

N O T I C E

THIS DOCUMENT HAS BEEN REPRODUCED FROM
MICROFICHE. ALTHOUGH IT IS RECOGNIZED THAT
CERTAIN PORTIONS ARE ILLEGIBLE, IT IS BEING RELEASED
IN THE INTEREST OF MAKING AVAILABLE AS MUCH
INFORMATION AS POSSIBLE

4/81

SEP

Report No. ANL-K78-4135-1
Distribution Category UC-94a
UC-98

Thermo Electron Report No. TE5484-88-79
NASA CR-159561

ENERGY

NOIIRKIFHON

**THERMAL ENERGY STORAGE FOR THE
STIRLING ENGINE POWERED AUTOMOBILE**

4-21-81

FINAL REPORT

Dean T. Morgan (Editor)



Date Published - March 1979

Prepared for
Argonne National Laboratory
Argonne, Illinois 60939

Work Performed Under Contract No. 31-109-38-4135

Thermo Electron Corporation
101 First Avenue
Waltham, Massachusetts 02154



U. S. DEPARTMENT OF ENERGY

Division of Energy Storage Systems

(NASA-CR-159561) THERMAL ENERGY STORAGE FOR
THE STIRLING ENGINE POWERED AUTOMOBILE
Final Report (Thermo Electron Corp.) 319 p
HC A14/MF A01 CSCL 10C

N81-22407

Unclass

82/44 21193

ABSTRACT

A detailed design of a thermal energy storage (TES) system for use with the Stirling engine as an automotive power system has been developed. The gravimetric and volumetric storage densities are competitive with electric battery storage systems. The TES/Stirling engine system meets all operational requirements for a practical vehicle and can be packaged in compact-sized automobiles with minimum impact on passenger and freight volume.

The TES/Stirling system is the only storage approach for direct use of combustion heat from fuel sources not suitable for direct transport and use on the vehicle. The particular concept developed in this study is also useful for a dual-mode TES/liquid fuel system in which the TES (recharged from an external energy source) is used for short-duration trips (~10 miles or less) and liquid fuel carried on board the vehicle used for long-duration trips (as in current automobiles). The dual-mode approach permits an automobile with the convenience and flexibility of current automobiles while offering the potential of 50-percent savings in the consumption of premium liquid fuels for automotive propulsion in the United States. Relative to the TES-only vehicle, the dual mode approach also reduces the TES cost significantly because of the much smaller TES capacity required.

PRECEDING PAGE BLANK NOT FILMED

ACKNOWLEDGEMENTS

This study effort was supported by the Chemical Engineering Division of the Argonne National Laboratory under Contract No. 31-109-38-4135; Dr. Madgy Farahat served as the program supervisor within the Argonne National Laboratory. Mr. David Namkoong of the NASA Lewis Research Center assisted in program monitoring. The work was performed during the period December 27, 1977 to September 1, 1978 by the Research and Development Center of Thermo Electron Corporation. The consulting engineering firm of Simpson, Gumpertz & Heger, Inc., Cambridge, Mass., was retained to perform the structural design and stress analysis of the TES reservoirs. Mr. Worth Piercival served as a consultant, particularly assisting in interface of the TES system to the Stirling engine.

The personnel involved in this study and their primary areas of contribution are listed below:

Thermo Electron Corporation, Waltham, Mass.

Dr. Dean T. Morgan	Program Manager TES Media Selection
Dr. Fred Huffman	Overall System Concept E-M Pump Design Thermal Insulation Design
Mr. George LaRue	Structural Design Including Detailed Drawings Coordination with Simpson, Gumpertz & Heger, Inc. Manufacturing Cost Estimating
Dr. Chi Chung Wang	Heat Transfer/Transport Analysis Vehicle Performance Analysis

Ms. Alexandra Zakak	Safety and Environmental Impact Assessment
Mr. Gabor Miskolczy	Heat Pipe Design Overall System Concept
Mr. Jim Shad	Overall System Concept
Dr. Chet Balestra	E-M Pump Design Fluoride Salt Properties
Dr. Seigo Matsuda	Materials-of-Construction

Simpson, Gumpertz & Heger, Inc., Cambridge, Mass.

Dr. Joseph Antebi	Detailed Structural Design and Analysis
Dr. Rene Luft	

Consultant

Mr. Worth Piercival Washington, DC	Interface with Stirling Engine Overall System Critique
---------------------------------------	---

Argonne National Laboratory, Argonne, Illinois

Dr. Mačgy Farahat	Program Supervisor
Mr. Al Chilenskask	Overall System Critique

NASA Lewis Research Center, Cleveland, Ohio

Mr. David Namkoong	Program Coordination
Mr. Joe Joyce	

U.S. Department of Energy, STOR, Washington, DC

Mr. C. J. Swet	Program Review
----------------	----------------

TABLE OF CONTENTS

<u>Chapter</u>		<u>Page</u>
	ABSTRACT	iii
	ACKNOWLEDGEMENTS	v
1	INTRODUCTION	1-1
	1.1 BACKGROUND	1-1
	1.2 GOALS AND APPROACH	1-4
	1.3 PERFORMANCE COMPARISON WITH THE ELECTRIC CAR	1-8
2	SELECTION OF ENERGY STORAGE MEDIA	2-1
	2.1 INTRODUCTION	2-1
	2.2 SENSIBLE, FUSION, OR CHEMICAL THERMAL STORAGE	2-2
	2.3 SELECTED MATERIALS AND CHARACTERISTICS	2-8
	2.3.1 Selection of Salts	2-8
	2.3.2 Properties of Selected Salts	2-18
3	CONCEPTUAL APPROACH AND MODES OF OPERATION	3-1
	3.1 INTRODUCTION	3-1
	3.2 DESCRIPTION OF OPERATION	3-10
	3.3 DUAL-MODE SYSTEM	3-15
	3.4 METHOD OF RECHARGING FROM EXTERNAL COMBUSTION SOURCE	3-17
4	HEAT TRANSFER AND TRANSPORT CHARACTERISTICS	4-1
	4.1 HEAT TRANSPORT BY POTASSIUM AND SODIUM VAPOR	4-3

TABLE OF CONTENTS (Cont'd)

<u>Chapter</u>		<u>Page</u>
4.2	EFFECT OF HYDROGEN LEAKAGE ON DISCHARGE HEAT PIPE OPERATION	4-14
4.3	EVAPORATION/CONDENSATION ΔT 's IN HEAT PIPES	4-24
4.4	SALT TEMPERATURE VARIATION DURING HIGH-POWER TRANSIENT	4-30
4.5	CHARGING HEAT PIPE, COMBUSTION SIDE	4-37
4.6	TRANSIENT RESPONSE	4-38
5	THERMAL INSULATION	5-1
5.1	HEAT TRANSPORT THROUGH MULTI-FOIL INSULATION	5-3
5.2	DESIGN CONSIDERATION AND PERFORMANCE	5-11
5.3	OVER ALL SYSTEM CHARACTERISTICS	5-15
6	TES RESERVOIR DESIGN	6-1
6.1	INTRODUCTION	6-1
6.2	DESIGN CRITERIA	6-6
6.2.1	Design Approach	6-8
6.2.2	Loads	6-9
6.2.3	Material Selection	6-10
6.2.4	Allowable Stresses for Inconel 617	6-12
6.3	RECTANGULAR DESIGN	6-16
6.3.1	Design Approach	6-16
6.3.2	Miscellaneous Details	6-75
6.3.3	Summary of Stresses, Weights, and Volume	6-82
6.4	CYLINDRICAL DESIGN	6-88
6.4.1	Design Approach	6-88
6.4.2	Summary of Results	6-103

TABLE OF CONTENTS (Cont'd)

<u>Chapter</u>		<u>Page</u>
6.5	DISCUSSION	6-107
	6.5.1 Alternate Designs	6-107
	6.5.2 Potential Problems	6-108
	6.5.3 Comparison and Evaluation	6-112
6.6	CONCLUSIONS	6-112
7	THERMOELECTRIC-ELECTROMAGNETIC PUMP DESIGN	7-1
	7.1 THERMOELECTRIC MODULE	7-3
	7.2 ELECTROMAGNETIC PUMP	7-10
8	CUSTOMER ACCEPTANCE AND APPLICATION CONSIDERATIONS	8-1
	8.1 MANUFACTURING COST	8-1
	8.2 ENERGY SOURCES AND RECHARGING	8-11
	8.3 VEHICLE RANGE	8-16
	8.4 SAFETY CONSIDERATIONS	8-24
	8.5 ENVIRONMENTAL CONSIDERATIONS	8-33
	8.6 MATERIAL AVAILABILITY CONSIDERATIONS	8-34
	8.7 DUAL-MODE TES/LIQUID FUEL SYSTEM...	8-35
9	CONCLUSIONS	9-1
	APPENDIX A MODEL USED FOR HEAT TRANSPORT CALCULATIONS FOR DISCHARGE HEAT PIPE DUCT ...	A-1

LIST OF FIGURES

<u>Figure</u>		<u>Page</u>
2.1	Phase Diagram for NaF-MgF ₂	2-20
2.2	Enthalpy vs Temperature for LiF and NaF/MgF ₂ Eutectic	2-21
2.2a	Thermal Diffusivity of Solid Lithium Fluoride (LiF).	2-27
2.2b	Thermal Diffusivity of Liquid Lithium Fluoride.	2-27
2.2c	Thermal Conductivity of Lithium Fluoride	2-27
3.1	TES Charging During Nonoperation.	3-4
3.2	TES Operation.	3-5
3.3	Short Period of Nonoperation (with charged TES).	3-6
3.4	Long Period of Nonoperation (with charged TES).	3-7
3.5	Dual-Mode Operation	3-8
3.6	Schematic of Dual-Mode TES/Liquid HC Fuel Vehicular Propulsion System Utilizing Stirling Engine	3-9
3.7	Schematic of Recharging System.	3-18
4.1	Schematic of Thermal Transport Model.	4-4
4.2	Heat Transport Characteristic for Sodium with D=2", L/D=60	4-6
4.3	Heat Transport Characteristic for Sodium with D=3", L/D=40	4-7
4.4	Heat Transport Characteristic for Sodium with D=4", L/D=30	4-8
4.5	Heat Transport Characteristic for Potassium with D=2", L/D=60	4-9
4.6	Heat Transport Characteristic for Potassium with D=3", L/D=40	4-10
4.7	Effect of L/D on Heat Transport Rate for Sodium with D=2", T _o =750°C	4-12

LIST OF FIGURES (Cont'd)

<u>Figure</u>		<u>Page</u>
4.8	Effect of Vapor Superheat for Potassium with D=2", L/D=60	4-13
4.9	Heat Transfer Rate vs. Source Temperature And Pipe Diameter	4-15
4.10	Minimum Source Temperature vs. Pipe Diameter ΔT , Source to Heater =25°C	4-16
4.11	Power and Efficiency Comparisons; Heat Pipe vs Direct-Fired Engines	4-19
4.12	Shaftpower vs. RPM For Engine 1-98 At Different Working Conditions	4-20
4.13	Indicated Power, PI, and Indicated Efficiency, NI, of a Phillips Stirling Engine as a Function of Speed, n, for H ₂ or He Working Gas and for Direct or Heat Pipe (Indirect) Heating	4-21
4.14	Pool Boiling Heat Flux vs. ΔT for Potassium And Sodium	4-29
4.15	Temperature Profile in Solid Salt Slab at Various Times After Step Increase in Heat Removal Rate From Zero to 200 kWth - Rectangular Design	4-33
4.16	Solid Salt Surface and Centerline Temperature As Function of Time With Initially Uniform Salt Temperature and Step Increase in Heat Removal Rate From Zero to 200 kWth - Rectangular Design	4-34
4.17	Centerline to Surface ΔT in Solid Salt As Function of Time With Initially Uniform Salt Temperature and Step Increase in Heat Removal Rate From Zero to 200 kWth - Rectangular Design	4-35
5.1	Multi-Foil Heat Transfer	5-2
5.2	Heat Flux as a Function of Applied Pressure for Multi-Foil Insulation	5-5
5.3	Multi-Foil Heat Flux Calculated from Function Fit Expression (Fitted to Experimental Data)	5-7

LIST OF FIGURES (Cont'd)

<u>Figure</u>		<u>Page</u>
5.4	Effects of Helium Pressure on the Heat Loss for a 9-Cup System (Run 10) With and Without a Water-Cooled Heat Sink	5-9
5.5	Time to Reach 10^{-3} Torr as a Function of Helium Leak Rate	5-10
5.6	Multi-Foil Insulation Heat Loss as Function of Number of Foils, $T = 850^{\circ}\text{C}$	5-12
5.7	Measured Temperature Distribution Through Cylindrical Foils	5-14
6.1	Location of TES Module in VW Transporter	6-3
6.2	Space in VW Transporter for TES Module	6-4
6.3	Location of TES Module in Ford Pinto-Size Car	6-5
6.4	Inside Box of Rectangular TES Assembly	6-19
6.5	Salt Container and Enclosure Frame	6-21
6.6	Inside Box with Reinforcing Skln (Corset) and Support Bushing	6-23
6.7	Side View of Inner Box	6-25
6.8	Enclosure Frame Assembly for Inner Box	6-28
6.9	Side Piece for Enclosure Frame (1 Hole)	6-29
6.10	Side Piece for Enclosure Frame (2 Hole)	6-30
6.11	Side Piece for Enclosure Frame (No Hole)	6-31
6.12	Top and Bottom Pieces for Enclosure Frame	6-32
6.13	Pressure Head on Doubly-Curved End Shells for Two Sides of Pressure Envelope	6-33
6.14	Primary Diaphragm Design	6-37
6.15	Bottom and Top Diaphragms	6-39
6.16	Drawn Sheets to Form Salt Capsules - For All Except End Capsules	6-41

LIST OF FIGURES (Cont'd)

<u>Figure</u>		<u>Page</u>
6.17	Drawn Sheets to Form Salt Capsules - Reduced Height for End Capsules	6-43
6.18	Truss for Reinforcing Skin on Side with Holes for Discharge Heat Pipe	6-47
6.19	Discharge Heat Pipe	6-49
6.20	Discharge Heat Pipe Assembly	6-51
6.21	Discharge Heat Pipe Header, Tube Side	6-53
6.22	Discharge Heat Pipe Header, Transport Pipe Side.	6-55
6.23	Return Liquid Distributor Tubing Assembly	6-57
6.24a	Discharge Heat Pipe Tube and Enclosure	6-59
6.24b	Closure Cap of Discharge Heat Pipe Tube	6-60
6.25	Multi-Foil Insulation Around Inner Box	6-62
6.26	Honeycomb Outer Box to Provide Vacuum in Multi-Foil Insulation	6-63
6.27	Assembly Drawing of Outer Box with Details of Pin Support	6-65
6.28	Top and Bottom Panels of Outer Box	6-67
6.29	Rear Panel of Outer Box	6-68
6.30	Side Panel of Outer Box (2 Req'd)	6-69
6.31	Front Panel of Outer Box	6-70
6.32	Pin Support Welded into Outer Box Opening	6-72
6.33a	Support Bushing Welded to Trusses of Inner Box.	6-73
6.33b	Support Ring for Inner Box	6-74
6.34a	Molded Salt Capsules for Charging; Short (for End Capsules	6-76
6.34b	Molded Salt Capsules for Charging; Long (For all Except End Capsules)	6-77

LIST OF FIGURES (Cont'd)

<u>Figure</u>		<u>Page</u>
6.35a	Pinch-Off Tube for Salt Capsules - Assembly	6-78
6.35b	Pinch-Off Tube for Salt Capsules - Details	6-79
6.36	Tabs for Tying Primary Diaphragms to Reinforcing Skin	6-81
6.37	Assembly Drawing of Cylindrical TES Reservoir (Dwg. No. 035-01-000)	6-91
6.38	Stock of Salt Inventory Capsules with Reinforcing Rings and Discharge/Charge Heat Pipe Tubes Incorporated	6-93
6.39	As In Figure 6.38 with Part of Inner Pressure Shell and Part of Discharge Heat Pipe Header Incorporated	6-94
6.40	Complete Inner Pressure Vessel	6-95
6.41	Installation of Multi-Foil Insulation, Outer Pressure Vessel With Stiffening Rings, and Support Pins	6-96
6.42	Salt Capsule Assembly Illustration	6-100
7.1	Potassium Vapor Transport Characteristics	7-2
7.2	Thermoelectric-Electromagnetic (TE-EM) Pump Concept	7-4
7.3	Thermoelectric-Electromagnetic (TE-EM) Pump Perspective Diagram	7-5
7.4	Thermoelectric Efficiency Versus Hot Junction Temperature	7-8
7.5	Electromagnetic Pump	7-11
7.6	Lumped Parameter Model of Electromagnetic Pump	7-12
7.7	Operating Characteristics of an EM Pump	7-13
8.1	Manufacturing Flow Diagram for Rectangular Configuration	8-3
8.2	Manufacturing Flow Diagram For Cylindrical Configuration	8-5

LIST OF FIGURES (Cont'd)

<u>Figure</u>		<u>Page</u>
8-3	Nonpetroleum Energy Sources and Options for Automotive Propulsion	8-12
8.4	Performance Map for ERDA-4 98DA Stirling Engine	8-18
8.5	SAE Metropolitan Area Driving Cycle, SAE J-2272 .	8-19
8.6	Performance Map: 4-98 Stirling Engine with Rollsock Seals	8-21
8.7	P-75 Stirling Engine Performance Map	8-22
8.8	Distribution of Trip Mileage and Fuel Consumption .	8-39

LIST OF TABLES

<u>Tables</u>	<u>Page</u>
1.1 TES Automotive Propulsion System Specifications . .	1-9
2.1 Entropy Change for Several Fusion and Chemical Transitions	2-6
2.2 Thermal Energy Storage Single Salts with Heat-of-Fusion ≥ 0.116 kwhrth/kg (100 cal/gm) . . .	2-10
2.3 Material Costs, 1976 Dollars	2-12
2.4 The 45 Most Abundant Elements in the Earth's Crust	2-13
2.5 Concentration of Some Elements Present in Solution in Seawater	2-14
2.6 Comparison of Li Required for Large-Scale Automotive Use to Estimated Resource and Recoverable Resource Potential	2-16
2.7 Selected TES Materials with Melting Points Greater than 1023°K	2-19
2.8 Thermal Energy Storage Density Over Temperature Range of 800°K to 1150°K	2-23
2.9 Density Variation of Reference Salts	2-25
4.1 Condensation Heat Flux and Heat Transfer Coefficient for Sodium and Potassium as Function ΔT	4-26
5.1 24-Hour Heat Loss as Percentage of Storage Capacity	5-17
6.1 Selected Allowable Stresses for Inconel 617	6-13
6.2 Stress Levels of Inconel 617	6-14
6.3 Inner Rectangular Box of Inconel 617 Stress Summary	6-83
6.4 Outer Rectangular Box of Tre-Metal Stress Summary	6-85
6.5 Summary of Structural Weight Rectangular Box . . .	6-86

LIST OF TABLES (Cont'd)

<u>Tables</u>	<u>Page</u>
6.6 Summary of Weights, Volumes, Heat Transfer Areas, and TES Capacity for Rectangular Configuration	6-87
6.7 Inner Cylindrical Container of Inconel 617 Stress Summary	6-97
6.8 Summary of Structural Weight Cylindrical Containers	6-105
6.9 Summary of Weights, Volumes, Heat Transfer Areas, and TES Capacity for Cylindrical Configuration (Two Cylinders)	6-106
6.10 Comparison of Cylindrical and Rectangular Configurations After Normalization to 500 kg Total Reservoir Weight	6-113
7.1 Thermoelectric Material Properties	7-7
7.2 Thermoelectric-Electromagnetic Reference Pump Summary	7-9
7.3 Pressures (psi) Required to Compensate for Frictional Losses in the EM Pump and Its Associated Plumbing	7-15
8.1 Manufacturing Cost Estimate for Rectangular TES Reservoir Configuration	8-7
8.2 Manufacturing Cost Estimate for Cylindrical TES Reservoir Configuration	8-9
8.3 Vehicle Range for 500 kg TES Reservoir Weight	8-20
8.4 Energy Requirement and Performance Predictions (Thermo Electron Corporation Calculations)	8-25
8.5 Estimated Potassium Charge for System	8-29
8.6 Comparison of Quantity of Strategic Metals for 100, 000, 000 Vehicles to Current World Production and Estimated Reserves	8-36

1. INTRODUCTION

1.1 BACKGROUND

When the world's petroleum reserves are depleted, alternative energy sources for automotive propulsion will be required. Current automobiles are based on the use of premium-grade liquid fuels, derived from petroleum as the energy source, and these fuels provide the convenience in personal transportation to which we are all accustomed. Passenger automobile propulsion currently utilizes 28 percent of the total petroleum consumption in the United States, corresponding to 13 percent of the total national energy consumption from all sources.¹

The world's petroleum resources are inadequate to sustain the present rate of consumption for very long, and there is no guarantee that synthetic fuels derived from coal or oil shale, our major fossil energy resources for the future, will be available in time and in sufficient quantities to replace petroleum-derived fuels. In addition, the thermal efficiency of current or projected processes to produce the synthetic premium fuels required for automotive propulsion is poor resulting in a waste of the coal energy resource, even if this approach were feasible in a timely and economic way.

The private automobile is an institution in the United States and severe restrictions in its use will result in severe economic and social repercussions. There is thus a very strong incentive to develop alternatives to premium liquid fuels for automotive propulsion. Several alternative options are under development, ranging from development of highly efficient engines such as the Stirling engine (to reduce the

consumption of premium liquid fuels from whatever source) to electric cars (which use electrical energy from central-station nuclear and coal-burning powerplants and thus are not dependent on use of premium liquid fuels). The energy storage options currently under development, such as the electric car with electric batteries for energy storage, have severe limitations relative to vehicle range between recharges, long recharge times, high cost, and limited life (limited number of discharge/recharge cycles).²

The Stirling engine is under intensive development for automotive propulsion by the U. S. Department of Energy, primarily because of its very high efficiency potential which reduces the consumption of premium liquid fuels.³ This reduction is important for either petroleum-derived or synthetic fuels. For the former, it extends the time when the petroleum reserves are depleted; for the latter, it reduces the capital investment in new plants to supply the fuel and provides additional time for implementation of synthetic liquid fuel plants.

The Stirling engine is an external combustion engine in which heat is transferred into the engine working fluid from combustion gases by a tubular heat exchanger; this is in contrast to the internal combustion engine in which the fuel is mixed with air and combusted directly in the engine cylinder. The Stirling engine can thus be adapted to practically any high-temperature heat source, including stored thermal energy by the sensible and/or latent-heat-of-fusion of selected materials. Thermal energy storage (TES) can also be utilized with other external combustion engines such as the closed-cycle Brayton or the Rankine engine, but these are considerably less efficient than the Stirling engine and have other disadvantages for automotive power

as well. The Stirling engine is the only external combustion engine currently under development for automotive propulsion.

In 1964, the General Motors Research Laboratories constructed and successfully operated a demonstration car, the "Calvair," using thermal energy storage combined with a small Stirling engine. In this installation, nitrogen was circulated through a tank of hot alumina pellets where it was heated; it was then circulated on to the Stirling engine where it heated the engine to about 1200°F. The tank was recharged by combustion of natural gas in an external combustor to reheat the alumina. The system was installed in a modified Corvair, but was too heavy and too expensive for a practical automotive vehicle installation.⁴

Meijer of the Philips Research Laboratories, Eindhoven, Holland, described application of the TES/Stirling engine system for automotive propulsion in a 1970 paper.⁵ In this study, the latent heat-of-fusion of LiF was used for TES, with heat transported from the TES reservoir to the Stirling engine heater by means of a heat pipe with sodium working fluid. Use of the heat-of-fusion of LiF greatly improved the gravimetric and volumetric thermal energy storage density relative to sensible heat storage in alumina or other materials. Transport of the thermal energy by means of the heat pipe also has many desirable features; demonstration Stirling engines (with helium working fluid) were successfully operated with sodium heat pipes.^{5,7} Separate testing of a TES system with LiF and using a sodium heat pipe for heat transport was also successfully demonstrated by the Philips Laboratories in Eindhoven.⁶ These studies demonstrated the basic technologies required for the TES/Stirling automobile as well as the excellent potential

of the TES/Stirling system relative to other energy storage concepts for automotive propulsion.

As a result of this potential, Mechanical Technology, Inc. performed a study to establish appropriate system parameters and initiate feasibility studies on the TES/Stirling automobile.⁸ This work resulted in the issuance of an RFD on August 8, 1977 to initiate a program to assess the technical and economic feasibility of the TES/Stirling car and to develop conceptual designs. As a result, a contract was issued to Thermo Electron Corporation on December 27, 1977 to perform this detailed assessment with the results described in this report. A parallel contract was also issued to Sigma Research, Inc. of Richlands, Washington.

1.2 GOALS AND APPROACH

In addition to the Stirling engine, any TES system for automotive propulsion includes the following major subsystems:

- TES Media and Containment
- Thermal Insulation
- Heat Transport to Engine With Controls for Regulating Heat Delivery Rate In Response to Engine Thermal Demand
- Thermal Recharge System

In this report, each of these major subsystems is discussed as well as their integration into a complete TES system that meets all operational requirements. In addition, critical factors related to customer acceptance and application are discussed, specifically packaging in the vehicle with minimum impact on passenger and freight volume, manufacturing cost, energy sources and recharging, vehicle range, safety

considerations, environmental considerations, and material availability considerations.

The application of the TES/Stirling system to dual-mode TES/liquid-fuel operation is also discussed. This approach, unique among energy storage methods for automotive propulsion, permits the Stirling engine to operate either from the TES unit charged from an external energy source or from liquid fuel carried on-board the vehicle as in current automobiles. The TES is used only for short-duration trips, with liquid fuel used for long-range trips. This approach offers a system with minimum cost for the TES system, retains the current flexibility and convenience of automobiles, and offers savings of up to 50 percent in the premium liquid fuel consumption for automotive propulsion. Because of the far less stringent technical requirements on the TES when used as a dual-mode TES/liquid fuel system, we believe that any future utilization of TES for automotive propulsion will be initiated as a dual-mode system, and that evolution to the total TES automobile will occur over an extended period of time as technology develops and social conditions change. The dual-mode system will greatly extend either petroleum or premium synthetic fuels for automotive propulsion by substitution of alternative energy sources not suited for direct on-board storage and/or use.

Two selections were made for the TES media, either of which can be used in the TES reservoir, LiF or a 70 w/o NaF - 30 w/o MgF₂ eutectic. Thermal energy storage is based on the use of both the sensible and latent heat-of-fusion with an operating temperature range of 800°K → 1150°K. The materials have good storage densities on both a gravimetric and volumetric basis; they have a

melting temperature that provides a good temperature match to the Stirling engine; they are very stable chemically and thermally; and they have low corrosion rates with suitable containment materials. LiF has the highest storage capacity and is the preferred material; however, there are questions concerning its availability and cost for large-scale automotive use. The NaF/MgF₂ eutectic has somewhat lower performance, but is made up of readily available and inexpensive materials.

In designing the reservoir or containment structure for the salt, the configuration was restricted to that judged best-suited for packaging in the vehicle. Packaging of the TES reservoir underneath the floorboard and between the wheels provides a low center-of-gravity, minimizes impact on the passenger/freight volume of the vehicle, provides equal weight distribution of the wheels, and provides maximum protection to the TES reservoir in the event of collision. This packaging location restricts the reservoir to a low profile (height) with large plan area. Two reservoir configurations were designed, a rectangular configuration and a cylindrical configuration made up of two identical cylindrical units. A key objective in the design of the reservoirs was maximizing the fraction of the total reservoir weight and volume comprised by the salt media. This required development of an efficient structural design to meet the system pressure loads as well as acceleration loads within the stress limits of the materials of construction. This goal of efficient structural design to minimize the structure weight is very important, since the design stress for continuously loaded parts of the structure is only 3000 psi because of the high operating temperature.

Extremely effective thermal insulation with low volume (thickness) and low weight is critical to minimize heat losses without compromising

other system requirements and severely degrading the overall system efficiency. The approach selected, which provides a significantly lower volume (thickness) and weight than any fiber insulation even under vacuum, is use of vacuum Multi-Foil insulation, which provides a 24-hour heat loss of 10 percent or less of the full-charged thermal storage capacity. Use of vacuum introduces severe difficulties in the reservoir structural design, but these difficulties were successfully resolved for both the rectangular and cylindrical reservoir configurations.

For heat transport from the TES media to the Stirling engine and for recharging, the only feasible approach is use of either potassium or sodium heat pipes. A unique approach was developed that uses three coupled heat pipes, one for recharging, one for internal heat transfer in the reservoir, and one for heat delivery or discharge to the Stirling engine. Precise control on the heat delivery rate to the engine is obtained by incorporating an E-M pump for liquid return to the TES reservoir, with the heat delivery rate controlled by modulation of the pumping rate. This system meets all operational requirements for the system with no moving parts.

A preliminary evaluation indicated that a recharging combustor could be developed to permit automotive recharging of the TES unit with the same convenience as operation of a home furnace. A key consideration is the source of energy for recharging. The most appropriate source is that used for home heating, since an extreme incentive exists to develop synthetic fuels for home heating as our petroleum resources are depleted. It can thus be hypothesized that a synthetic gas industry will develop to initially supplement, and eventually replace, natural gas. The extensive and expensive natural gas transmission/distribution infrastructure provides a strong economic incentive for

development of the synthetic gas industry. If this develops, this synthetic gas can be used for overnight recharging of the TES/Stirling automobile at home, as well as for home heating. Such gas is not suited for direct on-board storage; it is delivered to the majority of the homes in the United States by an existing infrastructure; and it is easily combusted with low emissions, permitting a compact external (to the vehicle) furnace for recharging.

In the design of the system, the detailed specifications on which the design was based, as given in the contract, are summarized in Table 1.1. The total TES system weight was specified as 500 kg, with a volume $\leq 0.4 \text{ m}^3$. The maximum heat delivery rate to the Stirling engine for peak power is 200 kwth. The designed system meets or exceeds all specifications and operational requirements. The vehicle range depends on the particular vehicle characteristics, including driving cycle and salt media, but is generally $\geq 161 \text{ km}$ (100 miles) for a 500-kg total system weight.

1.3 PERFORMANCE COMPARISON WITH THE ELECTRIC CAR

The prime competitor to the TES/Stirling engine system at present is the electric car; a brief comparison of the storage density by TES is compared with that of the electric battery in this section. From Table 6.10 of Chapter 6, the storage density of the TES reservoir is given as summarized below:

Salt Configuration		Gravimetric Storage Density (Kwhrth/Kg)		Volumetric Storage Density ₃ (Kwhrth/m ³)	
		Rectan-gular	Cylin-drical	Rectan-gular	Cylin-drical
LiF		0.30	0.28	400	400
NaF/MgF ₂ Eutectic		0.20	0.18	290	290

TABLE 1.1

TES AUTOMOTIVE PROPULSION SYSTEM SPECIFICATIONS

TES System: Weight	500 kg
Volume	$\leq 0.4 \text{ m}^3$
Vehicle Energy Requirement:	
Steady Speed at 88.5 km/hr	0.627 kwhrth/km
SAE Metropolitan Driving Cycle	0.824 kwhrth/km
Heater Head Temperature:	
Normal Operation	1023°K
Peak (Not to be exceeded)	1123°K
Minimum	$\sim 800^\circ\text{K}$
Heat Delivery Rates:	
Peak for Maximum Power (15 second duration)	200 kwth
Constant Speed at 88.5 km/hr	55.5 kwth
With Hill Climb (5 minute duration)	66.8 kwth
Maximum Heat Loss Rate	25% of Full Charge Over 12-Hour Period at 25° C Ambient
Thermal Control Requirements:	
Traffic Start from Idle*	5 → 15 kwth in 0.2 sec.
Traffic Stop	15 → 5 kwth in 0.2 sec.
Idle	Stable at 2 kwth Indefinitely
High Power Burst*	50 → 200 kwth in 1 sec.
Maximum Heat Leakage to Heat Transport Subsystem During Standby	0.5 kwth
Orientation Limits	Maximum Power $\pm 15^\circ$ From Horizontal in Any Direction Startup on 30% Grade With Minimum Heat Delivery Rate of 66.8 kwth.
Geometrical Constraints:	The TES System Shall be Configured to Fit Within a Compact-Sized Auto- mobile
Recharge:	Amenable to Recharge From External Com- bustion Heat Source
Operating Life:	10 Year Minimum 3000 Charge/Discharge Cycles
Transient Accelerations for Structural Integrity:	Vertical: 3.5 g Longitudinal: 6.0 g Vibration Rates: 10-20 Cycles/sec Slew Rate: 2 Radians/sec

* Minimum Heater Wall Temperature During Transient of 673°K

From the Lawrence Livermore Laboratory report on energy storage systems for automobile propulsion,² the storage characteristics of engineering batteries, those that have a reasonable chance of becoming commercially available within the next few years, are given as:

Storage Density Battery		State-of-the-Art			Improved (Goals)		
		Pb/Acid	Ni/Zn	Ni/Fe	Pb/Acid	Ni/Zn	Ni/Fe
Kwhre/kg		0.035	0.070	0.045	0.05	0.09	0.06
Kwhre/m ³		60	115	85	90	150	110

The most promising advanced batteries are given as the lithium/metal sulfide, sodium/sulfur (ceramic electrolyte), and zinc/chlorine systems. The energy storage densities of these batteries are uncertain since they are currently in development. Projected gravimetric storage densities for these batteries range from 0.1 to 0.15 kwhre/kg, and the volumetric storage densities are given as:

Battery	Volumetric Storage Density (kwhre/ft ³)
Li-Al/FeS _x	174
Na/S (ceramic)	135
Zn/Cl ₂	120

Exploratory batteries are also discussed, but they are not presented here since their storage densities are even more uncertain.

For comparison, it is assumed that the average Stirling engine efficiency in use is 25 percent so that, in terms of work output, the TES system has storage densities of:

Salt	Gravimetric Storage Density (kwhr work/kg)	Volumetric Storage Density (kwhr work/m ³)
LiF	0.069 → 0.076	100
NaF/MgF ₂	0.046 → 0.050	72

It is apparent from comparison of these values with those from the previous tables that, in terms of gravimetric and volumetric storage densities, TES with LiF media is superior to the current Pb/acid batteries and competitive to other state-of-the-art batteries. While the storage densities for TES are somewhat lower than for the advanced battery systems, it should be noted that the quoted values for advanced batteries are undoubtedly optimistic and will decrease as development continues. For example, a 20 kwhre Li-Al/FeS_x battery storage system currently under fabrication for automotive propulsion has a battery weight of 900 lbs, high temperature insulation and containment box weight of 150 lbs, and overall size of 12 in. x 18 in. x 65 in.⁹ These values correspond to storage densities of 0.042 kwhre/kg and 86.9 kwhre/m³, which are much lower than the values presented in Reference 2. Although some improvement in these values can be expected for larger battery units, it would appear that TES should be competitive in terms of storage density with even advanced battery systems.

In addition, TES is the only automotive storage system suited for direct use of combustion energy from fuels not suited for on-board storage and use. A very important and unique feature of the TES/Stirling system is its use as a dual-mode TES/liquid fuel system that provides the convenience and flexibility of current automobiles while offering 50-percent savings in premium liquid fuels in the United

States for automotive propulsion. The combination of excellent storage densities and this potential fuel savings justifies a development effort on the TES/Stirling automobile with initial emphasis on the dual-mode TES/liquid fuel system.

REFERENCES FOR CHAPTER 1

1. Shonka, D. B., et al., Transportation Energy Conservation Data Book, Edition 2, ORNL-5320, Oak Ridge National Laboratory, Oak Ridge, Tenn., October 1977.
2. Behrin, E., et al., Energy Storage Systems for Automobile Propulsion, Vol. I: "Overview and Findings," Vol. II: "Detailed Report," UCRL-52503; Vol. I and Vol. II, Lawrence Livermore Laboratory, Livermore, California, December 15, 1977.
3. DOE Highway Vehicle Systems Contractors Coordination Meeting, October 17-20, 1978, Dearborn, Michigan.
4. "Energy Storage Systems Complement the Stirling Engine," Paper Prepared by Technical Information Department, GM Research Laboratories, Warren, Michigan, May 1969.
5. Meijer, R. J., "Prospects of the Stirling Engine for Vehicular Propulsion," Philips Technical Review, Vol. 31, No. 5/6, pp. 168-185(1970).
6. Asselman, G. A. A., "Thermal Energy Storage Based on Lithium Fluoride," Energy Conversion, Vol. 16, pp. 35-47, Pergamon Press, 1976.
7. Meijer, R. J. and Spigt, C. L., Paper Presented at the Second Symposium on Low Pollution Power Systems Development, Committee on the Challenges of Modern Society of the North Atlantic Treaty Organization, Dfusseldorf, Germany, November 4-8, 1974.
8. Falsom, L. R. and Artiles, A. A., "Thermal Energy Storage/Heat Engine for Highway Vehicle Propulsion," Paper Presented at ERDA Highway Vehicle Systems Contractors Coordination Meeting, Dearborn, Michigan, October 4-6, 1977.
9. Personal Communication, Dr. Seigo Matsuda, Thermo Electron Corporation, Waltham, Mass., October 1978.

2. SELECTION OF ENERGY STORAGE MEDIA

2.1 INTRODUCTION

Thermal energy storage (TES) can be accomplished by utilization of sensible heat, latent heat-of-fusion, or thermally reversible chemical reactions. For the automotive application, the primary selection criteria are:

- High gravimetric storage capacity, kwhrth/kg
- High volumetric storage capacity, kwhrth/liter
- Low cost per unit of TES capacity
- Temperature range appropriate for integration with Stirling engine
- High thermal stability
- High chemical stability; i. e., compatible with available materials of construction and nonreactive with air and water
- Composed of readily available chemical elements permitting large-scale automotive use
- Low vapor pressure at maximum operating temperature
- Firm technology base (known properties, prior experience)

As with most engineering analyses, selection of the final material generally represents some compromise with respect to the selection criteria, based on the engineering judgment of the selector.

In this chapter, we present a summary of the characteristics of TES media leading to our selection of either LiF or a NaF/MgF₂ eutectic mixture for the TES media. For either material, TES is based on utilization of both the latent heat-of-fusion and sensible heat of the fluoride salt, with a significant contribution from the sensible heat. LiF has the highest gravimetric and volumetric storage densities, but is relatively costly and lithium has a low natural abundance—with questionable availability for large-scale automotive use. The NaF/MgF₂ eutectic has significantly lower gravimetric and volumetric storage densities, but is available at low cost and is made up of highly abundant and readily available elements. Both materials have excellent thermal and chemical stability—thus, the TES reservoir design presented in Chapter 6 can be charged with either material, depending on the relative importance attached to performance and cost. It should be noted that eutectics containing LiF are also available with storage densities intermediate between the two selected materials. However, achieving a significant improvement above the NaF/MgF₂ eutectic requires a substantial weight percentage of LiF (at least 30 to 50%) — so that the questions of cost and availability of LiF are not eliminated, but only somewhat reduced. The decision was thus made to use pure LiF and a material containing no LiF as the two alternative TES media for this study.

2.2 SENSIBLE, FUSION, OR CHEMICAL THERMAL STORAGE

A TES material having very high gravimetric and volumetric storage densities, as well as meeting the other criteria outlined

in Section 2.1, would have a very wide application potential. As a result, much effort has been expended by many organizations over the last 15 years on development of TES media, particularly those using the latent heat-of-fusion or reversible chemical reactions. In this section, we briefly discuss the basis for selection of latent heat-of-fusion as the best approach for TES for the automotive application.

One can, of course, use only the sensible heat of high-temperature oxides as the means of TES. For application with a Stirling engine, the minimum heat source temperature is already high, $\sim 1000^{\circ}\text{K}$ (1340°F), if high engine efficiency is to be achieved. Reliance on sensible heat alone thus requires a very high peak temperature of the TES media if acceptable storage densities are to be achieved for even a limited-purpose vehicle. As an example, for LiF with a latent heat-of-fusion of 0.29 kWhrth/kg (450 Btu/lb), the latent heat-of-fusion is equivalent to $\sim 1000^{\circ}\text{K}$ (1800°F) temperature differential for a material with heat capacity of $0.25 \text{ cal/gm-}^{\circ}\text{K}$. The heat capacity of Al_2O_3 is $0.29 \text{ cal/gm-}^{\circ}\text{K}$ at 1000°K . Since the technical difficulties with respect to materials-of construction, insulation and heat losses, and heat delivery to the engine increase rapidly with the peak storage temperature, the delivery of heat at a constant temperature by use of the latent heat-of-fusion has important advantages, and thus has been selected as the optimum approach for this application. Use of the sensible-heat, as well as the latent heat-of-fusion, can add significantly to the TES densities, primarily by using the sensible heat of the solid below the

melting point. For example, either solid or liquid LiF has a heat capacity of $\sim 0.6 \text{ cal/gm-}^\circ\text{K}$.

A potential alternative to the latent heat-of-fusion is the use of a thermally reversible chemical reaction. On charging, heat added to the TES media raises the temperature of the media, which results in the shift of a reversible chemical reaction. The energy is stored, therefore, both as sensible heat and as chemical energy resulting from the endothermic chemical reaction. On discharge, the temperature drops as heat is removed, and the reverse exothermic reaction occurs. This approach sounds extremely promising at first glance, due to the high energy available from certain chemical reactions. We believe, however, that once the practical restriction for motive power applications (and for most other applications) is made that components of the chemically reacting system must be either liquid or solid phases over the temperature range of the TES, it is extremely difficult for a thermally reversible chemical reaction to outperform the better latent heat of fusion materials. The reversible reaction cannot produce a gas because of the large storage volume required for a gas relative to a liquid or a solid.

For a latent heat transition, which occurs at a specific temperature,

$$\Delta F^\circ_{\text{Fusion}} = \Delta H^\circ_{\text{Fusion}} - T_{\text{MP}} \Delta S^\circ_{\text{Fusion}} = 0.$$

For a reversible chemical reaction, the temperature at which the reaction occurs can be represented by T^* , where the equilibrium

constant, $K=1$ and $\Delta F^\circ = -RT \ln K = 0$. Thus,

$$\Delta F^\circ_{\text{Reaction}} = \Delta H^\circ_{\text{Reaction}} - T^* \Delta S^\circ_{\text{Reaction}} = 0.$$

For either type of reversible transition, therefore,

$$\Delta H^\circ_{\text{Trans}} = T^* \Delta S^\circ_{\text{Trans}} \quad \text{in } \frac{\text{kilocal}}{\text{gm-mole}}$$

In terms of the transition heat per unit mass,

$$\frac{\Delta H^\circ_{\text{Trans}}}{M} = \frac{T^* \Delta S^\circ_{\text{Trans}}}{M} \quad \text{in } \frac{\text{kilocal}}{\text{gm}},$$

where

$$M = \text{Molecular Weight.}$$

From this relation, it is apparent that for high TES per unit mass, M must be small enough that only low molecular weight chemical elements should be considered, and that the entropy change, ΔS° (for given T^*), should be as large as possible.

In Table 2.1, the entropy of transition is presented for several fusion and chemical transitions classified according to the change in the number of gaseous products.¹⁵ Inspection of this table indicates that a relatively large ΔS° occurs only for those transitions in which the number of gas-phase particles in the products is greater than the number in the reactants, whatever the nature of phase of the other reactants or products may be. For those gas-phase reactions in which the number of product gas moles is equal to the number of reactant gas moles, the entropy change is very small. For the

TABLE 2.1

ENTROPY CHANGE FOR SEVERAL FUSION AND CHEMICAL TRANSITIONS ¹⁵

Type of Transition	Transition	ΔS° , cal/gm-mole \cdot K	
Fusion	$\text{LiF}(s) \rightleftharpoons \text{LiF}(l)$	5.8*	(1121°K)
	$\text{NaCl}(s) \rightleftharpoons \text{NaCl}(l)$	6.5	(1074°K)
	$\text{Al}(s) \rightleftharpoons \text{Al}(l)$	2.6	(659°K)
	$\text{CaF}_2(s) \rightleftharpoons \text{CaF}_2(l)$	4.3	(1691°K)
	$\text{MgCl}_2(s) \rightleftharpoons \text{MgCl}_2(l)$	10.5	(988°K)
	$\text{FeCl}_2(s) \rightleftharpoons \text{FeCl}_2(l)$	10.8	(950°K)
	Vaporization	$\text{LiF}(l) \rightleftharpoons \text{LiF}(g)$	17.6**
$\text{NaCl}(l) \rightleftharpoons \text{NaCl}(g)$		23.4	(1738°K)
$\text{Al}(l) \rightleftharpoons \text{Al}(g)$		25.1	(2767°K)
$\text{CaF}_2(l) \rightleftharpoons \text{CaF}_2(g)$		26.7	(2773°K)
$\text{MgCl}_2(l) \rightleftharpoons \text{MgCl}_2(g)$		19.4	(1691°K)
$\text{FeCl}_2(l) \rightleftharpoons \text{FeCl}_2(g)$		23.4	(1285°K)
Reactions in Which Gaseous Products Are Found From Solid or Liquid Reactants at 298°K		$1-1/2 \text{Br}_2(l) + 1/4 \text{P}_4(s) \rightarrow \text{PBr}_3(g)$	17.9
	$\text{Li}(s) + 1/2 \text{I}_2(s) \rightarrow \text{LiI}(g)$	34.9	(34.9)
	$\text{C}(\text{graphite}) + 2\text{S}(\text{rhombic}) \rightarrow \text{CS}_2(g)$	40.2	(40.2)
	$\text{H}_2\text{O}(l) \rightarrow \text{H}_2(g) + 1/2 \text{O}_2(g)$	40.0	(26.7)
	$\text{NaCl}(s) \rightarrow \text{Na}(g) + \text{Cl}(g)$	58.1	(29.1)
	$\text{NH}_4\text{Cl}(s) \rightarrow \text{NH}_3(g) + \text{HCl}(g)$	68.1	(34.1)
Reactions in Which There is an Increase in the Number of Gaseous Particles at 298°K	$\text{BiCl}_3(g) \rightarrow \text{Bi}(s) + 1/2 \text{Cl}_2(g)$	8.1	(16.2)***
	$\text{PbO}_2(s) \rightarrow \text{PbO}(s) + 1/2 \text{O}_2(g)$	22.5	(45.0)
	$\text{Pb}_3\text{O}_4(s) \rightarrow 3\text{PbO}(s) + 1/2 \text{O}_2(g)$	22.7	(45.4)
	$\text{SiCl}_4(l) + 2\text{H}_2\text{O}(l) \rightarrow \text{SiO}_2(s) + 4\text{HCl}(g)$	98.0	(24.5)
	$\text{ZnS}(s) + 2\text{H}_2\text{O}(l) \rightarrow \text{Zn}(\text{OH})_2(s) + \text{H}_2\text{S}(g)$	21.7	(21.7)
	$\text{PbCO}_3(s) \rightarrow \text{PbO}(s) + \text{CO}_2(g)$	36.1	(36.1)
	$\text{NaCl}(s) \rightarrow \text{Na}(s) + 1/2 \text{Cl}_2(g)$	21.5	(43.0)
	$\text{PH}_3(g) \rightarrow \text{P}(s, \text{white}) + 1-1/2 \text{H}_2(g)$	7.2	(14.4)
	$\text{KHF}_2(s) \rightarrow \text{KF}(s) + \text{HF}(g)$	32.5	(32.5)
	$\text{AsF}_3(l) \rightarrow \text{As}(s, \text{grey}) + 1-1/2 \text{F}_2(g)$	38.0	(25.3)
Gas Phase Reactions at 298°K in Which There is an Increase in the Number of Gas Phase Particles	$\text{O}_2(g) \rightarrow 2\text{O}(g)$	28.0	(28.0)***
	$\text{NH}_3(g) \rightarrow 1/2 \text{N}_2(g) + 1-1/2 \text{H}_2(g)$	23.7	(23.7)
	$\text{P}_4(g) \rightarrow 4\text{P}(g)$	81.7	(27.2)
	$\text{S}_8(g) \rightarrow 8\text{S}(g)$	218.9	(31.3)
	$\text{NO}_2(g) \rightarrow 1/2 \text{N}_2(g) + \text{O}_2(g)$	14.3	(28.6)
	$\text{N}_2\text{O}_4(g) \rightarrow \text{N}_2(g) + 2\text{O}_2(g)$	71.0	(35.5)
	$\text{H}_2\text{O}(g) \rightarrow \text{H}_2(g) + 1/2 \text{O}_2(g)$	10.5	(21.0)
	$\text{Ni}(\text{CO})_4(g) \rightarrow \text{Ni}(g) + 4\text{CO}(g)$	136.7	(34.2)
Gas Phase Reactions at 298°K in Which No Change Occurs in the Number of Gas Particles	$\text{H}_2(g) + \text{F}_2(g) \rightarrow 2\text{HF}(g)$	3.3	
	$\text{H}_2(g) + \text{Cl}_2(g) \rightarrow 2\text{HCl}(g)$	4.8	
	$\text{H}_2(g) + \text{Br}_2(g) \rightarrow 2\text{HBr}(g)$	5.0	
	$\text{H}_2(g) + \text{I}_2(g) \rightarrow 2\text{HI}(g)$	5.0	
	$\text{N}_2(g) + \text{O}_2(g) \rightarrow 2\text{NO}(g)$	6.0	
	$\text{Br}_2(g) + \text{Cl}_2(g) \rightarrow 2\text{BrCl}(g)$	2.6	
	$\text{I}_2(g) + \text{Cl}_2(g) \rightarrow 2\text{ICl}(g)$	2.6	
	$\text{NO}(g) + \text{Cl}_2(g) \rightarrow \text{NOCl}(g) + \text{Cl}(g)$	-1.2	

* At fusion temperature.

** At normal boiling temperature.

*** Normalized to an increase of 1 gm-mole of gas in the reaction.

fusion transitions, all of which have a relatively large latent heat-of-fusion, the ΔS change, though small, is intermediate between these two cases.

From this analysis, it would appear that the only way to obtain a thermally reversible and large transition ΔH (by use of a thermally reversible chemical reaction) is to use a transition that produces gaseous molecules. Since space limitations prevent the use of this type of transition, it will be difficult to find any thermally reversible chemical reaction that is significantly better than the best of the fusion transition materials now available. This difficulty is best illustrated by the fact that no thermally reversible chemical reaction has yet been discovered (to our knowledge) that is competitive with the better fused-salt TES materials.

The difficulty is further illustrated by TES by liquid hydrocarbon fuels as used in current automobiles. Using n-hexane as representative of gasoline, the lower heating value (LHV) is 12.41 kwhrth/kg and 8.26 kwhrth/liter (as compared to 0.29 kwhrth/kg and 0.53 kwhrth/liter for the latent heat-of-fusion of LiF)—values which result in the excellent range of the current automobiles with a relatively small fuel tank and mass of fuel. However, the excellent TES storage capacity of liquid hydrocarbon fuels is due, in part, to the fact that one of the components, O_2 , is freely available from the atmosphere and does not have to be transported. Including the 3.53 kg of O_2 required per kg of fuel reduces the TES capacity to 2.74 kwhrth/kg. Thus, even for a highly-exothermic and in-situ irreversible chemical reaction, the gravimetric storage capacity for all reactants is only 9.4 times the latent heat-of-fusion of LiF as compared to a factor of 42.8 for the hydrocarbon mass alone.

Thus, the excellent storage capacity of liquid hydrocarbon fuels is due primarily to the fact that a major portion of this TES system does not have to be transported by the vehicle, and secondarily to the highly exothermic (and in situ irreversible) reaction.

In summary, the latent heat-of-fusion represents a highly competitive means of storing thermal energy when all materials must be solid or liquid and in-situ reversibility is required for recharging. Use of the sensible heat of the solid and/or liquid can add significantly to the storage capacity for the heat-of-fusion, where temperature variation in the heat-source temperature can be tolerated. Thus, the combination of latent heat-of-fusion/sensible heat has been selected as the best approach for thermal energy storage for automotive use.

2.3 SELECTED MATERIALS AND CHARACTERISTICS

2.3.1 Selection of Salts

Based on the specifications for the Stirling engine, the normal operating head temperature (outside tube wall maximum) is 1023°K (1381°F), and the maximum head temperature, which should not be exceeded, is 1123°K (1561°F). Because of the low strength of metallic materials at temperatures above 1150°K (1610°F), 1150°K has been assumed as an upper limit on the heat source temperature. Since it is highly desirable to operate the Stirling engine at its highest efficiency and highest temperature to maximize the vehicle range for a given TES capacity, and assuming an ~50°K temperature difference from the heat source to the Stirling engine heater head,

the optimum temperature range for the melting point of the TES material is:

$$1075^{\circ}\text{K} (1475^{\circ}\text{F}) \leq T_{\text{M. P.}} \leq 1150^{\circ}\text{K} (1610^{\circ}\text{F}).$$

In searching for TES media in this temperature range, reliance has been placed primarily on survey reports by Borucka¹, Eichelberger, J. L.², and Schröder³. In Table 2.2, a summary is given of the TES characteristics of single salts having latent heats-of-fusion ≥ 0.116 kwhrth/kg (100 cal/gm). For automotive propulsion, both the gravimetric and volumetric energy storage densities are very important. The gross vehicle mass has a strong effect on the energy economy of the vehicle, and the space is very restricted for incorporation of any energy system. From inspection of Table 2.2, LiH has by far the highest storage capacity per unit mass, and near the highest per unit volume. This is primarily the result of the very low molecular weight of this material rather than an unusually high entropy change on fusion. It also has a very high heat capacity for both the liquid and solid phases. However, LiH is very hazardous to handle due to its high flammability, and has an appreciable decomposition pressure of H₂ [H₂ pressure = 1 atm at 1223°K (1741°F)], which is difficult to contain because of the high diffusion rate of H₂ through most materials of construction at high temperature. LiH is not suitable for this application.

Once LiH is eliminated, it is apparent that the metal fluorides, in particular LiF, NaF, and MgF₂, have high latent heats-of-fusion on both a gravimetric and volumetric basis, as well as reasonably

TABLE 2.2
 THERMAL ENERGY STORAGE SINGLE SALTS WITH
 HEAT-OF-FUSION ≥ 0.116 kwhrth/kg (100 cal/gm)

Material	Melting Point (°K)	Latent Heat of Fusion		Heat Capacity at Melting Point (cal/gm-°K)		Density (gm/cm ³)	
		kwhrth/kg	kwhrth/L (Based on liquid density at melting point)	Solid	Liquid	Solid at 85°C	Liquid at Melting Point
LiOH	723	0.243	~0.28	0.731	0.866	1.46	~1.17
LiCl	887	0.130	0.196	0.331	0.355	2.07	1.50
LiH	962	0.790	0.46	1.89	1.87	0.82	0.58
MgCl ₂	981	0.126	0.211	0.221	0.231	2.32	1.68
Li ₂ CO ₃	996	0.168	0.308	0.533	0.549	2.11	1.83
NaCl	1074	0.133	0.209	0.262	0.274	2.17	1.56
LiF	1121	0.290	0.531	0.567	0.598	2.64	1.83
KF	1131	0.135	0.259	0.246	0.275	2.48	1.92
NaF	1269	0.219	0.428	0.364	0.391	2.56	1.95
MgF ₂	1536	0.259	0.630	0.33	0.363	3.00	2.43
CaCO ₃	1612	0.147	~0.41	0.388	-	2.93	-

high heat capacities. From a performance viewpoint, LiF is the preferred material, since it has a melting temperature of 1121°K (1558°F) (almost optimum for integration with a Stirling engine); it has the second highest gravimetric storage density (after LiH), 0.29 kwhrth/kg heat-of-fusion; it has the second highest volumetric storage density (after MgF₂), 0.53 kwhrth/liter heat-of-fusion; and has high solid/liquid heat capacities of 0.57 and 0.60 cal/gm-°K, respectively. However, lithium has a low abundance in the earth's crust and is relatively expensive, so that its use for automotive propulsion can be questioned from a viewpoint of both availability and cost. Eichelberger² has performed an evaluation of the potential cost of LiF, as well as the other fluoride salts of interest, with results as presented in Table 2.3. For a TES system with 300 kg of LiF, the LiF cost alone would amount to \$800 to \$1000, based on the estimated production cost range of Table 2.2. Both NaF and MgF₂ are considerably less expensive (lower by a factor of 4 to 25) and are made up of abundant and readily accessible elements.

In Table 2.4, a summary is given of the 45 most abundant elements in the earth's crust (Hurlich⁴). In Table 2.5, the concentration of elements present in seawater is given (McLellan⁵). Both Na and Mg have a high abundance in either the earth's crust or seawater. Fluorine is the 13th most abundant element in the earth's crust, with an average concentration of 625 ppm (0.0625% by weight); thus, its availability should not be a problem. Lithium has an average abundance in the earth's crust of 20 ppm and a negligible concentration in seawater (70 ppb). It is thus a relatively scarce element,

TABLE 2.3

22-478

MATERIAL COSTS, 1976 DOLLARS*

Material	Current Selling Price (\$/kg)	Estimated Production Cost Range** (\$/kg for 91,000 Metric Tons/Year)
LiF	5.38	2.58 - 3.27
NaF	0.74	0.11 - 0.58
MgF ₂	0.87-1.71	0.18 - 0.76

* Estimated by Eichelbarger.²

** Range due to different process assumptions relative to cost of the source of fluorine.

TABLE 2.4
THE 45 MOST ABUNDANT ELEMENTS IN THE EARTH'S CRUST

Relative Abundance	Element	Abundance, ppm/wt
1	Oxygen	466,000
2	Silicon	277,000
3	Aluminum	81,300
4	Iron	50,000
5	Calcium	36,300
6	Sodium	28,300
7	Potassium	25,900
8	Magnesium	20,900
9	Titanium	4,400
10	Hydrogen	1,400
11	Phosphorus	1,050
12	Manganese	950
13	Fluorine	625
14	Barium	425
15	Strontium	375
16	Sulfur	260
17	Carbon	200
18	Zirconium	165
19	Vanadium	135
20	Chlorine	130
21	Chromium	100
22	Rubidium	90
23	Nickel	75
24	Zinc	70
25	Cerium	60
26	Copper	55
27	Yttrium	33
28	Lanthanum	30
29	Neodymium	28
30	Cobalt	25
31	Scandium	22
32	Lithium	20
33	Columbium	20
34	Nitrogen	20
35	Gallium	15
36	Lead	13
37	Radium	13
38	Boron	10
39	Krypton	9.8
40	Praseodymium	8.2
41	Protoactinium	8.0
42	Thorium	7.2
43	Neon	7.0
44	Samarium	6.0
45	Gadolinium	5.4

TABLE 2.5

CONCENTRATION OF SOME ELEMENTS PRESENT IN SOLUTION
 IN SEAWATER

Element	Concentration gm/metric ton on parts per million
Cl	18980
Na	10561
Mg	1272
S (as Sulfate)	884
Ca	400
K	380
Br	65
C (as Bicarbonate)	28
Sr	13
B	4.6
F	1.4
SiO ₂	1.0
N (NO, NO ₂ , NH ₃)	1.0
Rb	0.20
Al	0.12
Li	0.07

but cannot be eliminated from consideration on this basis alone, since relative accessibility (that is: Has the element been concentrated by nature into ore deposits or is it uniformly spread through the earth's crust?) is also an important consideration. Copper and lead, for example, are produced at relatively low cost, even though their average abundance is 55 ppm and 13 ppm, respectively. Some evaluation of their availability for large-scale automotive use can be obtained by comparison of the amount required for large-scale automotive use with the current yearly production, identified reserve, and identified reserves considered economically recoverable by the year 2000, as summarized in Table 2.6⁶. The identified reserves in the U. S. and world are obviously insufficient to support complete turnover of automobiles to this system. Substantial implementation would be feasible, however, since with the U. S. reserves alone, subtracting the cumulative demand to the year 2000 leaves 643,000 metric tons of lithium — which, if totally committed to automotive propulsion, would provide 8,000,000 automobiles — a very substantial number.

In addition, the U. S. and world resources of any metal or mineral may be very much larger than the published data on reserves. Quoting from Hurlich⁴: "A considerable portion of the world's crust has yet to be thoroughly investigated for mineral deposits; many known deposits have not been quantitatively studied as to size, concentration, and total quantity of metals which may be extracted. Reserves of many metals may be expected to increase from year to year as more exhaustive surveys of mineral resources are made around the world". With a mean concentration of 20 ppm, the earth's crust to

TABLE 2.6
COMPARISON OF LI REQUIRED FOR LARGE-SCALE AUTOMOTIVE
USE TO ESTIMATED RESOURCE AND RECOVERABLE
RESOURCE POTENTIAL⁶

AMOUNT REQUIRED (MAXIMUM)

No. of Vehicles (U. S.)	100,000,000
Mass of Li Per Vehicle (300 kg LiF)	80.26 kg ₉
Total Li Mass	8.03 x 10 ⁹ kg
	8,030,000 metric tons

AVAILABILITY

U. S. Demand (Lithium Content)	
1970	2440 metric tons
1974	4120 metric tons
2000 (Average 5% Annual Rate of Increase)	13100 metric tons
1973 - 2000 Cumulative Demand	201,000 metric tons

Availability

Identified Reserves	
U. S.	298000 metric tons
World	677000 metric tons

Identified Reserves Considered Economically recoverable by 2000	
U. S.	546000 metric tons
World	1239000 metric tons

Total Identified Reserves	
U. S.	844000 metric tons
World	1916000 metric tons

a depth of 1 km (0.6 mile) contains $\sim 10^{13}$ metric tons of Li — a factor of 10^6 greater than that needed for 100,000,000 automobiles. While most of this is economically unrecoverable, it would appear highly likely that new resources will be uncovered when the need exists. With a current U. S. demand of 4120 metric tons, and identified reserves of 298,000 metric tons economically recoverable at present prices, there is obviously little incentive at present for extensive prospecting for new Li resources.

Because of its superior properties, LiF has been included in this study as one of the reference materials. Its availability is sufficient for significant automotive usage, particularly if the liquid hydrocarbon fuel/TES hybrid, as discussed in Chapter 7, is used — since this decreases the mass required per vehicle by a factor of ~ 10 .

Because of the questions on the price and availability of LiF, a second reference salt was selected, namely an eutectic mixture of NaF and MgF_2 . While mixtures containing LiF do exist and could be used, a significant contribution by LiF to the TES performance requires a substantial percentage of LiF in the salt ($\geq 30\%$). The potential problems of LiF because of cost and availability would thus be only alleviated and not eliminated. The decision was thus made that the second salt should have no LiF and should be made of materials about which there could be no question regarding availability and low cost. From Table 2.2, the materials with the best TES gravimetric and volumetric densities after LiF are NaF and MgF_2 ; but, their melting points are unacceptably high. However, a

eutectic mixture of these two salts exists with a melting point in the desired range for integration to the Stirling engine with TES properties as given in Table 2.7. The phase diagram of the 70 w/o NaF-30 w/o MgF_2 mixture which has a melting point of $1103^\circ K$ ($1525^\circ F$) is given in Figure 2.1. From Table 2.6, the latent heat-of-fusion of the eutectic is 0.18 kwhrth/kg and 0.39 kwhrth/liter, 62% and 74%, respectively, of the corresponding values for LiF. The heat capacity is 0.33(s) and 0.39(l) at the melting point - ~60% of the values for LiF. From Table 2.7, it is apparent that the eutectic mixture of NaF/ MgF_2 has a lower heat-of-fusion than the individual components. This can be interpreted as a result of the decrease in melting temperature by mixing the two components with approximately the same entropy change on fusion.

In summary, then, two alternative fluoride salts have been selected as reference materials with melting points in the desired range, pure LiF and the 70 w/o NaF-30 w/o MgF_2 eutectic. Lithium fluoride (LiF) is preferable from a performance viewpoint, but has questionable cost and availability for large scale automotive application. The NaF/ MgF_2 eutectic has gravimetric and volumetric storage densities in the range of 60 to 70% of that of LiF, but is inexpensive and has unquestioned availability for large-scale application.

2.3.2 Properties of Selected Salts

2.3.2.1 Enthalpy and Storage Capacity

The enthalpy is presented as a function of temperature in Figure

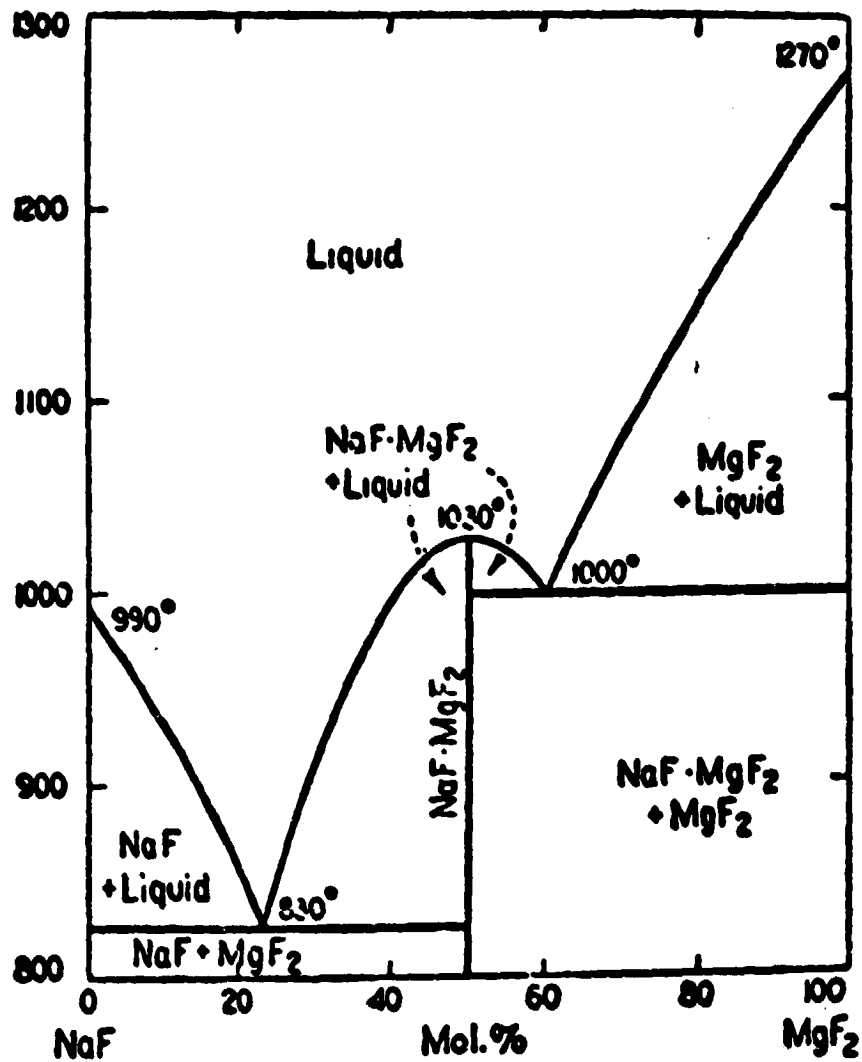
TABLE 2.7

23-478

SELECTED TES MATERIALS WITH MELTING POINTS
GREATER THAN 1023°K

Material	Temperature (°K)	ΔH_f		C_p at Melting Point (cal/g-°C)
		$\frac{\text{kWhrth}}{\text{kg}}$	$\frac{\text{kWhrth}^*}{\text{liter}}$	
LiF	1115	0.29	0.53	0.57(s);0.59(l)
NaF	1261	0.22	0.43	0.37(s);0.40(l)
MgF ₂	1543	0.26	0.63	0.33(s);0.36(l)
70 w/o NaF - 30 w/o MgF ₂	1103	0.18	0.39	0.32(s);0.39(l)

*Based on liquid density at melting point.

NaF-MgF₂Figure 2.1 Phase Diagram for NaF-MgF₂

A-3019

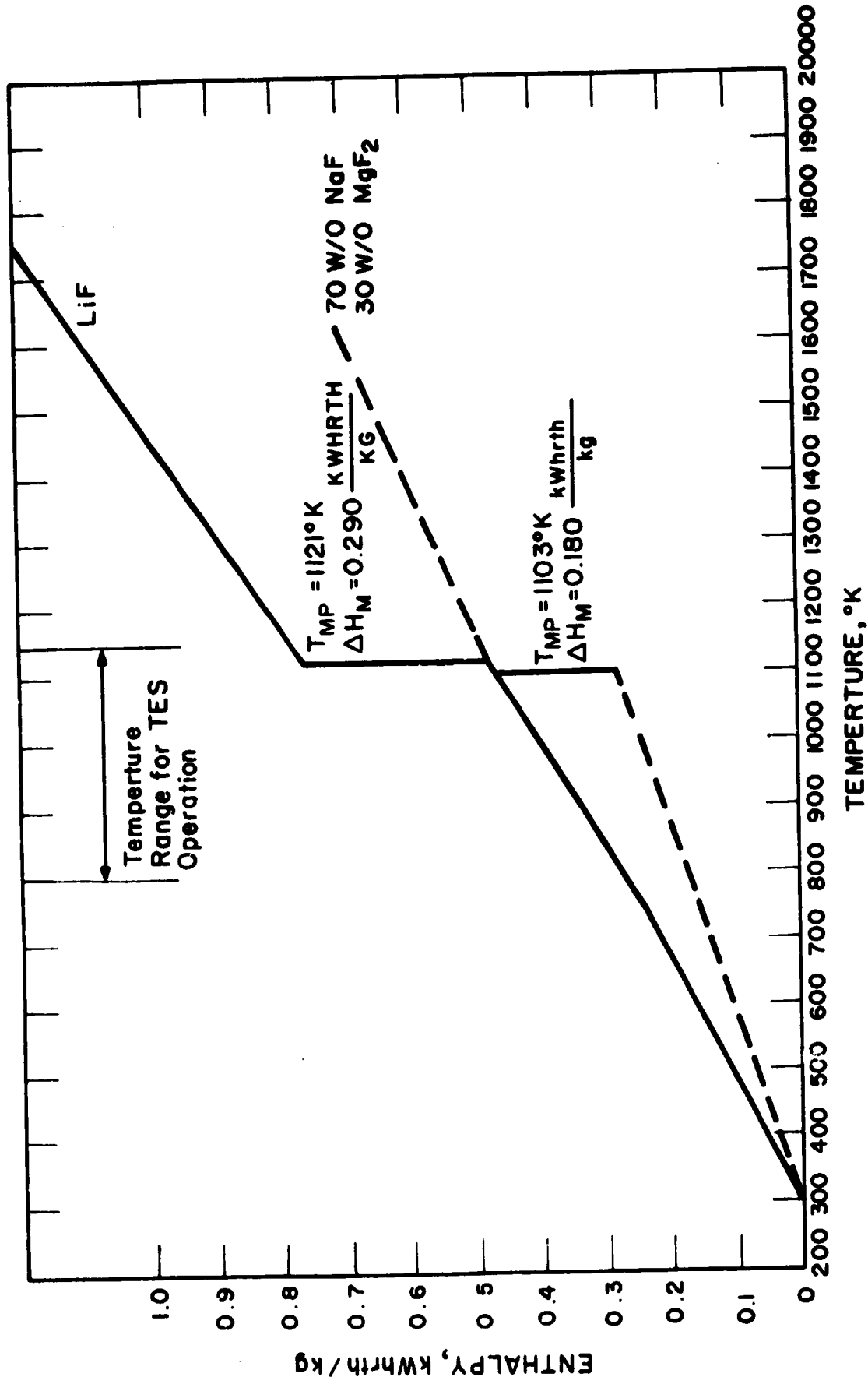


Figure 2.2 Enthalpy vs Temperature for LiF and NaF/MgF₂ Eutectic

2.2 for LiF and the 70 w/o NaF-30 W/o MgF₂ eutectic. The LiF curve is based on the Janaf tables⁷. For the NaF/MgF₂ eutectic, the heat-of-fusion reported by Schroder³ and used by Eichelberger² was used, namely 0.180 kwhrth/kg (155 cal/gm). The enthalpy change of the solid and liquid for the eutectic was based on the weighted average of the values for the solid and liquid phases of the pure components, NaF and MgF₂, again using the Janaf tables.

The LiF enthalpy should be quite accurate. For the eutectic, the heat-of-fusion is based on only one source; however, the value reported is considerably below the well-established values for each of the pure components, and application of Kirchhoff's method for estimating the value for mixtures^{8,14} resulted in a substantially higher value (16%) than that reported by Schroder³. Thus, the heat-of-fusion of the eutectic would not be expected to be lower than the quoted value of 0.18 kwhrth/kg. The solid/liquid heat capacities calculated from the pure components should be accurate.

For performance evaluation, the temperature range over which the TES system operates is taken as 800°K to 1150°K. Below the somewhat arbitrary limit of 800°K (980°F), the Stirling engine power and efficiency are reduced to unacceptable levels. As discussed earlier, 1150°K (1610°F) represents the upper limit based on material strength considerations. In Table 2.8, the energy storage capacity is given for each salt, based on these limits. The importance of the sensible heat in maximizing the TES capacity is apparent, representing an increase of 76% for LiF and 72% for the NaF/MgF₂ eutectic above the heat-of-fusion.

TABLE 2.8

THERMAL ENERGY STORAGE DENSITY
OVER TEMPERATURE RANGE OF 800°K TO 1150°K

LIF

Solid, 800°K → 1121°K	0.20	Kwhrth/kg
Heat of Fusion	0.29	
Liquid, 1121°K → 1150°K	<u>0.02</u>	
Total	0.51	Kwhrth/kg (0.92kwhrth/L)*

70 W/O NaF - 30 W/O MgF₂ Eutectic

Solid, 800°K → 1103°K	0.11	Kwhrth/kg
Heat of Fusion	0.18	
Liquid, 1103°K → 1150°K	<u>0.02</u>	
Total	0.31	Kwhrth/kg (0.68 kwhrth/L)*

* Based on liquid density at melting point

2.3.2.2 Density

The density variation is important in assuring sufficient volume for the salt at its maximum temperature and in designing for the volume change which occurs during melting. Values for the two salts are summarized in Table 2.9^{1,3}. The liquid density variation from the melting point to 1150°K is small enough to be neglected.

2.3.2.3 Vapor Pressure

The vapor pressure of LiF liquid at the maximum operating temperature of 1150°K is 0.048 mm Hg. The vapor pressure of the eutectic mixture has not been measured, but can be estimated from the vapor pressure of the pure components. At 1150°K, the vapor pressure of MgF₂ is 2.8×10^{-5} mm Hg, and that of NaF is 0.030 mm Hg, based on extrapolation of the liquid vapor pressures. Thus, the vapor pressure of the eutectic should be primarily determined by the NaF component which, with a mole fraction ratio of 77.4% NaF, corresponds to a vapor pressure of approximately 0.02 mm Hg.

The vapor pressure decreases rapidly with temperature for all components. Thus, at the minimum storage temperature of 800°K, the vapor pressure of NaF is 9.9×10^{-8} mm Hg.

The vapor pressures given above are based on relations from Barin and Knacke⁹.

2.3.2.4 Thermal Conductivity and Diffusivity

Since heat must be transferred from the solid salt to the heat

A-2961

TABLE 2. 9
DENSITY VARIATION OF REFERENCE SALTS

Salt	Density, gm/cm ³ (kg/liter)			% Increase in Volume	
	25° C	Solid at Melting Point	Liquid at Melting Point	25° C to Liquid at Melting Point	At Melting Point
LiF	2.64	2.34	1.81	44.0	29.4
70 w/o NaF 30 w/o MgF ₂	2.94	2.69	2.19	34.2	22.8

transport media with an acceptable ΔT , the thermal conductivity of the salt (and thermal diffusivity) is an important property in the system design. Generally, conduction through the solid state is the controlling thermal resistance in the removal of thermal energy from the salt, since natural convection assists the heat transfer once the salt is molten.

The thermal conductivity of LiF is well established. In Figure 2.3, the thermal diffusivity and thermal conductivity of solid and liquid LiF are presented, as measured by Chang, et al¹⁰ and Sreenivasan, et al¹¹. In the temperature range of 800°K to 1150°K, average design values are:

Thermal Conductivity

Solid LiF	0.059 watt/cm°K (3.4 Btu/hr-ft-°F)
Liquid LiF	0.019 watt/cm°K (1.1 Btu/hr-ft-°F)

Thermal Diffusivity

Solid LiF	0.0105 cm ² /sec (0.0407 ft ² /hr)
Liquid LiF	0.0042 cm ² /sec (0.0162 ft ² /hr)

For the NaF/MgF₂ eutectic Maru⁸, reports the thermal conductivity at the melting point to be in the range of 2.4 to 4.8 Btu/hr-°F-ft for the solid and 2.69 Btu/hr-°F-ft for the liquid, with reference to work reported by Philips. These values are consistent with thermal conductivity values for MgF₂ as well as other fluoride salts for which detailed measurements are available. Reasonable design values are thus:

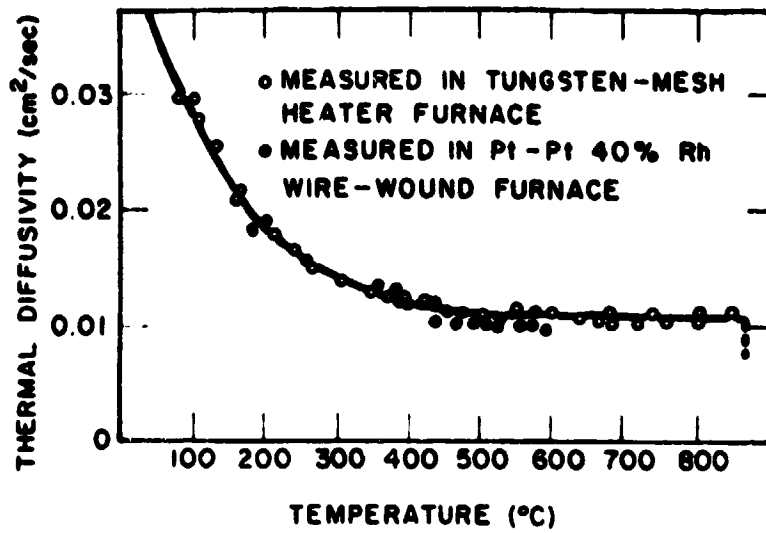


Figure 2.3a Thermal Diffusivity of Solid Lithium Fluoride (LiF)

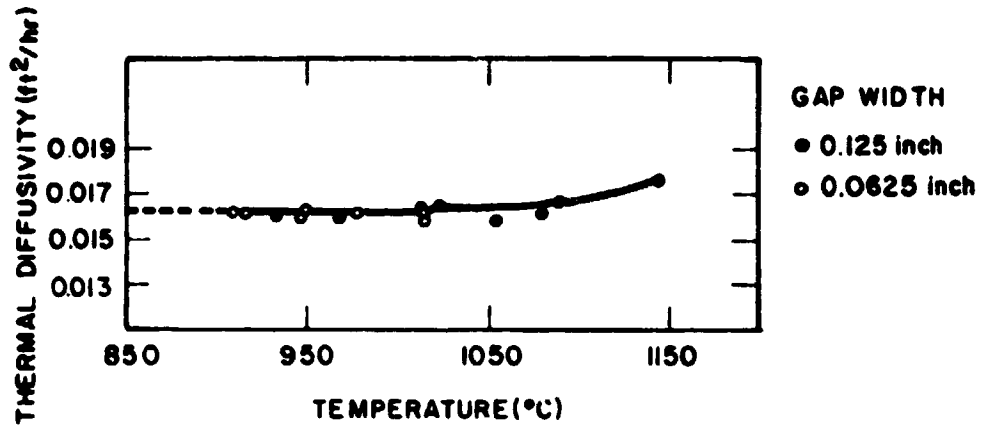


Figure 2.3b Thermal Diffusivity of Liquid Lithium Fluoride

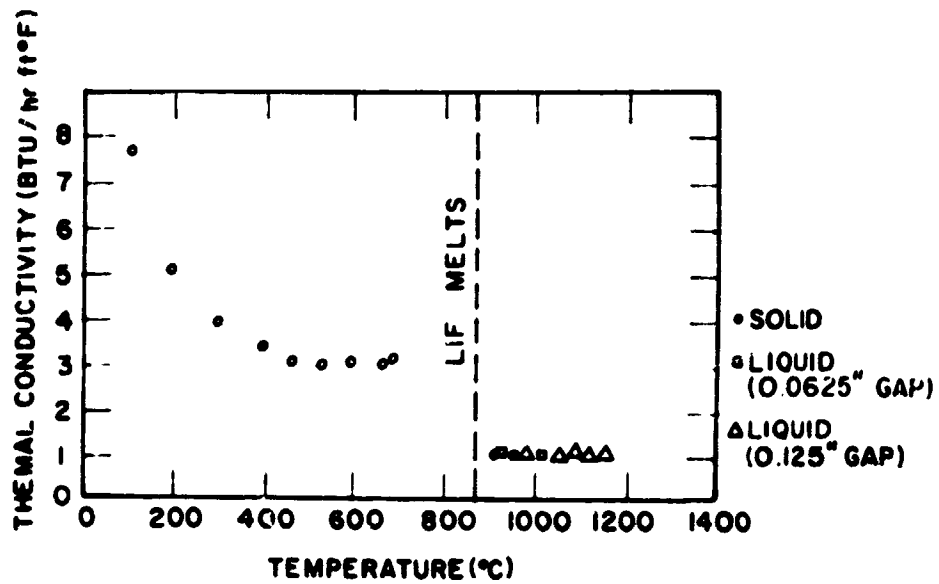


Figure 2.3c Thermal Conductivity of Lithium Fluoride

Thermal Conductivity

Solid Eutectic 0.059 watt/cm-°K (3.4 Btu/hr-ft-°F)

Liquid Eutectic 0.047 watt/cm-°K (2.7 Btu/hr-ft-°F)

Thermal Diffusivity

Solid Eutectic 0.016 cm²/sec (0.063 ft²/hr)

Liquid Eutectic 0.013 cm²/sec (0.051 ft²/hr)

It should be noted that even though the thermal transfer properties of the NaF/MgF₂ eutectic are not well known, the system design requires transfer through relatively thin salt layers, with a large surface area and resulting small ΔT's. Thus, the thermal conductivity and diffusivity are not crucial factors in the system performance, and large variations could be tolerated without seriously affecting the design or performance.

2.3.2.5 Thermal and Chemical Stability

All three of the fluorides of interest, LiF, NaF, and MgF₂ are extremely stable compounds that are unreactive with conventional materials-of-construction, water, or air. Because of this high chemical stability, these metal fluorides show little corrosive action on alloy steels and other high temperature alloys at temperatures to 1150°K. Asselman¹² demonstrated that technical grade LiF, when purified for the removal of hydrogen fluoride, water, and oxygen, is noncorrosive to Inconel 600 capsules as used in his demonstration unit. Asselman, as well as Schröder³ indicated that adding a small quantity of aluminum to the fluoride salt permits use of technical grade LiF as well as other fluoride salts without the slightest corrosion of

AISI 321 stainless steel after prolonged heating at 1123°K (1561°F). In a more pertinent series of tests, Beam¹³ performed an experimental evaluation of the compatibility of several eutectic fluorides with the specific material selected for the high temperature parts of the TES system, Inconel 617. Eleven different capsules were fabricated and filled with the following eutectics: LiF/MgF₂, LiF/MgF₂/NaF, and LiF/MgF₂/KF. From the initial 2000 hours of testing at temperatures of about 950°K to 1000°K, no significant corrosion of the Inconel 617 was observed, with the eutectic temperatures remaining stable. The testing was to be continued to a 10,000-hour test.

In a separate evaluation by Bramlette¹⁴, it was concluded: "Turning now to chemical properties of molten fluoride eutectics, it has been conclusively demonstrated that these mixtures are stable for many years up to 1023°K if maintained under an inert gas atmosphere. Suitable containment materials are Hastelloy N, titanium-modified Hastelloy N, and Inconel".

While additional experimental work on corrosion rates is required, this prior work establishes a high degree of confidence that Inconel 617 should be suitable for this TES system with negligible corrosion rates, particularly if a small quantity of aluminum is added to the salt to act as a corrosion inhibitor.

2.3.2.6 Other

While the liquid viscosity is unimportant since the salt is contained in sealed capsules, Eichelberger² reports the viscosity for many fluoride salts. He concludes: "In general, the fluorides are

highly fluid, with viscosities on the order of 1.7 to 15 centipoise at the melting point and decreasing as temperature is increased". While not important in the TES system operation, this low viscosity could be important in filling of the system during manufacture.

An additional consideration is the possibility of supercooling of the fluoride salt. Again quoting from Eichelberger: "Metal fluoride salts apparently do not have this problem (supercooling). . . . Reports of work on metal fluorides performed at Oak Ridge and Philips Laboratories state that supercooling is not evident".

REFERENCES FOR CHAPTER 2

1. Borucka, A., "Survey and Selection of Inorganic Salts for Application to Thermal Energy Storage", Report to U. S. Energy Research & Development, Administration Report No. ERDA-59, Borucka Research Company, Livingston, New Jersey, June, 1975.
2. Eichelberger, J. L., "Investigation of Metal Fluoride Thermal Energy Storage Materials: Availability, Cost, and Chemistry", Report to U. S. Energy Research & Development Administration, Report No. C00-2990-6, Pennwalt Corporation, King of Prussia, Pennsylvania, December, 1976.
3. Schroder, J., "Thermal Energy Storage and Control", ASME Paper No. 74-WA/OcT-1, ASME Annual Meeting, November 17-22, 1974.
4. Hurlich, "Planet Earth's Metal Resources", Metal Progress, 112, No. 5, October, 1977, pp. H1 - H16.
5. McLellan, H. J., Elements of Physical Oceanography, Pergamon Press, New York, 1965.
6. Mineral Facts and Problems, 1975 Edition, Bureau of Mines Bulletin 667, U. S. Department of the Interior, 1976.
7. Stull, D. R., and Prophet, H., "Janaf Thermochemical Tables," Second Edition, Report No. NSRDS-NBS 37, United States Department of Commerce, June, 1971.
8. Maru, H. C., et al, "Molten Salt Thermal Energy Storage Systems: Salt Selection", Report No. C00-2888-1, Institute of Gas Technology, Chicago, Ill., August, 1976.

REFERENCES FOR CHAPTER 2 (Cont'd)

9. Barin I., and Knacke, O., "Thermochemical Properties of Inorganic Substances," Springer-Verlag, Berlin/Heidelberg/New York, 1973.
10. Chang, H., et al, "The Determination of Thermal Diffusivities of Thermal Energy Storage Materials, Part I: Solids Up to Melting Point," ASME Paper No. 66-WA/Ener-5, presented at Winter Annual Meeting, New York, N. Y., November 27 — December 1, 1966.
11. Sreenivasan, K., and Altman, M., "The Determination of Thermal Diffusivities of Thermal Energy Storage Materials, Part II: Molten Salts Beyond the Melting Point," ASME Paper No. 68-WA-Ener-5, presented at ASME Winter Annual Meeting, New York, N. Y., December 1-5, 1968.
12. Asselman, G. A. A., "Thermal Energy Storage Unit Based on Lithium Fluoride," Energy Conversion, 16, pp. 35-47, Pergamon Press, 1976.
13. Beam, J. E., "Evaluation of Eutectic Fluoride Thermal Energy Storage Unit Compatibility: Part II - Test Procedures and Post-Test Evaluation Results," Report No. AFAPL-TR-75-92, Part II, Air Force Aero - Propulsion Laboratory, Wright-Patterson AFB, March 1977.
14. Bromlette, T. T., et al., "Survey of High Temperature Thermal Energy Storage," Report No. SAND75-8063, Sandia Laboratories, March 1976.
15. Dasent, W. E., Inorganic Energetics, Penguin Books, Baltimore, 1970.

3. CONCEPTUAL APPROACH AND MODES OF OPERATION

3.1 INTRODUCTION

The operational requirements of an automotive TES/Stirling engine system are severe:

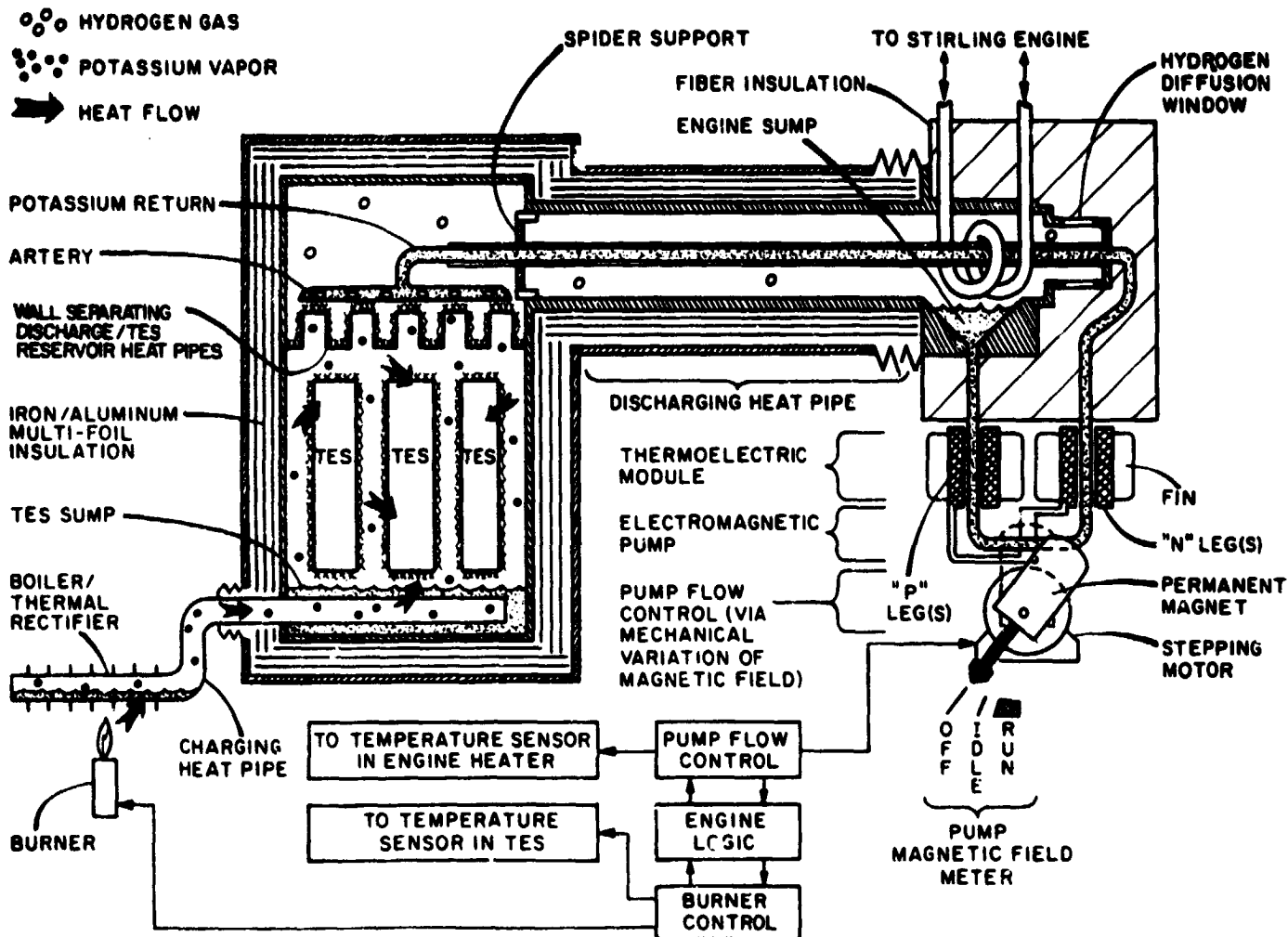
- Heat Transfer from TES Media to Stirling Engine Heater Head at High Temperature during Vehicle Operation
 - Normal engine heater head temperature of 1023° K
 - Small ΔT from TES media to engine heater head
 - Variable heat delivery rate from 2 kwth to 200 kwth
 - Very rapid transient response
 - 2 kwth to 200 kwth in $\leq 2-1/2$ sec
 - 200 kwth to 2kwth w/o exceeding heater head temperature of 1123° K
 - Temperature control to prevent exceeding head temperature of 1123° K
 - Separate location of TES/engine with small connecting line for heat transport
 - Rapid startup of engine from cold or standby condition
- Minimal Heat Losses for High Energy Efficiency
 - Highly effective insulation on TES Reservoir
 - For automotive application, volume and weight of insulation reduced to absolute minimum

- With engine shutdown, very low heat transfer rate to engine
- Recharging from External (to Vehicle) Combustion Heat Source
 - Heat exchanger external to vehicle structure required with means of conveying thermal energy to TES media
 - Heat losses through recharging heat exchanger very low when not in use
- Dual Mode Operation (As Described in Section 3.4).
 - Operation from TES alone
 - Operation from on-board liquid hydrocarbon fuel
 - Use of TES for peak thermal requirements when operating on hydrocarbon fuel, permitting relatively steady combustion (thermal flywheel)
 - Minimum inventory of high temperature heat transport fluid from safety viewpoint
 - High reliability — no seals, no moving parts

After considerable and iterative evaluation of alternative approaches, a concept evolved which meets all of these operational requirements. It is remarkable that such a wide variety of operations can be accomplished in a relatively simple system with no moving parts. In this chapter, the concept and its operational modes are described in qualitative fashion to serve as a basis for the detailed evaluation and design presented in succeeding chapters of this report.

The system concept and its modes of operation are described schematically in Figures 3.1 through 3.6. All heat transport operations are accomplished by means of potassium heat pipes. Three separate, but coupled, heat pipes are used in a specific manner to decouple the charging/discharging modes of operation and to provide the required operational flexibility. In addition, heat pipes are well adapted to coupling low heat flux surfaces to high heat flux surfaces, and vice versa. One heat pipe is used for recharging, the second for transfer of heat into and out of the TES media, and the third for discharging or transport of the thermal energy from the TES reservoir to the Stirling engine heater head. For control purposes, and to decrease the connecting-pipe size by permitting a higher ΔP along the heat pipe than is feasible with capillary pumping, this latter discharging heat pipe uses an electromagnetic pump to return the condensed potassium. Power is supplied to the E-M pump by a small thermoelectric generator operating on heat extracted from the pumped potassium liquid. This E-M pump provides a means for conveniently regulating the potassium flow, and hence heat transport rate, to the Stirling engine heater head by means of a permanent magnet rotated to vary the magnetic field. If no potassium is pumped to the wall supporting the discharge/TES reservoir heat pipes, no heat transport to the Stirling engine heater occurs. It should be noted that the wall separating the discharge/TES reservoir heat pipes (illustrated schematically in Figures 3.1 through 3.5) is formed by multiple tubes in the detailed designs presented in Chapter 6 for both the rectangular and cylindrical configurations; heat transfer considerations are presented in Chapter 4, and the E-M pump design is presented in Chapter 7.

To provide for very low heat losses with minimum volume and weight, high performance Multi-Foil insulation is used. Multi-Foil



1 TES CHARGING DURING NONOPERATION. BURNER ON; PUMP CONTROL SET AT OFF.

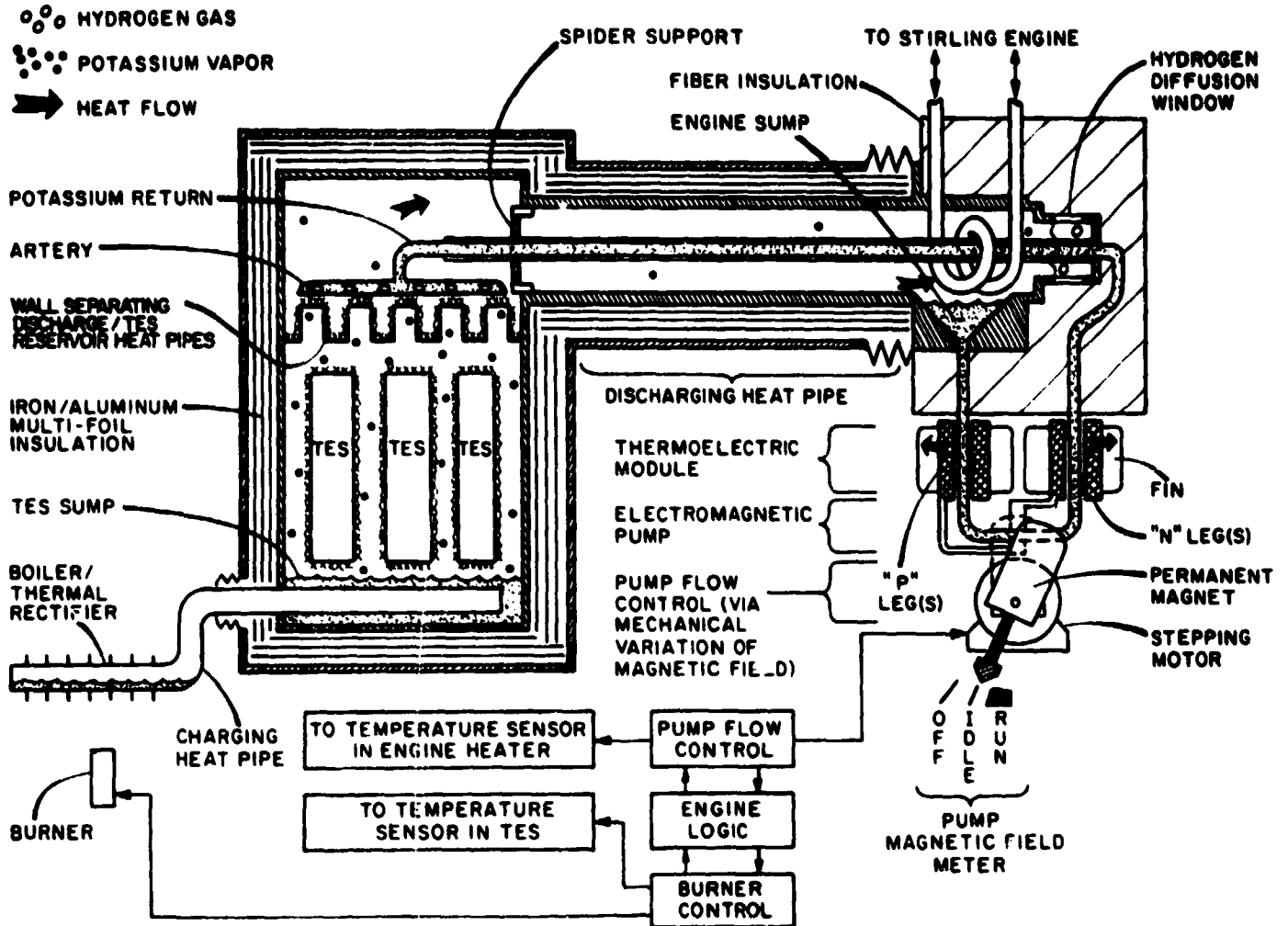
The potassium in the boiler is vaporized by combustion heat and condenses in the charging heat pipe section located in the TES sump. The condensed potassium returns by gravity to the boiler.

The charging heat pipe vaporizes potassium in the TES sump which condenses and transfers boiler heat into the TES material and walls. The condensed potassium returns by gravity to the TES sump.

Heat is not supplied to the engine head since the pump flow control has rotated the stepping motor to the off position so that the magnetic field is not perpendicular to the thermocouple current flow (consequently there is no "E x H" force to circulate the potassium in the electromagnetic pump circuit).

NOTE: Auxiliary electric heaters powered from the vehicle battery will be used to maintain or raise the potassium line temperature above the melting point of potassium.

Figure 3.1 TES Charging During Nonoperation



4. SHORT PERIOD OF NONOPERATION (with charged TES). BURNER OFF. PUMP CONTROL SET AT IDLE.

If the vehicle is not expected to be used for short periods (e. g., order of an hour), the pump control will be set on idle. This location will position the magnet (via the stepping motor) so that: (1) the heat loss from the system will be reduced, and (2) the heat leakage to the engine will maintain the engine at near operating temperature so that the vehicle can start relatively quickly.

Note that with the pump control in the idle position, a "trickle" flow of potassium is maintained to keep the engine heater at an intermediate temperature somewhat below the usual operating temperature.

Figure 3.3 Short Period of Nonoperation (with charged TES)

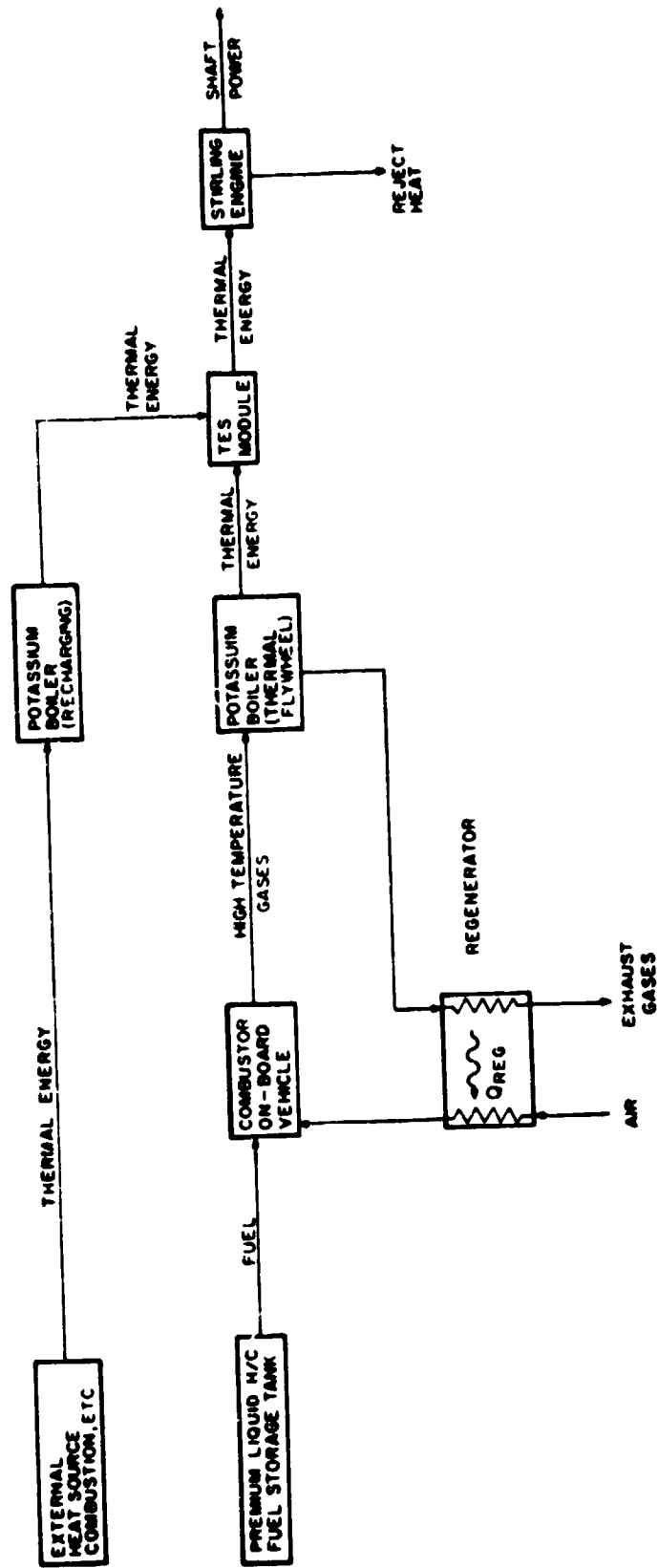


Figure 3.6 Schematic of Dual-Mode TES/Liquid HC Fuel Vehicular Propulsion System Utilizing Stirling Engine

denotes a high temperature thermal insulation system developed by Thermo Electron Corporation in which thin metal foils (90 in this case) are spaced in a vacuum by oxide particles. The vacuum and oxide particles eliminate conduction losses, and the foils serve as multiple radiation shields so that a 1/2 inch insulation thickness results in very low heat losses from the high temperature parts of the system. This insulation and its characteristics are described in detail in Chapter 5. The Multi-Foil is used to insulate the TES reservoir and the primary heat transport line to the Stirling engine. Conventional fiber insulation (e. g., Fiberfrax or Min-K is used to insulate the heater head of the Stirling engine for ease in maintenance of the engine.

Use of the vacuum insulation does introduce difficult structural problems in design of the TES reservoir, and a major portion of the reservoir design effort was concentrated on development of a practical means of structurally supporting this vacuum with minimum structural weight. The TES reservoir structural designs for rectangular and cylindrical envelopes are given in Chapter 6.

3.2 DESCRIPTION OF OPERATION

The means of charging the TES system is illustrated schematically in Figure 3.1. Thermal energy is added to the system by means of the charging heat pipe. The charging heat pipe functions as a thermal rectifier which transfers heat in one direction only. Thus, when the burner is "ON", heat is transferred by vaporization of potassium vapor in the boiler section heated by the burner. The

vapor flows to the condensing section, which is located in the TES reservoir sump and is surrounded by liquid potassium in the TES reservoir heat pipe. The vapor in the charging heat pipe is condensed, transferring heat to the boiling potassium in the TES heat pipe. The condensed liquid drains by gravity back to the boiler section. Rectification is obtained by use of this gravity return of the potassium to the boiler section, rather than by capillary return as in a conventional heat pipe. Thus, if the TES reservoir is at a higher temperature than the boiler section of the charging heat pipe, no condensation or heat transfer occurs, and the K inventory is collected in the burner section. In other words, with gravity return of the condensed K, reverse vapor-condensation is impossible, eliminating heat loss by this mechanism from the TES reservoir via the recharging heat pipe. Conduction heat losses are minimized by use of an extended length of thin-wall tubing in the charging heat pipe and by use of low thermal-conductivity metal in the adiabatic section connecting the boiler/condenser sections of the heat pipe.

In the reservoir, the charging heat pipe is immersed in a sump into which the liquid potassium in the TES reservoir heat pipe collects. The sump is configured to minimize the inventory of potassium in the TES reservoir required to assure that the charge heat pipe in the reservoir is immersed in, and wet with, potassium liquid during charging. During charging, heat transfer from the charging heat pipe results in boiling of the potassium in the reservoir containing the TES salt capsules. This vapor condenses on any cold surfaces, transferring heat to these surfaces and heating/melting the salt media, with the liquid potassium draining back to the sump. In other words, the TES reservoir operates isothermally with uniform recharging of the TES media.

During recharging, heat transfer from the TES reservoir to the Stirling engine by the discharging heat pipe does not take place, since no liquid potassium is pumped to the wall separating the discharge/TES reservoir, and no vapor is generated (the permanent magnet is rotated out of the E-M pump so that no magnetic field exists and no pumping occurs).

The charging concept thus meets the functional objectives of no heat loss by vapor transport through the charging system when not charging, no heat loss by vapor transport to the Stirling engine during charging, minimum potassium inventory in the charging/reservoir heat pipes, uniform heating of the TES salt containers, and no moving parts. It does require that the boiling section of the charging heat pipe be located at a lower level than the TES reservoir during recharging, and, to minimize the K inventory in the TES reservoir, that the vehicle be level during recharging so that the liquid potassium can be constrained to flow to the sump in the reservoir. These restrictions can be satisfied in a practical vehicle. There will be a small heat transport rate from the hot TES reservoir to the cold Stirling engine by thermal radiation and conduction.

With a charged TES system, normal operation of the vehicle is as illustrated in Figure 3.2. The permanent magnet is rotated into the E-M pump, producing a magnetic field and resulting in pumping of liquid potassium in the discharge heat pipe. This pumped potassium is distributed onto the wall separating the discharge heat pipe and the TES reservoir heat pipe. Provided the Stirling engine heater head is at a lower temperature

than the TES media, boiling of this pumped potassium occurs with vapor flow down the discharge heat pipe and condensation on the Stirling engine heater tubes. Temperature of the engine heater is controlled by modulation of the pumping rate in the discharge heat pipe via rotation of the permanent magnet, to regulate the magnetic field. Thus, the normal operating temperature of the heater head, 1023°K, can be obtained under all-load conditions (i. e., small or large TES/engine head ΔT), even though the TES media has a maximum charged-temperature of 1150°K and melting point of 1121°K or 1103°K, depending on the salt used.

Within the TES reservoir itself, boiling of potassium on the wall separating the discharge/TES reservoir heat pipes removes heat from the wall with a reduction in the wall temperature. Vapor in the TES reservoir heat pipe immediately condenses on the TES reservoir side of the wall to liquid potassium. This liquid drains or drips into the salt capsules, where it vaporizes with extraction of heat from the salt; this condensation/vaporization cycle continues until the pressure in the reservoir heat pipe equals the vapor pressure of K at the TES media temperature. The salt capsules have their surface textured to assist in distribution of the dripping K liquid over the capsule surfaces. Also, the bottoms of some of the capsules are immersed in the liquid potassium in the reservoir sump to provide potassium vapor and to ensure isothermal conditions in the reservoir, including the sump; the slight capillarity on the salt capsule surfaces assists in this function and ensures sufficient heat transfer from the capsules to the liquid in the sump to maintain its temperature at the salt temperature.

During short periods of nonoperation with a charged TES, it may be desirable to maintain the engine head at an intermediate temperature between ambient and the normal operating temperature. This would minimize heat losses through the engine while still providing instantaneous startup of the vehicle. This function can be easily accomplished, as illustrated in Figure 3.3, by switching the control to an idle position which changes the set point of the engine temperature control to a lower temperature. The system then functions as in normal operation to maintain this new temperature. For long periods of nonoperation with a charged TES, the permanent magnet is simply moved from the E-M pump, preventing any K pumping and any heat transfer (except by radiation) from the high temperature TES media to the low temperature engine head. A longer startup is required, since the engine head must be heated from a cold condition instead of an intermediate temperature. Startup time should be no more than that required for the combustion-heated Stirling engine.

The operational concepts as described above meet the important functional requirements of minimal heat loss to the engine during long periods of nonoperation, absolute control on the engine head temperature, rapid transit response both in turndown and turnup, no moving parts (except for the permanent magnet), and minimum inventory of potassium. In addition, as will be described in Chapter 4, the discharge heat pipe diameter to carry 200 kwth from the TES reservoir to the engine at the minimum heat source temperature of 800°K is only 10 cm (3.94 in), with a 25°C ΔT from the TES salt to the engine heater (outer tube wall).

3.3 DUAL-MODE SYSTEM

As discussed in Chapter 9, the dual mode of operation, in which the Stirling engine can be operated from stored thermal energy for short duration trips or from liquid hydrocarbon fuels for long duration trips, provides an attractive alternative to the TES-only vehicle. This method can provide (1) a vehicle with the convenience of current automobiles and (2) substantial savings of premium liquid hydrocarbon fuels by use of TES via an external heat source for short-duration trips. In addition, the TES can be used to provide peak thermal energy requirements, so that the combustion system can operate at approximately steady-state; a resultant reduction in emission levels can be expected relative to the direct-fired Stirling engine where the combustor must track the highly transient engine power demand. It is much easier to achieve low emissions with steady-state combustion than in highly-transient combustion, particularly where a turndown of ~20:1 is required. In other words, the TES would function as a thermal "flywheel."

The functional operation as a dual mode system is illustrated schematically in Figure 3.5, and in terms of a block diagram in Figure 3.6. For dual-mode operation, the TES size would be reduced to about one-tenth of the size required for TES-only operation, since the TES by itself would be used only for short trips. In addition to the external charging combustor and its associated heat-pipe, a second combustor/heat pipe system would be operated in parallel to that for the external heat source, using liquid hydrocarbon fuel carried on the vehicle. The external charging system would be

operated exactly as on the TES-only system, with overnight recharging from an external heat source. The on-board unit would function in a similar manner — with fuel tank, combustor, and a second charging heat exchanger carried on board. The boiler section of this heat pipe would be located below the TES reservoir, with gravity return of condensed potassium to eliminate heat losses when the on-board combustor was not in operation in an analogous fashion to that described earlier.

For dual-mode operation as illustrated in Figures 3.5 and 3.6, the TES reservoir is located in series between the on-board combustor and the Stirling engine. It is thus necessary that the TES module be at least partially charged and at a sufficiently high temperature for proper operation of the Stirling engine ($> 800^{\circ}\text{K}$), since the heat input to the engine is always taken from the TES reservoir. This disadvantage is alleviated because of the small storage capacity (~ 10 percent) of the TES reservoir relative to the TES-only vehicle and the increased thermal charging rate possible with the on-board combustor. Thus, even with a cold and uncharged TES reservoir, the startup time will be relatively small (a matter of minutes). Normally, the TES reservoir would be maintained either charged or partially charged so that instant operation of the vehicle is possible. It would be desirable, of course, to be able to bypass the TES reservoir, with the on-board combustor directly heating the Stirling engine via a heat-pipe. Such an approach would greatly complicate the system and the extra complication was not felt warranted, relative to the inconvenience of delayed startup only when the TES reservoir is cold.

3.4 METHOD OF RECHARGING FROM EXTERNAL COMBUSTION SOURCE

An external burner producing combustion gases with a temperature of at least 2000°F is required. These gases must be ducted to the vehicle and passed through the evaporator section of the recharging heat pipe as described earlier. The gases leaving, still at a high temperature considerably in excess of 1600° F, must then be ducted back to the furnace and passed through a recuperator for an efficient utilization of the combustion energy. The exhaust gases, which are at a low temperature, are then ducted to a stack or chimney. The combustor must also be connected to the fuel source, either gas or liquid, with a burner suited to the fuel. As a final note, the recharging must be safely accomplished.

Such a system can obviously be operated by trained engineers/technicians on prototype vehicles. The question of whether it can be operated by the normal layman must be considered. Although a definitive answer requires design and evaluation, the following discussion describes, in qualitative terms, one technique that appears feasible. It is based on the supposition that the recharging system must be as convenient to operate as a central home-heating system, i. e., completely automatic.

For overnight recharging (50,000 Btu/hr transfer rate to the TES system), two recharging heat pipes are used, each with a finned evaporator having a tube O. D. of 1 inch, a length of 12 inches, and a fin/tube area ratio of 3. One possible method of recharging is illustrated in Figure 3.7. The two finned tubes are located beneath the car in an insulated cavity as illustrated. The cavity matches with a special

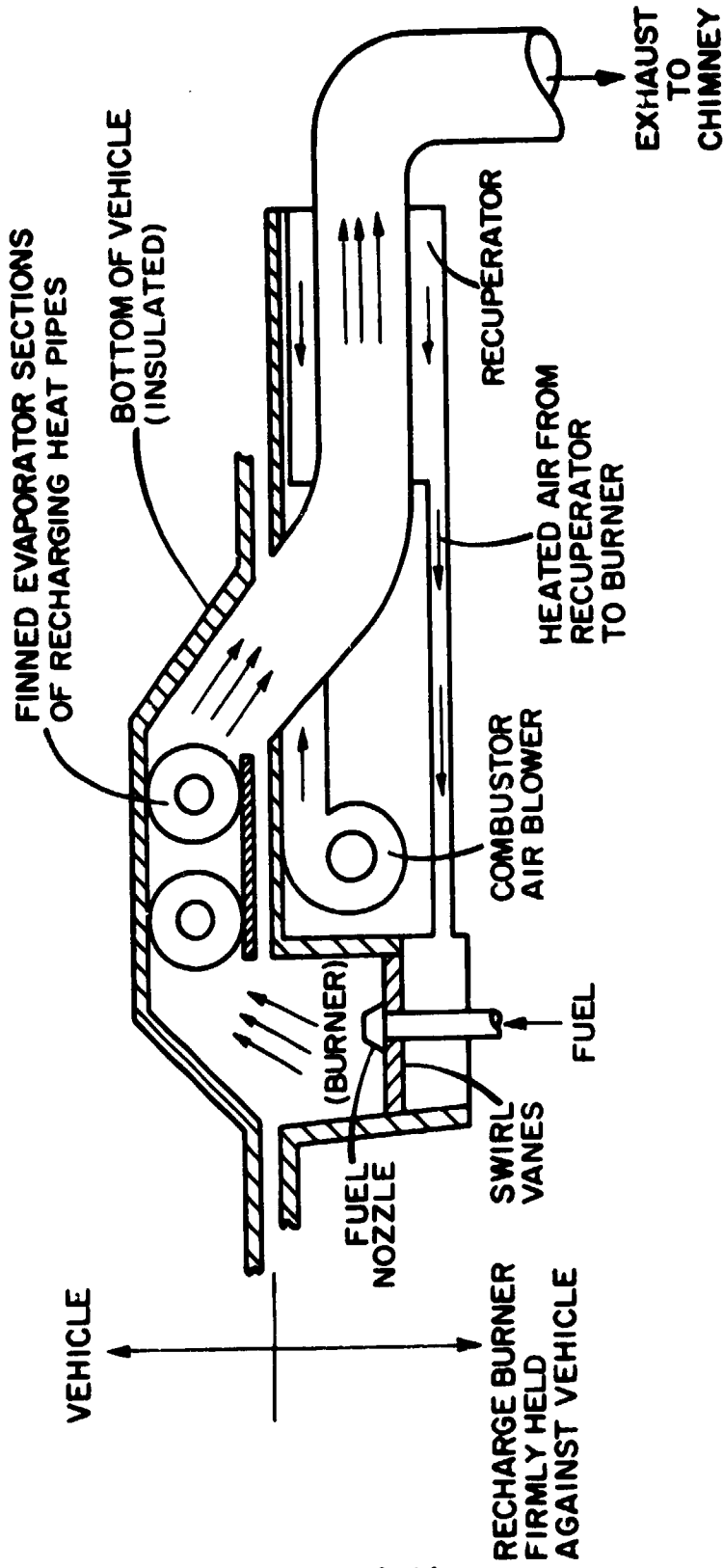


Figure 3.7 Schematic of Recharging System

combustor configuration, as illustrated schematically. The combustor would be located permanently in the garage floor so that the car could be driven over the unit. Special metal wheel indents and guides fastened to the floor would be used for accurate positioning of the vehicle to match the burner cavity and the exchanger cavity on the vehicle. Once positioned, the recharging sequence would be completely automatic and actuated by pressing a switch in the garage. On actuation, the burner assembly would be automatically raised by an electric motor and pushed against the bottom of the vehicle with considerable force, providing an effective gas seal around the perimeter and forming a closed furnace. The blower would then be started and the air pressure checked automatically to ensure proper positioning and a good gas seal. If satisfactory the gas burner (or liquid burner) would be actuated and the recharging started. The burner would continue to operate until a thermocouple indicated that the desired temperature of 1600°F in the TES reservoir had been reached. The burner would be turned off and the air flow continued until the furnace surfaces had cooled to near room temperature, at which point, the blower would be turned off and the burner assembly lowered into the garage floor, completing the cycle.

Safety sensors would be incorporated to shut down the recharging in the event of overheating in any part of the system, such as one of the finned tubes. An electrical connector would automatically be coupled, connecting sensors carried on the vehicle to the burner control assembly. Fuel and exhaust lines would be brought into the cavity beneath the furnace and connected to the burner by flexible lines.

4. HEAT TRANSFER AND TRANSPORT CHARACTERISTICS

In the TES/Stirling engine system, key considerations are: transfer of 200 kwth for at least 15 seconds from the TES media to the engine heater with a ΔT small enough to have an insignificant effect on the engine performance; small connecting line for heat transport between the TES reservoir and the engine; rapid transient response; and low parasitic power. The ΔT between the TES media and the Stirling engine working gas can be divided into the following:

ΔT in Salt

ΔT in Transport of Heat Removed From Salt to Engine Heater Plenum

ΔT in Transfer of Heat From Engine Heater Plenum to Working Gas

In Section 4.4, the transient temperature profile in the solid (frozen) salt-slab is calculated for a step increase in the heat removal rate from zero to 200 kwth with an initially uniform temperature in the salt. Transfer from the solid salt represents the worst case, since natural convection assists heat transfer and reduces the ΔT where liquid exists. After 15 seconds with 200 kwth removal rate, the salt capsule surface temperature has decreased by only 20°C (36°F); most full-power transients last 15 seconds or less. This small temperature decrease will have only a small effect on the Stirling engine performance during the full-power transient. Even when 200 kwth is removed continuously for longer periods, the asymptotic centerline-to-surface ΔT in the solid salt is only 43°C (77°F).

Relative to heat transport from the salt to the engine working gas, evaluation of alternative means of heat transport (such as use of an inert gas) rapidly leads to the conclusion that the only practical means of heat

transport are heat pipes using, at the temperatures of interest for the Stirling engine, either sodium or potassium vapor. The proposed system is thus based on three potassium heat pipes for charging, internal heat transfer in the TES reservoir, and transport of thermal energy to the Stirling engine, as described in detail in Chapter 3.

In Section 4.3, the evaporation/condensation ΔT 's for potassium are estimated for the systems designs presented in Chapter 6. For 200-kwth heat transport, the ΔT 's for evaporation/condensation are all substantially less than 1°C and thus negligible. The major ΔT in heat transport is thus that resulting from the ΔP required to transport potassium or sodium vapor in the discharge heat pipe from the TES reservoir to the engine heater plenum in a connecting pipe of reasonable size. This heat transport is evaluated in Section 4.1. At the minimum storage temperature of 800°K , the ΔT resulting from the 4-inch diameter connecting pipe used in the system design is 25°C with a vapor transport rate corresponding to 200 kwth transport. This ΔT decreases rapidly with increasing TES media temperature. Thus, the maximum TES media-to-engine heater tube temperature is 45°C , with 200 kwth supplied continuously for 15 seconds. Under almost all actual operating conditions, the ΔT is less than this worst-case value. The effect of this ΔT on the Stirling engine performance is small and the operational requirements of the system are therefore satisfied.

Use of potassium as a heat transfer medium does introduce safety questions because of its high reactivity. The approach followed in the design has been to reduce the potassium inventory to an absolute minimum, thereby reducing this hazard to a low level compared to other hazards. Safety of this system is discussed in Chapter 9. Also, use of a potassium heat pipe for transport of thermal energy to the Stirling engine heater

head introduces questions regarding the effect of H_2 diffusion through the heater tubes on the heat transport rate or performance of the heat pipe. This issue is discussed in Section 4.2 of this chapter.

Transient response of the TES system is discussed in Section 4.6, and meets the operational requirements of the system.

4.1 HEAT TRANSPORT BY POTASSIUM AND SODIUM VAPOR

Consideration of the large volume and weight of the TES reservoir requires packaging of the TES reservoir and the Stirling engine at different locations in the vehicle. Thermal energy at 200 kwth (for peak engine power) is transported from the TES reservoir to the Stirling engine by means of the discharge heat pipe. In a conventional heat pipe, with capillary liquid return, the pressure drop for sodium- or potassium-vapor flow is very small and limits the transport rate per unit duct area, kwth/cm². As discussed in Chapter 3, a separate E-M liquid return pump is incorporated so that a larger ΔP can be generated over the vapor transport line, thereby greatly increasing the transport rate per unit area. (The E-M pump also provides a means of controlling the heat transport rate.)

The effect of ΔP on the vapor transport rate, and hence thermal transport rate, was analyzed parametrically for both sodium and potassium vapor, based on the flow schematic of Figure 4.1. The model used for the calculations (given in Appendix A) treated the vapor flow as compressible flow in a frictional duct. The metal vapor was assumed to obey the ideal gas law, with good approximation; other properties, such as vapor pressure and heat-of-vaporization were taken from Schins.¹ While some condensation may occur during flow of the vapor down the duct, this effect was neglected, since it has a small effect on the vapor flow rate (≤ 10 percent), and results in a slightly higher transport rate

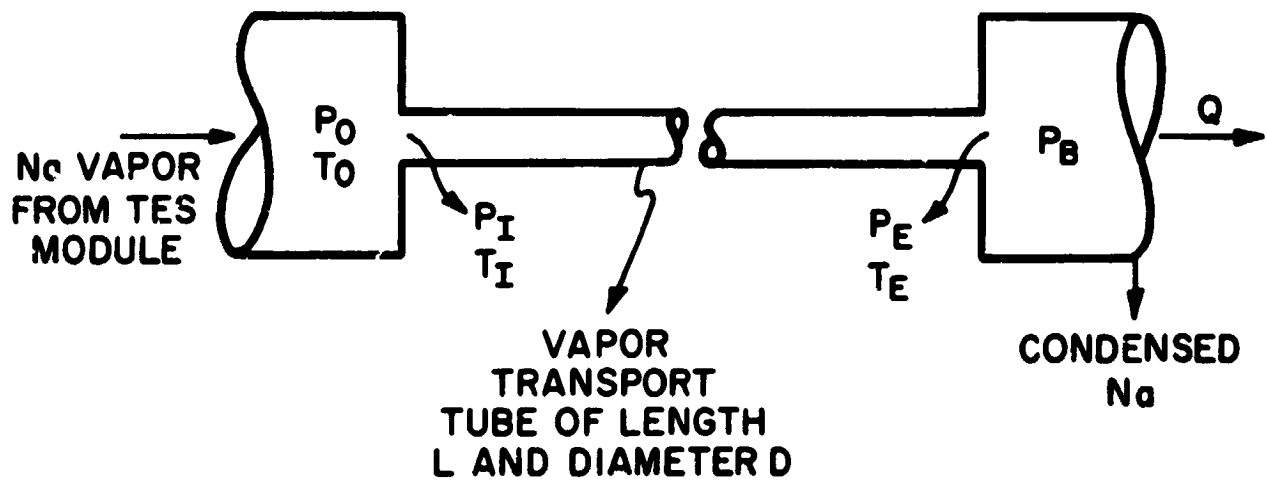


Figure 4.1 Schematic of Thermal Transport Model

than that based only on compressible flow. The heat transport rate is determined as the product of the vapor mass flow rate and the latent heat-of-vaporization of the metal.

With reference to Figure 4.1, for given conditions of pressure, P_0 , and temperature, T_0 , at the TES reservoir, the back pressure, P_B , at the Stirling engine heater head determines the flow rate in the duct. This back pressure in turn is determined by the temperature of the engine heater tubes and determines the temperature at which the metal vapor condenses on the heater tubes. If $P_B = P_0$, no flow occurs and no heat transport occurs. As P_B is reduced (by extraction of heat by the Stirling engine), the flow rate responds to the ΔP , and vapor flow and heat transport occur. The flow rate continues to increase until the back pressure is reduced to the level where the flow velocity at the duct exit equals the sonic velocity of the vapor. At this point, the flow is choked, and a further decrease in P_B does not result in a further increase in vapor flow rate and heat transport rate; this condition represents the maximum thermal transport capability of the heat pipe duct.

Results of the calculations are given in Figures 4.2 through 4.4 for sodium vapor and in Figures 4.5 and 4.6 (and Figure 7.1 of Chapter 7) for potassium vapor. These figures are based on a duct length of 10 feet, taken as the maximum length of interest for the automotive calculation. It is also assumed that P_0 and T_0 correspond to saturated conditions, with the condensing temperature determined by the back pressure, P_B (as established by P_0 and the pressure ratio P_0/P_B). From these figures, the following conclusions can be drawn:

- At a given heat source temperature (P_0), the heat transport rate increases rapidly as the back pressure is reduced.

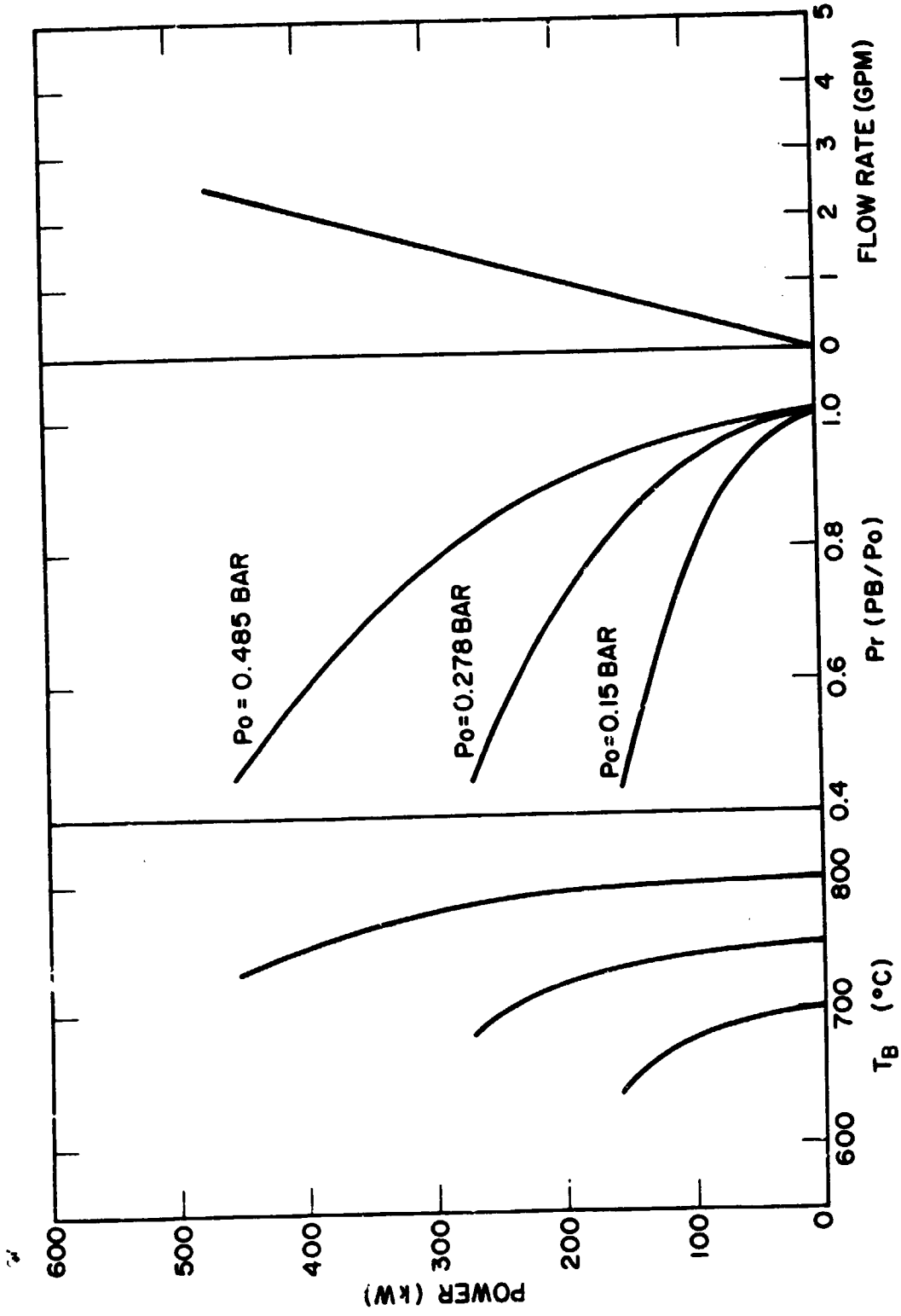


Figure 4.2 Heat Transport Characteristic for Sodium with $D=2''$, $L/D=60$

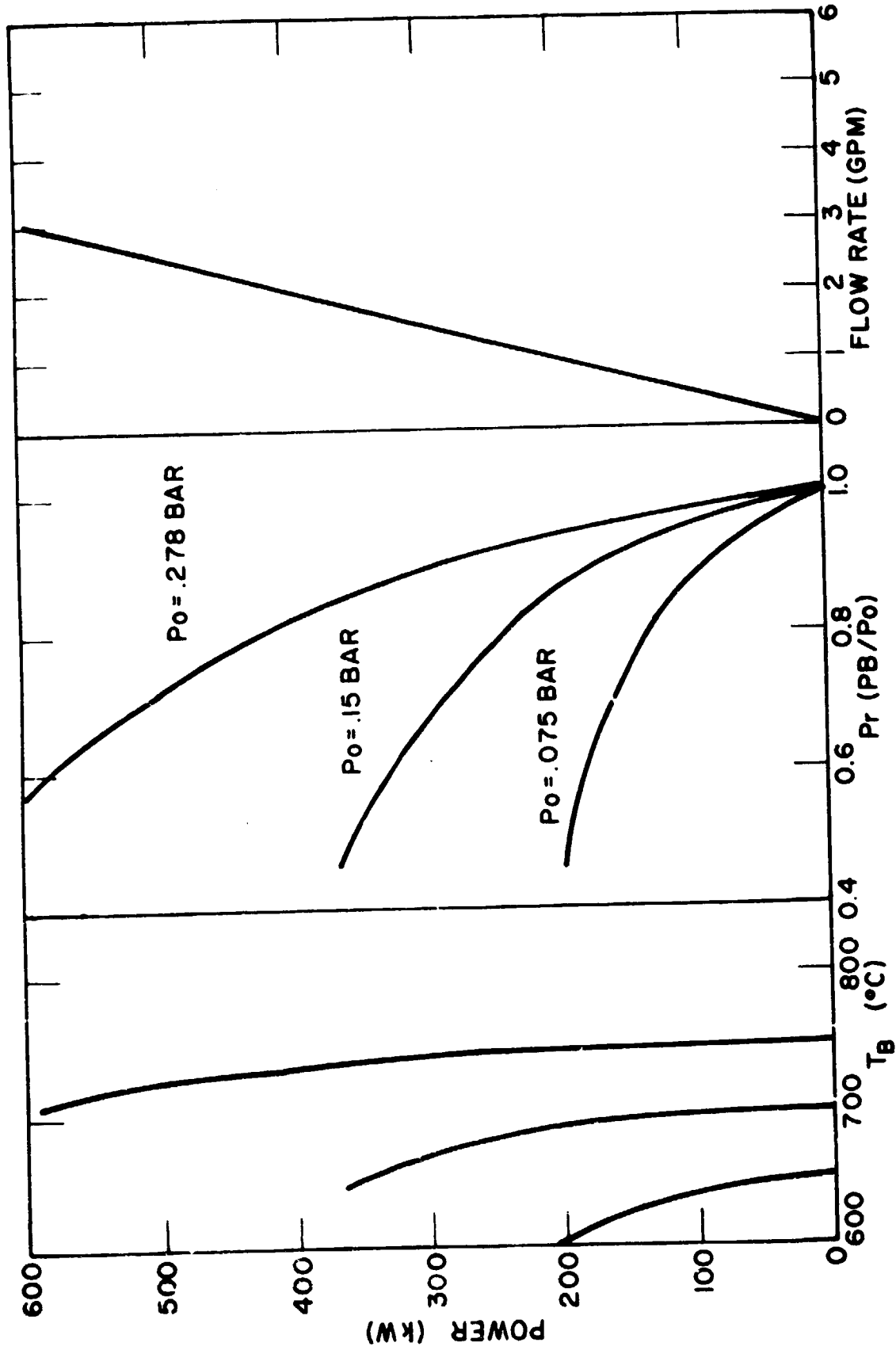


Figure 4.3 Heat Transport Characteristic for Sodium with $D=3"$, $L/D=40$

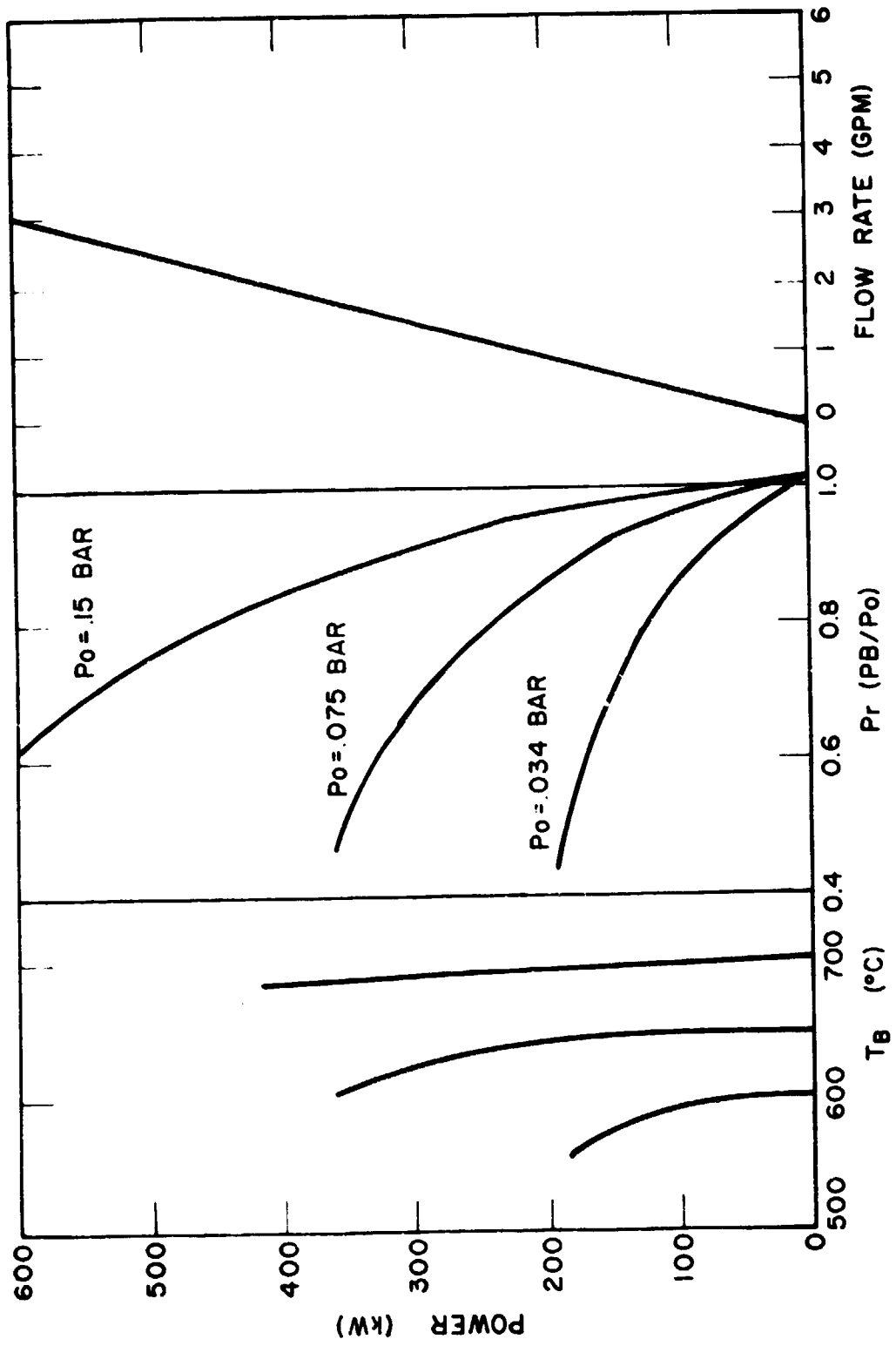


Figure 4.4 Heat Transport Characteristic for Sodium with D=4", L/D=30

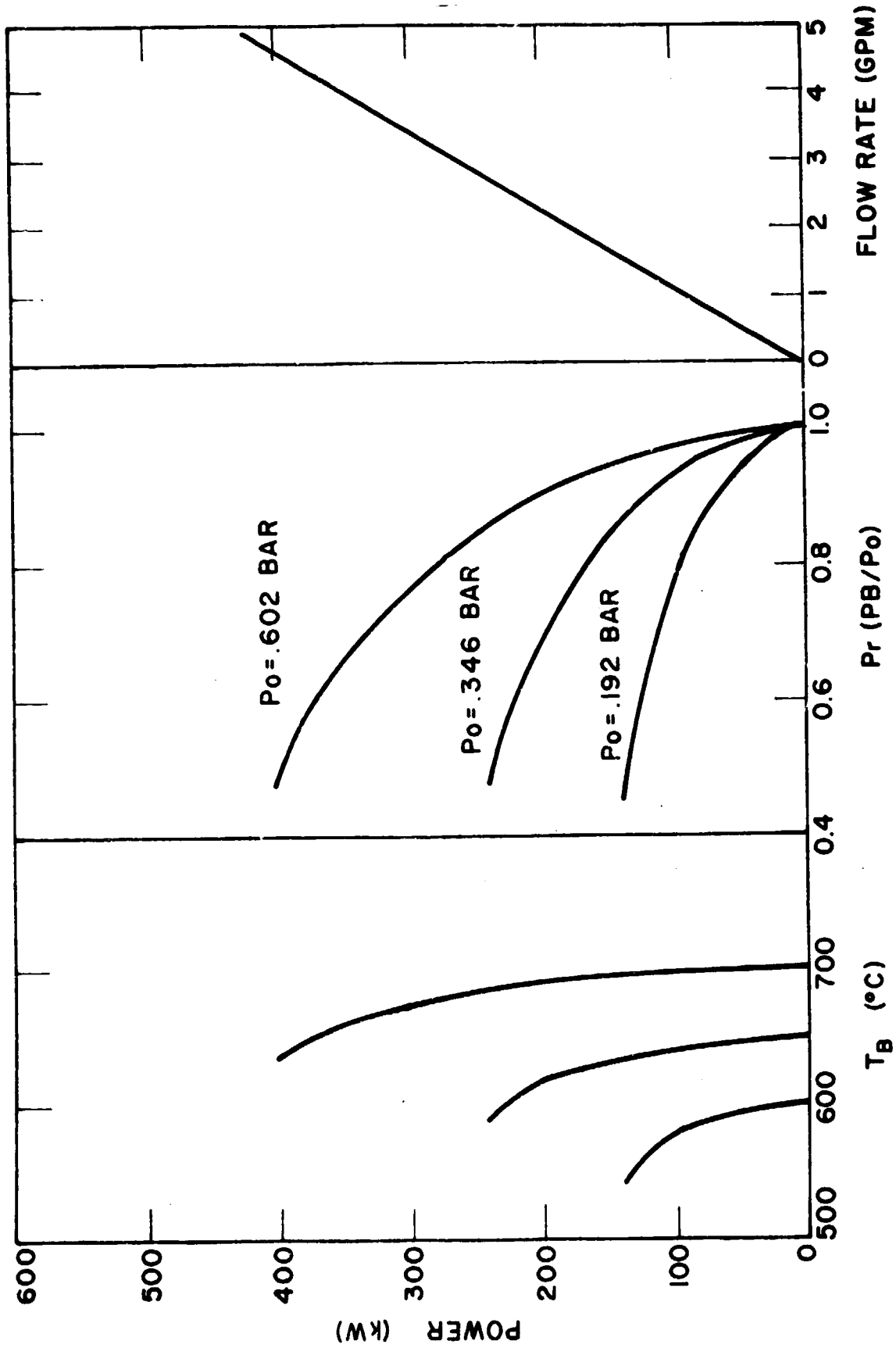


Figure 4.5 Heat Transport Characteristic for Potassium with D=2", L/D=60

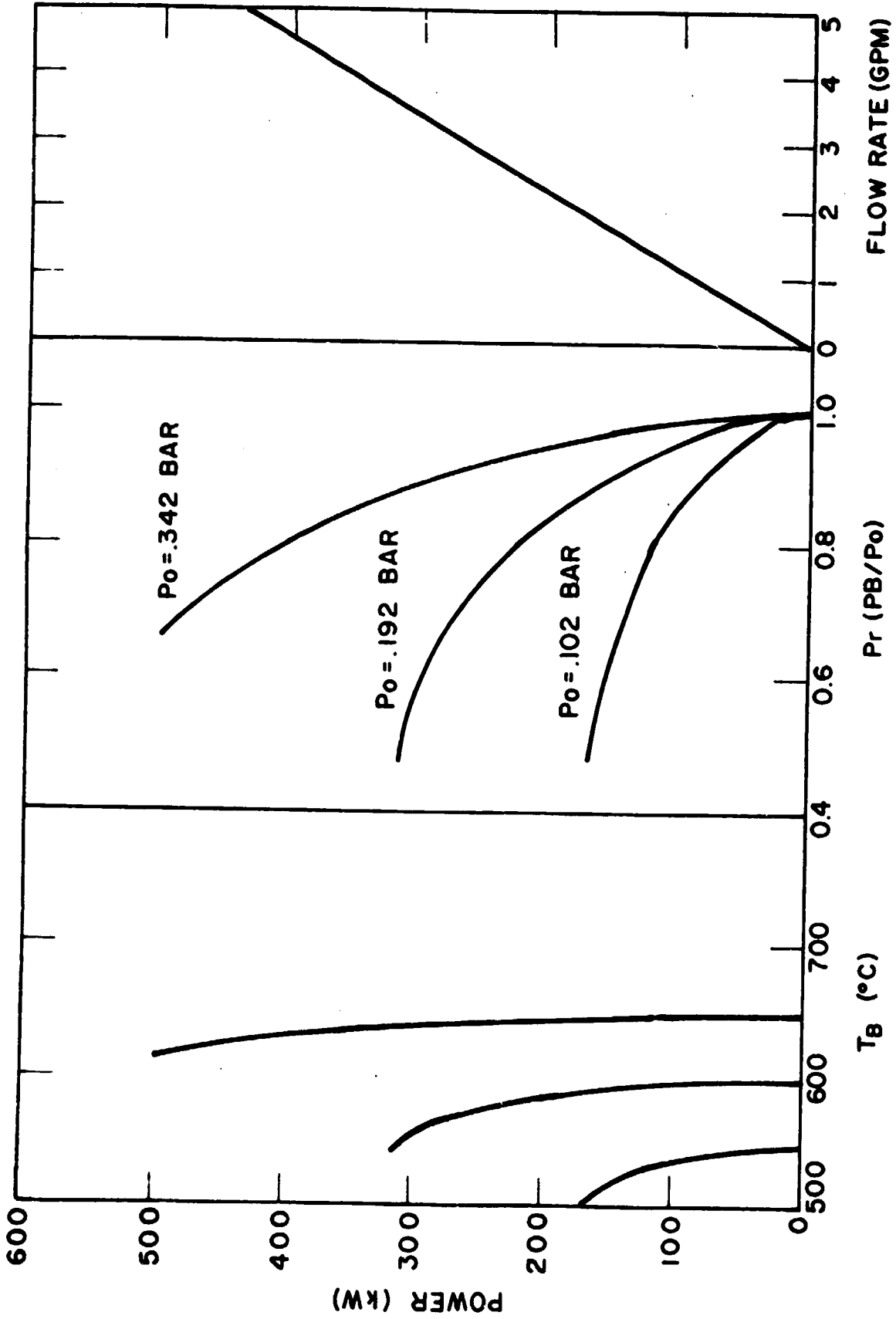


Figure 4.6 Heat Transport Characteristic for Potassium with $D=3"$, $L/D=40$

- The reduction in back pressure for fixed P_0 corresponds to an increase in the temperature differential between the heat source and the condensing temperature.
- The heat source temperature has an extremely strong influence on the heat transport capability of a given diameter duct, with the capability decreasing rapidly as the heat source temperature is reduced. This effect is very important, since it is proposed to utilize the TES system over the temperature range of $800^\circ\text{K} - 1150^\circ\text{K}$ to maximize the storage capacity per unit mass. The duct diameter required to transport 200 kwth is determined by the lower storage temperature. If the TES were restricted only to higher temperatures, a very small duct (~ 1 inch with potassium at 750°C) would be required to transport 200 kwth.
- The liquid flow rate for 200 kwth transport is 1.0 gal/min. for sodium and 2.2 gal/min for potassium.
- At a given heat source temperature and, temperature difference, potassium has a significantly higher thermal transport capability through a duct of a given diameter.

Calculations were also performed to determine the effect of the L/D ratio and the effect of superheated vapor from the TES reservoir, with results as given in Figures 4.7 and 4.8, respectively. The L/D ratio has only a small effect on the thermal transport capability; thus, the duct length, and the exact locations of the TES reservoir and Stirling engine, are not important in establishing the duct diameter. Relative to superheat, for a given pressure, P_0 , at the TES reservoir, the specific vapor temperature, T_0 , or degree of superheat, has a minor effect on the thermal transport capability of a

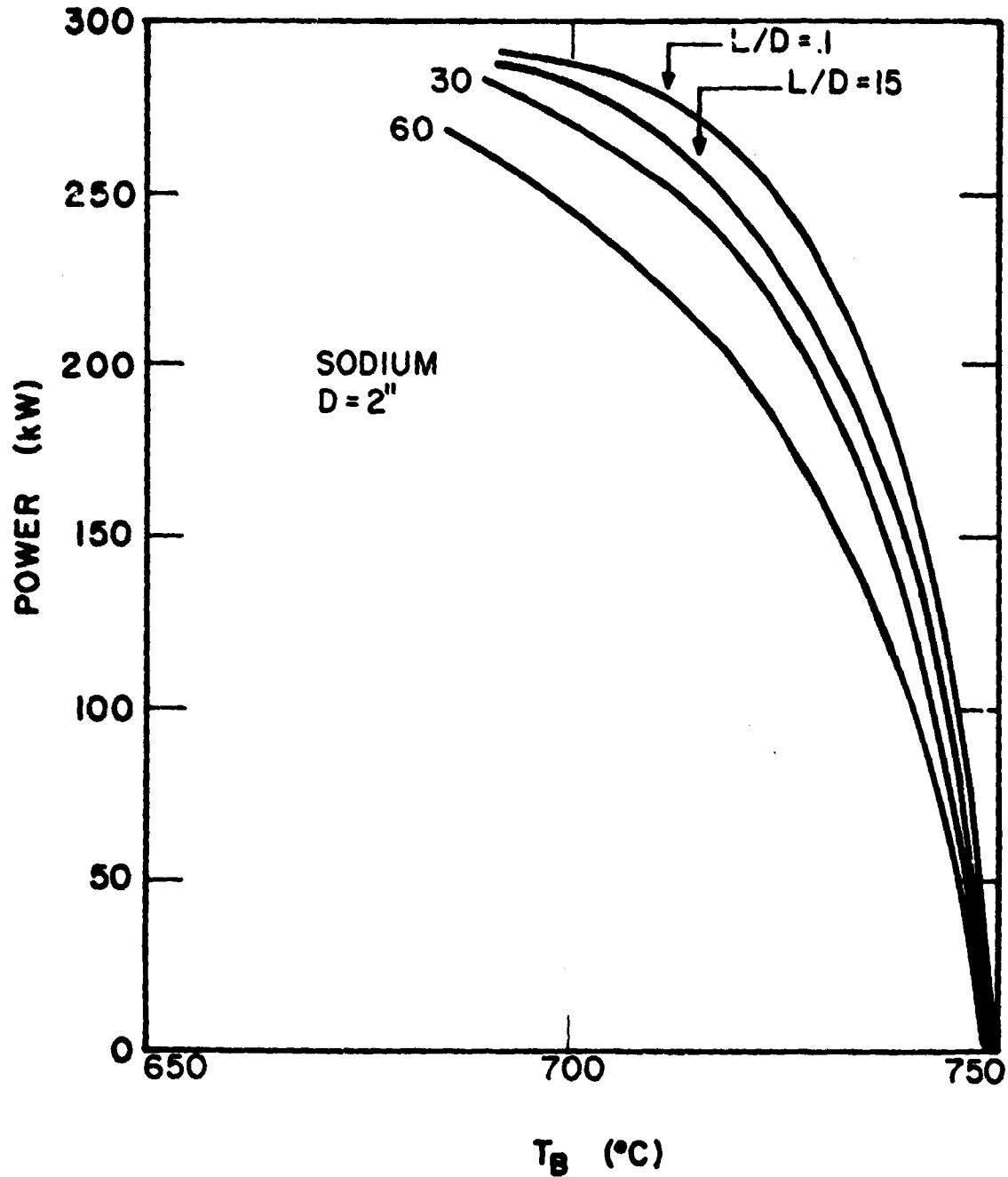


Figure 4.7 Effect of L/D on Heat Transport Rate for Sodium with D=2", $T_o = 750^\circ\text{C}$

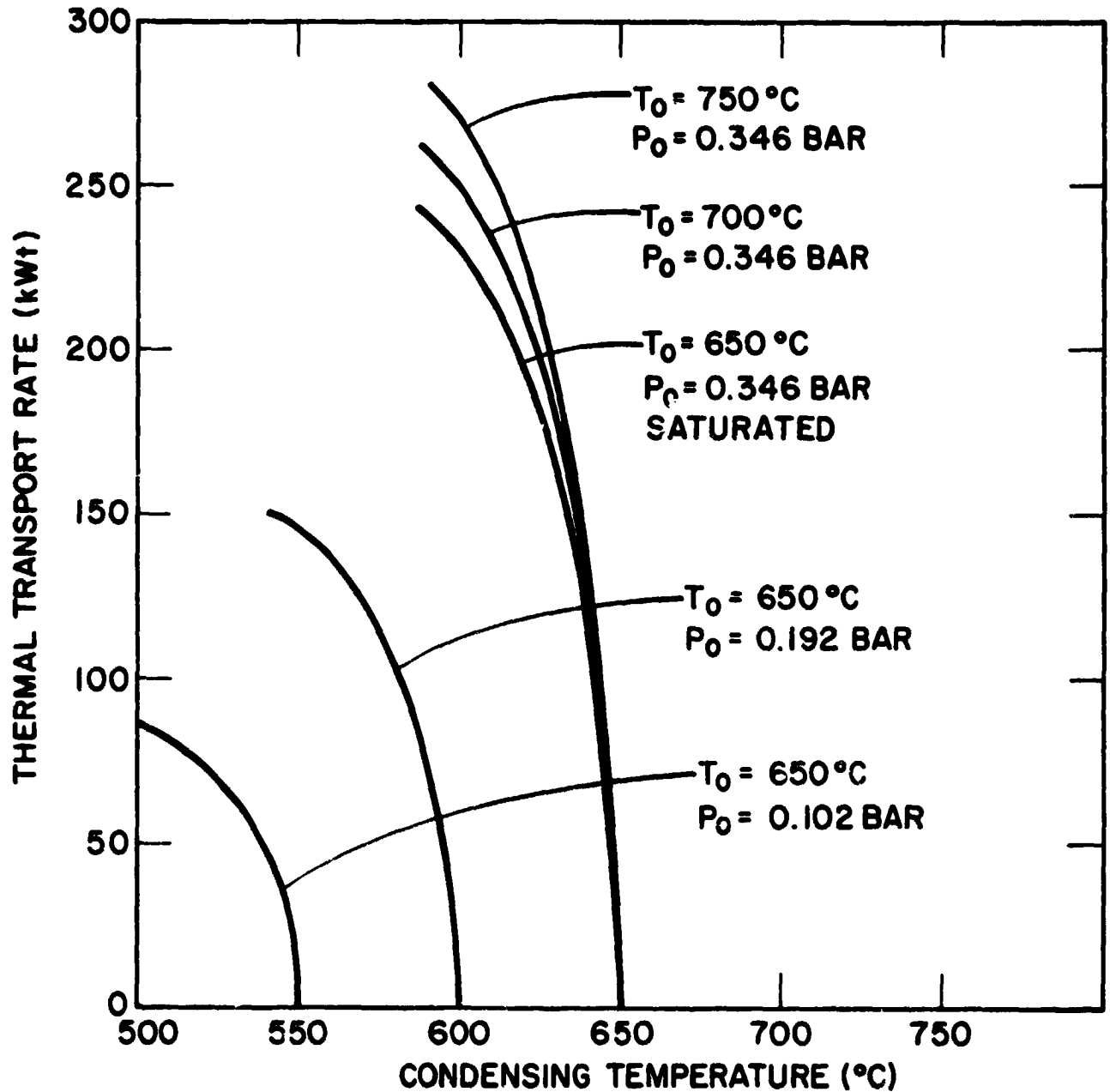


Figure 4.8 Effect of Vapor Superheat for Potassium with $D=2''$, $L/D=60$

given duct — as illustrated by Curves 1, 2, and 3 of Figure 4.8. However, if superheat is obtained at a given vapor temperature, T_o , by reducing the vapor pressure, a significant change in the thermal transport capability occurs — as illustrated by Curves 4 and 5 of Figure 4.8. In other words, the thermal transport capability is determined primarily by the pressure, P_o , at the reservoir, with superheat of the vapor having a minor effect.

The results presented previously were cross-plotted to determine the duct diameter for the discharge heat pipe, based on a transport rate of 200 kwth with a 25°C ΔT from the heat source to the Stirling engine and with a heat source temperature of 800°K . Results are given in Figures 4.9 and 4.10. Based on these results, potassium was selected as the best fluid for the discharge heat pipe, and a duct diameter of 4.0 inches was determined to be sufficient to transport 200 kwth at 800°K . At higher heat-source temperatures, the TES media/Stirling engine heater ΔT will be substantially less than 25°C . If sodium were used, the required duct diameter would be 6.0 inches. The potassium liquid flow rate is about double that of sodium, so that the potassium inventory in the liquid return line is somewhat greater than that for sodium.

4.2 EFFECT OF HYDROGEN LEAKAGE ON DISCHARGE HEAT PIPE OPERATION

The heater tubes of the Stirling engine are metallic, contain high-pressure hydrogen, and operate at high temperature (1023°K). Under these conditions, hydrogen gas diffuses at a relatively rapid rate through the heater tubes into the discharge heat pipe. The

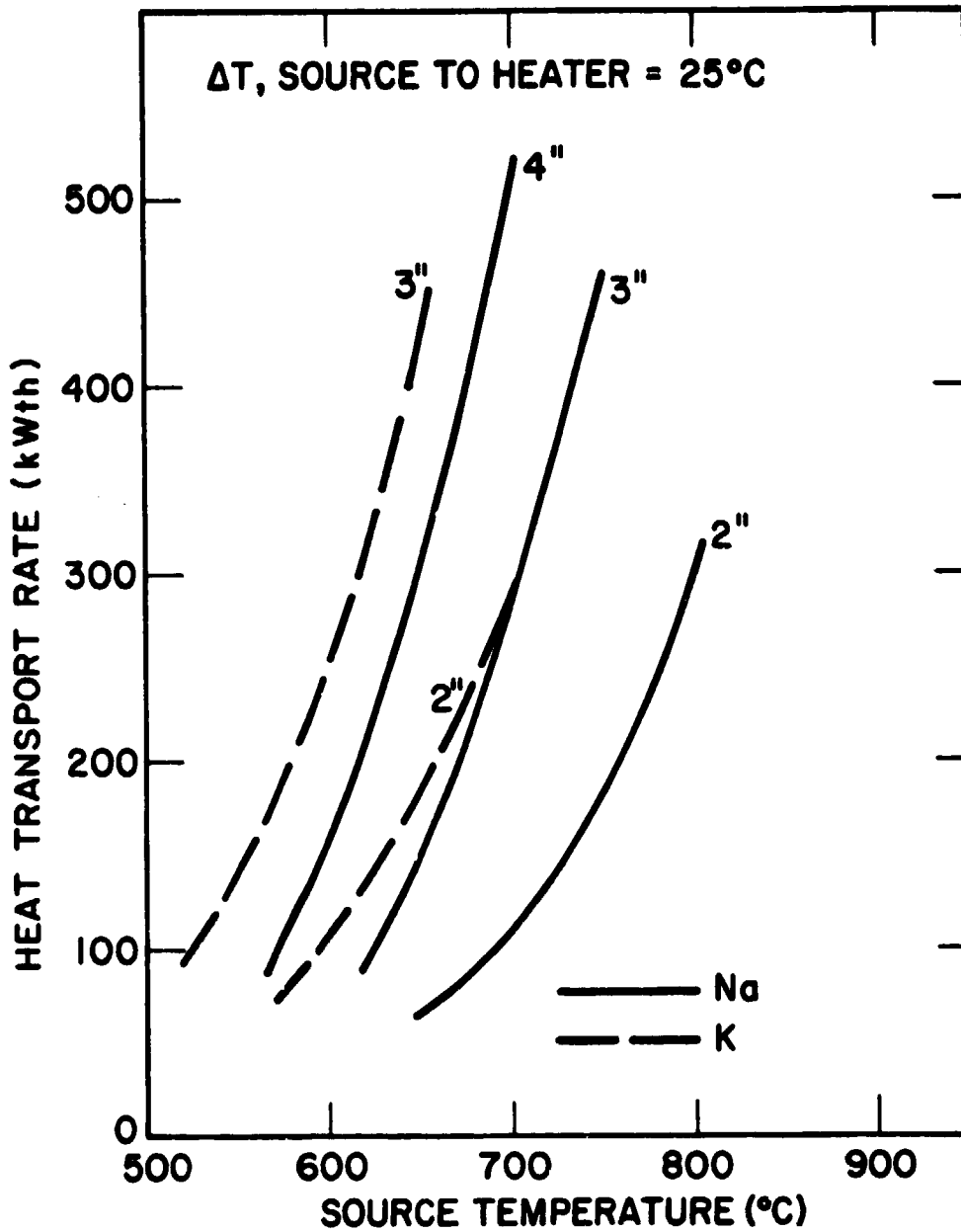


Figure 4.9 Heat Transfer Rate vs. Source Temperature And Pipe Diameter

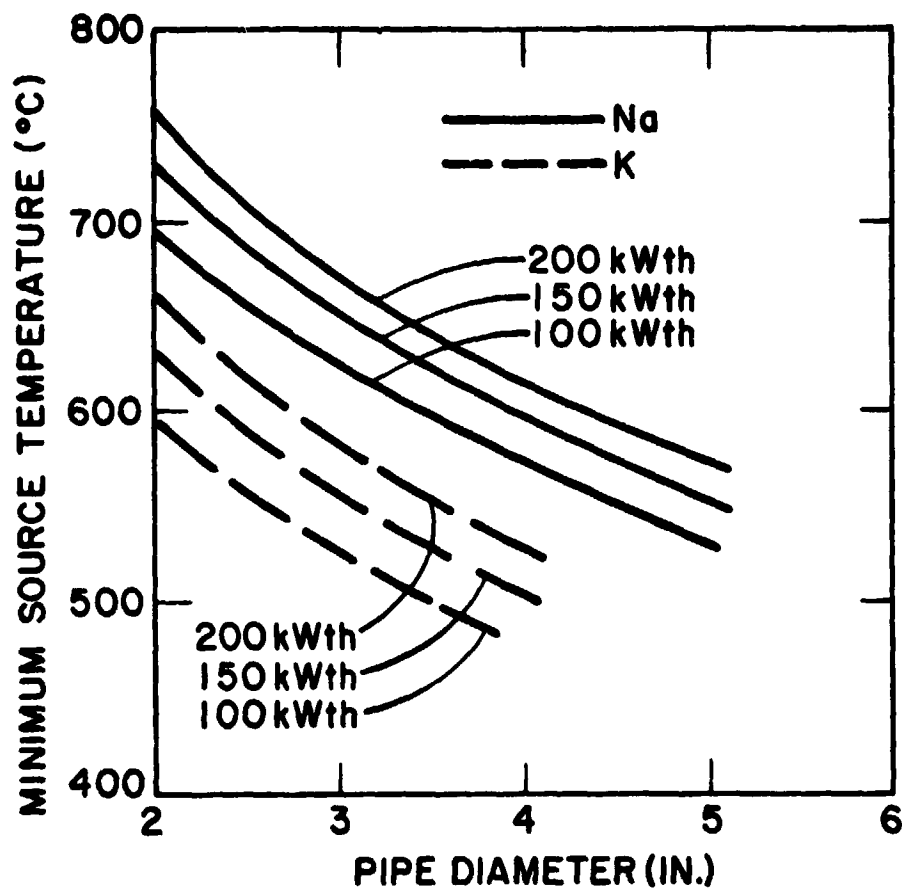


Figure 4. 10 Minimum Source Temperature vs. Pipe Diameter
 ΔT , Source to Heater = 25°C

presence of an inert gas in a heat pipe can have very serious effects on its heat transfer performance, and this leakage of hydrogen is of obvious concern. Stirling engines have been operated with excellent performance, using heat pipes for thermal transport to the engine heater.² All of the engines tested in this fashion have used helium instead of hydrogen as the Stirling engine working fluid, since helium does not diffuse through the tube walls. Indeed, as pointed out below, use of heat pipe heating of the Stirling engine permits use of helium as a working fluid, with comparable or better power and efficiency relative to the direct-combustion heated Stirling engine of the same displacement with hydrogen working fluid. This opportunity to eliminate use of hydrogen as the working fluid deserves careful attention, even without use of thermal energy storage. Without experimental work, it is impossible to give a definitive answer as to whether it is feasible to operate a heat-pipe heated Stirling engine with hydrogen working fluid. Since it is a complicated problem to model analytically, there are strong doubts that a reliable analysis can be made without experimental measurements to both provide an understanding of the phenomena occurring and to back up the analysis. Such experiments should simulate as closely as possible the expected configuration of the Stirling engine heater head and be carried out with both H₂ and He.

If H₂ diffusion does develop as a serious problem in operation of the discharge heat pipe, one alternative is to take advantage of the heat-pipe "bonus" effect as outlined by Hoagland and Percival.³

In Figure 4. 11, a power and efficiency comparison is presented for high specific power, double-acting engines optimized for direct heating with He and H₂ working gases and for indirect heating by a heat pipe with helium working gas.² In Figure 4. 12, experimental measurements on a directly heated and heat-pipe heated Stirling engine are presented.³ The information in both of these figures is from United Stirling, Malmo, Sweden, a major developer of Stirling engines. In Figure 4. 13, a similar comparison prepared by Philips of Eindhoven, Netherlands and reported by Meijer is presented,⁴ based on use of the same high specific power engine in which the engine heater is not optimized for each working gas and mode of heating. All of this information indicates that, because of the "bonus effect" of heat-pipe heating, the power and efficiency of a heat-pipe heated engine with helium working gas is equal to or greater than that of the direct-fired Stirling engine with hydrogen working gas.

The "bonus effect" of heat-pipe heating vs. direct heating results primarily from two effects as follows:

- The use of condensing potassium (or sodium) as a heat source provides a nearly constant wall temperature of the Stirling heater. In addition, control of the potassium pressure around the Stirling heater provides extremely tight control over the tube temperature, since the pressure directly determines the temperature at which potassium can condense. In a direct-fired heater, heat is being transferred from combustion gases with a widely varying temperature. Furthermore, small perturbations in the tube spacings due to manufacturing tolerances can lead to nonuniform combustion gas flow, through heater tubes - with resultant heat-flux variation. Both of these effects result in a nonuniform tube-wall temperature. To assure

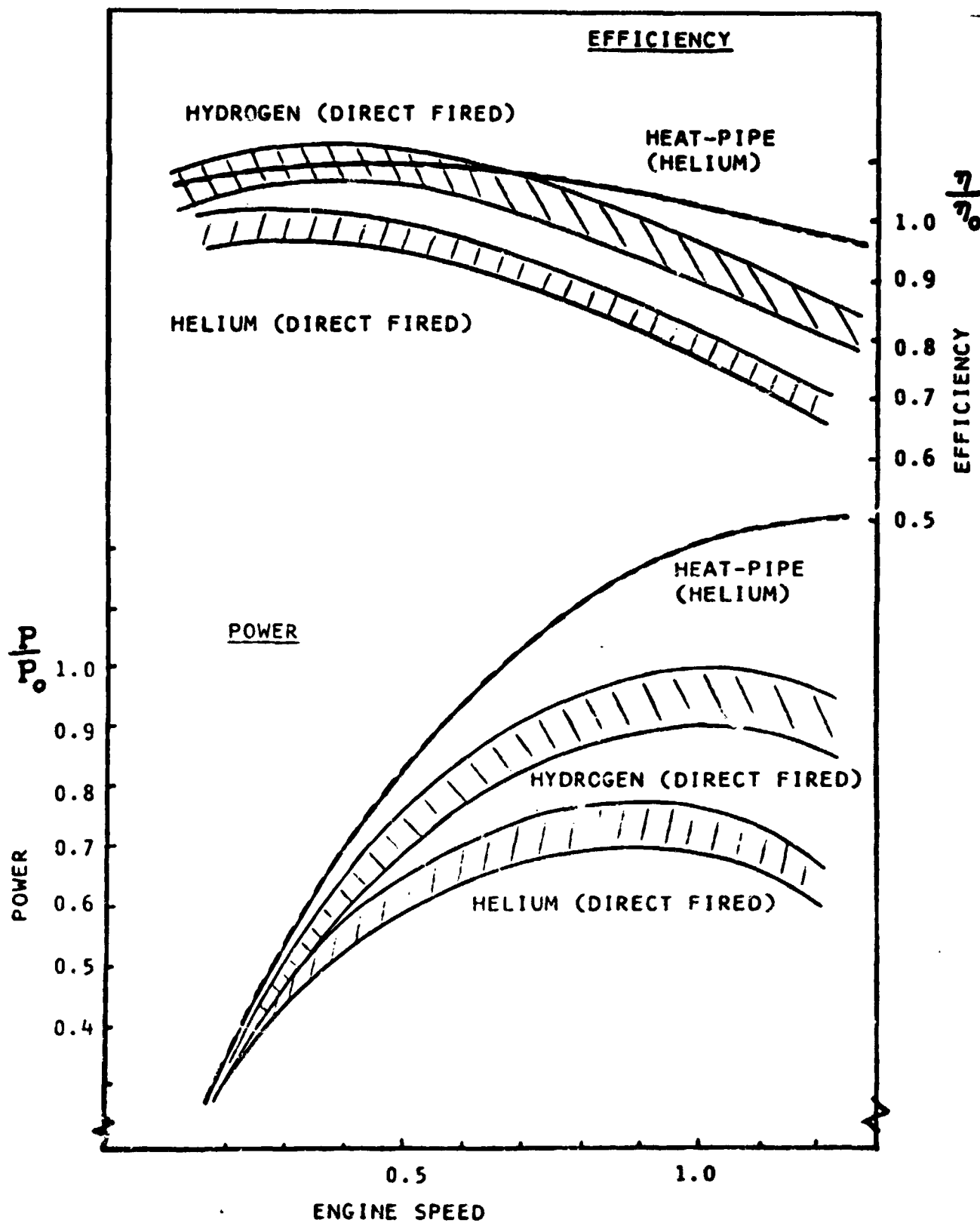


Figure 4.11 Power and Efficiency Comparisons; Heat Pipe vs Direct-Fired Engines

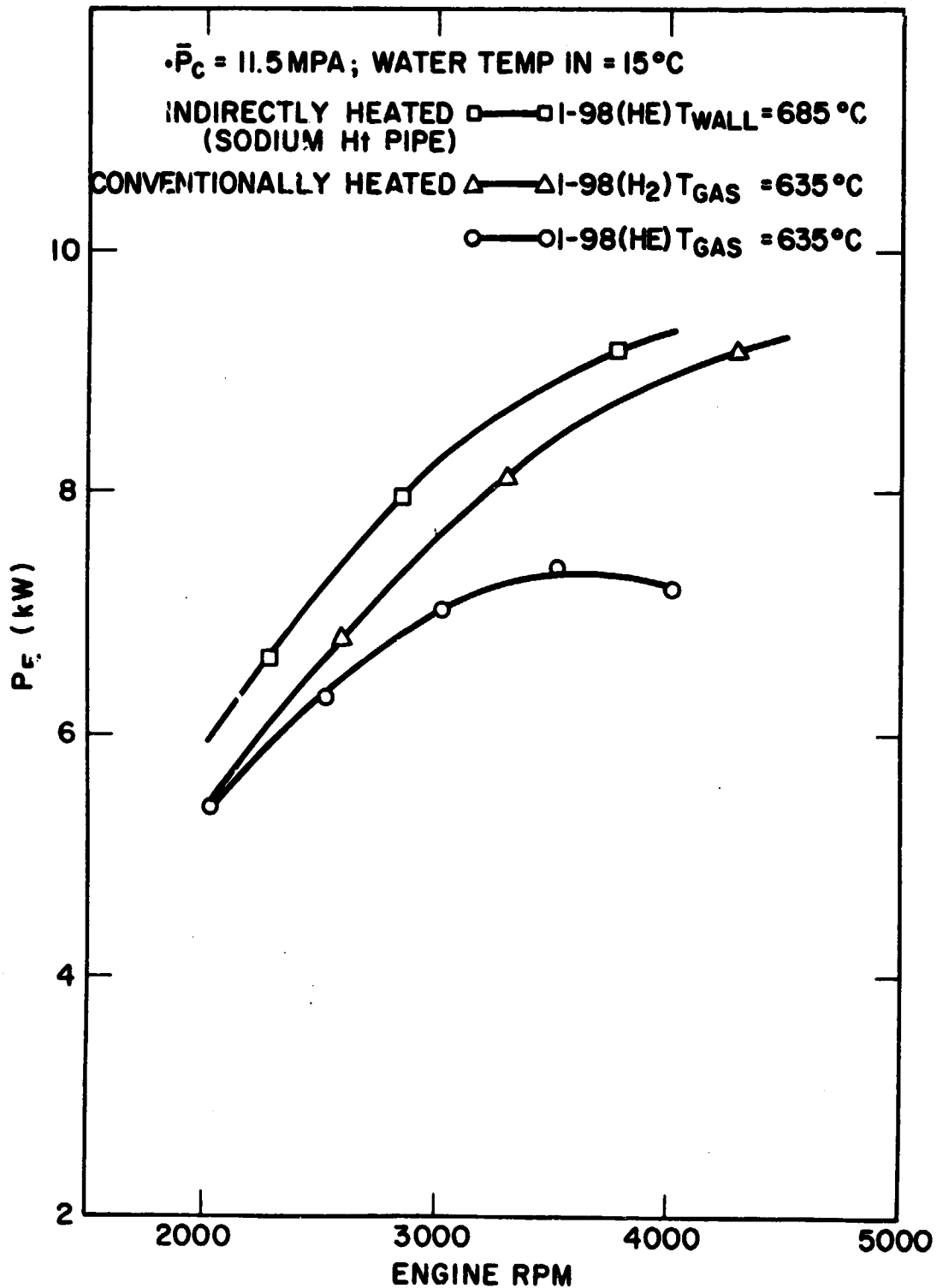


Figure 4.12 Shaftpower vs. RPM For Engine 1-98
At Different Working Conditions³

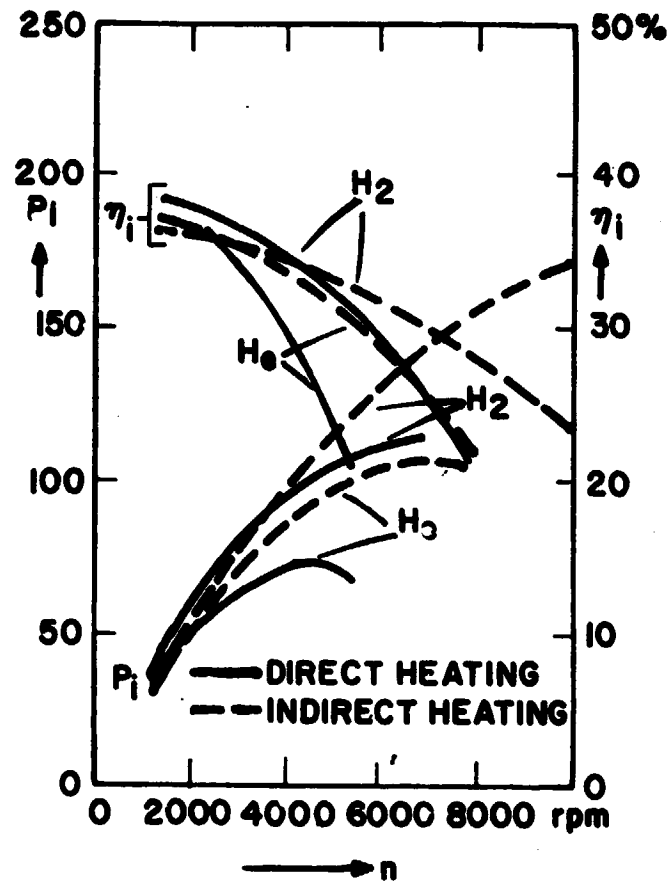


Figure 4. 13 Indicated Power, P_i , and Indicated Efficiency, η_i , of a Philips Stirling Engine as a Function of Speed, n , for H_2 or He Working Gas and for Direct or Heat Pipe (Indirect) Heating⁴

that the safe working temperature of the tubes is not exceeded, the average heater tube temperature is substantially below the "hot spot" temperature — which is governed by material creep properties. The net result is that with heat-pipe heating, the average heater tube temperature (and peak working gas temperature) can be boosted to the creep temperature limit, an increase of about 50°C to 75°C above that for the direct-fired engine, thereby improving engine output and efficiency substantially.

- Due to its high condensing heat transfer coefficient, the potassium heat pipe allows the heater tubes to operate at a substantially higher heat flux than with direct combustion heating. Reoptimization of the heater head for heat pipe, rather than direct heating, results in a larger number of smaller-diameter and shorter tubes. This modification improves the internal heat transfer performance, reduces the internal gas pressure loss through the heater, and reduces the dead volume of the engine — all leading to higher engine specific power and efficiency.

Thus, a viable solution to the hydrogen diffusion problem is to use helium working gas. Relative to the H₂/combustion-heated engine, nothing is lost by going to He in terms of engine size, engine power, and engine efficiency. In addition, elimination of H₂ has some advantages relative to safety and to the elimination of the need to periodically charge the engine with makeup H₂ to replace leakage. Even without TES, heat-pipe heating should be given serious evaluation for the automotive Stirling engine. In addition to use of He working gas with the same engine displacement and higher power and efficiency, the heat pipe decouples the burner/combustion heater from the Stirling engine, permitting,

for example, placement of the burner/combustion heater in the rear of the vehicle with the Stirling engine in the front. Elimination of the burner from the Stirling engine, coupled with the shorter heater tube, reduces the overall length of the Stirling engine — thus, facilitating packaging.

The heat pipe also decouples the heat transfer surface at the burner from that at the Stirling engine — permitting separate optimization of each. Thus, the burner/combustion heater can be designed larger, with a much lower pressure drop and parasitic power loss, resulting in an additional improvement in the overall system energy efficiency. In the direct-heated Stirling engine, several percent of the gross engine power is required for the combustion air blower. The heat pipe acts as a very effective heat-flux transducer, using the low heat-flux in the combustion heater and providing a very high heat-flux to the Stirling heater.

Use of H_2 with the heat pipe would result in a smaller Stirling engine for the same power and efficiency, and could greatly improve the attractiveness of the automotive Stirling engine. Thus, even though the heat-pipe heated engine with He is competitive with the direct-heated engine with H_2 , there is still an incentive to use H_2 with the heat-pipe heated engine. Two approaches can be followed to potentially eliminate the effect of H_2 diffusion leakage on the heat pipe. First, the heater head can be designed so that high-velocity flow of the metal vapor cleans the tubes of H_2 , with pumping of the H_2 to a H_2 diffusion window in a manner analogous to a diffusion pump. This technique is suggested in the concept schematics of Chapter 3

for elimination of H_2 from the discharge heat pipe, but requires experimental development and demonstration before its success can be assured. Second, to reduce any effect, materials or coatings that greatly reduce the diffusion rate can be used as (or on) the heater tubes. It should be noted that diffusion rates through the tubes in operation of actual Stirling engines have been substantially less than would have been predicted from steady-state, isothermal, laboratory diffusion measurements.³ The reason for this reduction is not known, but may be due to the oscillating pressure as well as thermal gradient in the tube wall.

4.3 EVAPORATION/CONDENSATION ΔT 's IN HEAT PIPES

In general, the evaporation/condensation heat transfer coefficients of alkali metals, specifically potassium and sodium, are high enough so that the ΔT 's for evaporation and condensation of potassium in each of the three heat pipes are negligible compared to other heat-transfer operations. In this section, typical heat transfer coefficients are presented and used with the system heat transfer areas to justify the negligible ΔT 's wherever potassium is evaporated or condensed.

For condensation of liquid metals, the liquid metal film on the condensing surface has a negligible ΔT and heat transfer resistance. The liquid film is basically isothermal at the temperature of the surface on which condensation is occurring. The primary resistance is thus at the liquid-vapor interface, with a continual interchange of molecules being condensed from the vapor and molecules evaporating from the surface. With a net flow of molecules toward the surface,

there exists a temperature drop, $T_s - T_i$, whose magnitude depends on the fluid being condensed, on the saturation pressure, and on the rate of condensation. T_s is the saturation temperature of the vapor, and T_i the surface temperature at the liquid film interface (wall temperature in this case). The heat transfer flux, q/A , is thus related to the net mass flow $(W/A)_{\text{net}}$ toward the liquid-vapor interface,

$$q/A = \left(\frac{W}{A}\right)_{\text{Net}} h_{fg}$$

where, h_{fg} = heat-of-vaporization of condensing vapor. Schrage⁵ has analyzed this problem with kinetic theory with the result:

$$\left(\frac{q}{A}\right)_{\text{Cond}} = \left(\frac{M}{2\pi R}\right)^{1/2} \left(\frac{2\sigma}{2-\sigma}\right) \left(\frac{P_i}{\sqrt{T_s}}\right) \left(\frac{P_s - P_i}{P_i} - \frac{T_s - T_i}{2T_i}\right) h_{fg}$$

where M = vapor molecular weight

R = ideal gas constant

σ = accommodation coefficient, defined as fraction of molecules striking surface that actually do condense

P_s = saturation pressure

P_i = interface pressure

The heat transfer flux and heat transfer coefficient are summarized in Table 4.1 for sodium and potassium at a film surface temperature of 650°C and for several ΔT 's. The condensing heat transfer coefficients are extremely high, so that small ΔT 's result wherever condensing heat transfer occurs. Presented below are heat transfer fluxes and the ΔT 's for a condensing surface temperature of 650°C for the

TABLE 4. 1

CONDENSATION HEAT FLUX AND HEAT TRANSFER COEFFICIENT
FOR SODIUM AND POTASSIUM AS FUNCTION ΔT

T_i = Interface or Condensing Surface Temperature = 650°C

T_s = Saturation Temperature of Vapor

$\Delta T = T_s - T_i$ (°C)	q/A (w/cm ²)		h (watts/cm ² -°C)	
	Na	K	Na	K
5	300	800	60	160
10	600	1600	60	160
30	1800	4800	60	160
50	3000	8000	60	160

TES system as presented in this report (based on a rectangular configuration):

● Recharge heat Pipe (Condensing in TES Reservoir)

A	718 cm ² (0.77 ft ²)
q	14.65 kwth (5 x 10 ⁴ Btu/hr)
q/A	20.4 w/cm ²
ΔT (650°C)	0.13°C

● Reservoir Heatpipe (Condensing on Discharge Heatpipe)

A	1.724 x 10 ⁴ cm ² (18.6 ft ²)
q _{max}	200 kwth (6.826 x 10 ⁵ Btu/hr)
(q/A) _{max}	11.7 w/cm ² (3.6 x 10 ⁴ Btu/hr-ft ²)
ΔT(650°C)	0.07°C

● Stirling Engine Heater Head (Condensing on Heater tubes)

A	~5000 cm ² (5.38 ft ²) (for automotive Stirling engine)
q	200 kwth (6.826 x 10 ⁵ Btu/hr)
q/A	40 w/cm ²
ΔT (650°C)	0.25°C

From these values, it is apparent that the condensing ΔT is small enough to neglect in all parts of the system.

The evaporative section of a heat pipe normally includes a wick, and evaporation occurs from the liquid surface without bubble formation. While wicks are not required for capillary pumping, they are used on all evaporative surfaces to ensure wetting of the surface and

to provide good distribution of liquid potassium over the hot surface. In this respect, then, the evaporation from a hot surface (relative to the vapor saturation temperature) is similar to the condensation on a cool surface, and the same molecular kinetic model applies for evaporation as for condensation; that is, the heat transfer represents the net mass flow resulting from molecular evaporation and condensation at the liquid interface, with the wall (or liquid) temperature in this case higher than the vapor saturation temperature:

$$(q/A)_{\text{Evap}} = \left(\frac{M}{2\pi R}\right)^{1/2} \left(\frac{2\sigma}{2-\sigma}\right) \left(\frac{P_i}{\sqrt{T_s}}\right) \left(\frac{P_i - P_s}{P_i} - \frac{T_i - T_s}{T_i}\right) h_{fg}$$

The evaporative heat transfer coefficient at a given temperature is thus identical to the condensing coefficient, and equivalent ΔT 's exist for the same heat flux as for boiling. This type of heat transfer definitely applies in the evaporative section of the discharge heat pipe, and this ΔT would be $\sim 0.07^\circ\text{C}$. This mode of evaporative heat transfer also occurs in the charging heat pipe for which the evaporative ΔT should be basically zero, since the external thermal resistance for heat transfer from combustion gases to the evaporative section of the charge heat pipe is totally dominant in the heat transfer.

In the reservoir heat pipe, liquid potassium may immerse the charging heat pipe, so that heat transfer by pool boiling could occur. The heat flux of 20 w/cm^2 ($6.34 \times 10^4 \text{ Btu/hr-ft}^2$) is small enough so that only small ΔT 's will occur. In Figure 4.14 the heat fluxes for pool boiling of sodium and potassium at several temperatures are presented, based on the results of Subbotin, et al.⁶ Heat transfer coefficients at 1400°F are $35,000 \text{ Btu/hr-ft}^2\text{-}^\circ\text{F}$ for potassium, and $13,500 \text{ Btu/hr-ft}^2\text{-}^\circ\text{F}$ for sodium, respectively. It is apparent that the ΔT for

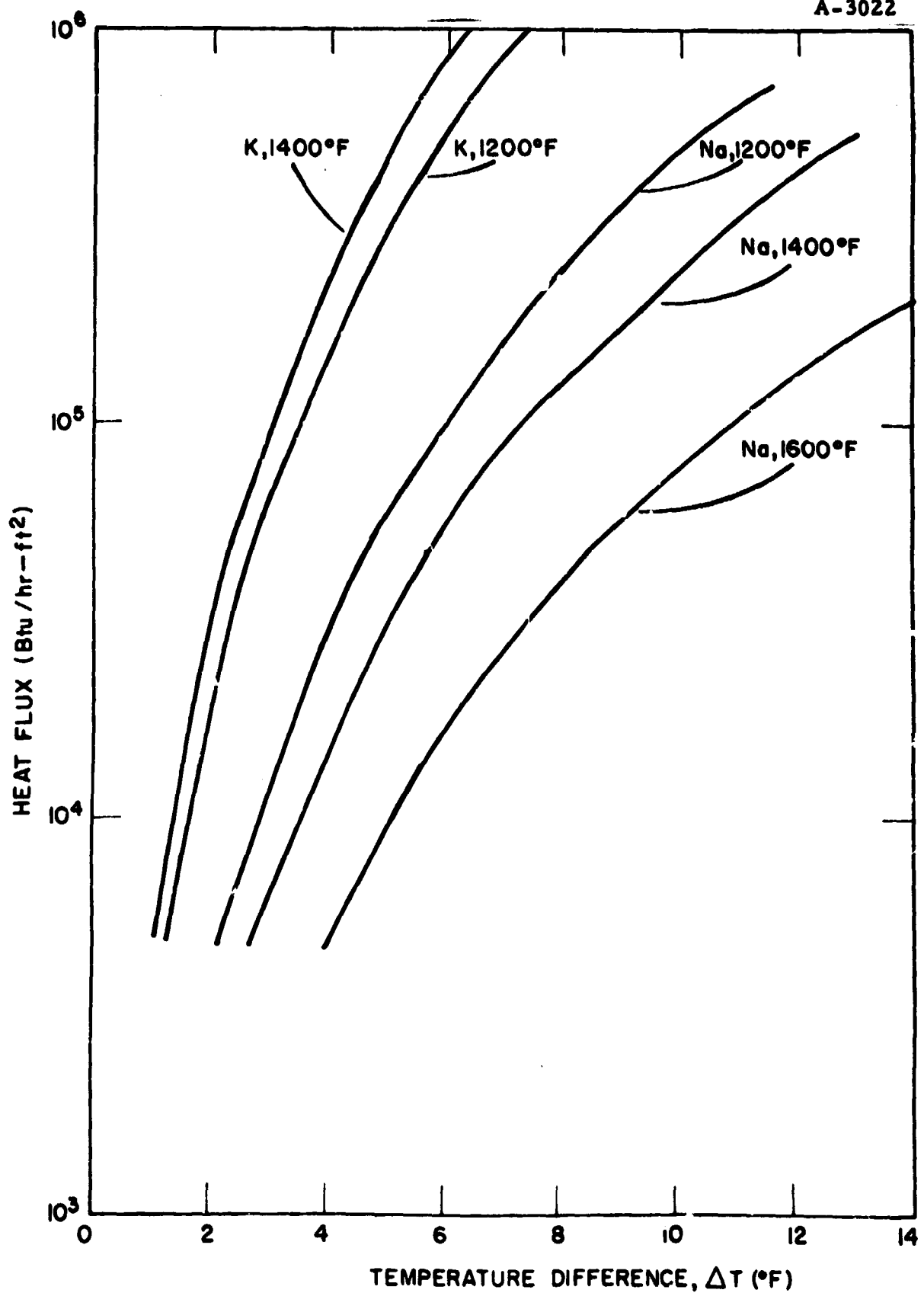


Figure 4. 14 Pool Boiling Heat Flux vs. ΔT for Potassium And Sodium

pool boiling of potassium at a heat flux of 6.3×10^4 Btu/hr-ft² is in the range of 0.8°C to 1.2°C (2°F to 3°F), and thus is negligible.

In summary, all ΔT 's for heat transfer by evaporation/boiling or condensation of potassium are sufficiently small to be neglected at the maximum heat fluxes required.

4.4 SALT TEMPERATURE VARIATION DURING HIGH-POWER TRANSIENT

During wide-open throttle operation, 200 kwth must be supplied by the salt capsule for at least 15 seconds. It is important in this transient that the salt capsule surface temperature is not significantly reduced, since both the Stirling engine power and efficiency are reduced as the head temperature decreases. In this section, an estimate is given of the transient temperature distribution in the solid salt slab following a step change in power demand from zero to 200 kwth. The worst case occurs when the salt is completely frozen, as assumed in the calculation, since natural convection assists the heat transfer in liquid salt and reduces the ΔT relative to that obtained with the completely frozen salt slab.

The heat transfer problem is that of a flat plate of thickness $2L$, initially at a uniform temperature, T_∞ . For times $t \geq 0$, a constant heat flux, q'' is applied to both surfaces of the flat plate; q'' is positive for heat addition and negative for heat removal. The solution to this unsteady-state thermal conduction problem, expressed in terms of dimensionless parameters d , is:⁸

$$\frac{\theta(x,t)}{(q''L/k)} = \frac{\alpha t}{L^2} + \frac{1}{2} \left(\frac{x}{L}\right)^2 - \frac{1}{6} - 2 \sum_{n=1}^{\infty} \frac{(-1)^n}{\eta^2 \pi^2} e^{-\frac{\alpha t}{L^2} \eta^2 \pi^2} \cos \eta \pi \frac{x}{L}$$

where $\theta(x,t) = T(x,t) - T_\infty$, °F

x = distance in plate from plate centerline, $0 \leq x \leq L$, ft

L = plate half-thickness, ft

t = time after application of constant heat flux, hr

q'' = constant heat flux applied to both surfaces of plate for $t \geq 0$, Btu/hr-ft²

k = plate thermal conductivity, Btu/hr-ft-°F

α = thermal diffusivity of plate, $k/(\rho C_p)$, ft²/hr

ρ = plate density, lb/ft³

C_p = plate heat capacity, Btu/lb-°F

T_∞ = initial constant plate temperature, °F

$T(x, t)$ = plate temperature at position x and time t , °F

For large times where $\alpha t/L^2$ is large, this relation reduces to:

$$\frac{\theta(x, t)}{q''L/k} \approx \frac{\alpha t}{L^2} + \frac{1}{2} \left(\frac{x}{L}\right)^2 - \frac{1}{6} \text{ for } \frac{\alpha t}{L^2} > 0.5$$

The temperature profile across the plate thus asymptotically becomes invariant with time, with the temperature at any x changing linearly with time and at the same rate. The plate centerline-to-surface ΔT thus asymptotically approaches a constant value, given by:

$$\theta(0, t) - \theta(L, t) = T(0, t) - T(L, t) = -\frac{q''L}{2k}$$

For the designs presented in Chapter 6, the total capsule surface areas are 132 ft² for the rectangular configuration and 153 ft² for the cylindrical configuration, with a salt thickness of 1.5 in. for each configuration and heat removed from both surfaces of the salt slab. However, the salt capsules are only partially filled with solid salt, since allowance has been made in the design for thermal expansion of the salt as well as the volume increase on melting. Thus, only a fraction

of the capsule surface is effective in heat transfer from the solid salt. Using the rectangular design because of its smaller capsule heat transfer area, and assuming that the salt freezes with a flat surface across the capsule (uniform height in capsule), the effective heat transfer area for heat removal from the surface is 81.5 ft^2 or about 62 percent of the total capsule surface area. For 200-kwth heat removal rate, this surface area corresponds to a heat flux of 8372 Btu/hr-ft^2 . The parameters used in calculating the salt slab temperature profile are summarized below, based on LIF:

$$q'' = -8372 \text{ Btu/hr-ft}^2 \text{ (for 200-kwth heat removal rate)}$$

$$L = 0.0625 \text{ ft}$$

$$k = 2.4 \text{ Btu/hr-ft-}^\circ\text{F}$$

$$C_p = 0.57 \text{ Btu/lb-}^\circ\text{F}$$

$$\rho = 146 \text{ lb/ft}^3$$

$$\alpha = \frac{k}{\rho C_p} = 0.0409 \text{ ft}^2/\text{hr}$$

$$T_\infty = 1400^\circ\text{F}$$

With these parameters, the temperature profile in the salt slab is presented in Figure 4.15 for various times after a step increase in the heat removal rate from zero to 200 kw^h; the plot is based on an assumed initial uniform temperature of 1400°F. In Figure 4.16, the salt centerline and surface temperatures are presented as a function of time and in Figure 4.17, the centerline-to-surface ΔT is presented as a function of time.

With reference to Figures 4.15, 4.16, and 4.17, the initial heat removal is taken only from the salt in the immediate vicinity of the surface with a relatively rapid decrease in the surface temperature. After 15 seconds, the surface temperature of the salt has decreased

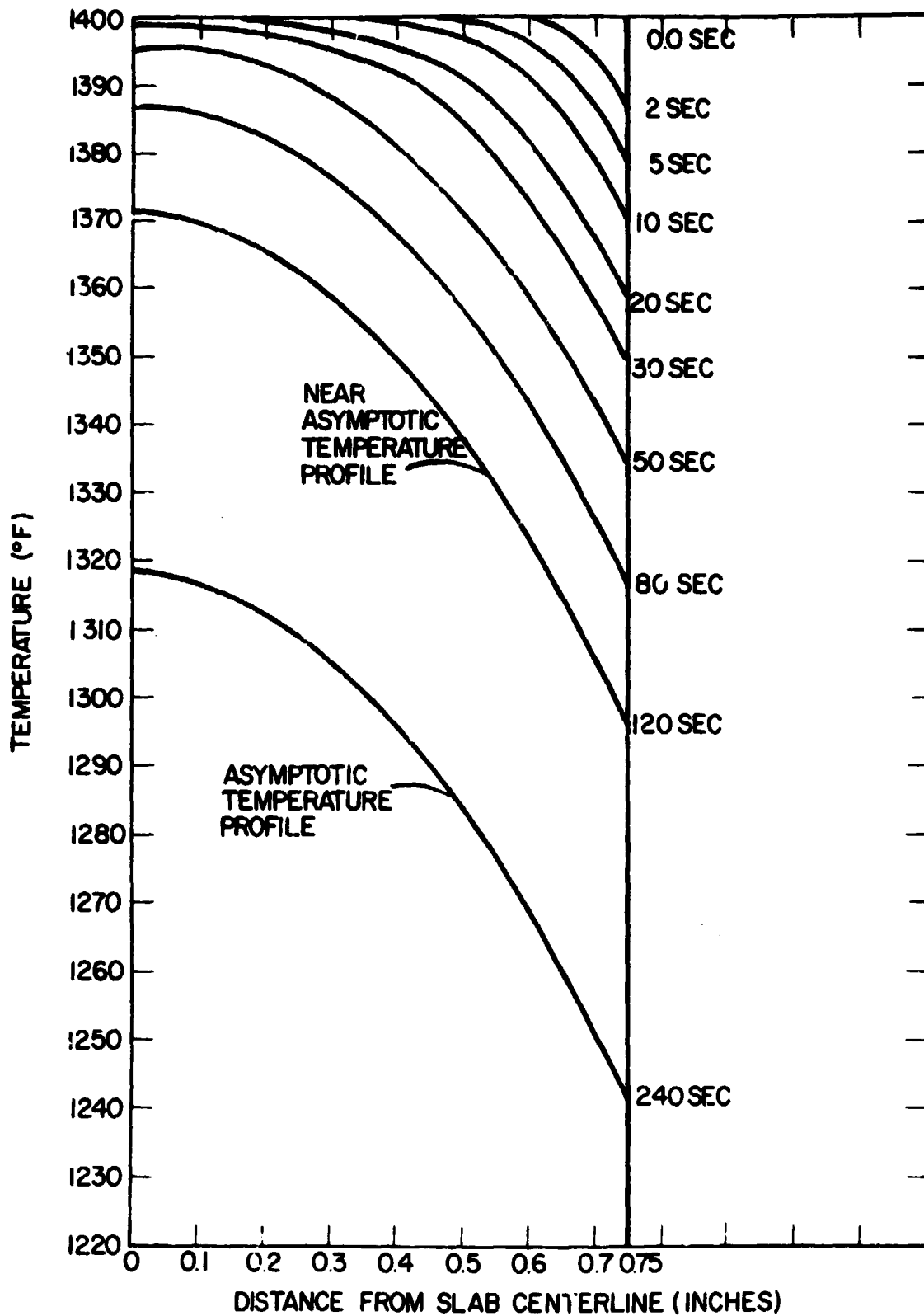


Figure 4.15 Temperature Profile in Solid Salt Slab at Various Times After Step Increase in Heat Removal Rate From Zero to 200 kWth - Rectangular Design

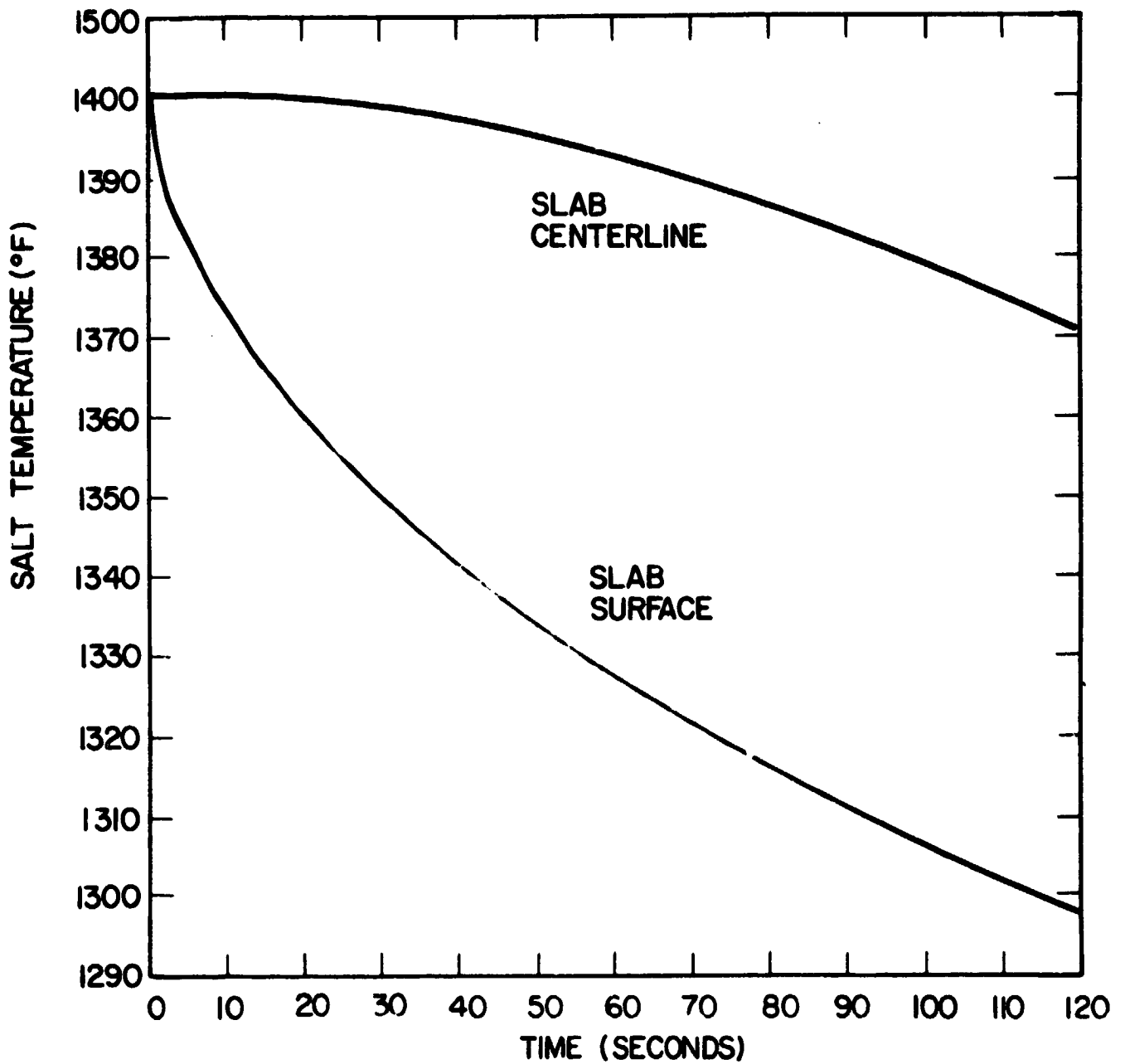


Figure 4. 16 Solid Salt Surface and Centerline Temperature As Function of Time With Initially Uniform Salt Temperature and Step Increase in Heat Removal Rate From Zero to 200 kWth - Rectangular Design

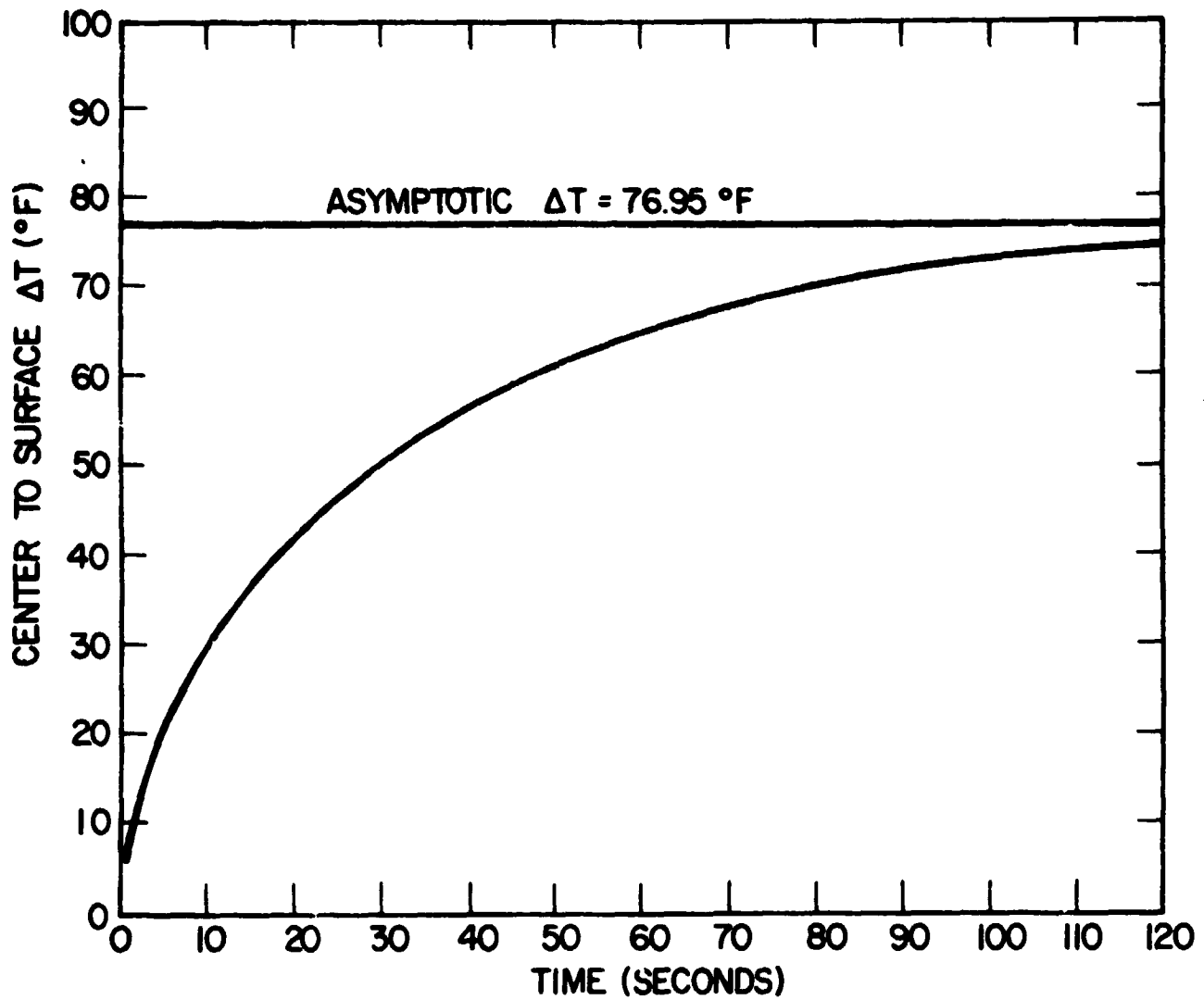


Figure 4.17 Centerline to Surface ΔT in Solid Salt As Function of Time With Initially Uniform Salt Temperature and Step Increase in Heat Removal Rate From Zero to 200 kWth - Rectangular Design

by only 20°C (36°F); most full-power transients last 15 seconds or less. This small temperature decrease will have only a small effect on the Stirling engine performance during the full-power transient.

If 200 kwth continues to be removed, the temperature wave reaches the centerline of the slab after about 30 seconds, and the centerline temperature then also starts to decrease; the centerline-to-surface ΔT is 28°C (51°F) at this time. After 120 seconds, the temperature profile in the salt has closely approached the asymptotic profile; the asymptotic centerline-to-surface ΔT is 43°C (77°F). For times >120 seconds, continued removal of 200 kwth occurs with a constant temperature profile and constant centerline-to-surface ΔT of 77°F ; with this asymptotic temperature profile, all parts of the solid salt are decreasing in temperature at the rate of $0.447^{\circ}\text{F}/\text{sec}$ or $26.8^{\circ}\text{F}/\text{min}$. After 240 seconds (4 minutes) with continuous 200 kwth heat removal, the centerline and surface salt temperatures are 1319°F and 1242°F , respectively, relative to the 1400°F initial temperature, and both temperatures are decreasing at the rate of $26.8^{\circ}\text{F}/\text{min}$.

In summary, the surface temperature of the salt capsule decreases by a maximum of 20°C (36°F) during wide-open throttle acceleration, when 200 kwth is removed from the solid salt for 15 seconds. This decrease is small enough to have an insignificant effect on the Stirling engine performance. The design is capable of delivering 200 kwth continuously from the solid salt, until discharged, with an asymptotic 43°C (77°F) centerline-to-surface ΔT and a corresponding $14.9^{\circ}\text{C}/\text{min}$ ($26.8^{\circ}\text{F}/\text{min}$) uniform rate of temperature decrease.

4.5 CHARGING HEAT PIPE, COMBUSTION SIDE

The combustion side of the charging heat pipe was not considered in detail, since this must be integrated and designed with the specific combustion system to be used with the vehicle. The single tube inside the reservoir can be manifolded to two or more tubes in the combustor heat exchanger. Use of multiple, finned tubes manifolded to the single tube in the reservoir can be used to provide whatever heat transfer area is required. A rough estimate is summarized below for perspective on the heat exchanger size.

The required recharging rate is ~ 50,000 Btu/hr (14.6 kwth) for overnight recharging. It is assumed that the combustion heat exchanger is made of 1.0-inch O.D. finned tubing, with a total heat transfer/bare tube area ratio of three (i. e., relatively low fin density). With an average heat-transfer coefficient of 15 Btu/hr-ft²°F, and neglecting any radiant transfer, the required tubing length (in feet) is given as follows:

$$50,000 \frac{\text{Btu}}{\text{hr}} = (15 \frac{\text{Btu}}{\text{hr-ft}^2 \cdot \text{F}}) \left(\frac{(\pi)(1.000)(L)(3)}{12} \text{ft}^2 \right) (\Delta T)$$

where ΔT is the average gas-to-tube wall temperature.

Thus,

$$L\Delta T = 4244 \text{ ft-}^\circ\text{F}$$

If $\Delta T = 1500^\circ\text{F}$, which is feasible with a combustion heat source, $L = 2.8$ ft. The combustion recharger could thus be made of two finned tubes, each having a length of 1.4 feet based on convection alone. With radiation considered, a tube length of 12 inches would probably be adequate. The combustion heat exchanger section of the recharging

heat pipe is thus of reasonable size for integration with the vehicle, as illustrated schematically in Figure 3.7 of Chapter 3.

4.6 TRANSIENT RESPONSE

The transient response of the TES system must be adequate to assure that the Stirling engine heater tube temperature does not decrease significantly during rapid power increases and that overheating does not occur during rapid power decreases. Response to rapid power increases is more crucial, since the heater tube temperature cannot be heated to a temperature higher than the TES media, a maximum of 1150°K. It is thus impossible to drastically overheat the Stirling engine.

Extremely rapid (0.2 sec) transient response of the TES system in response to a rapid power increase by the Stirling engine is not required, since the engine heater tubes themselves provide a small TES capacity for transient operation. The magnitude of the TES transient response requirement can be estimated as follows: The heater tubes of the Ford Motor Company 4-98 Stirling engine have a mass of 3.96 kg; an additional mass of 8.49 kg is located in the cylinders, cylinder walls, regenerator caps, and regenerator walls, at least part of which operate at the heater head temperature.⁷ On an idle-to-full-power transient, the heat transfer rate in the heater head rapidly goes from ~2 kwth to the maximum requirement of 200 kwth as the pressure level of the engine is increased in response to the power requirement. Even with no thermal input into the Stirling engine heater head, the engine will continue to operate at full power for a short period using thermal energy stored in the heater head. Assuming the tubes alone are effective for

TES, the rate of temperature decrease of the tube temperature with no thermal input and a removal rate of 200 kwth is $94^{\circ}\text{C}/\text{sec}$, using a heat capacity for the tubes of 540 joules/kg- $^{\circ}\text{C}$. Assuming that 2.5 kg of the 8.5 kg in the engine head is also effective reduces the rate of temperature decrease to $57^{\circ}\text{C}/\text{sec}$. Thus, if a momentary decrease in the tube wall temperature of 150°C is acceptable, $\sim 2\text{-}1/2$ seconds are available for the TES system to increase its thermal delivery rate from idle (~ 2 kwth) to the full power demand of 200 kwth. This response requirement is consistent with the response rate of the combustor for the direct-combustion-heated Stirling engine. Mr. Worth Percival, who managed Stirling engine development at General Motors, indicated that the combustor typically responds from idle to full-firing rate in ~ 3 to 4 seconds so that faster transient response is not needed.

The turnup response of the TES system described conceptually in Chapter 3 is controlled primarily by the speed with which the potassium flow rate to the TES reservoir can be modulated by the E-M pump and by the rate at which potassium vapor is generated in the discharge heat pipe, thereby building up the pressure differential in the discharge heat pipe to the level required to meet the thermal transport demand of 200 kwth. Increasing the liquid potassium flow rate involves rotation of the permanent magnet on the E-M pump (see Chapter 7 for the E-M pump design) and should require only a few tenths of a second. Since the liquid lines will normally be filled with liquid potassium, this increase in liquid potassium pumping rate immediately results in spray of liquid potassium into the tubes of the discharge heat pipe located in the TES reservoir. Because of the large heat-transfer rates for evaporation/condensation of potassium with small ΔT 's, generation of

potassium vapor in the discharge heat pipe will very rapidly increase the pressure differential to the level required to transport the required 200 kwth. Vapor transport down the 4-inch connecting pipe occurs with sonic velocity at the discharge end and represents a completely negligible time delay. In short, the turnup response of the TES system developed in this report should be much faster than that for the direct combustion-fired system where both air and fuel must be increased in a controlled ratio into the combustion chamber in response to the idle-to-full-power transient. The transient response on turnup of the designed TES system is more than adequate to meet the demands of the Stirling engine for automotive propulsion.

For turndown, the response time is controlled by the liquid potassium flow rate cutoff time, by any liquid potassium existing on discharge heat-pipe walls which can flash to vapor, and by potassium vapor in the discharge heat pipe. The liquid potassium flow rate can be rapidly stopped by the E-M pump, and the TES storage by potassium vapor is very small. The primary limitation is thus any residual liquid in the reservoir tubes of the discharge heat pipe. It is believed that this liquid holdup is small enough so that the thermal transport potential from this source is small relative to TES capacity of the Stirling engine heater tubes. In addition, as pointed out earlier, it is impossible to heat the Stirling engine heater to a temperature higher than the TES media under any circumstances, and thus impossible to drastically overheat the Stirling engine.

REFERENCES FOR CHAPTER 4

1. Schins, H. E. J., "Liquid Metals for Heat-Pipes, Properties, Plots and Data Sheets," European Atomic Energy Community, Joint Nuclear Research Center, Ispra, Italy, 1967.
2. Hoagland, L. C., and Percival, W. H., "A Technology Evaluation of the Stirling Engine for Stationary Power Generation in the 500 to 2000 Horsepower Range," Amtech, Inc., Newton, Mass., January 5, 1978.
3. Percival, W. H., Consultant and United Stirling U. S. Representative, Washington, D. C., Personal Communication, June 1978.
4. Meijer, R. J., "Prospects of the Stirling Engine for Vehicular Propulsion," Philips Technical Review, 31, No. 516, page 168-185, 1970.
5. Schrage, R. W., A Theoretical Study of Interphase Mass Transfer, Columbia University Press, New York, 1953.
6. Subbotin, et al., (Na/K Pool Boiling Reference).
7. Stirling Engine Feasibility Study of an 80-100 HP Engine and of Improvement Potential for Emissions and Fuel Economy, Final Report Prepared For U. S. Department of Energy by the Ford Motor Company, Report No. COO/2631-22, November 1977.
8. Arpacı, V. S., Conduction Heat Transfer, Addison-Wesley Publishing Company, Reading, Mass. 1966.

5. THERMAL INSULATION

The thermal insulation represents an extremely important part of the TES system. The TES system operates at high temperature (up to 1150°K) and should have capability for extended standby in the charged condition without excessive heat loss. Any heat losses, either while operating or in standby, degrade the energy efficiency of the system and represent an economic loss, and thus must be minimized. In addition, space is extremely limited — so that the volume of the insulation is very important relative to packaging of the system. Weight is also important, since weight contributes indirectly to poor energy efficiency (or vehicle range for a fixed salt weight), and a TES system is by nature heavy. For a fixed TES system weight, it is obviously desirable to maximize the ratio of the salt weight to total system weight.

For this application, Multi-Foil insulation has been selected as the best method of insulating the TES reservoir and vapor transport pipe to the Stirling engine. Multi-Foil denotes a thermal insulation in which many thin metal foils are loosely stacked and enclosed in a vacuum space; the metal foils are coated with small oxide particles which space the individual foils — preventing their contact and minimizing thermal conduction losses. As illustrated in Figure 5. 1, the multiple foils are effective thermal radiation shields; the vacuum environment eliminates convective heat transport; and the oxide particles provide a high thermal impedance

• CONVECTION — ZERO

1077-3

• RADIATION — REDUCED BY MULTIPLE REFLECTING FOILS

• CONDUCTION — MINIMIZED DUE TO:

1. SMALL FRACTION OF PARTICLES BRIDGE FOILS
2. LOW THERMAL CONDUCTIVITY OF OXIDE PARTICLES
3. HIGH PARTICLE-TO-FOIL CONTACT RESISTANCE
4. OPTIMIZED PARTICLE SIZE AND AREAL DENSITY
5. LOW THERMAL CONDUCTANCE IN PLANE OF FOIL

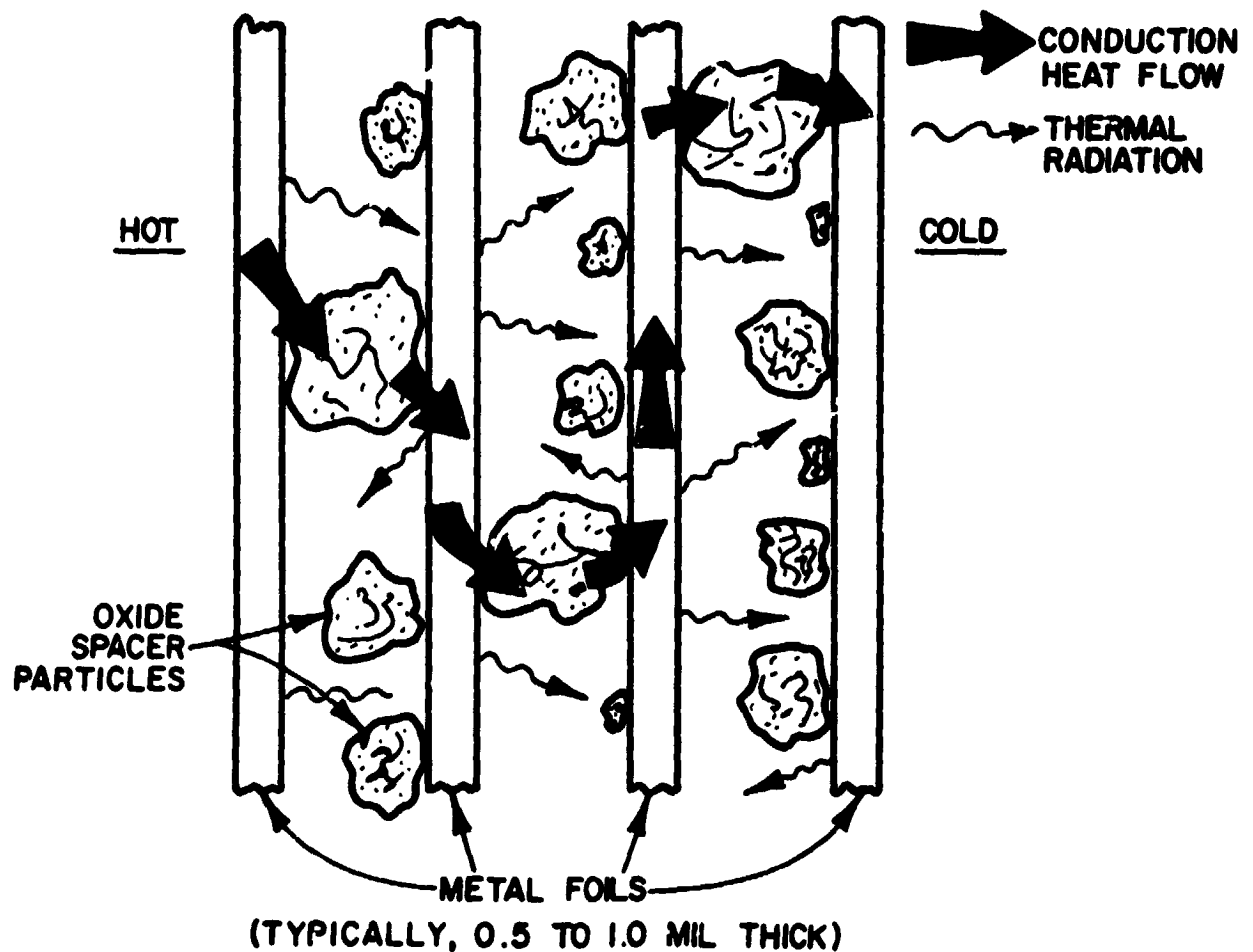


Figure 5.1 Multi-Foil Heat Transfer

to conduction by selection of oxides with low thermal conductivity, providing an extremely effective high temperature thermal insulation with small thickness (~ 0.5 in.) and low weight (~ 2 lb/ft²). The oxide particles are selected on the basis of low thermal conductivity and foil compatibility at the application temperature.

5.1 HEAT TRANSPORT THROUGH MULTI-FOIL INSULATION

The heat flux, ϕ , through Multi-Foil thermal insulation with a hard vacuum (no convection) is a function of the following parameters:

$$\phi = \phi \left(\underbrace{(T, N, P, S)}_{\substack{\text{1st} \\ \text{Order}}}, \underbrace{(T_C, \alpha, d, k_p)}_{\substack{\text{2nd} \\ \text{Order}}}, \underbrace{(\epsilon, k_{\text{FOIL}}, t_{\text{FOIL}})}_{\substack{\text{3rd} \\ \text{Order}}} \right)$$

where	T	= Heat source temperature
	N	= Number of foil layers
	P	= Pressure applied to foils
	S	= Spacing between foil layers
	T _C	= Heat sink temperature
	α	= Particle density per unit area
	d	= Characteristic dimension of particles
	k _p	= Thermal conductivity of particle spacers
	ϵ	= Emissivity of foils
	k _{FOIL}	= Thermal conductivity of foils
	t _{FOIL}	= Thickness of foils

From previous work at Thermo Electron Corporation, zirconia particles have been established as an excellent powder for coating

the foils, and the optimum particle density, α , and particle size, d , established. Thus, α , d , and k_p can be eliminated from the ρ relation.

For effective performance, it is essential that the foils be loosely stacked with no external pressure exerted, that is, the foils are not load bearing. Heat flux is given in Figure 5.2 as a function of applied pressure for Multi-Foil insulation made of nickel foils. It is apparent that an atmosphere of applied pressure greatly increases the thermal conductance of Multi-Foil insulation. With foil thickness of 0.0005 in. to 0.001 in., a total space thickness which allows at least 0.002 in. between foils is adequate. With these precautions, P and S can be eliminated from the ρ relation.

Because of the effectiveness of the insulation (low heat flux), the outer surface of Multi-Foil insulation is very close to the surrounding ambient temperature. For most terrestrial applications, T_C is about 300°K. Particularly for high-heat source temperatures, variation in T_C has very little influence on the heat flux, considering the rapid increase in radiation heat flux with temperature. T_C can thus be eliminated as an important variable from the ρ equation.

Finally, it has been experimentally demonstrated that the foil characteristics, ϵ , k_{FOIL} , and t_{FOIL} have very little influence on ρ , and can be eliminated from the equation. While it might be expected that ϵ would have an important effect, coating of the foils with the zirconia particles, evidently results in approximately the same ϵ for all foils.

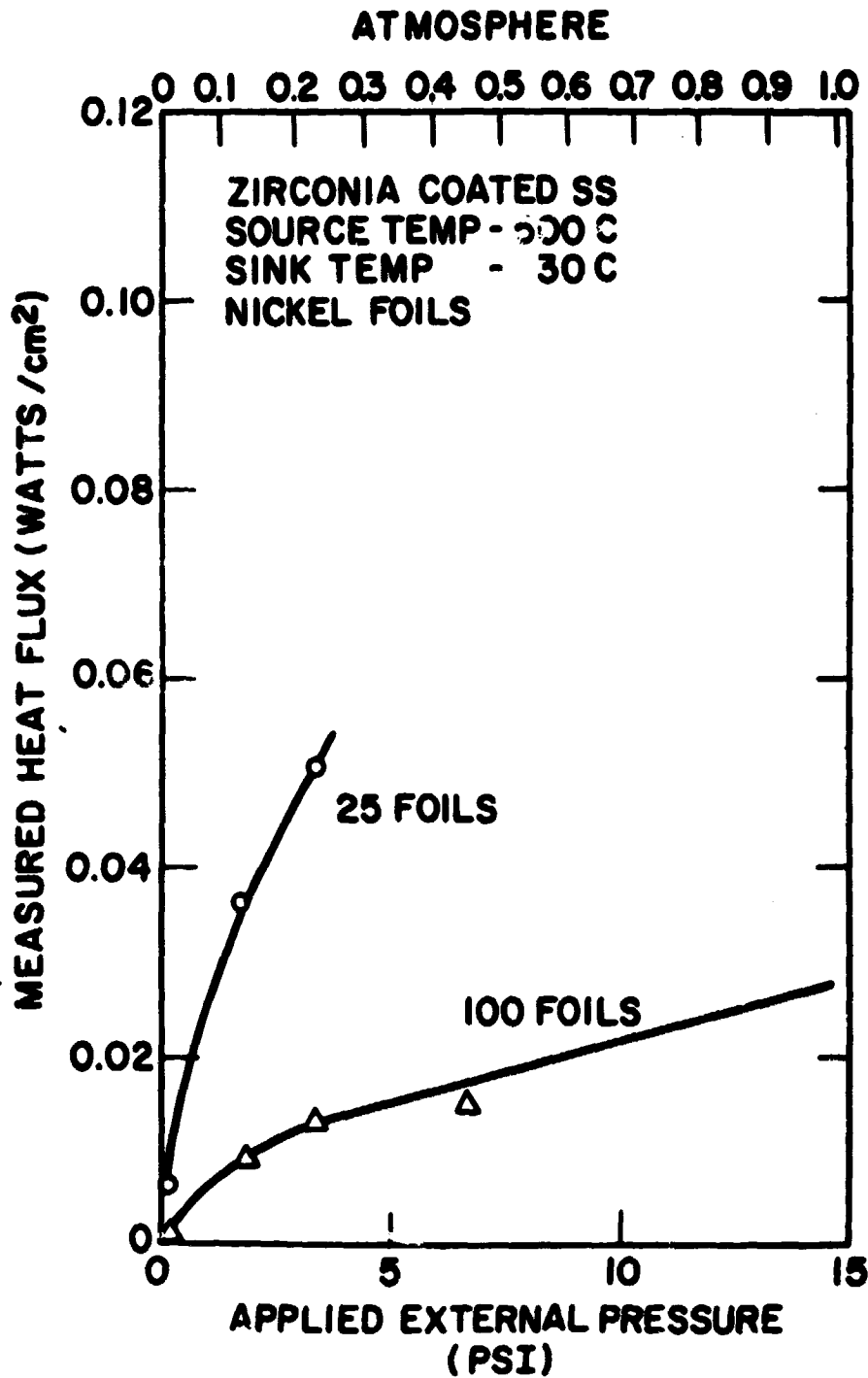


Figure 5.2 Heat Flux as a Function of Applied Pressure for Multi-Foil Insulation

Thus, for practical purposes:

$$\phi \sim \phi(T, N)$$

Assuming an ambient temperature of 300°K, analysis of measured heat flux curves (for a given number of foils) gave the theoretically expected fourth power dependence on source temperature. However, for a given source temperature, a 1/(N + 1) dependence was not satisfactory, especially for N < 20 foils. For the "Conventional" Multi-Foil data, the following function was found to give reasonable agreement to the measurements:

$$\phi \frac{\text{watt}}{\text{cm}^2} = \frac{1.06 \times 10^{-12} [T^4 - (81 \times 10^8)]}{0.778 N + (1.11 \times 10^{-2}) N^2}$$

where ϕ = Heat flux perpendicular to the foils

T = Heat source temperature, /°K

N = Number of foils

Heat flux as a function of source temperature, parametric in number of foils, is given in Figure 5.3. Although these curves were developed from measurements on nickel Multi-Foil assemblies, they are applicable to insulation packages fabricated from stainless steel, aluminum or other metal foils, since, as pointed out above, the heat flux is insensitive to the foil metal.

It should be noted that great care must be taken in the design and fabrication of Multi-Foil assemblies to minimize heat losses at joints, such as the intersection of two edges which cannot be wrapped with continuous foil. Typically, these joint losses can be as high as the heat losses directly through the foil. Several

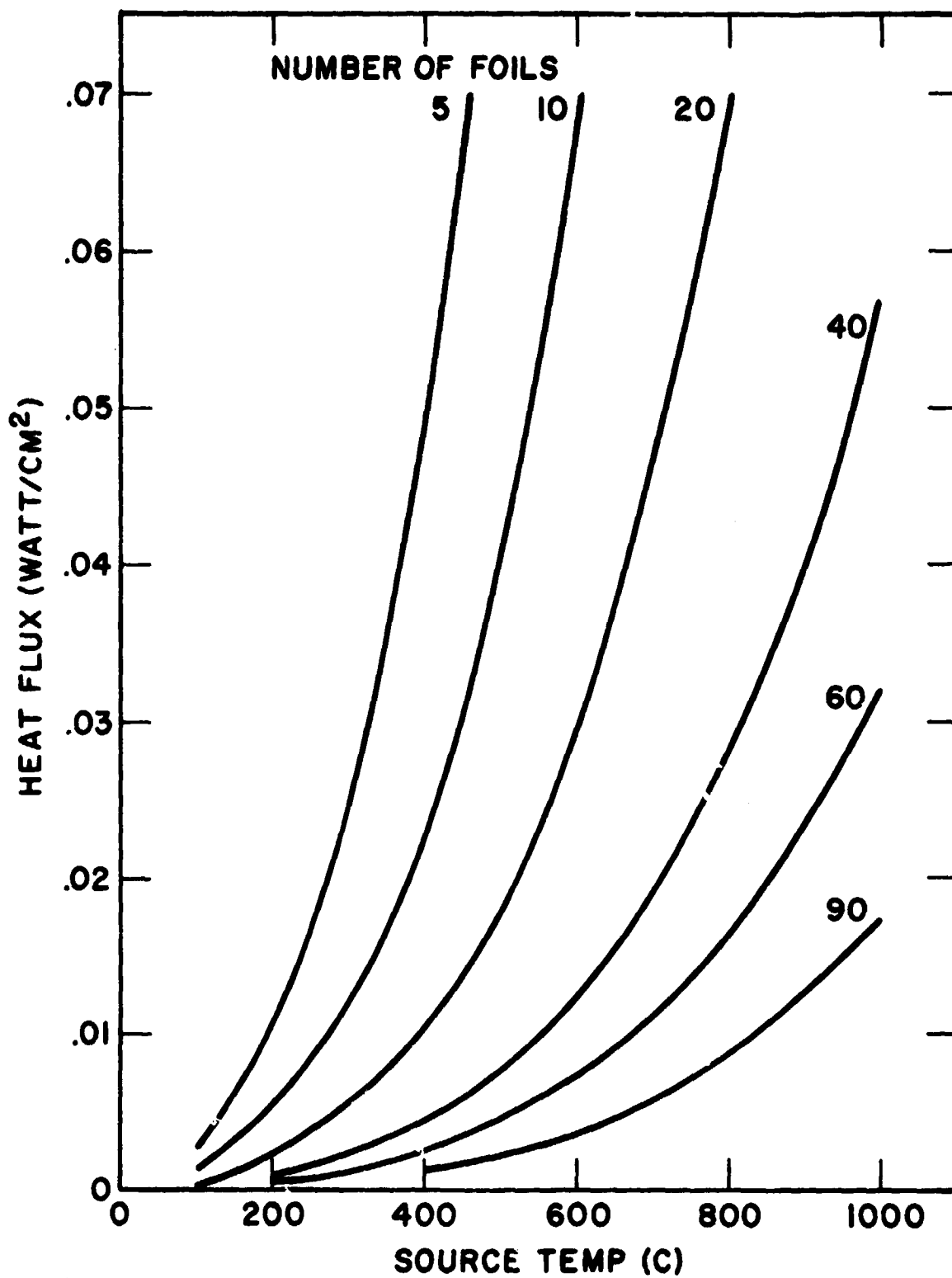


Figure 5.3 Multi-Foil Heat Flux Calculated from Function Fit Expression (Fitted to Experimental Data)

techniques have been developed at Thermo Electron Corporation to minimize these joint heat losses. It should also be noted that methods have been developed for application to ducting bends, flanges, penetrations, and other irregularly shaped surfaces, by use of a "tape" Multi-Foil insulation, rather than wide sheets. In this technique, a tape of suitable metal foil coated with the optimized oxide coating is used to continuously wrap with reverse bias the areas to be thermally insulated. On large flat surfaces or straight cylinders, much wider sheets of foil are used, with the sheets either precut to the proper size and stacked on the surface, or wrapped as a continuous sheet around a straight cylinder or box.

A high vacuum must be maintained in the foil if good insulating performance is to be achieved, since the insulating properties degrade above 10^{-4} torr. In Figure 5.4, the effect of helium pressure on heat loss from a 9-layer foil insulation is illustrated; the effect of pressure is greater when a much larger number of foils are used with $\sim 10^{-3}$ to 10^{-4} torr required for 90 foils. It is therefore essential that the foil enclosure be leaktight and the entire unit be thoroughly degassed prior to pinchoff. The stringent requirements on leak-tightness are evident from Figure 5.5, which gives the time to reach 10^{-3} torr as a function of initial helium leak rate for an insulation enclosure of approximately the same size as for the TES system. The sensitivity limit for available leak detectors is approximately 10^{-8} cm³/sec. A leak of this size will degrade the vacuum in the foil insulation to an unacceptable level in about 500 hours. Leaks of this magnitude can be gettered by commercially

A-1144

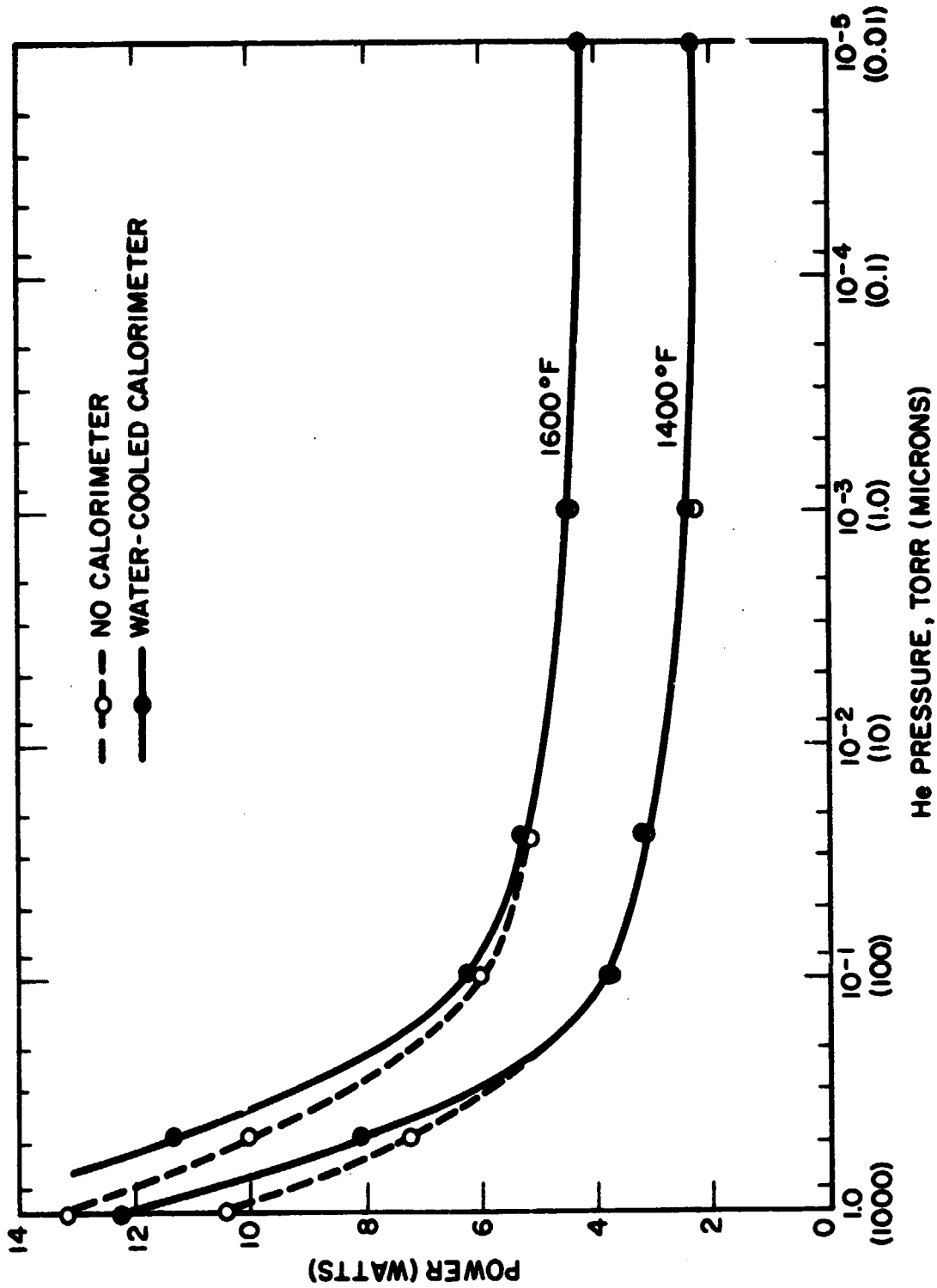


Figure 5.4 Effects of Helium Pressure on the Heat Loss for a 9-Cup System (Run 10) With and Without a Water-Cooled Heat Sink

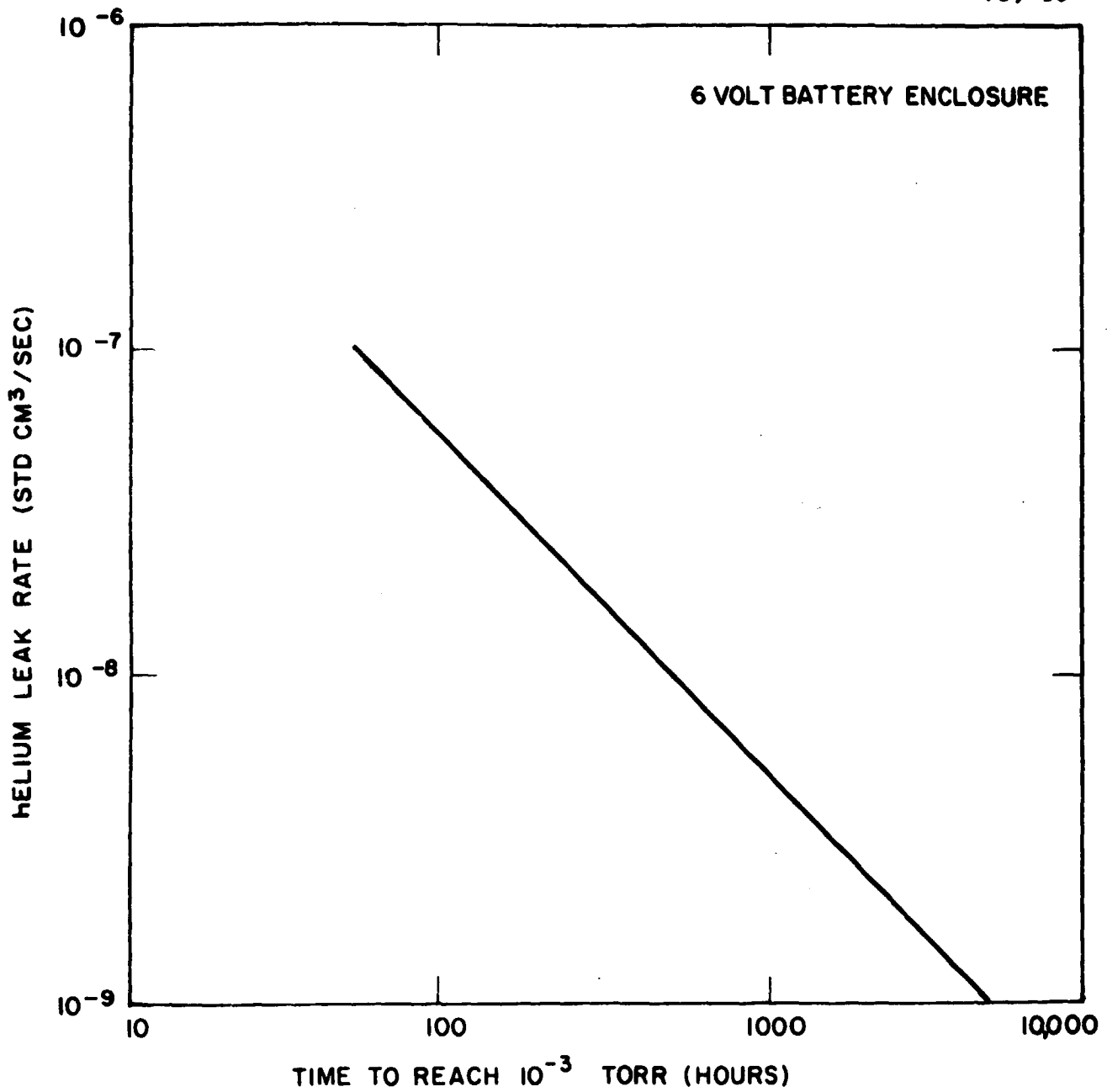


Figure 5.5 Time to Reach 10⁻³ Torr
as a Function of Helium
Leak Rate

available materials used in the electronics industry. For example, a recent Multi-Foil battery enclosure has utilized copper turnings to getter oxygen and CerAlloy 400 (which is an alloy of rare earth metals, aluminum and thorium) to getter nitrogen and other gases.

5.2 DESIGN CONSIDERATIONS AND PERFORMANCE

A key design requirement is provision of a vacuum-tight envelope for the space containing the Multi-Foil insulation. This envelope must be structurally self-supporting, since pressure on the Multi-Foils severely degrades their performance. Even though this requirement introduces great design difficulties for larger systems, successful designs were developed for both the cylindrical and rectangular configurations as described in detail in Chapter 6.

The number of foils is an important design consideration. In Figure 5.6, the heat loss is presented as a function of the number of foils with a heat source temperature of 850°C (1123°K), near the melting point of the two reference salts. Based on this curve, 90 foils was selected for the reference design, since the heat loss decreases slowly with additional foils above 90. With 90 foils, the heat loss is 0.01 watts/cm².

For the foils, it is desirable to use as thin a foil as possible (i. e., a very ductile metal which can be rolled to thin foils) with a metal which has low density and is inexpensive. The best material is aluminum, provided the temperature is low enough for its use. Aluminum obviously cannot be used at temperatures near or above its melting point of 660°C (933°K). A composite foil package can

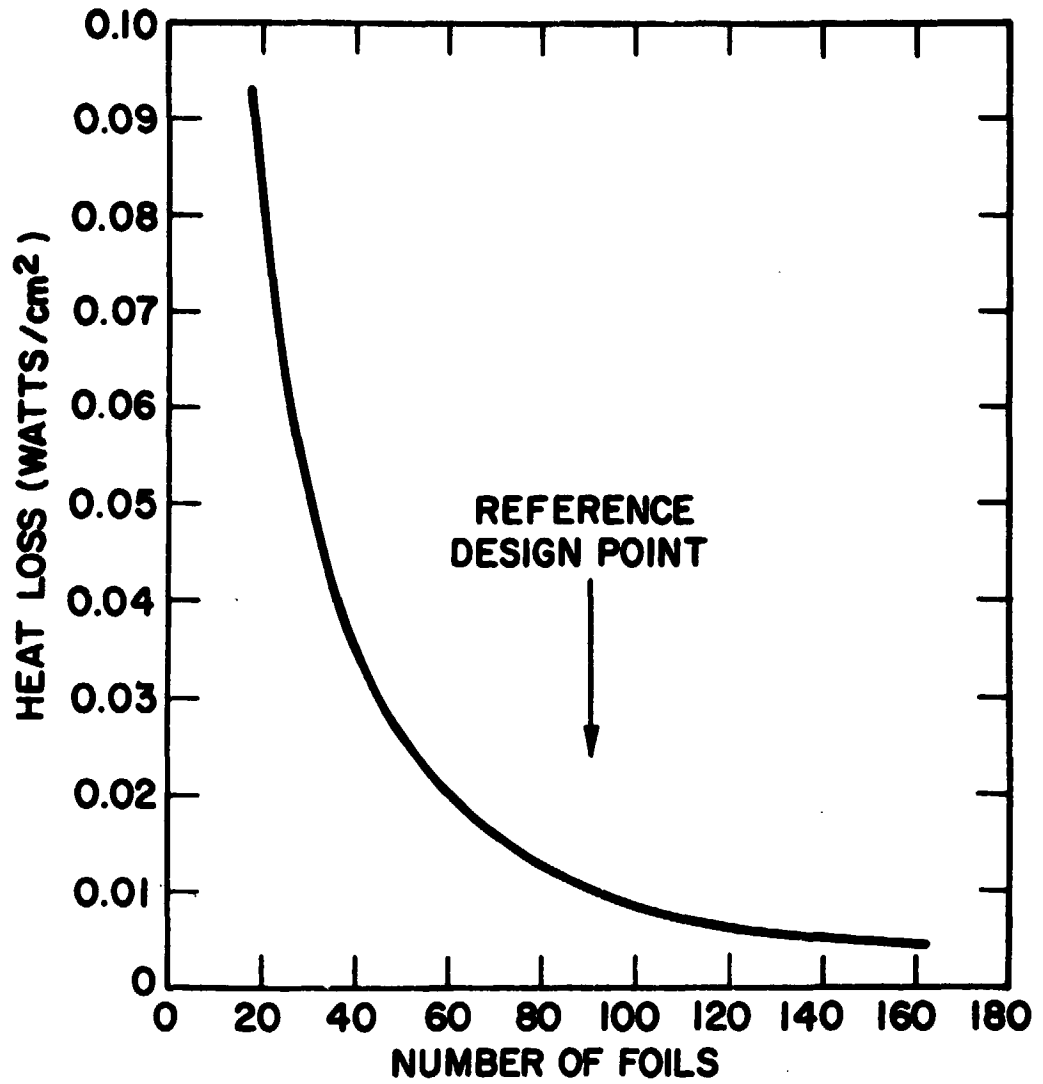


Figure 5.6 Multi-Foil Insulation Heat Loss as Function of Number of Foils, $T = 850^{\circ}\text{C}$

be used, however, in which aluminum foil is used in the lower temperature part of the insulation and a different material in the high-temperature region. The temperature profile across the foil insulation is not linear, as illustrated in Figure 5.7, for measured temperature profiles across 60 zirconia-coated foils. These temperature distributions are more linear than calculated on the assumption that the only mode of heat transfer is radiation. Conduction across metal oxide particle bridges tends to linearize the temperature profile.

To minimize the weight and cost, the insulation for the present application is a composite foil package consisting of 50 layers of 0.001-inch thick stainless steel foil in conjunction with 40 layers of 0.0005-inch thick aluminum foil. The interface temperature between the hot stainless steel and the cooler aluminum foils is $\sim 450^{\circ}\text{C}$. It should be noted that use of 0.0005-inch thick stainless steel foils would reduce the insulation weight, and that use of soft iron foils (feasible because of the vacuum/environment) would reduce the cost. However, neither of these options was selected, since a check of vendors indicated considerable doubt in the technical feasibility of their manufacture at reasonable cost. Stainless steel foil 0.001-inch thick was thus selected for the reference design.

An envelope spacing of 0.5 inch was selected for the 90 foils, providing an average space for each foil of 0.0056 inch. This spacing is sufficient to assure loose packing of the foils, even with some deflection of the envelope structure. With this spacing, and

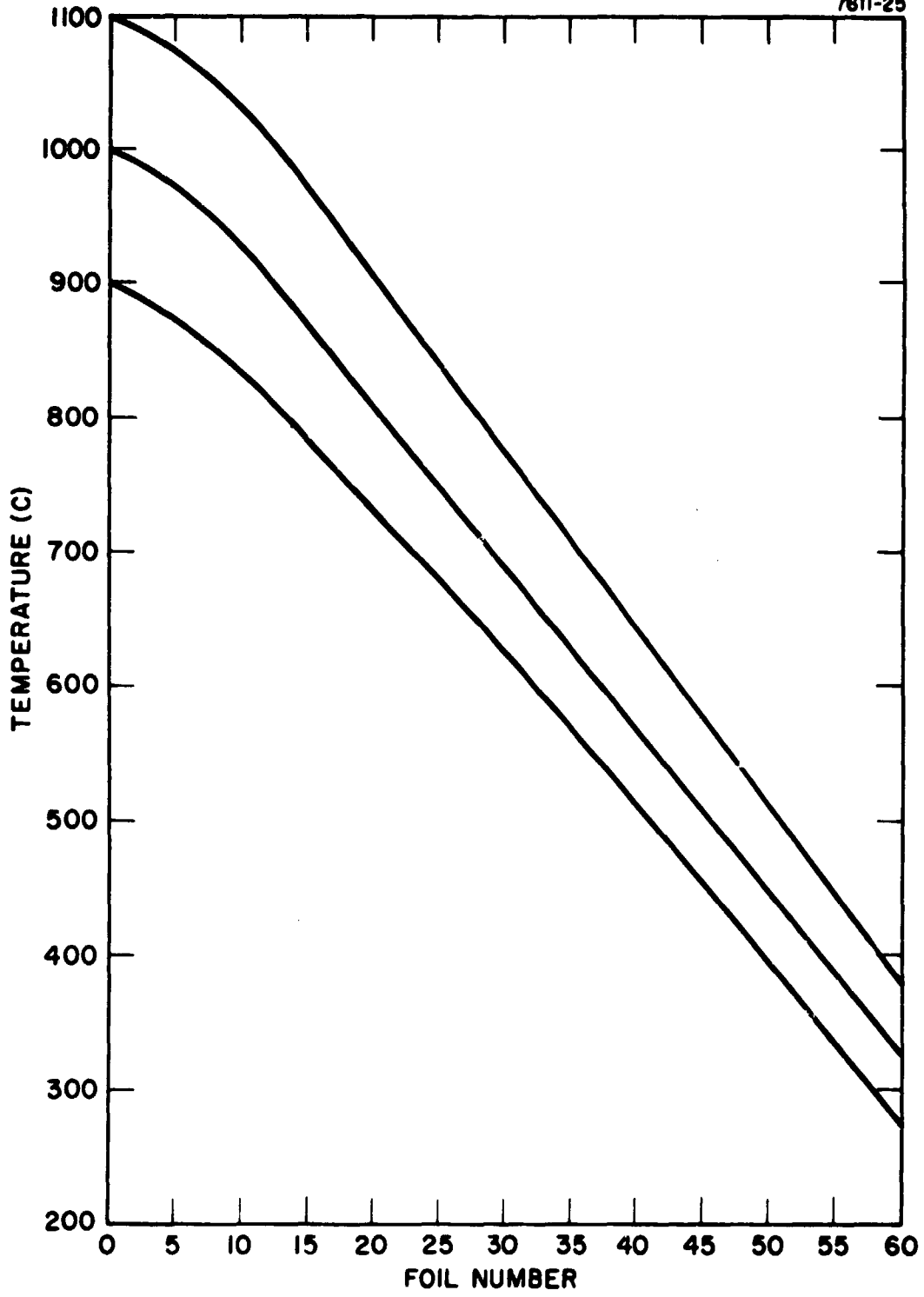


Figure 5.7 Measured Temperature Distribution Through Cylindrical Foils

heat source temperature of 850°C, the effective thermal conductivity of the insulation is 1.54×10^{-5} watt/cm-°C (8.9×10^{-4} Btu/hr-ft. °F). This k is lower by a factor of at least 25 than the best fibrous insulation in air (Min-K with $k \approx 3.9 \times 10^{-4}$ w/cm-°C). Furthermore, the spacing could be reduced somewhat from 0.5 inch without affecting the insulating performance with a corresponding reduction in the effective k.

With the spacing of 0.5 inch and the selected foils, the insulation weight per unit area is 2.33lb/ft² [11.35kg/M²], with the 50 stainless steel foils contributing 88 percent of the weight, and the 40 aluminum foils only 12 percent. If 0.0005-inch thick stainless steel foil could be used, the insulation weight would be reduced to 1.30lb/ft², with 78-percent due to the stainless steel and 22 percent to the aluminum.

In summary, Multi-Foil vacuum insulation provides an extremely effective high-temperature insulation, with very low weight and very low volume characteristics, which are extremely important for an automotive TES system.

5.3 OVERALL SYSTEM CHARACTERISTICS

The two configurations have outer shell areas of 38 ft² (35300 cm²) for the rectangular box and 40 ft² (37200 cm²) for the two cylinders described in detail in Chapter 6. Total heat loss rates through the container walls (at 0.01 watts/cm²) are therefore 0.35 kwth for the rectangular box and 0.37 kwth for the two cylinders, respectively, with an interior temperature of 850°C. This heat loss rate

over 24 hours represents the percentage of the total storage capacity for the two units as shown in Table 5. 1. The total energy loss over 24 hours is, however, relatively small — amounting to ~29,500 Btuth per day. At \$4.0 per million Btuth (typical of current fuel energy price to home owner), this lost energy has a value of only \$0.12, and is thus acceptable from a cost point-of-view. Other heat losses, such as from the discharge heat pipe when operating or radiation from the TES reservoir down the discharge heat pipe when not operating, will add somewhat to the direct heat loss through the containment envelope of the TES reservoir.

The overall insulation weight (at 2.33 lb/ft²) is 88 lbs and 93 lbs, respectively, for the rectangular and cylindrical units. The values were increased to 95 lbs and 100 lbs, respectively, to allow for forming of joints.

It is useful to compare the performance of the Multi-Foil with a conventional, high-performance, high-temperature insulation — specifically, molded Min-K insulation (Johns-Manville Corporation) with a thermal conductivity of 3.9×10^{-4} w/cm-°C and density of 0.32 gm/cm³ (20.0 lb/ft³). The heat loss from the insulation can be expressed as follows:

$$q = \frac{T_{HS} - T_{Amb}}{R_I + R_S}$$

where q = heat loss, w

T_{HS} = temperature of heat source on hot surface, °C.
 T_{Amb} = temperature of surrounding air, °C.
 R_I = thermal insulation heat transfer resistance

TABLE 5.1
24-HOUR HEAT LOSS AS
PERCENTAGE OF STORAGE CAPACITY

<u>Configuration</u>	<u>LiF</u>	<u>NaF/MgF₂</u>
Rectangular	5.0%	6.8%
Cylindrical	6.6%	9.0%

$$= \frac{\bar{X}}{k_I A}, \frac{^\circ\text{C}}{\text{w}}$$

R_S = thermal resistance for convection and radiation from the insulation surface

$$= \frac{1}{(h_c + h_r) A}, \frac{^\circ\text{C}}{\text{w}}$$

\bar{X} = insulation thickness, cm.

k_I = insulation thermal conductivity, w/cm- $^\circ\text{C}$

$h_c + h_r$ = heat transfer coefficient representing convection and radiation loss from surface, $\frac{\text{w}}{\text{cm}^2 \cdot ^\circ\text{C}}$

A = heat transfer area, cm^2

For the present case,

$$q = 360 \text{ watts}$$

$$A = 36000 \text{ cm}^2$$

$$T_{HS} = 850^\circ\text{C}$$

$$T_{\text{Amb}} = 25^\circ\text{C}$$

$$k_I = 3.9 \times 10^{-4} \text{ w/cm-}^\circ\text{C}$$

$$h_c + h_r \approx 9.0 \times 10^{-4} \text{ w/cm}^2 \cdot ^\circ\text{C}$$

The Min-K thickness required to achieve the same heat transfer rate as the Multi-Foil insulation with these parameters is 31.7 cm (1.04 ft) with a specific weight of 20.8 lb/ft². The insulation volume

is 25 times greater and the weight 9 times greater than for the Multi-Foil. For the two systems described in Chapter 6 and for equivalent heat loss, the Min-K weight (for 40 ft²) would be 380 kg, which can be compared to the total TES system weight specification of 500 kg.

A composite insulation of Min-K/Multi-Foil was also considered, with the thought of either reducing the temperature of the Multi-Foil sufficiently so that aluminum foils could be used throughout (Min-K on high temperature side), or reducing the amount of high-temperature foil required (stainless steel), by placing Min-K on the low-temperature side. For effective performance of the composite, approximately equal thermal resistances would be required or:

$$\frac{\bar{X}_{\text{Min-K}}}{k_{\text{Min-K}} A} \approx \frac{\bar{X}_{\text{Multi-Foil}}}{k_{\text{eff}}^{\text{Multi-Foil}} A}$$

$$\frac{\bar{X}_{\text{Min-K}}}{\bar{X}_{\text{Multi-Foil}}} \approx \frac{k_{\text{Min-K}}}{k_{\text{eff}}^{\text{Multi-Foil}}} = \frac{3.9 \times 10^{-4}}{1.54 \times 10^{-5}} = 25$$

Thus, the Min-K volume of the composite would be about 25 times that of the Multi-Foil (and the weight ratio about 9 times). Consideration of these ratios, coupled with the fact that the problem of a vacuum enclosure still exists, eliminated this composite approach from further consideration.

In summary, Multi-Foil vacuum insulation was selected as the best approach for an automotive TES system operating at high temperature.

It provides an extremely effective thermal insulation, with very low heat loss, and with an absolute minimum of volume and weight — all extremely important considerations for this application. It does introduce the problem of a self-supporting vacuum enclosure on a relatively large structure with minimum weight. Practical designs for the vacuum enclosure were developed, however, as described in detail in Chapter 6. The vacuum enclosure must also be extremely leak-tight, and considerable development will be required to develop reliable seam-welding techniques for large-scale manufacture which provide this leak-tightness. For both design configurations, a design criterion has been to restrict the design to straight seam welds suited for automated machine welding, and there should be no reason why the required leak-tightness cannot be achieved, either in large volume production or in prototype construction. The cylindrical configuration has much less welding than the rectangular configuration, an important advantage.

6. TES RESERVOIR DESIGN

6.1 INTRODUCTION

Thermal energy storage systems are much heavier and require a much larger volume than the liquid hydrocarbon storage (gasoline) now used. The criteria important in packaging such a system in a vehicle are:

- Low center of gravity
- Equal weight distribution on wheels
- Minimum encroachment on passenger/freight volume
- Maximum impact protection
- Short vapor transport line to engine
- Relatively large diameter 10 cm transport line to engine
- Maximum collision protection and minimum hazard to passengers feasible

In the TES system design, great emphasis was placed on selecting a configuration (outer envelope) that permitted passenger and freight volume equivalent to that of current automobiles. Rather than fit the vehicle around the TES, the TES was to be fit into the vehicle with minimum deviation from the current automobile, as far as trunk/freight volume and passenger volume and seating are concerned.

With this prime consideration in mind, as well as the other criteria, the best location for the TES reservoir is between the wheels and beneath the floorboard of the vehicle. This location requires a relatively low height for the TES reservoir with a large

plan area to provide the required internal volume. In Figures 6.1 and 6.2, the space available for the TES system in a Volkswagen transporter is illustrated; the available space is

41 in.(w) x 60 in.(l) x 15 in.(h), without

modification to the vehicle. Incorporation into a conventional compact car would require substantial modification of the vehicle to incorporate the height of the TES unit, while still retaining the trunk and passenger volume. As illustrated in Figure 6.3 for a Ford Pinto-size automobile, the vehicle roofline would have to be raised approximately the height of the TES reservoir (perhaps less by 2-4 cm), providing a relatively boxy vehicle. With this modification, a volume of 48 in.(w) x 60 in.(l) x 12 in.(h) can be utilized for the TES reservoir. A significant design effort would be required to develop a non-van compact automobile with the TES integrated as illustrated in Figure 6.3; but such a vehicle appears practical and would still provide trunk/freight and passenger volume equivalent to current automobiles.

The optimum configuration of the TES reservoir for integration into a practical automobile of either the van or conventional automobile type is one which has relatively low overall height (≤ 15 in) and a large plan area. Two approaches were evaluated with detailed structural analysis and preliminary detail design drawings prepared. One was a rectangular box with an overall height of 15 in. and plan dimensions of 41 in. x 41 in. The other was a cylindrical configuration with ellipsoidal heads; two cylindrical

28-478

AVAILABLE SPACE APPROXIMATELY : 41"W x 60"L x 12.9"H (18.4 FT³)

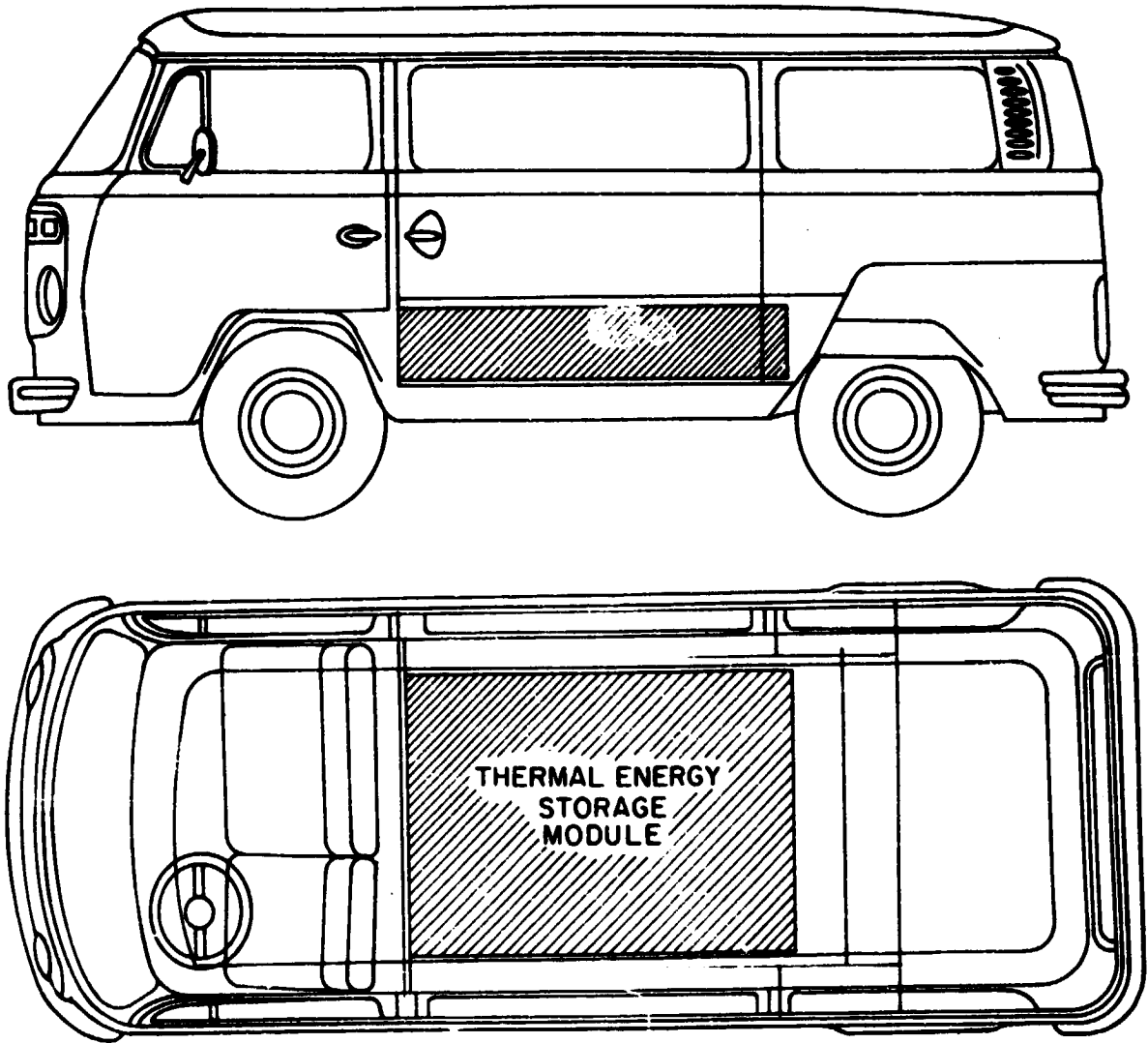


Figure 6.1 Location of TES Module in VW Transporter

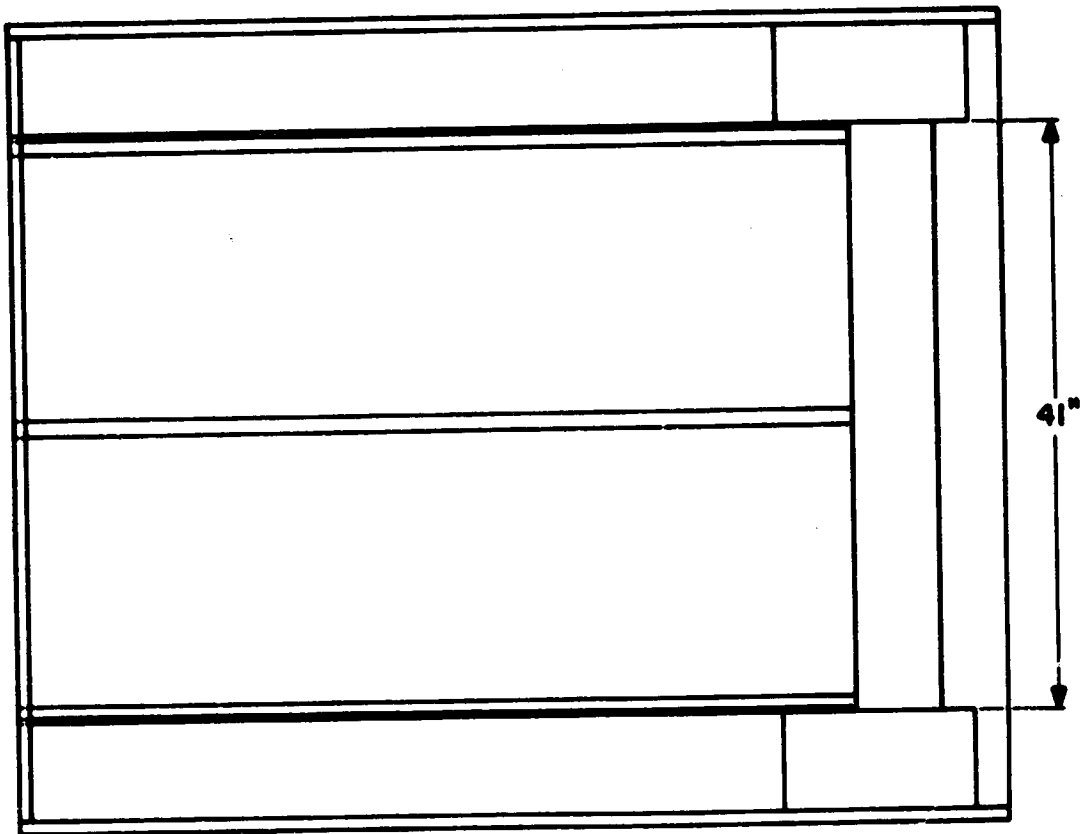
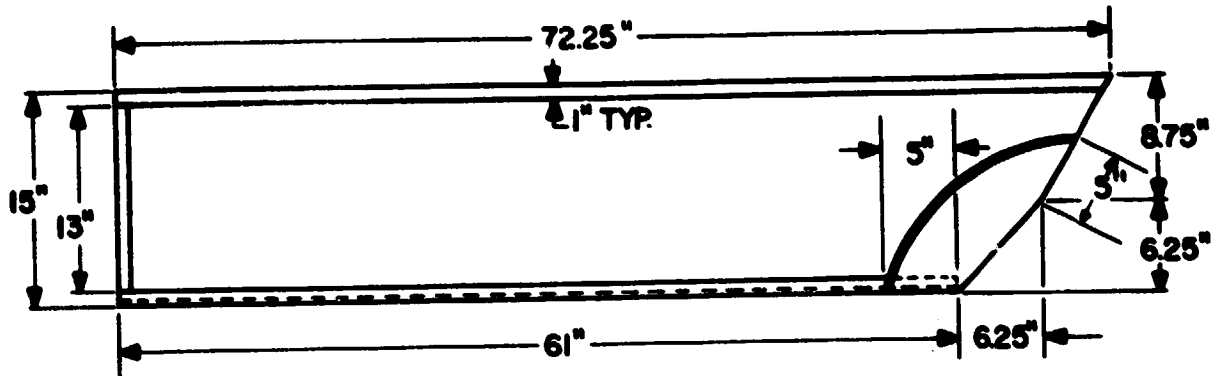


Figure 6.2 Space in VW Transporter for TES Module

60-478

HEIGHT
INCREASE
~10" (7")

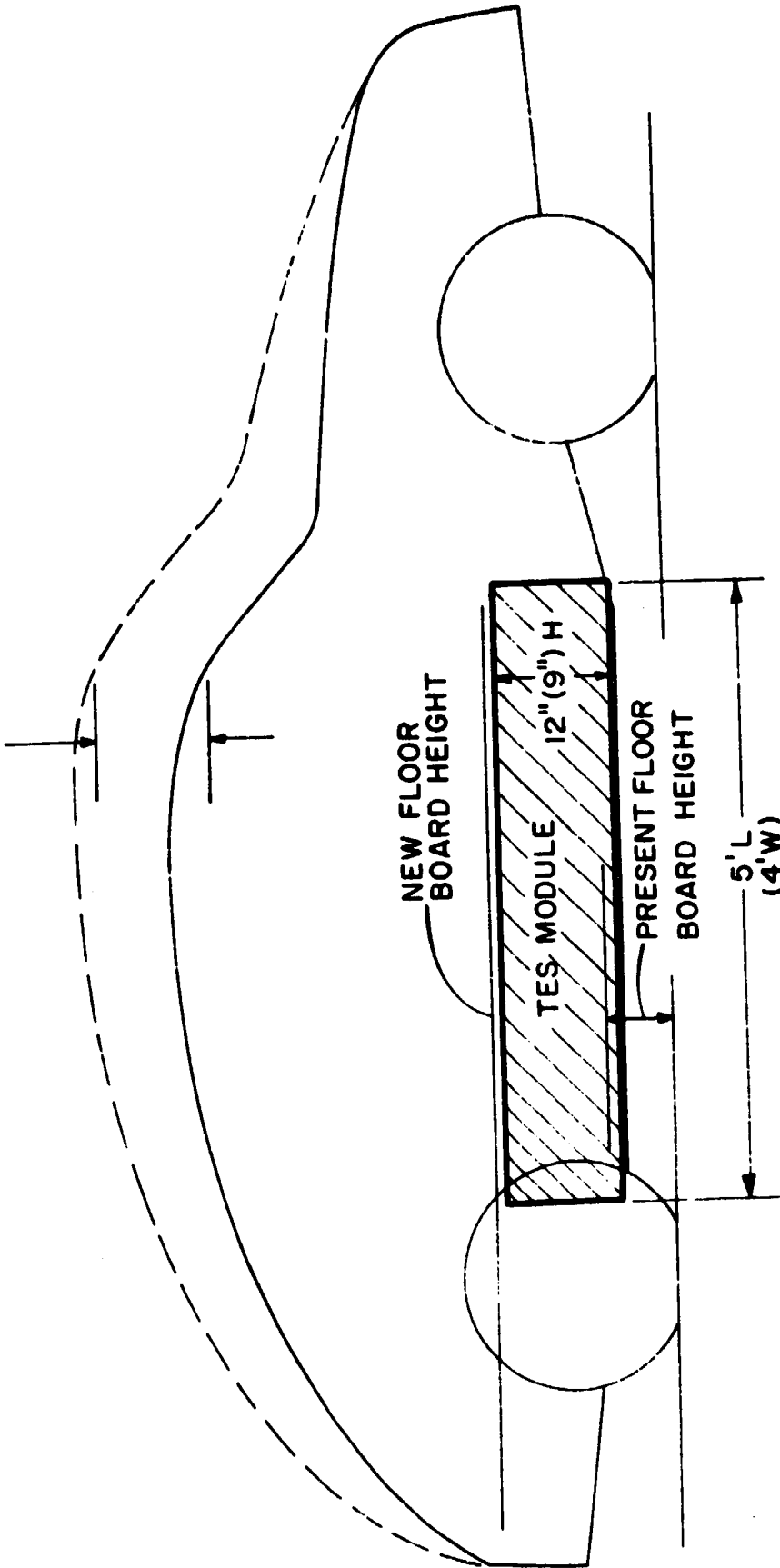


Figure 6.3 Location of TES Module in Ford Pinto-Size Car

units with overall dimensions of 15 in. (OD) x 60 in. (L) are required, to be packaged side-by-side in the selected space in the vehicle. The rectangular configuration is better suited for integration into the vehicle, but the necessity for use of vacuum, Multi-Foil insulation introduces structural design and manufacturing problems. These problems arise because of the necessity of self-supporting flat surfaces of relatively large area and minimal weight across which a substantial pressure differential exists. The cylindrical unit is efficient as a pressure vessel and easier to manufacture, but does not use the vehicle space as efficiently as the rectangular configuration.

Feasible designs were developed for both the rectangular box and cylindrical shell configurations and are described in this section. An important consideration in the evolution of the designs was adaptability to automated, high-volume production. A detailed manufacturing and cost analysis was carried out for each configuration with the results presented in Chapter 8. Another consideration in the design was a large surface area or heat transfer area for the salt containers, with the maximum salt thickness through which heat must be transferred small enough to result in an insignificant ΔT in the salt.

6.2 DESIGN CRITERIA

The thermal energy storage reservoir must function at temperatures slightly higher than the melting point of the salt, and

maintain its integrity in a corrosive environment that includes solid and liquid salt and liquid and gaseous potassium. In addition, the TES reservoir must function in the mechanical environment typical of a car, including accelerations and vibrations inherent in normal driving and accelerations due to collisions or road hazards.

Loss of heat from the TES reservoir is minimized by using Multi-Foil insulation, which requires a vacuum. To achieve the required vacuum, the TES reservoir uses two containers, one inside the other. The inside unit stores the salt and is used to perform the heat transfer function; the space between the two containers is filled with Multi-Foil insulation.

The functional requirements can be summarized as follows:

● Environment

- Liquid and solid salt (LiF or NaF/MgF_2)
- Potassium liquid and vapor

● Mechanical

- Vacuum between inner and outer container
- Operating and collision accelerations and vibrations for an automobile

The design goal for the TES reservoir is a unit that will store a minimum 300 kg of salt and will meet the functional requirements during a 10-year design life. To achieve the design goal, the functional requirements must be translated into design criteria.

An important consideration in the design was to maximize the ratio of salt weight to total reservoir weight and salt volume to total reservoir volume, that is, to reduce as much as possible the TES structural weight and the volume required for the structure and heat transfer media.

6.2.1 Design Approach

The primary design requirements for the TES reservoir are to (1) provide a containment system for solid or liquid salt, (2) provide a means of heat transfer in and out of the salt, and (3) provide an efficient insulation around the contained salt. The first and second requirements lead to the need for a container that can operate at high temperature up to 1150°K (1610°F), and that can sustain internal pressure resulting from the vapor pressure of potassium used as the heat transfer medium. If the third requirement is met with Multi-Foil insulation, a system that requires a vacuum for its operation, then a second container that encloses the inner container and the insulation is needed. Therefore, the TES reservoir consists of two containers, one inside the other, separated by the Multi-Foil insulation.

Any structural design must allow thermal expansion and contraction of the inner container to occur without overstress; because of the very large magnitude of these movements, it was decided that they should be allowed to occur freely. Thus, the inner container must be supported so that it can expand and contract without causing restraint forces. As a consequence of allowing thermal movement, both the inner and the outer containers must be designed as independent pressure vessels with no support from each other.

Two designs were developed, one rectangular and one cylindrical; these are described in detail later. In both designs, the inner container is supported on four sliding pins which provide support but do not restrain expansion and contraction. The outer container is also supported by these pins at the points where they pierce through the outer container. Consequently, the containers are structurally independent of one another. Adequate clearance between them must be maintained to accommodate deformation due to pressure and acceleration loads, and the thermal movement.

6.2.2 Loads

Mechanical loads to be considered are differential pressures acting on the container walls, dead weight, inertia loads due to longitudinal and vertical accelerations, and temperature loads.

The pressure inside the inner container of the TES reservoir varies from 0 to 30 psia — depending on the salt and potassium temperature; the pressure outside the outer container is atmospheric; and the Multi-Foil insulation between the inner and outer containers is in a vacuum. Therefore, the design pressures are:

- Inner container 0-30 psi internal pressure
- Outer container 15 psi external pressure

The transient accelerations for structural integrity are specified by the contract as:

- Vertical 3.5 g
- Longitudinal 6.0 g

- Vibration Rates 10-20 cycles/sec
- Slew Rate 2 rad/sec

The temperatures inside the inner container are slightly higher than the melting point of the salt. Lithium fluoride has a melting point of 1121°K (1559°F) and the sodium fluoride/magnesium fluoride eutectic has a melting point of 1103°K (1526°F). The thermal energy storage capacity of the reservoir is based on a temperature range of 800°K (980°F) to 1150°K (1610°F); this is also the design temperature range for the reservoir. Thermal loads are a function of temperature and configuration of the structure.

6.2.3 Material Selection

The material selection for the inner box is governed primarily by the sustained high pressure (30 psia) at high temperatures (1150°K) and the corrosive environment (liquid salts and potassium). In addition, the requirements of fabricability and minimum weight must be considered. These requirements narrowed the possible materials to high-nickel alloys, and of these, to the ones exhibiting the highest strength properties at the maximum operating temperatures. The critical properties considered in this selection were (1) stress to rupture in 10,000 hrs and (2) creep strength (1% minimum creep rate in 10,000 hrs). The alloy selected is Inconel 617 (a registered trademark); its composition is given as 54% nickel, 22% chromium, 12.5% cobalt, 9% molybdenum, and 1% aluminum. Of the alloys reviewed, it had the highest stress to rupture (6.7 ksi) in 10,000 hours at 1600°F.

The manufacturer (Huntington Alloys, Inc.) indicates that Inconel 617 is a relatively new alloy and only limited corrosion test data are available for it in contact with liquid salts or potassium vapor; however, this alloy does have good-to-excellent resistance to cyclic oxidation and to carburization at temperatures to 2100° F, to corrosion by sulfuric, phosphoric, and hydrofluoric acid, to corrosion by sodium hydroxide, and to stress corrosion cracking. As described in Chapter 2, test data with several fluoride salts at ~1000° K indicate excellent compatibility for long-term exposure. In summary Inconel 617 would be expected from its alloy composition to have excellent corrosion resistance, and available data support this conclusion. More extensive corrosion testing must be performed for the particular conditions of this application before a definitive conclusion can be reached, however.

The outer box operates under ordinary ambient conditions, and therefore carbon steels, high-strength low-alloy steels, or aluminum may be used. When the container is designed as a cylindrical shell, buckling, and not high strength, is the governing criterion; ordinary carbon steel is therefore selected for this application. For the rectangular container, the design is governed by the bending of panels with large span-to-thickness ratios; to control deflections while minimizing weight, honeycomb sandwich panels were selected. The selection of the specific panels is discussed in Section 6.3, describing the rectangular structure.

6.2.4 Allowable Stresses for Inconel 617

Design allowable stresses for Inconel 617 were based on data published by the manufacturer, Huntington Alloys, Inc.,¹ supplemented by engineering judgement in use of the data for this application. Considerations in selecting allowable stresses were:

- Type of Stress - e. g. , primary membrane stress,
secondary bending stress.
- Duration of Stress - e. g. , sustained load, dynamic
load of short duration.

The selection of allowable stresses is complicated by the cyclical operation of the TES system with the temperature varying over each cycle. Since the internal pressure in the inner container depends on the salt temperature (vapor pressure of potassium), this cyclical operation results in a stress-time history in the TES reservoir that depends on the mode of use of each vehicle. There are no codes or other authoritative criteria for selecting design stresses under these conditions, and improvisation was required to set allowable stresses, as summarized in Table 6. 1. Selected strength properties of Inconel 617 are summarized in Table 6. 2.

For sustained loads, the creep strength is the important stress value. The selected value of 3. 0 ksi was based on 90 percent of the 0. 5 percent creep strength over 10, 000 hours at 1600°F (1144°K). This level is believed to be consistent with a design life of 10 years (87, 600 hours), since the system will operate at substantially lower temperatures than 1144° over most of its life period. The TES

TABLE 6.1
SELECTED ALLOWABLE STRESSES FOR INCONEL 617

Type of Stress	Allowable Stress (ksi)
Primary membrane stress due to pressure.	3.0
Primary membrane stress due to pressure plus membrane stress due to gravity load.	3.0
Primary membrane stress due to pressure plus local bending discontinuity stress.	6.7
Primary membrane stress due to pressure plus membrane stress due to gravity plus local bending discontinuity stress.	6.7
Primary membrane stress due to pressure plus membrane stress due to gravity plus local bending discontinuity stress plus membrane or bending stress due to acceleration loads.	16.0

TABLE 6.2
STRESS LEVELS OF INCONEL 617

A. For 10,000 hr Sustained Load

Temperature (°F)	Stress Rupture	1% Creep Strength (ksi)	0.5% Creep Strength
1550	9.0	5.0	4.0
1575	7.8	4.4	3.6
1600	6.7	3.9	3.3

B. For Dynamic Loads

Temperature (°F)	Yield Strength (0.2% Offset) (ksi)	Tensile Strength (ksi)
1000	27	82
1200	24	81
1400	25	63
1600	27	40

reservoir will be at temperatures above the melting point of the salt, [1121°K(1558°F) for LiF and 1103°K(1525°F) for NaF/MgF₂] for only a very small fraction of the time, and substantial time may be spent at temperatures below the melting point down to 800°K, since use is made of the solid sensible-heat as a significant contribution to the total storage capacity.

For load combinations that include secondary stresses (discontinuity stresses) in addition to primary bendings, the ASME code² specifies: "The allowable stress shall be 3.0 times the allowable value for primary membrane stress, but not to exceed the rupture stress". The allowable stress for this loading was thus taken as the rupture stress at 1144°K(1600°F), for 10,000 hours — 6.7 ksi.

The primary bending and gravity stresses, as well as the discontinuity stresses, are sustained loads; of course, as previously stated, the temperature fluctuates and so does the pressure — nevertheless, there are primary membrane stresses at all times. This is not the case for collision accelerations which are one-time occurrences; therefore, the allowable stresses for collision acceleration loads can be based on the high-temperature yield strength (0.2-percent offset). The allowable stress for combined static and acceleration loads is chosen as two-thirds of the lowest yield strength, or 16.0 ksi. The lowest yield strength is not at the highest temperature, and the allowable stress is therefore based on the lowest yield strength in the operating temperature range.

Another concern is acceleration loads encountered in normal driving, and the problem of low-amplitude fatigue. Considering that for normal driving vertical impact accelerations are often taken as 0.25g (14 times smaller than design collision acceleration), and that longitudinal accelerations are taken as 0.33g (18 times smaller than design collision acceleration), and also considering that the allowable stress for collision accelerations is 16 Kips/in² (ksi) for Inconel 617, it is concluded that normal driving accelerations would cause stresses that are 1 ksi or smaller. This stress is low enough that low amplitude fatigue due to normal driving accelerations should not be important.

6.3 RECTANGULAR DESIGN

A rectangular box is one of the shapes selected for the TES reservoir. It appears that a rectangular box best utilizes the space between the axles and below the passenger compartment of an automobile. A box size of approximately 44 in x 44 in x 14 in, outside dimensions, was chosen to meet the packaging constraints and to provide the space required to store at least 300 kg of salt.

6.3.1 Design Approach

The TES reservoir, as noted earlier, consists of two containers, one inside the other, separated by insulation which requires a vacuum. The function of the outer box is to contain the thermal insulation around the inner box.

The inner box must function under internal pressure varying from 0 to 30 psi and at temperatures up to 1150°K (1610°F). The

outer box is under an external pressure of 15 psi and is at ambient temperatures. Because of the large thermal expansions/contractions that the inner box undergoes, the design must allow relative movements to occur without restraint between the boxes.

The most efficient structural action is direct tension or compression in contrast to bending. A widely used configuration for pressure vessels is a cylinder with ellipsoidal heads. Under internal or external pressure loads, these vessels are primarily in tension or compression. By contrast, in a hollow rectangular box under pressure loads, each side must act as a plate in bending to deliver the pressure loads to its edges; a rectangular box is therefore not a structurally efficient shape for a pressure vessel.

The structural efficiency of a rectangular box can be increased, however, by adding structural elements inside the box. The function of these elements is to reduce the bending span of the surface plates by providing intermediate supports. For internal pressure, the reactions on symmetrically located supports on two opposite sides of the rectangular box are equal, and of opposite sign. This means that if a symmetrical structure is located between opposite faces of the box, this structure will be subjected to a system of self-equilibrating forces.

In the rectangular TES reservoir, internal structure can be used with the inner box. In the outer box, the sides can have no intermediate supports, since these supports would pass through the inner box.

The design of the inner and outer boxes are therefore quite different. The inner box is under internal pressure at high temperature. It supports itself, the heat pipes, and the 300 kg of salt, and is internally braced. The outer box is under external pressure at near ambient temperature, and supports only its own weight plus part of the Multi-Foil insulation; however, it can have no internal bracing, and the side plates must be self-supporting to the pressure differential.

6.3.1.1 Inner Box

All metal parts of the internal box must operate at high temperature (up to 1150° K), and are therefore constructed of Inconel 617. In developing a concept for the structure of the inner box, the primary considerations were that the design be of minimum weight and practical to fabricate. Since minimum weight is achieved by structural efficiency, the design approach was based on developing an efficient structure, that is, one that to the maximum extent possible relies on direct tension and compression rather than bending.

The concept developed is illustrated in the perspective of Figure 6.4, which presents the inner box with the discharge and charge heat pipes in place. The inner box has overall dimensions of approximately 41 in x 41 in x 10 in. The dominant considerations in arriving at the design were:

- Tying the top and bottom (41 in x 41 in) surfaces together

A-2979

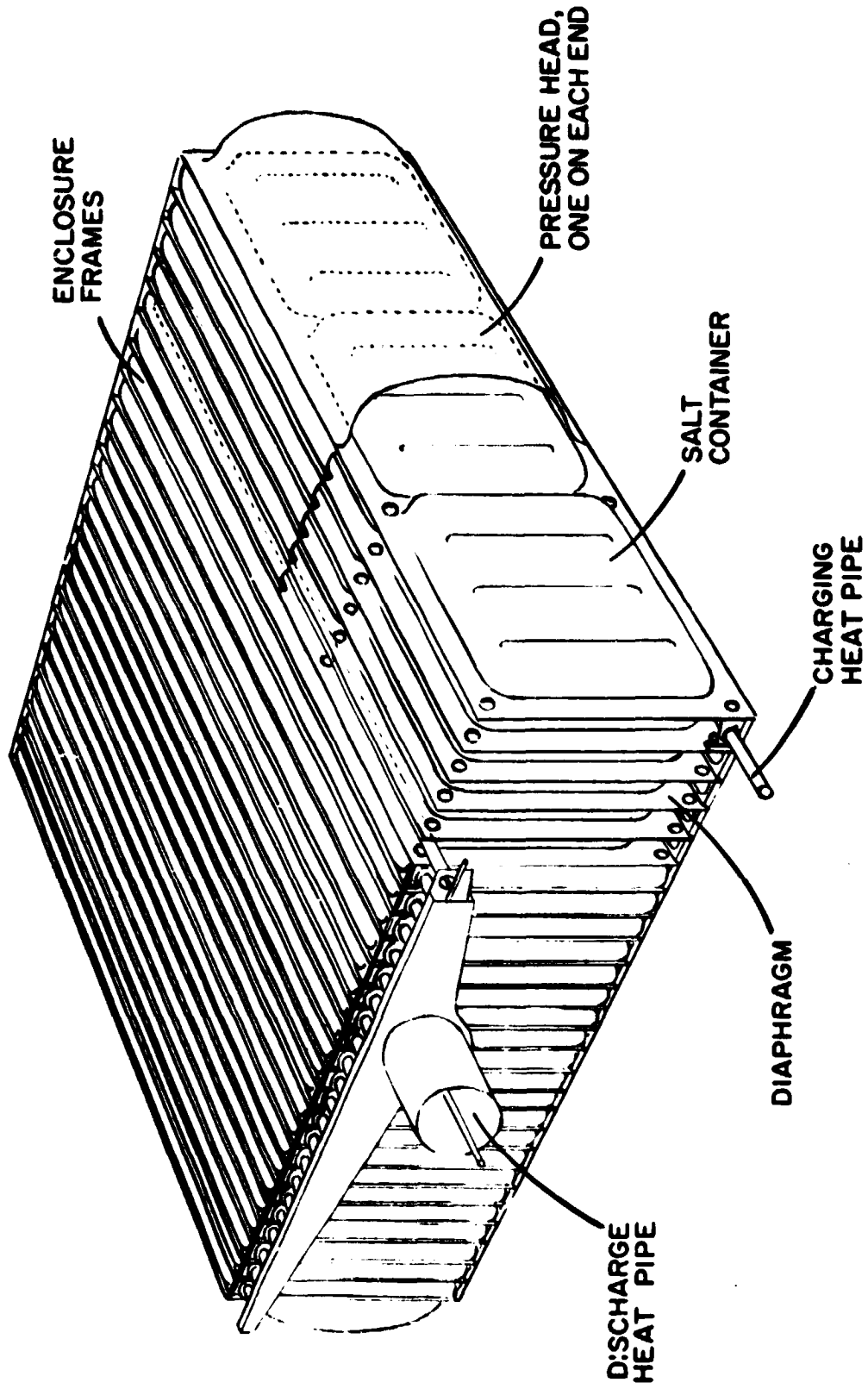


Figure 6.4 Inside Box of Rectangular TES Assembly

- Providing salt containment with a small centerline to surface salt thickness for heat transfer from salt with minimum ΔT .
- Fabrication from sheet stock of Inconel 617 for automated manufacture at minimum cost.
- Design amenable to stacked-assembly for manufacturing ease

As illustrated in Figure 6.5, the inner box is made as a stacked assembly of salt containers consisting of a flat diaphragm, a pressed plate with indentations for the salt TES media and an enclosure frame to position the salt containers and provide a vacuum-tight seal with space for the discharge heat pipe tubes (these tubes form the wall separating the discharge/ TES reservoir heat pipes illustrated schematically in Figures 3.1 through 3.5 of Chapter 3). This construction ties the two 41 in. x 41 in. surfaces together by the diaphragms, reducing the clear span to be supported by the top and bottom surfaces. Under internal pressure, the forces on the top and bottom surfaces are equal and opposite and the diaphragms between the top and bottom surfaces carry these self-equilibrating forces.

The concepts examined for the top and bottom surfaces, divided into a series of short spans by the supporting diaphragms, were:

- Plate of uniform thickness
- Corrugated sheet
- Honeycomb sandwich panels
- A series of adjacent cylindrical shells.

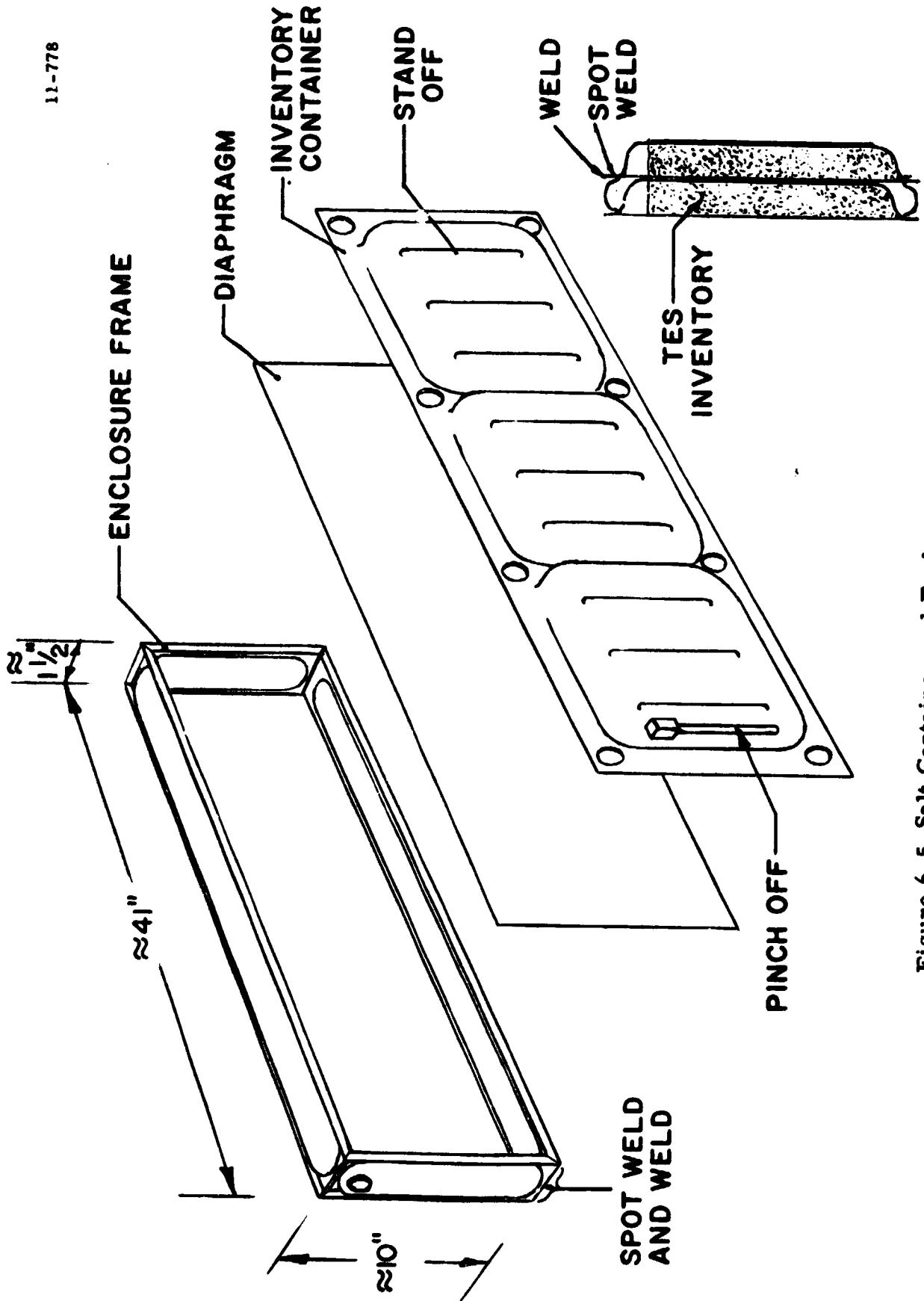


Figure 6.5 Salt Container and Enclosure Frame

The uniform plate was rejected because of its excessive weight; the corrugated sheet is more efficient, but is very difficult to weld to the diaphragms. The honeycomb sandwich plates appeared to be an efficient solution, but was not selected because of lack of such panels capable of operating at 1150° K.

In the concept using a series of adjacent cylindrical shells, as illustrated in Figure 6.6, the pressure load is carried by direct tension in the shells and by direct tension in the diaphragms. The same concept of adjacent cylindrical shells is also used on the other two opposite sides of the box — which are divided by the diaphragms into short spans. The diaphragms are thus loaded in direct tension in two orthogonal directions. In addition, the diaphragms can perform still another function as part of the salt containment capsules to minimize weight.

For the remaining pair of opposite faces of the box which are parallel to the diaphragms and approximately 41 in x 10 in, the concepts considered were: a corrugated skin to span 10 inches, the provision of vertical stiffeners 5 inches on center and corrugated skin spanning 5 inches horizontally, and doubly curved shallow-end shells (pressure heads) across the entire span. The end shell concept was selected over the corrugated skins because it had slightly less weight and avoided the complex welding of corrugated skins at the box edges. The end shells, or pressure heads, apply reaction forces along each of the four support sides of the shell. These edge forces are carried by the end diaphragm (forming the end salt capsule) lying in the plane of the shell perimeter and by top and bottom

A-2980

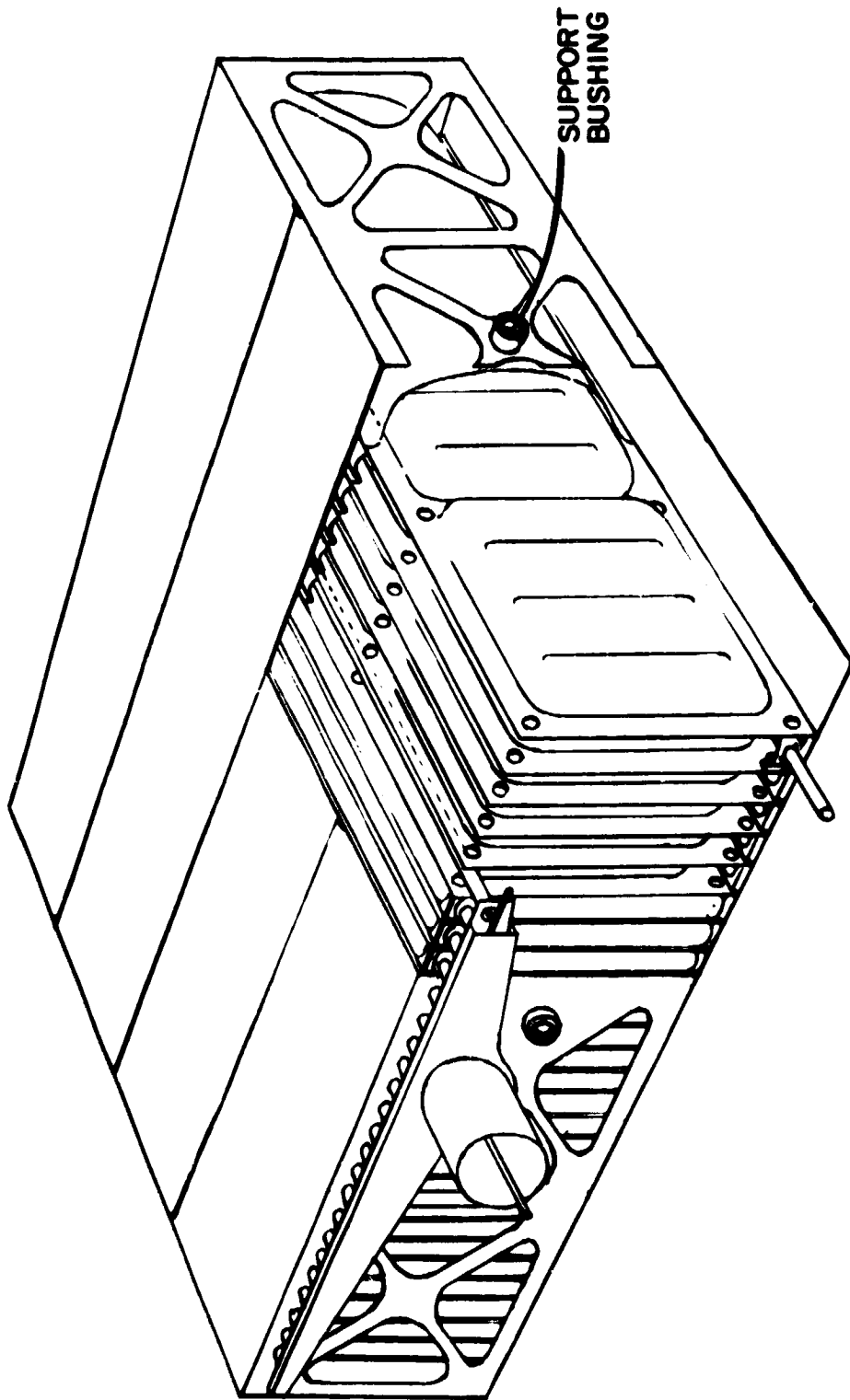
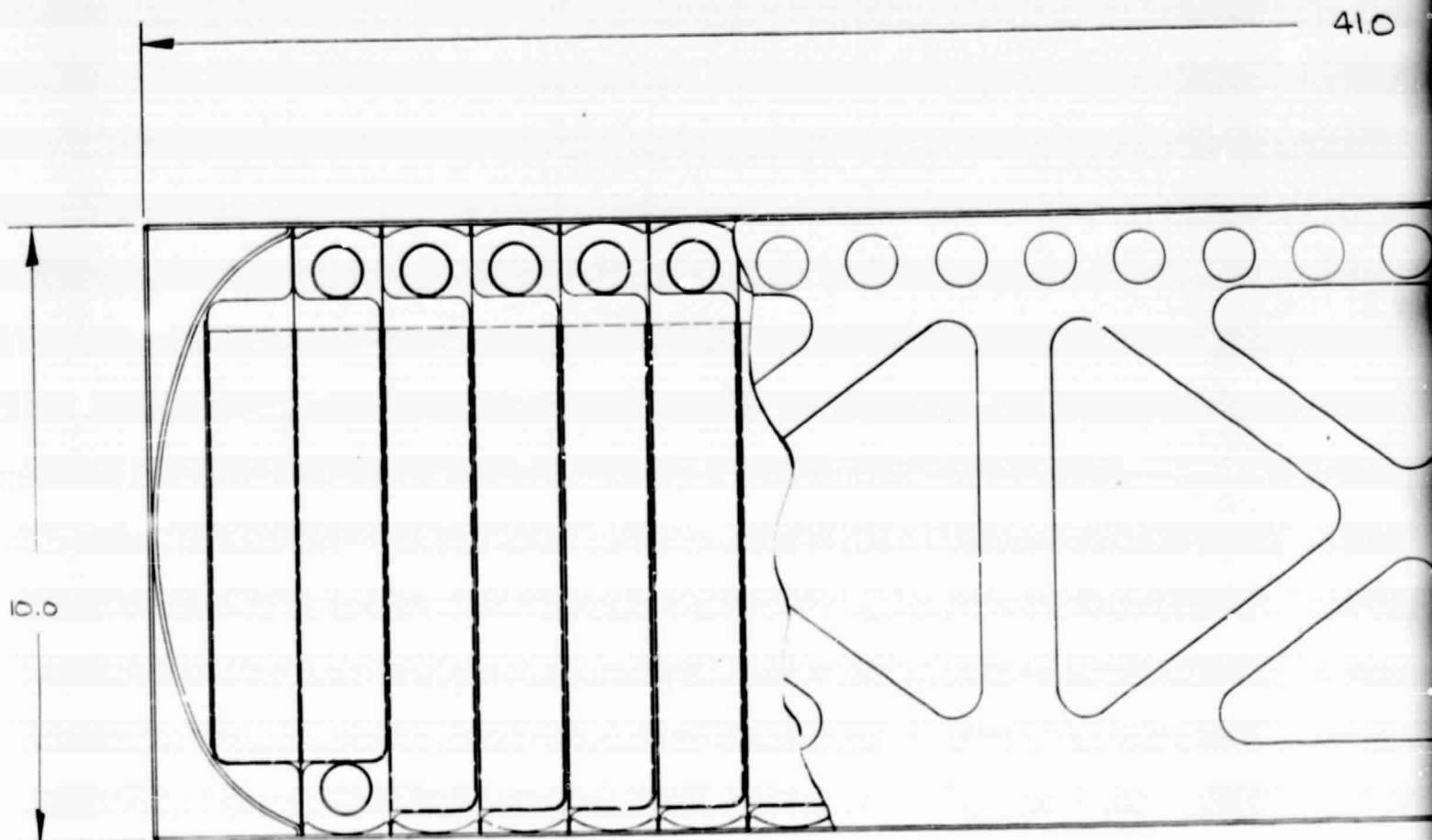


Figure 6.6 Inside Box with Reinforcing Skin (Corset) and Support Bushing

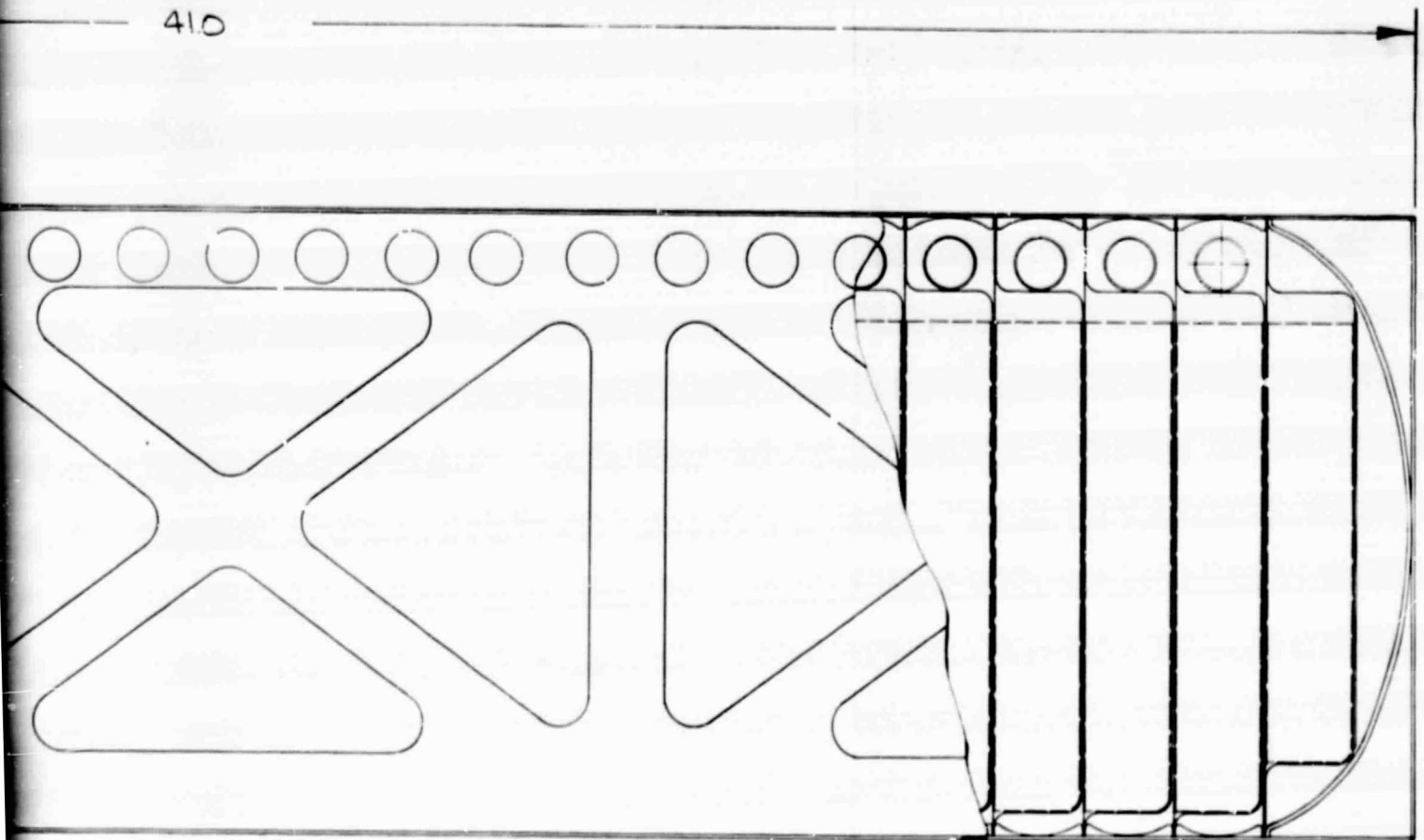
diaphragms, which, with the support trusses, form a reinforcing skin (or corset) around the entire capsule assembly as illustrated in Figures 6.6 and 6.7. Tabs are spot-welded along the perimeter of each capsule diaphragm. The top and bottom diaphragms, as well as the two side trusses, perpendicular to the capsule diaphragms, are then spot-welded to these tabs, thereby tying the edges of the pressure heads to the top and bottom diaphragms and the side trusses. The in-plane base diaphragms act in compression, and the top and bottom diaphragms (and trusses) act in tension to support the two pressure heads.

The closely spaced cylindrical shells on four sides of the box and the end shells on the remaining two sides are the pressure vessel envelope in the rectangular box concept. These shells, however, are not adequate to transfer gravity and acceleration loads to the supports. For these loads, additional structural elements are needed. The supports are formed by four sliding pins in a support bushing that can transmit only shear forces; this support system restrains the box from displacements and rotations, but allows free thermal expansion of the inner box. The concentrated loads at the supports are transferred to the edges of the rectangular box by a set of four perimeter trusses and top and bottom diaphragms which act as a rigid structure capable of channeling the loads to the supports. As discussed earlier, this reinforcing skin is connected to the capsule diaphragms along all edges of the capsule diaphragms by tabs spot welded to both the capsule diaphragms and the top/bottom diaphragms and side trusses. Had the honeycomb sandwich panels been selected



FOLDOUT FRAME

410



SAT INVENTOR 

Figure 6.7 Side View of Inner Box

ORIGINAL PAGE IS
OF POOR QUALITY

FOLDOUT FRAME 2
6-25

rather than the several shells, the panels could have been designed to act as pressure-containing units and to transfer the acceleration loads to the supports; that is, the side trusses and top/bottom diaphragms would not be required.

The structural behavior for acceleration loads is as follows:

- Vertical loads are carried by the beams formed by the top and bottom diaphragms acting as flanges and the primary diaphragms acting as webs. These beams are supported at their ends by two trusses; these trusses are supported by pins at their centers and elastically supported at each end by the other two trusses, which in their turn are supported by pins.
- Horizontal loads parallel to the primary diaphragms are transferred from these to the top and bottom diaphragms by the spot-welded tabs, and from these to the trusses, and thence to the pins.
- Horizontal loads perpendicular to the primary diaphragms are carried by these diaphragms by out-of-plane bending, the edge supports being provided by the top and bottom diaphragms via the spot-welded tabs. The loads would then be carried by in-plane action to the perimeter trusses.

In summary, the inner box is approximately 41 in x 41 in x 10 in (h), and can be described as follows:

- The pressure envelope consists of a series of adjacent cylindrical shells for four faces (the top and bottom faces and two sides) and doubly curved shells for the remaining two faces. The cylindrical shells each span 1.5 inches and are 0.010-inch thick; the enclosure frame assembly (welded) is illustrated in Figure 6.8, with the details of required pieces given in Figures 6.9 through 6.12. The doubly curved end shells or pressure heads span 41 in x 10 in and are 0.07 inch-thick with details given in Figure 6.13.

A-2982

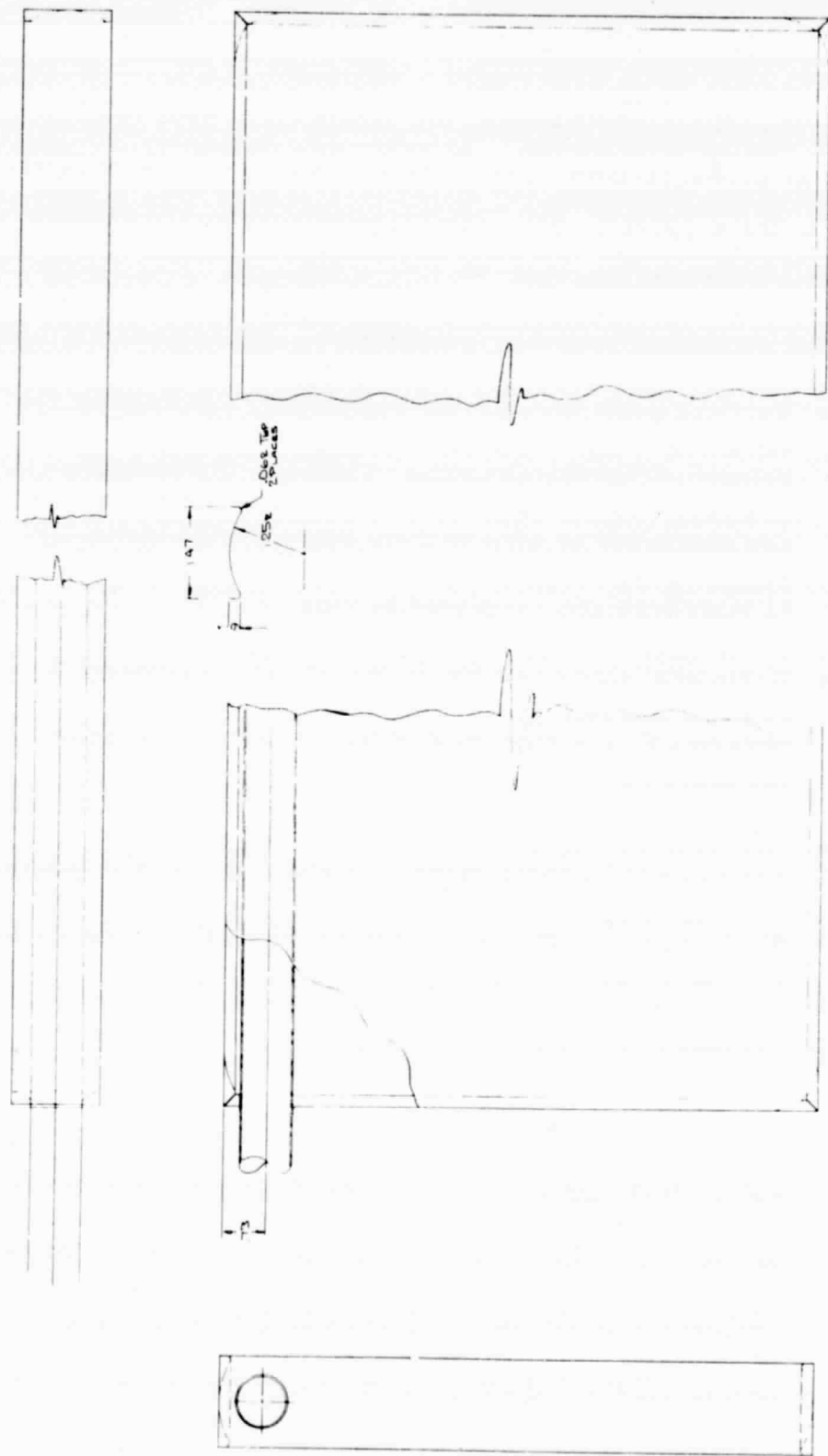
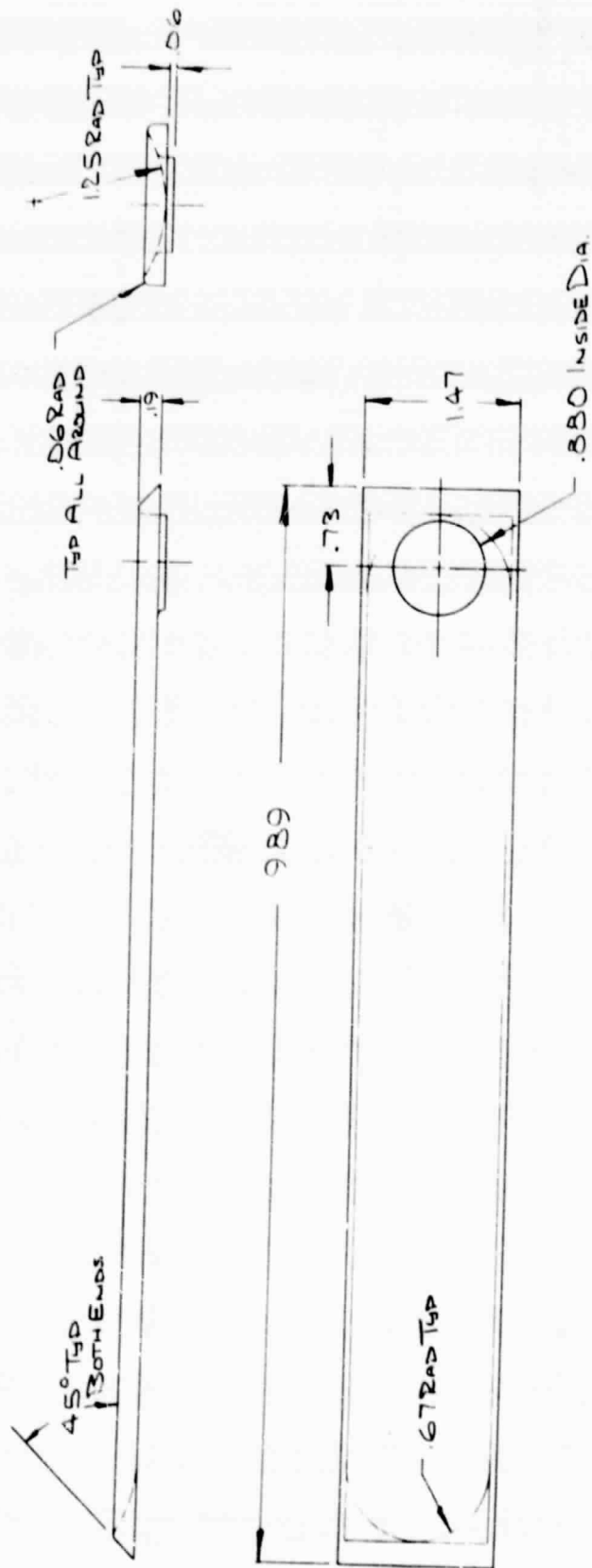


Figure 6.8 Enclosure Frame Assembly for Inner Box

A-2983



MATERIAL DRAWN TO .010 THICK

Figure 6.9 Side Piece for Enclosure Frame (1 Hole)

A-2984

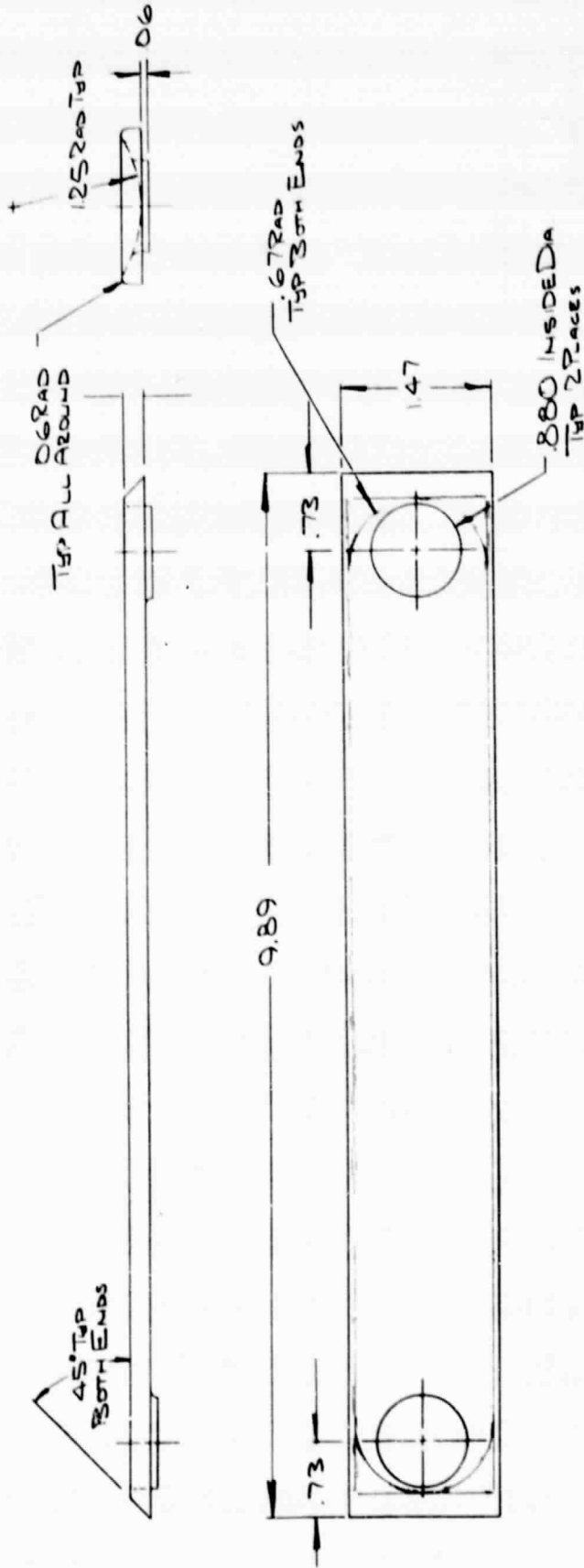
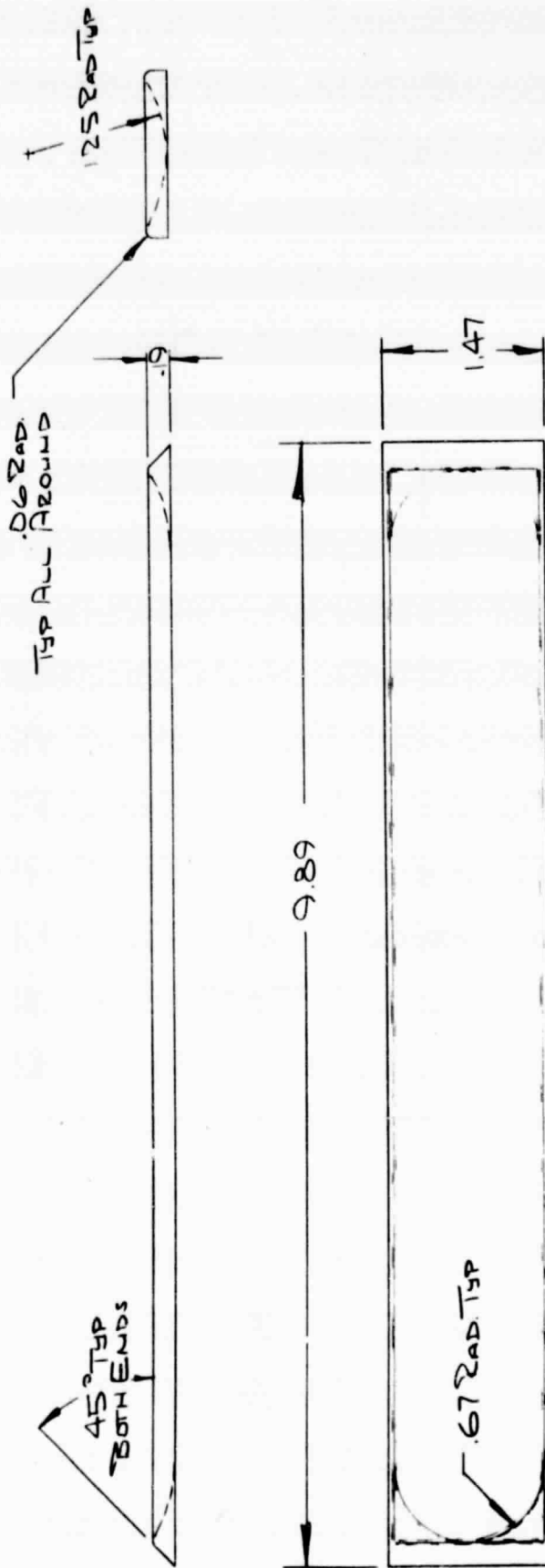


Figure 6.10 Side Piece for Enclosure Frame (2 Hole)

A-2985



MATERIAL DRAWN TO .010 THICK

Figure 6. 11 Side Piece for Enclosure Frame (No Hole)

A-2986

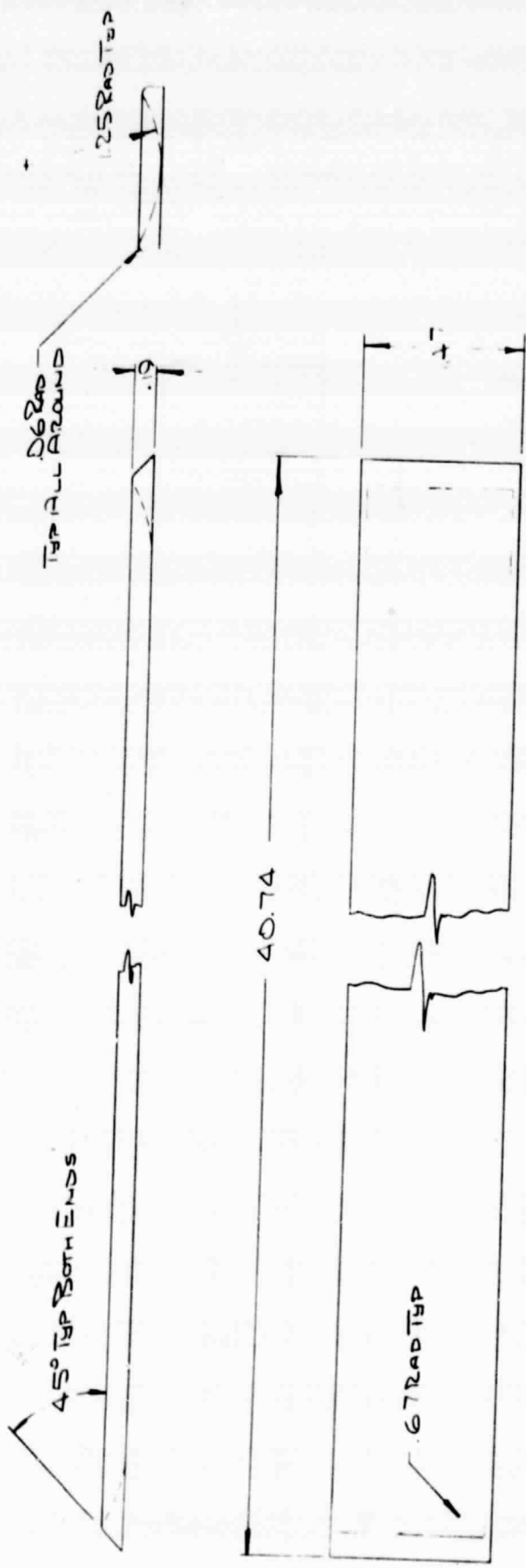
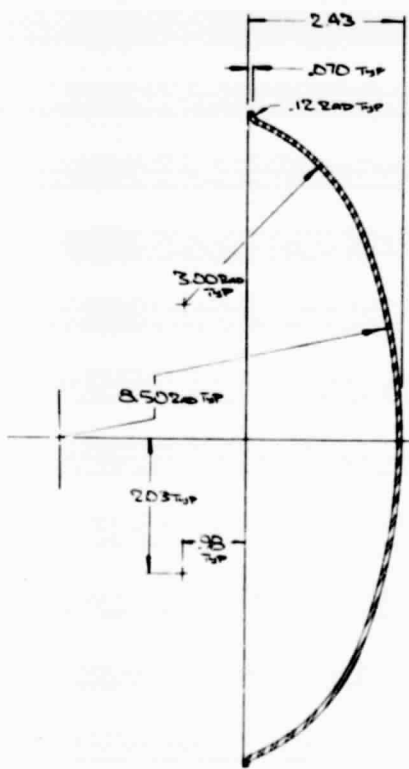
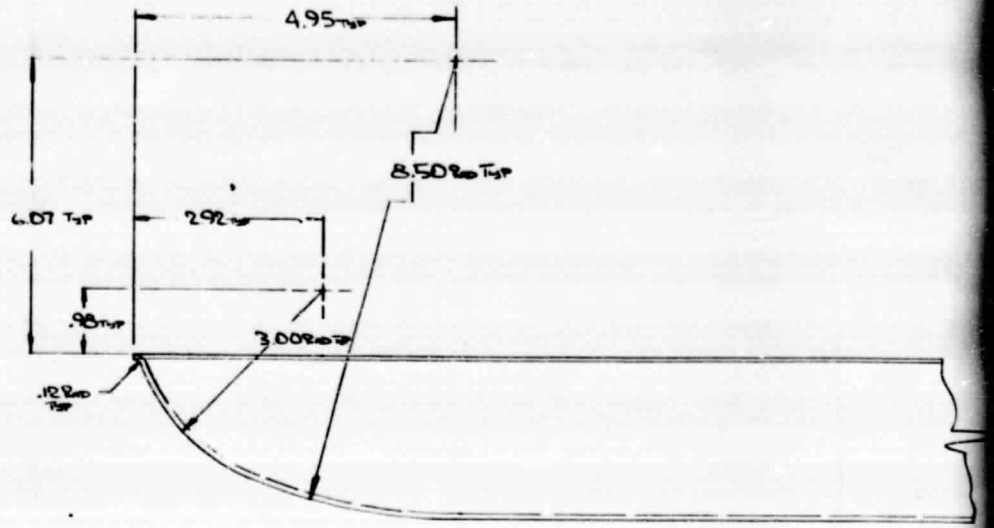
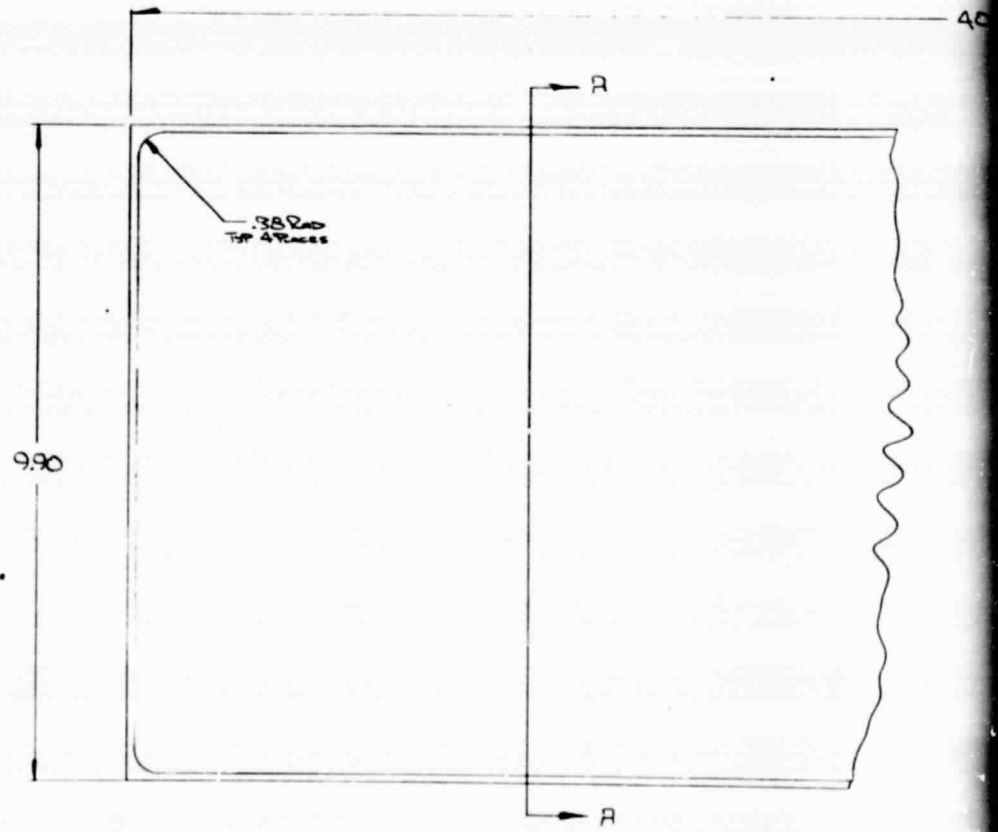


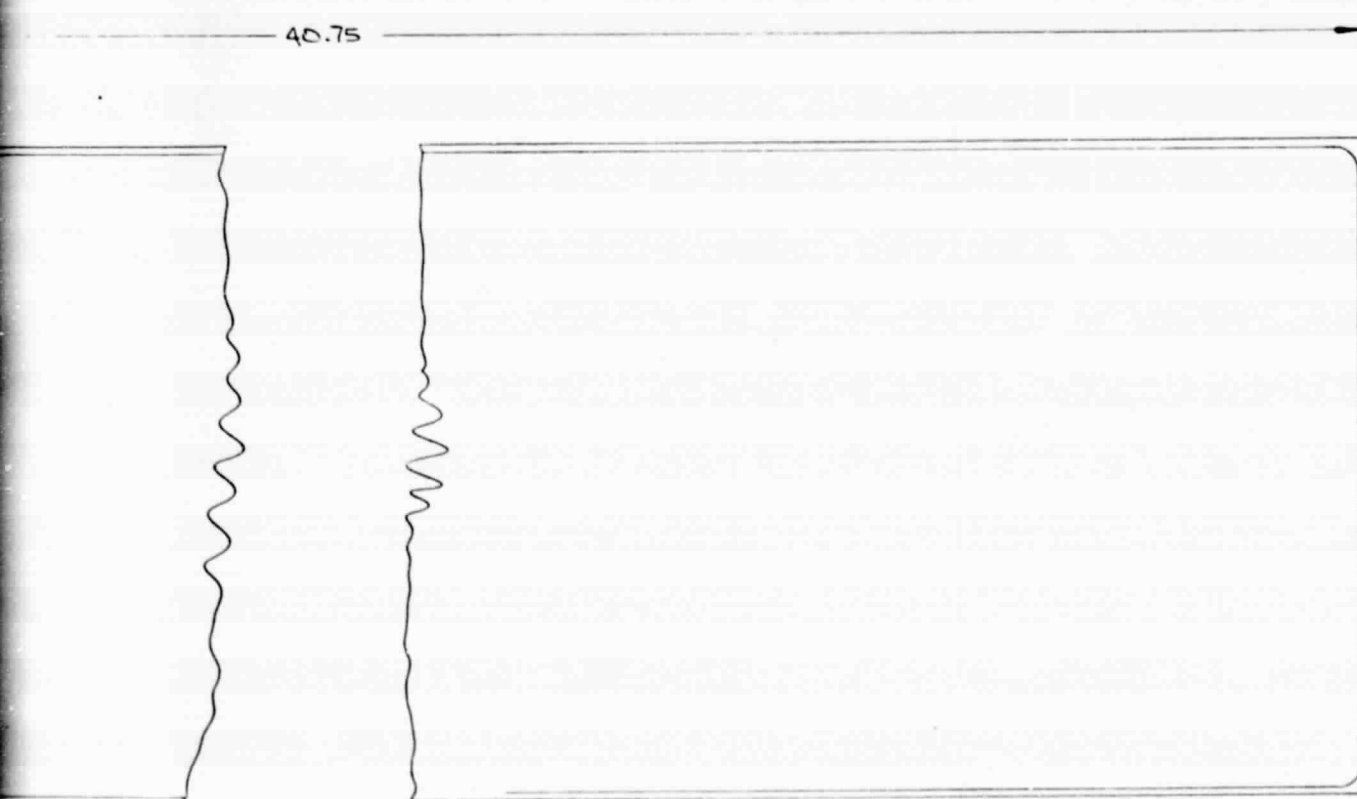
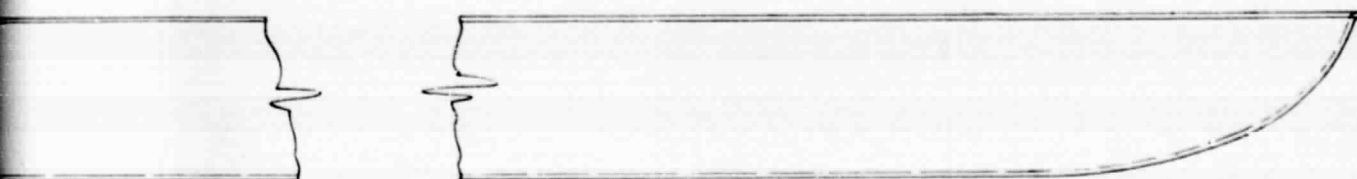
Figure 6.12 Top and Bottom Pieces for Enclosure Frame



SECTION AA



FOLDOUT FRAME

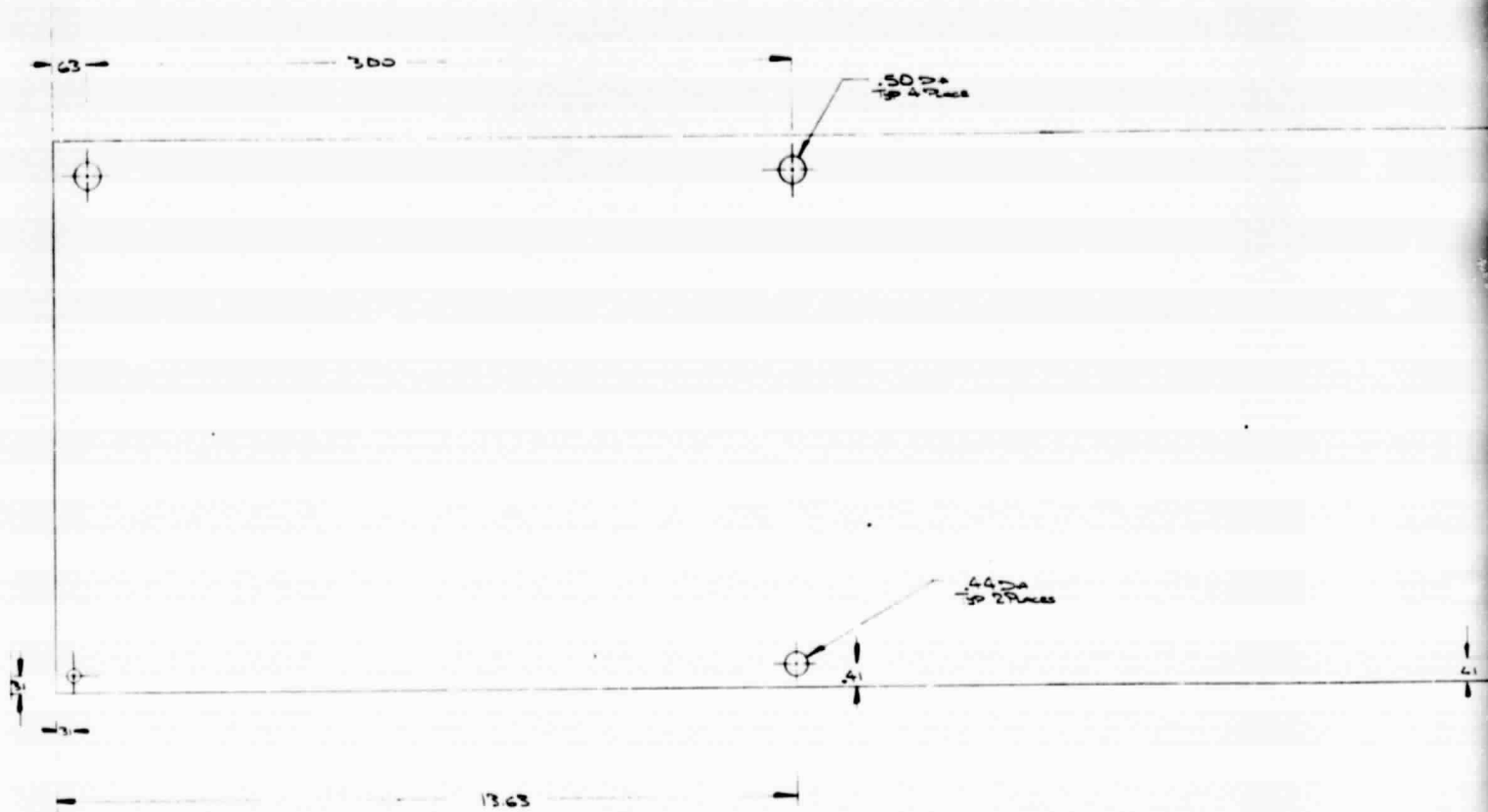


MATERIAL: INCONEL 617
DRAWN TO .070 THICK

FOLDOUT FRAME 2

Figure 6.13 Pressure Head on Doubly-Curved End Shells for Two Sides of Pressure Envelope

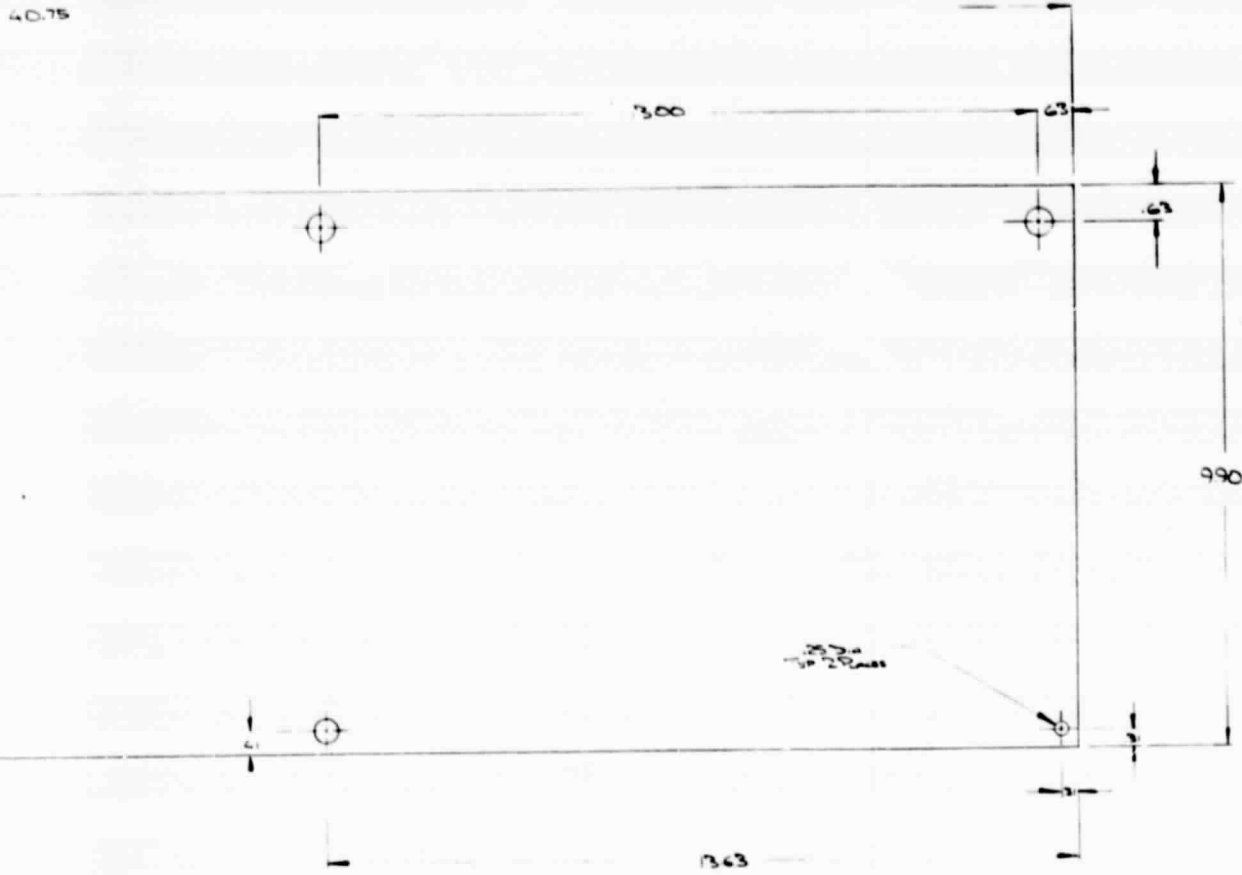
- A series of primary diaphragms 0.015-inch thick and 1.5 inches on center support the longitudinal edges of the cylindrical shells. Under internal pressure loads each diaphragm carries self equilibrating tension forces between the cylindrical shells on opposite faces. Since each diaphragm is attached to shells along all four edges, it carries equal tension in two orthogonal directions. Each primary diaphragm is also used as a side of a salt capsule. The diaphragm design is illustrated in Figure 6.14, and includes holes for pressure equalization in the entire volume outside the salt capsules comprising the reservoir heat pipe.
- The two end primary diaphragms carry in-plane compression forces from the end shells and are thicker than the others (0.19-inch thick). Their design, other than thickness, is identical to that of the other diaphragms.
- Diaphragms on the top and bottom surfaces 0.05 -inch thick support the edges of the end shells. These diaphragms are connected to the primary diaphragms by spot welding to tabs on the diaphragms. To assist in welding to the tabs, the diaphragm is split into four segments as illustrated in Figure 6.15.
- A deep-drawn sheet, 0.010-inch thick, is welded to each primary diaphragm to form a salt capsule. Each salt capsule is 1.49-inch deep and has stiffeners stamped into it. The capsule sheet designs are illustrated in Figure 6.16 for most of the capsules, with the design for the end capsules (lower height) given in Figure 6.17.
- Trusses are attached to the four sides of the box. These trusses are 10-inches deep and made of 0.05-inch thick material; they are attached by segment welding to the top and bottom surface diaphragms, and to the primary diaphragms by spot welding to tabs on the diaphragm.



PRECEDING PAGE BLANK NOT FILMED

ORIGINAL PAGE IS
OF POOR QUALITY

FOLDOUT FRAME

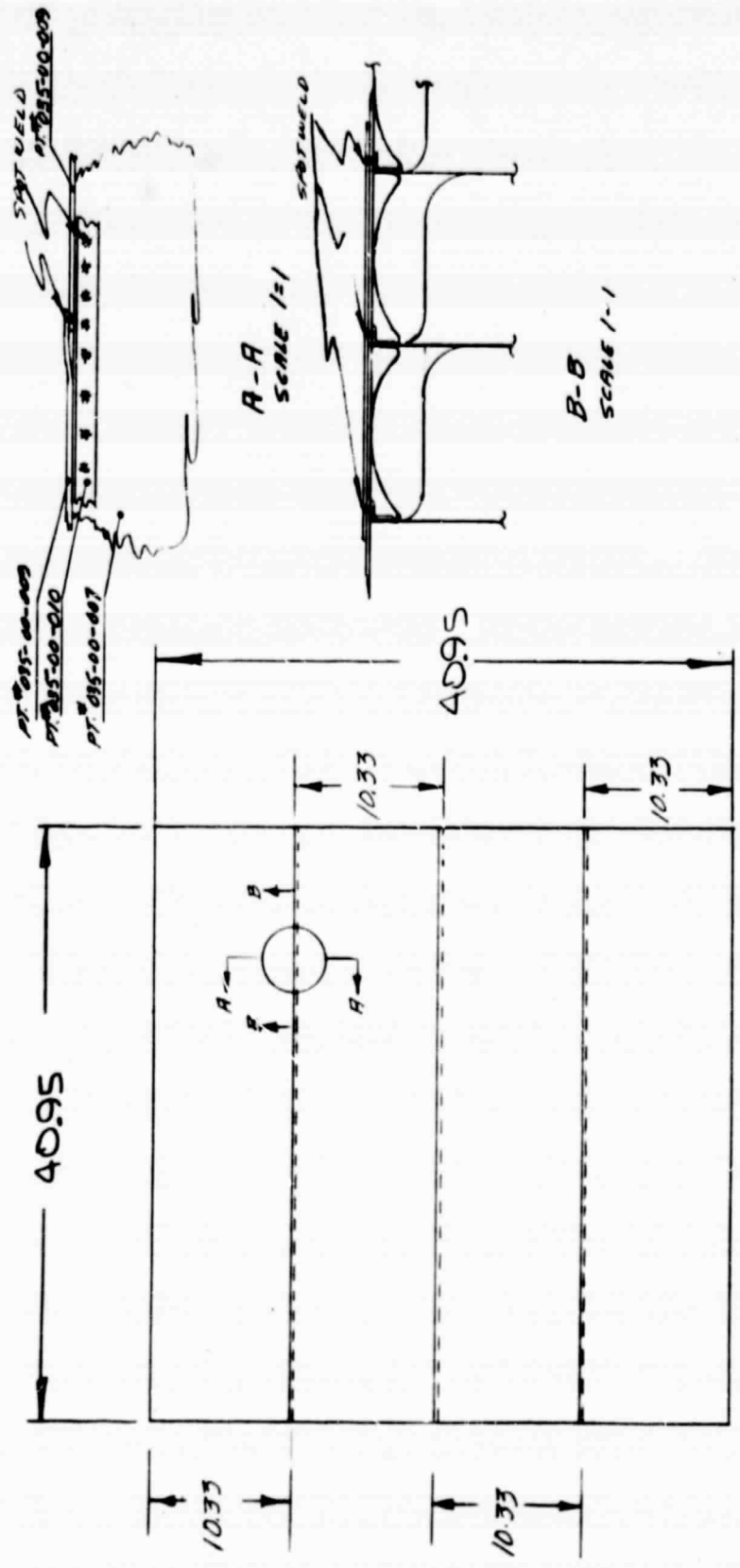


MATERIAL: ALUMINUM 6061 T6
DOWEL: 6061 T6
DOWEL THICK: 0.0625

Figure 6.14 Primary Diaphragm Design

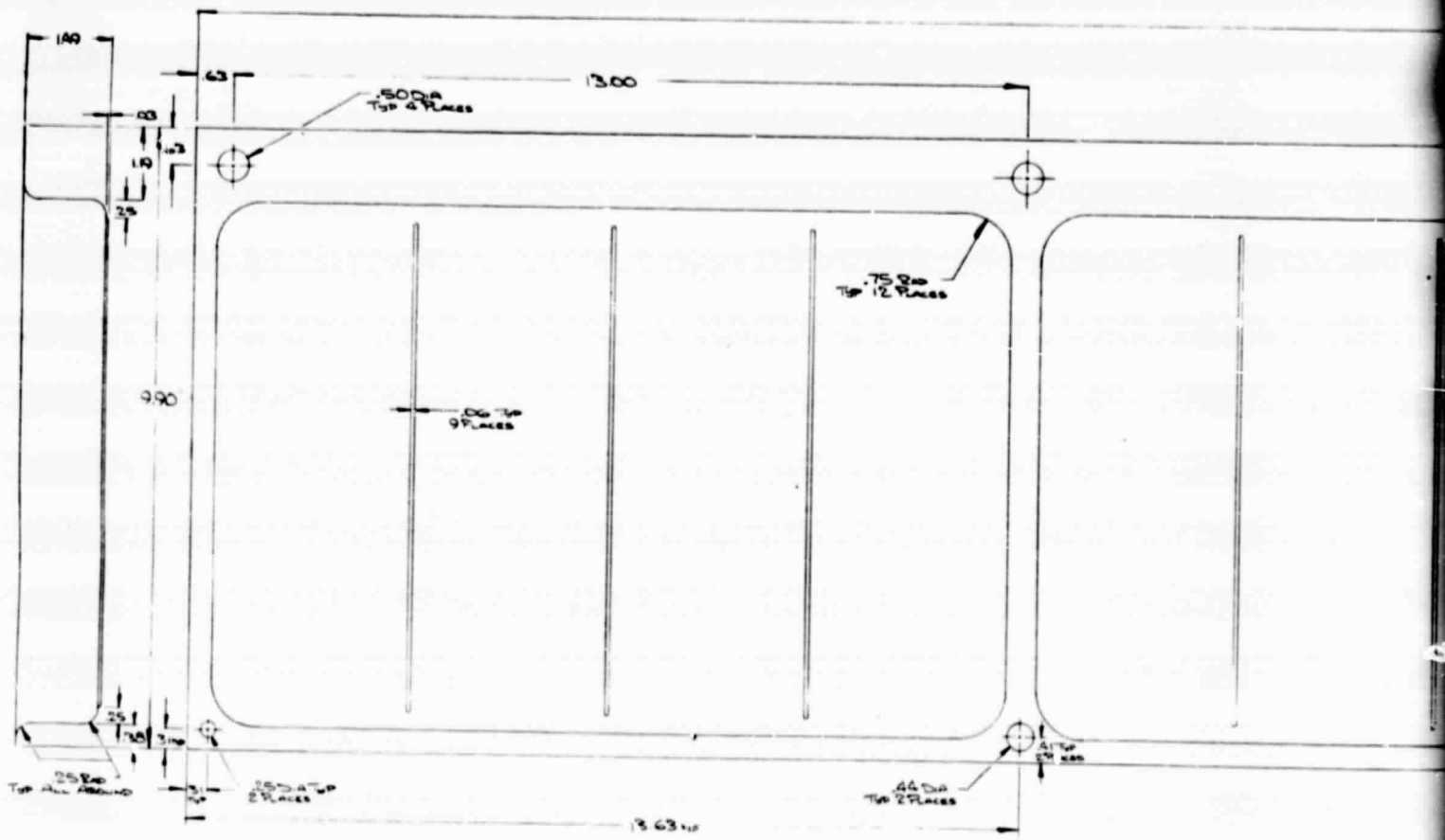
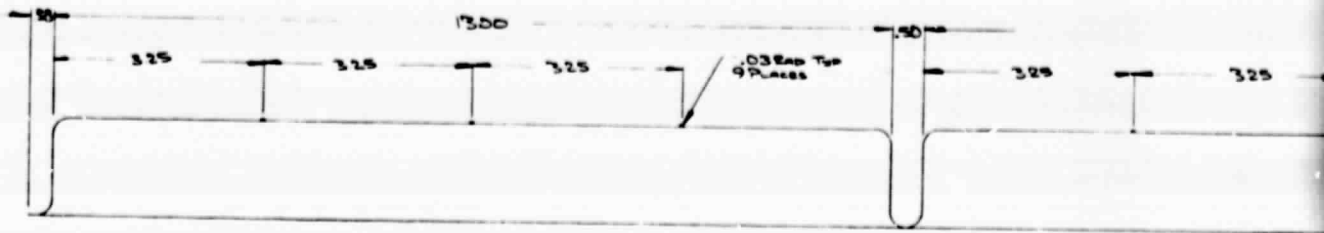
FOLDOUT FRAME 2

A-2989



• 050 SHEET

Figure 6. 15 Bottom and Top Diaphragms



PRECEDING PAGE BLANK NOT FILMED

FOLDOUT FRAME

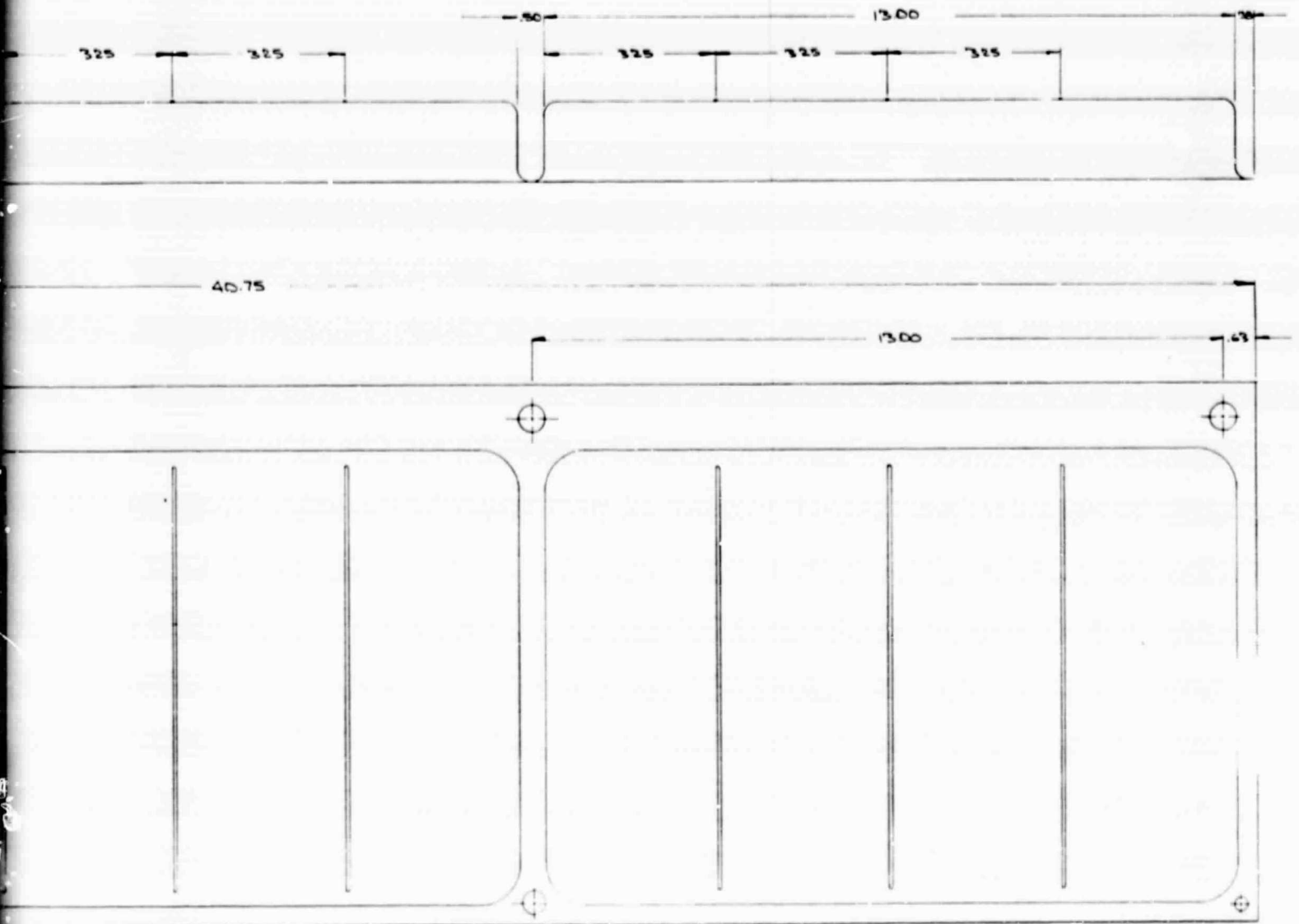
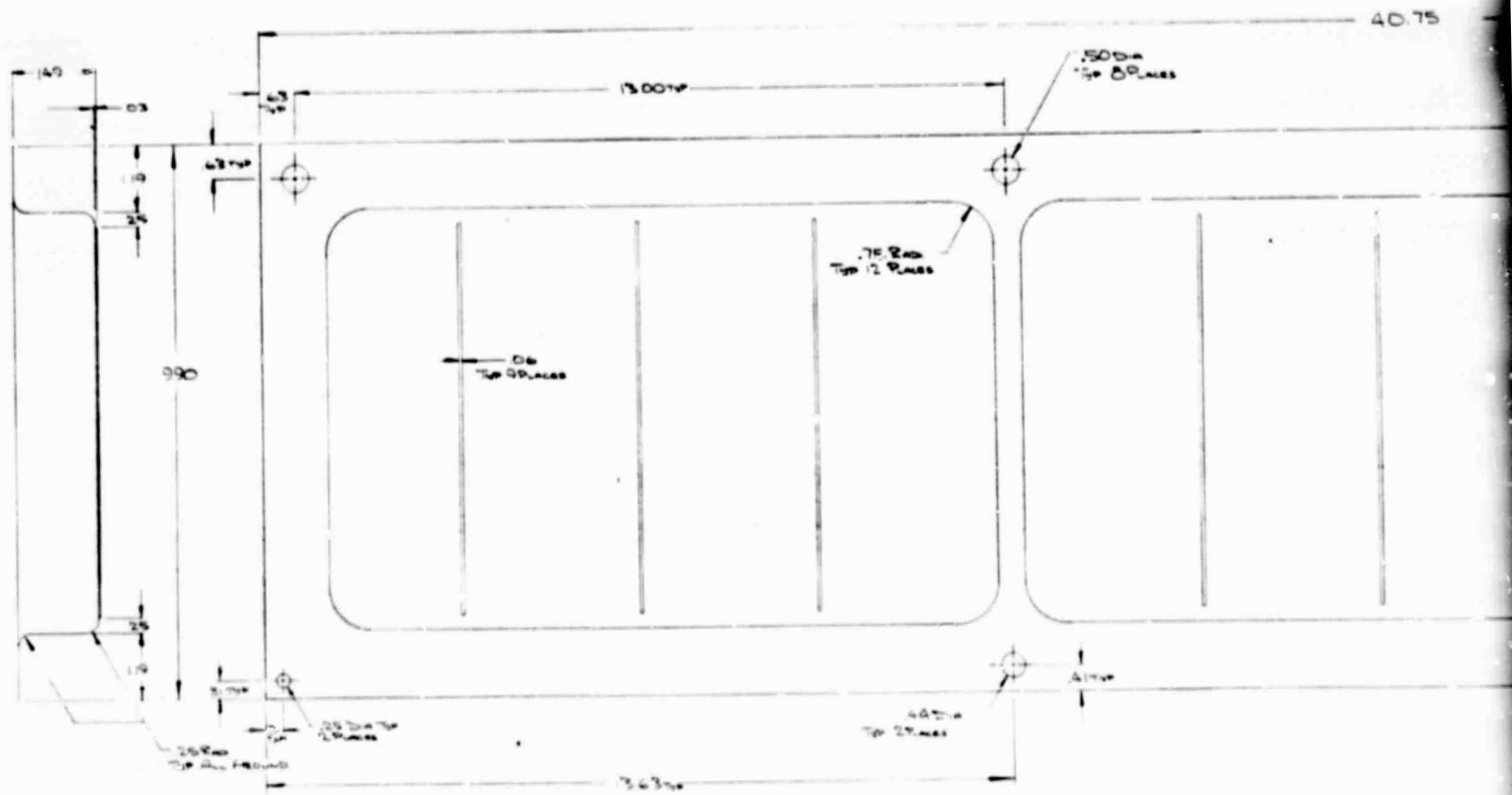
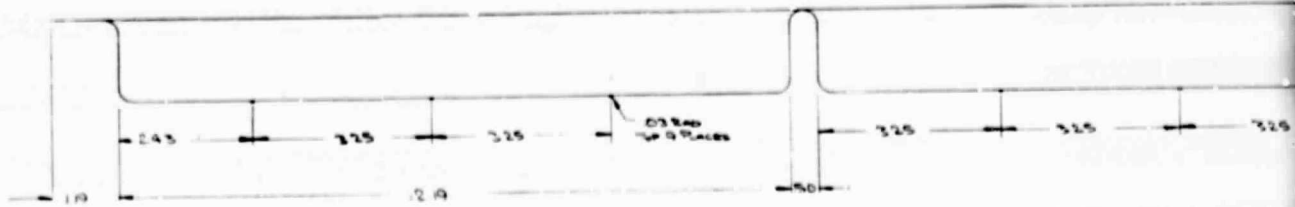
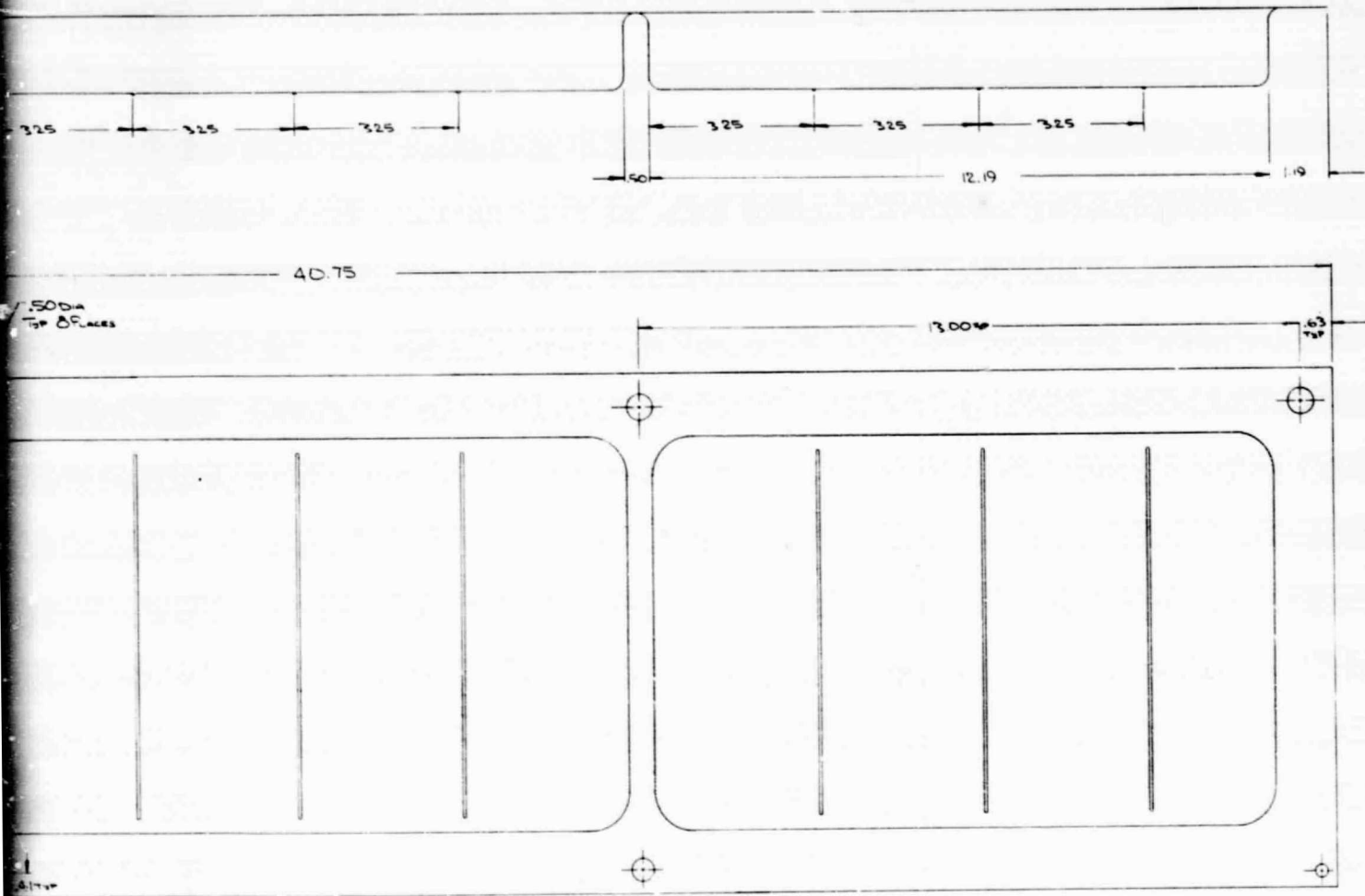


Figure 6.16 Drawn Sheets to Form Salt Capsules - For All Except End Capsules



FOLDOUT FRAME

PRECEDING PAGE BLANK NOT FILMED



MATERIAL: INCONEL 6017
DRAWN TO
D10 THICK

FOLDOUT FRAME 2

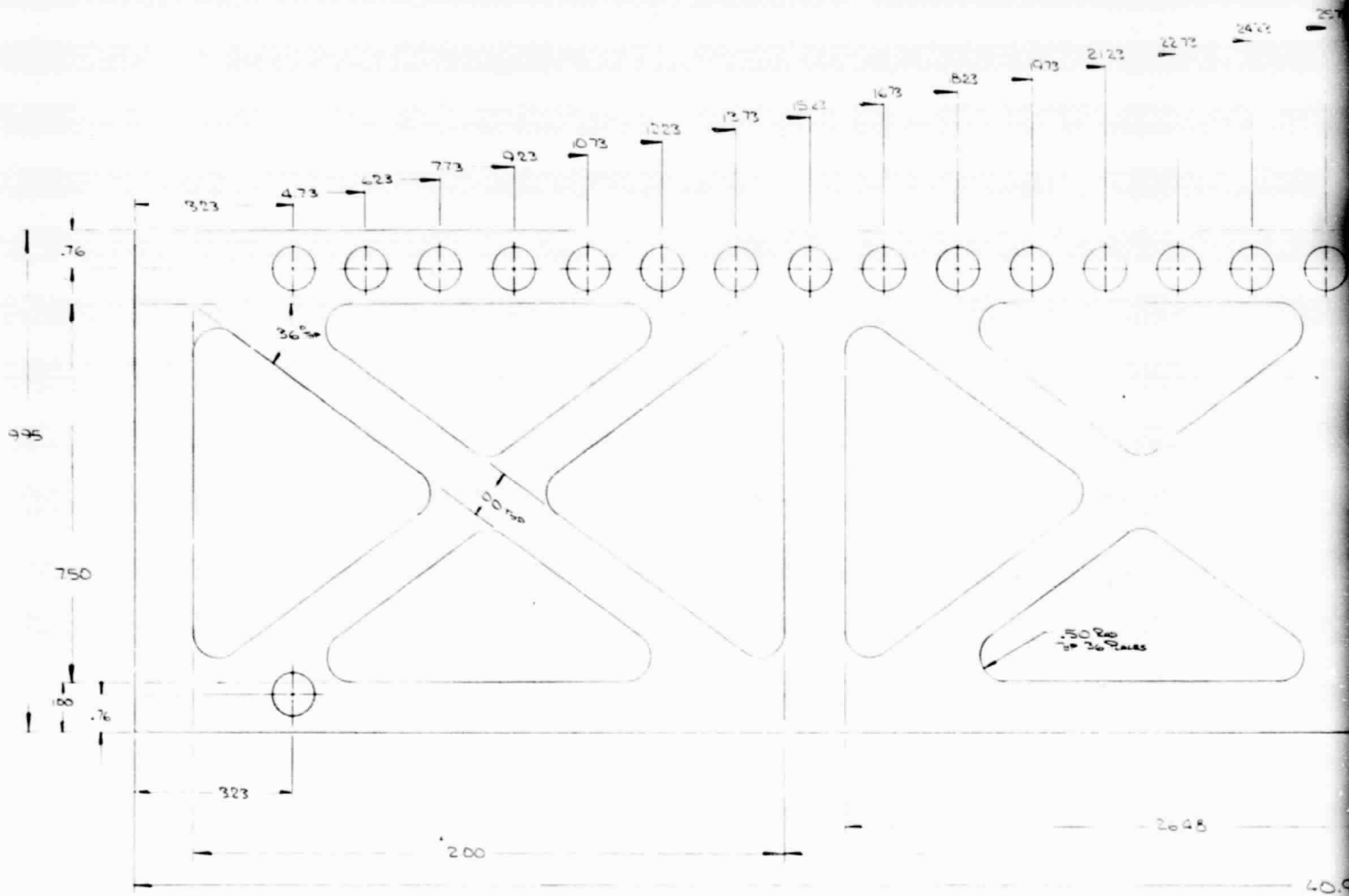
Figure 6.17 Drawn Sheets to Form Salt Capsules - Reduced Height for End Capsules

The design is illustrated in Figure 6. 18 for the truss with the holes for the discharge heat pipe. The other three trusses are identical except they do not have the heat pipe holes at the top.

- Four bearing supports are provided, one at, or near, the center of each truss. Pins cantilevering inwards from the exterior, where they are assumed held, fit into bushings in these bearings. The sliding interface between the pins and the bushings must accommodate the thermal movements plus deformations due to pressure and acceleration loads. A support bushing is welded to each truss with each bushing near the center of the truss. The bearing supports are described in detail in Section 6. 3. 1. 2, which describes the outside box.
- Tubes run along the top of each capsule, and connect into a manifold located along one side of the box. These tubes form the wall separating the discharge/ TES reservoir heat pipes. A 4-inch diameter pipe goes from the manifold to the Stirling engine for transport of K vapor to the engine. The discharge heat pipe assembly is illustrated schematically in Figure 6. 19, with a detailed assembly in Figure 6. 20. Part details are presented in Figures 6. 21 - 6. 24, inclusive.
- The charge heat pipe consists of one tube with the same dimensions inside the reservoir as for the discharge heat pipe, namely 0. 875 in. (OD) x 0. 020 in. (wall) x 40. 50 in. (L). To ensure that the exterior of this heat pipe is wet with liquid potassium with a minimum potassium inventory in the reservoir heat pipe, the entire reservoir should be installed slightly tilted, so that any liquid potassium drains to the charge heat pipe. Holes in the diaphragm at top and bottom permit vapor to reach all capsules in the reservoir, and the liquid potassium to drain to the heat pipe.

6. 3. 1. 2 Outside Box

With the inner box assembly completed, the Multi-Foil insulation is installed around the inner box, followed by the outside box designed to support the internal vacuum in the Multi-Foil insulation over the



PRECEDING PAGE BLANK NOT FILMED

FOLDOUT FRAME

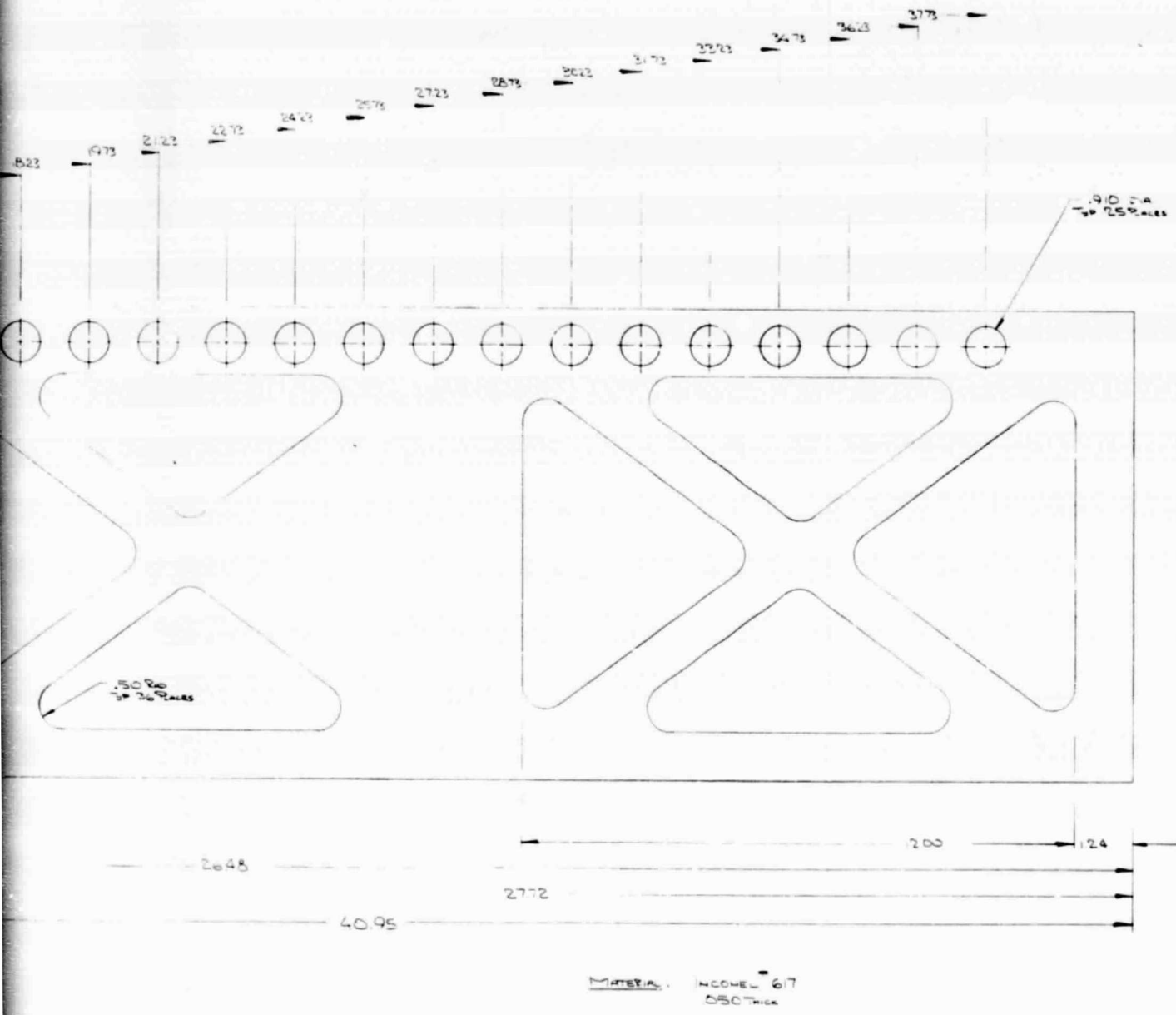
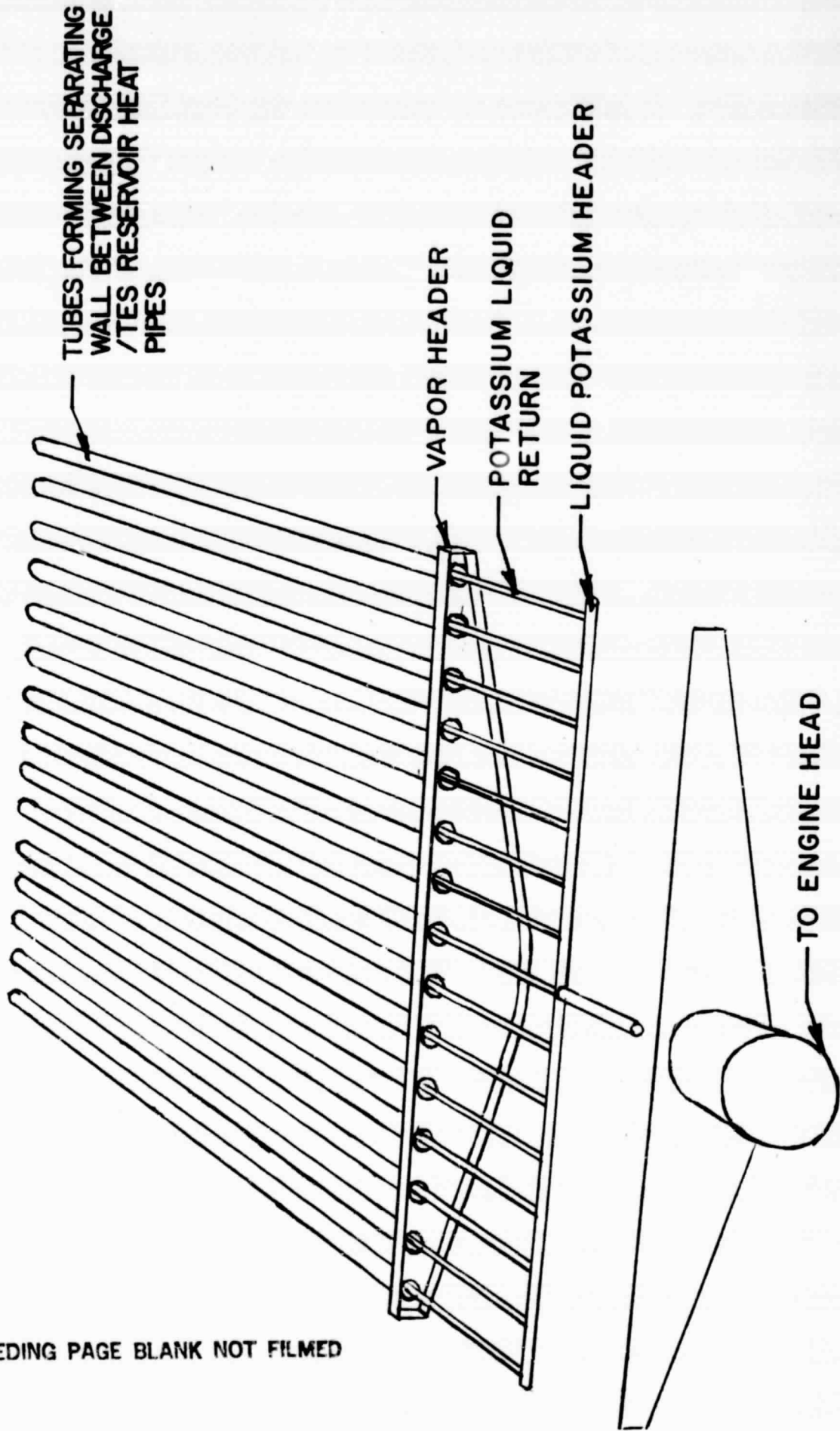


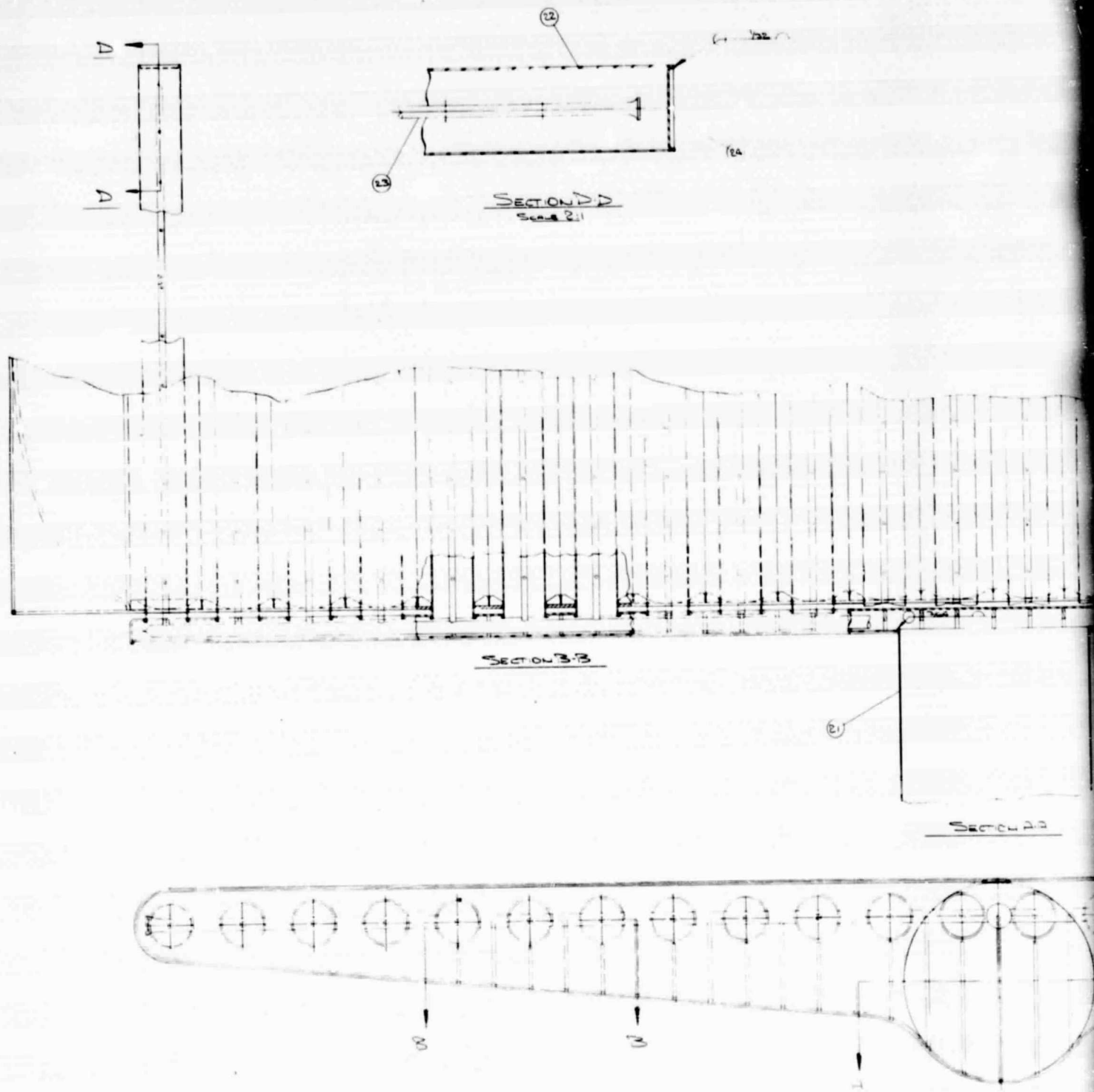
Figure 6.18 Truss for Reinforcing Skin on Side with Holes for Discharge Heat Pipe

13-778



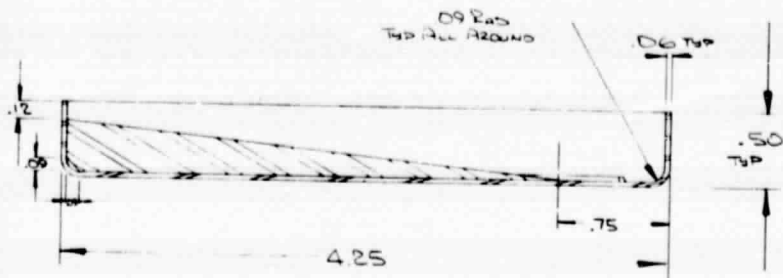
PRECEDING PAGE BLANK NOT FILMED

Figure 6. 19 Discharge Heat Pipe

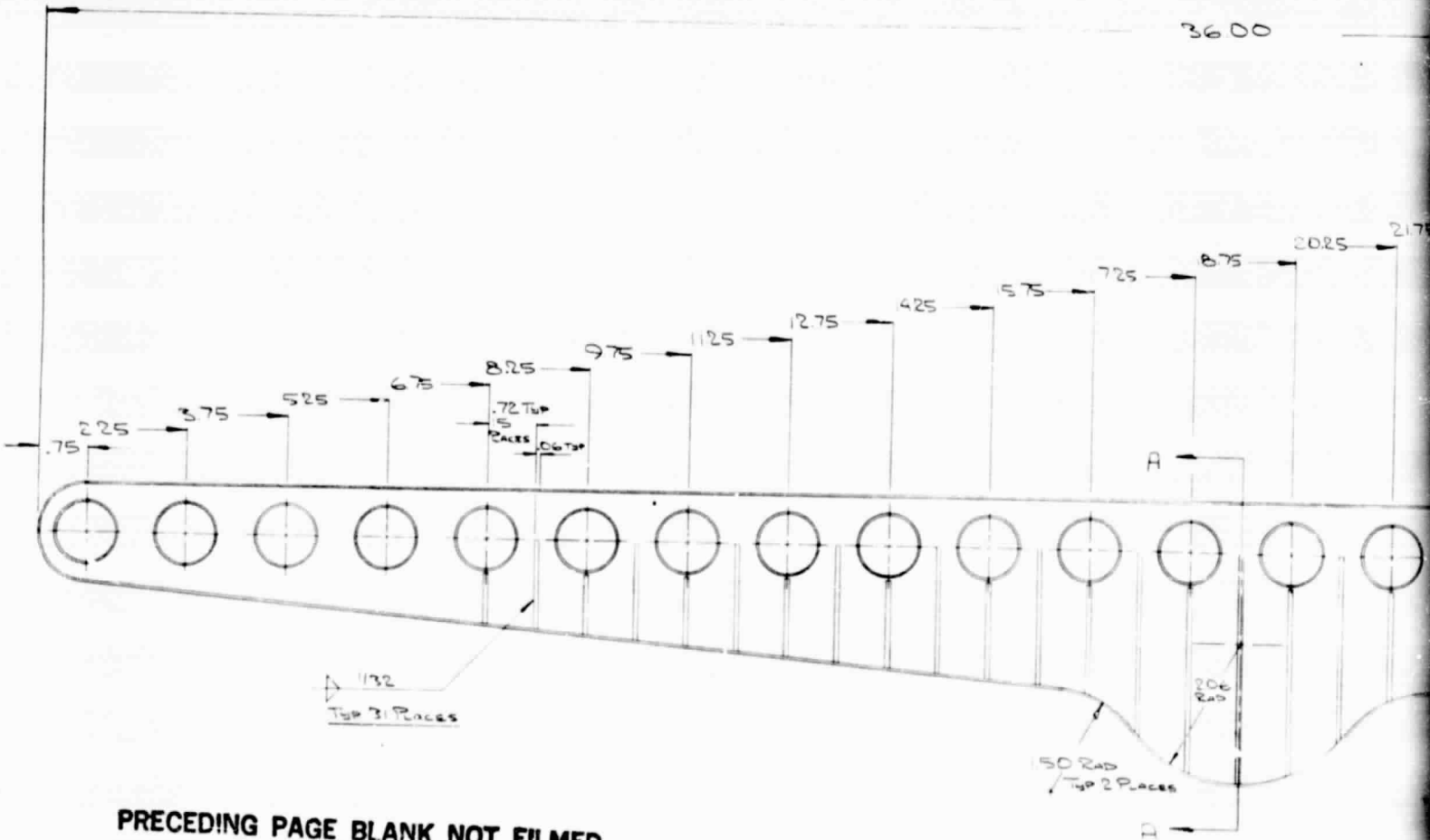
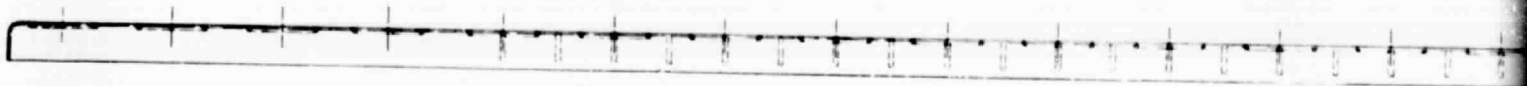


PRECEDING PAGE BLANK NOT FILMED

FOLDOUT FRAME



SECTION A-A
SCALE 2:1



PRECEDING PAGE BLANK NOT FILMED

FOLDOUT FRAME

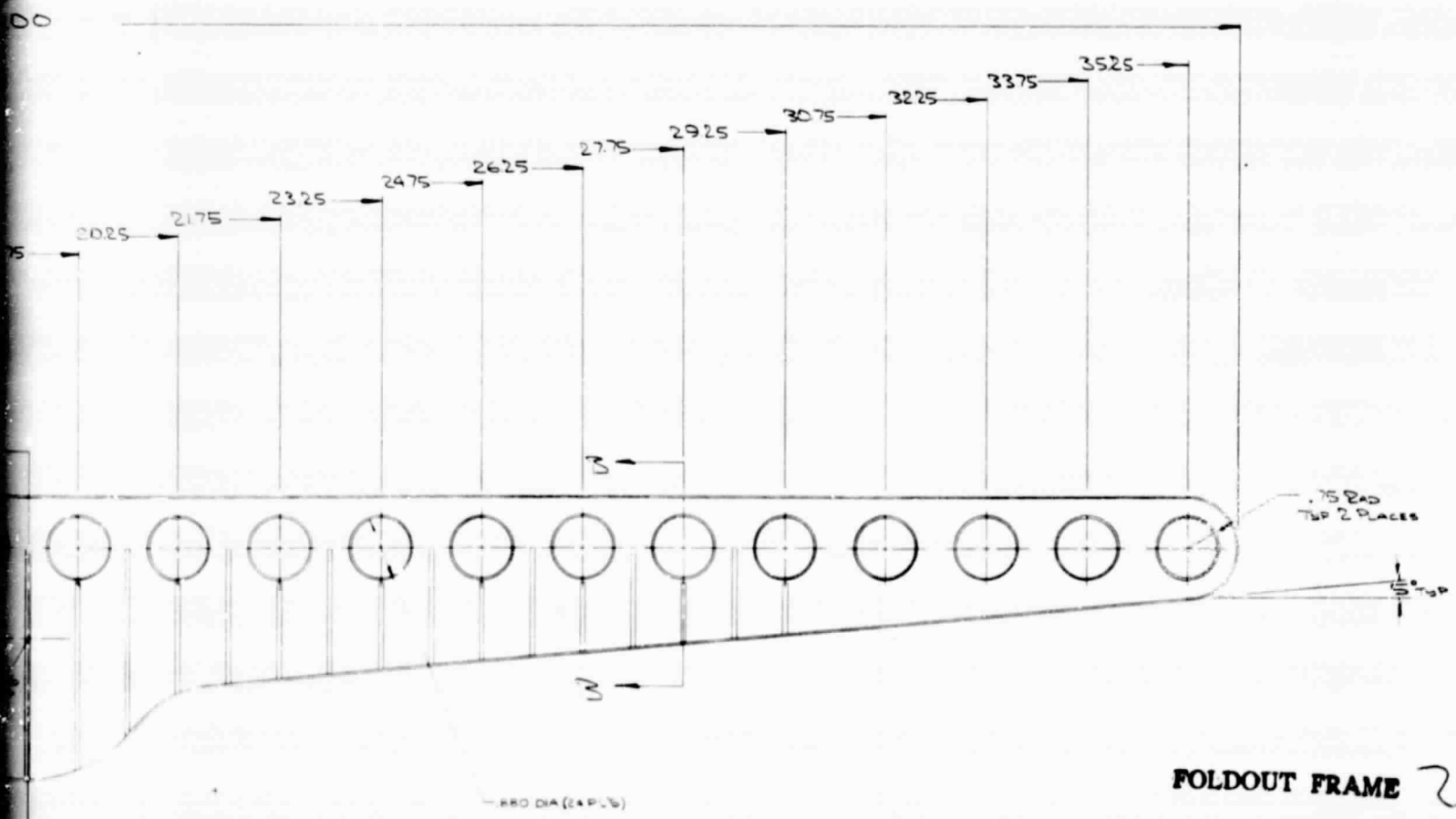
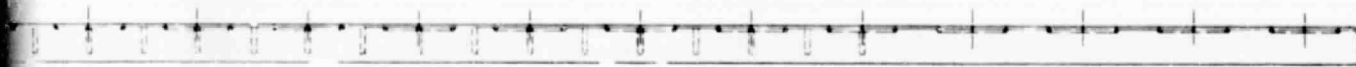
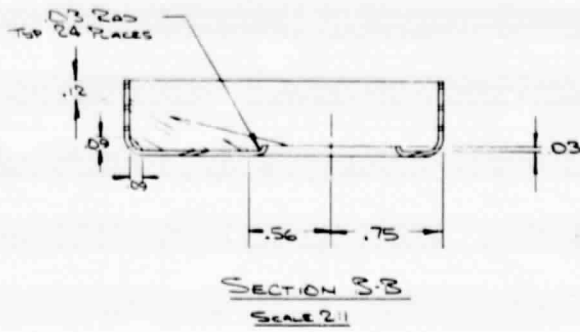
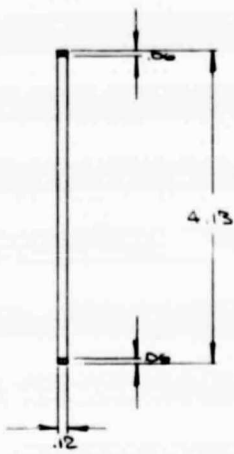
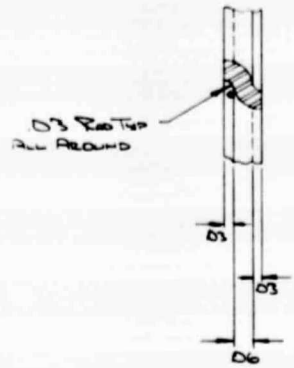


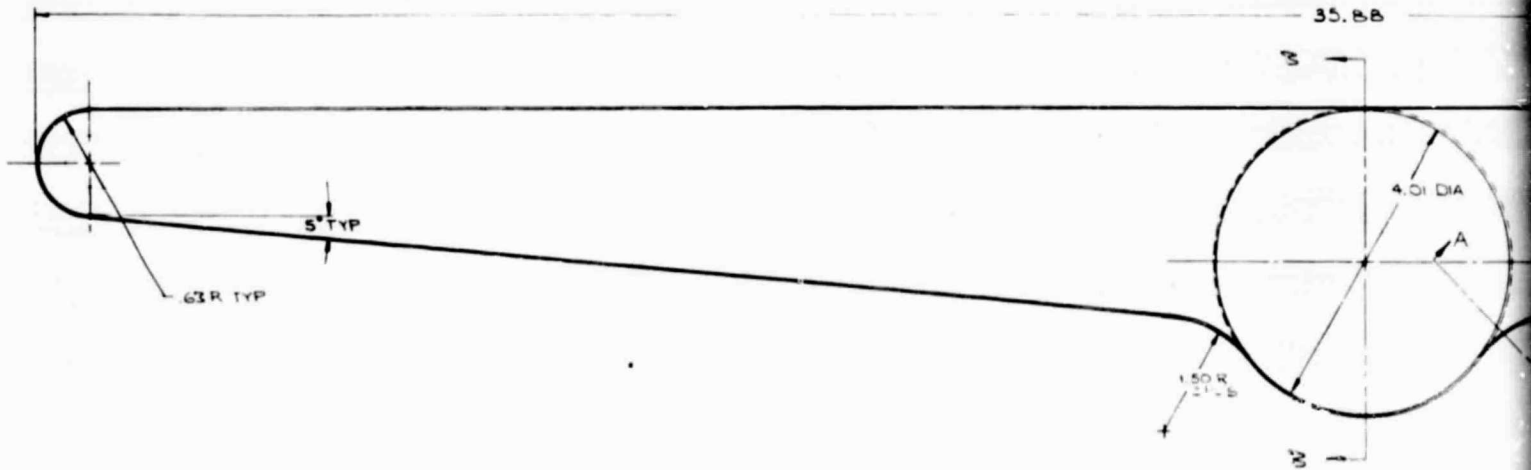
Figure 6.21 Discharge Heat Pipe Header Tube Side



SECTION B-B
SCALE F₁₀₀

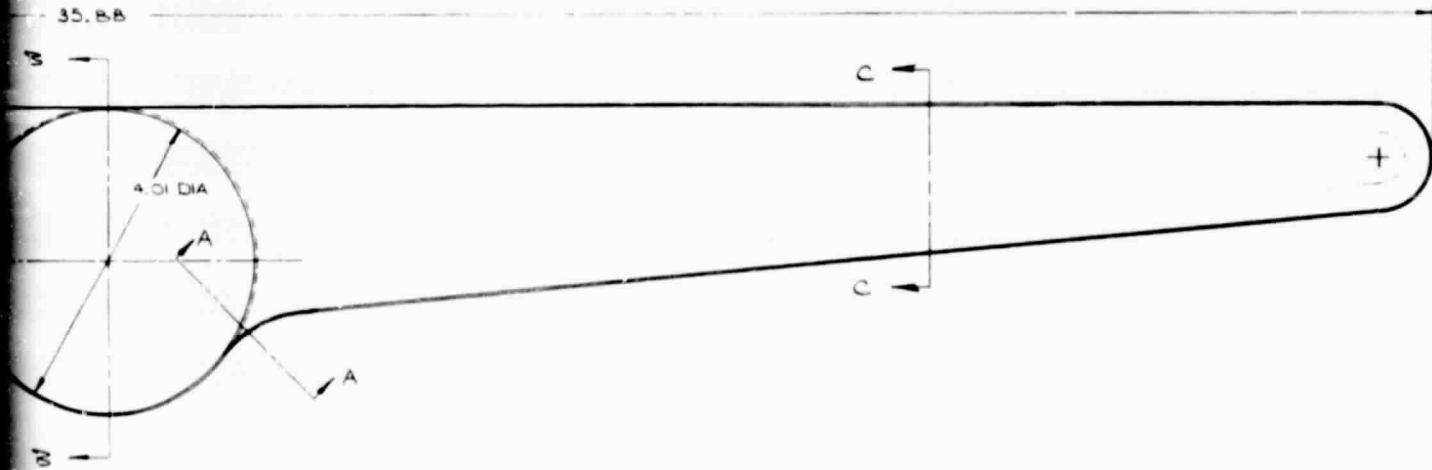
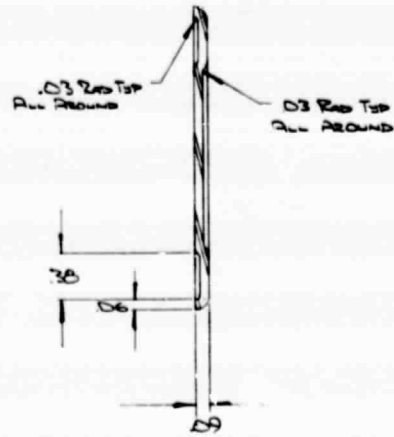
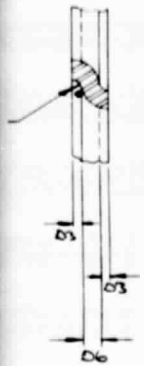


SECTION A-A
SCALE 4:1



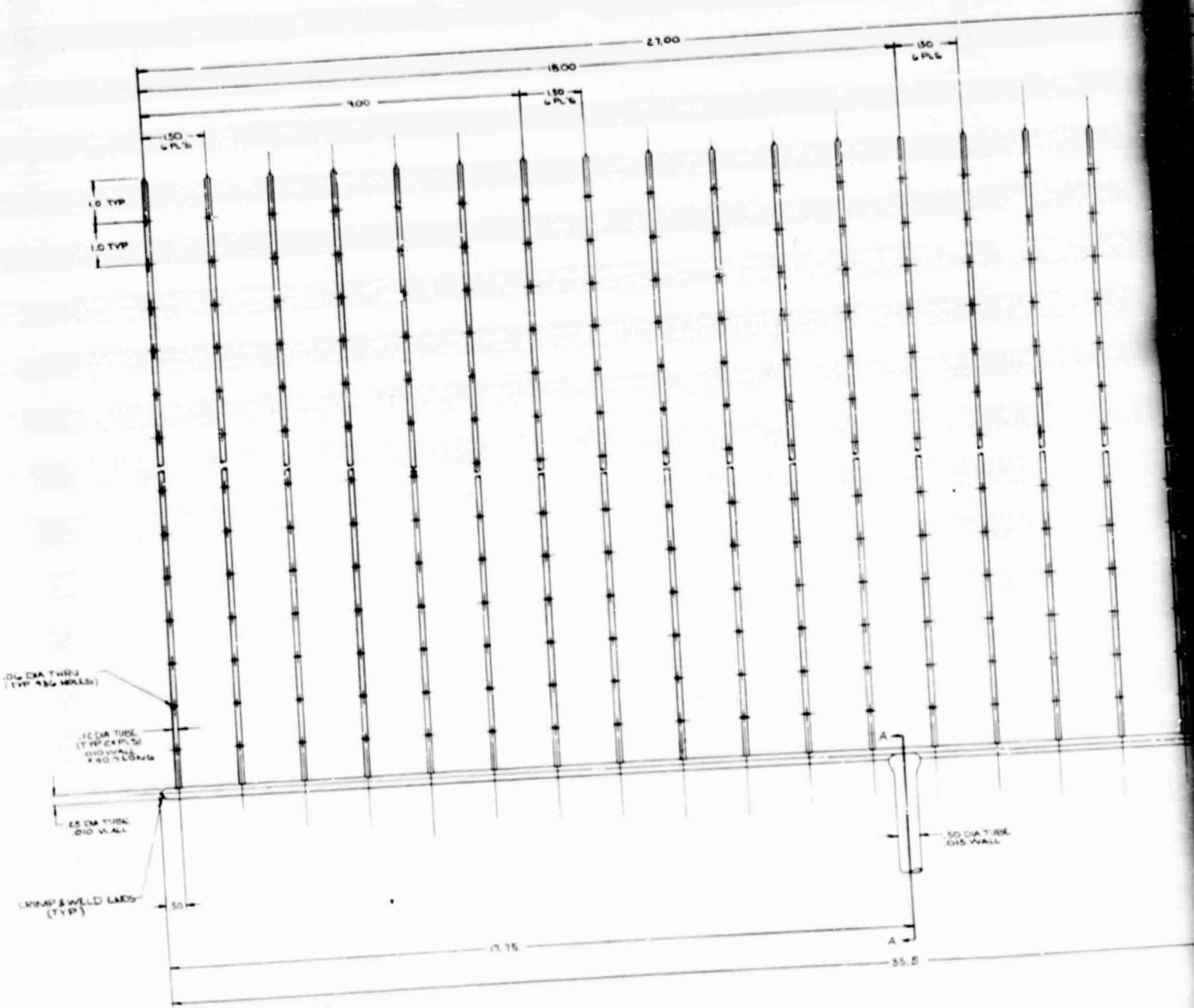
PRECEDING PAGE BLANK NOT FILMED

FOLDOUT FRAME



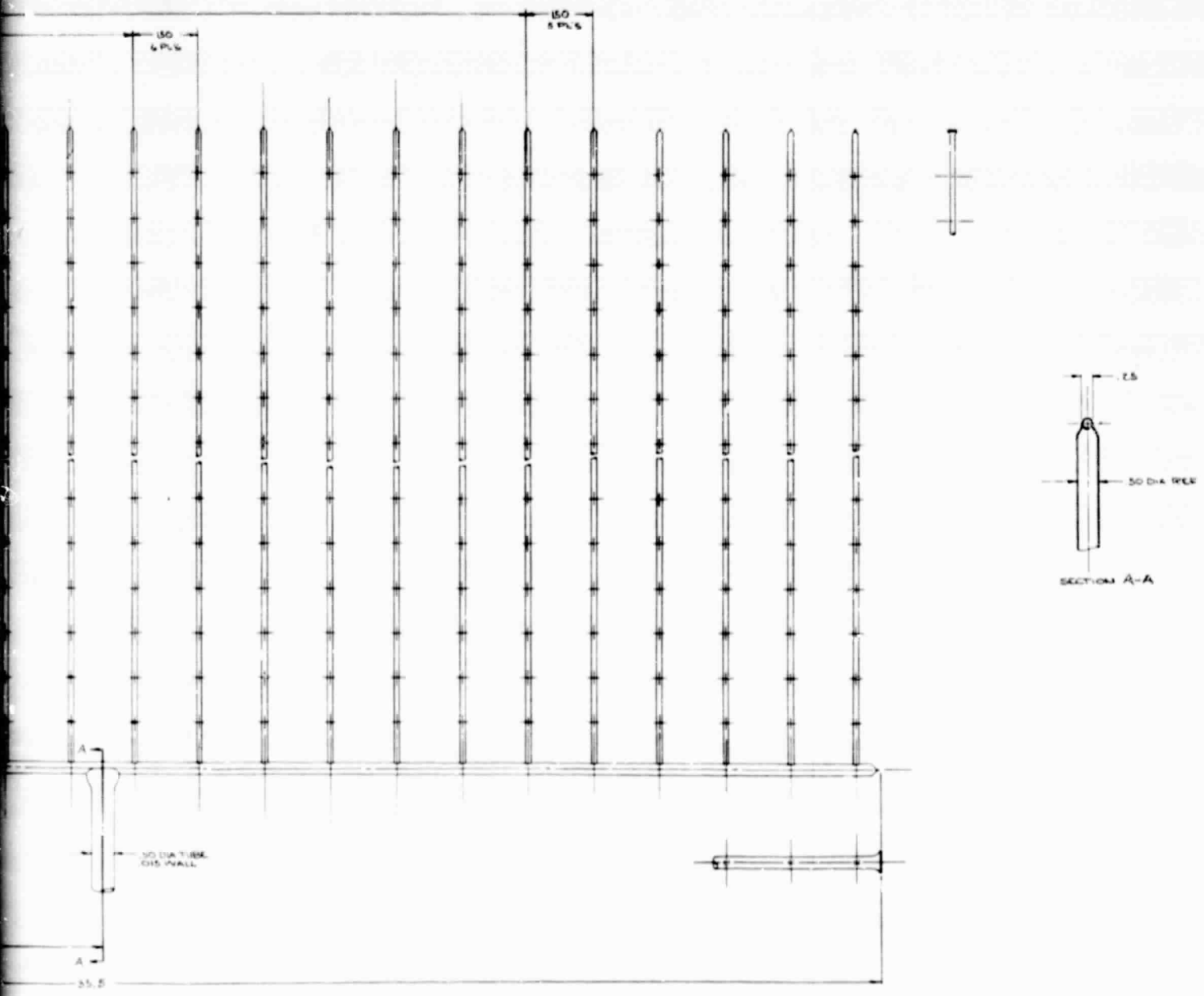
MATL: INCONEL 617

Figure 6.22 Discharge Heat Pipe Header, Transport Pipe Side



FOLDOUT FRAME

PRECEDING PAGE BLANK NOT FILMED



MATL
CONEL 617

Figure 6.23 Return Liquid Distributor Tubing Assembly

FOLDOUT FRAME 2

A-2997

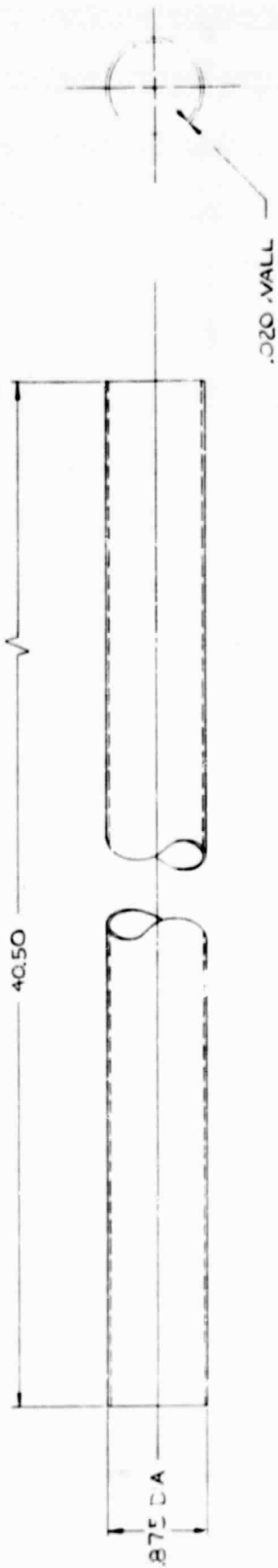
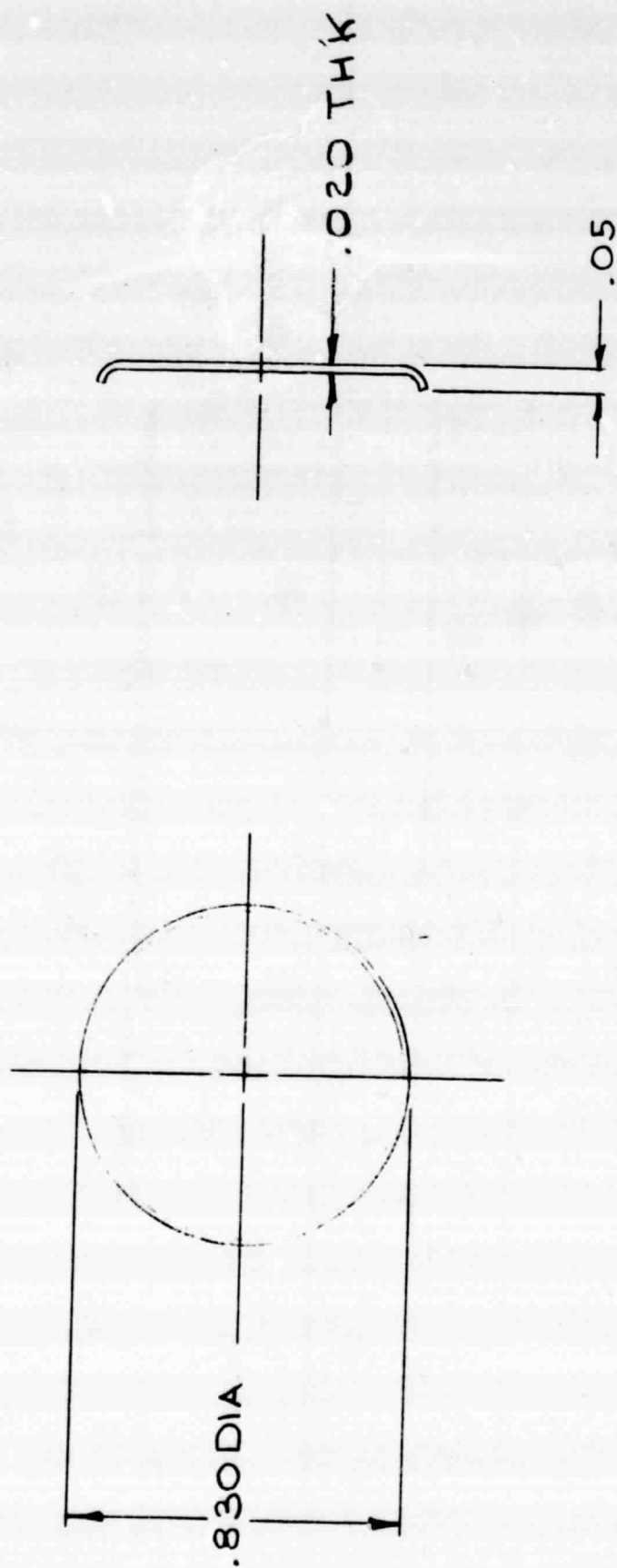


Figure 6.24a Discharge Heat Pipe Tube and Enclosure

A-2998



6-60

Figure 6.24b Closure Cap of Discharge Heat Pipe Tube

C-3

flat sides, as illustrated in Figures 6.25 and 6.26. Of prime concern in the design was an outer box structure which could support the internal vacuum over the large flat surfaces with minimum weight while still requiring only straight seam welds to facilitate manufacture of a vacuum-tight box.

The loads on the outside box are of the same nature as those on the inside box, namely, pressure and acceleration loads. There are, however, some differences:

- The outside box is at ambient temperature, and therefore carbon steel, low alloy steel or aluminum can be used.
- The outside box surrounds the inside box, and therefore no cross members or diaphragms can be used to brace the walls of the outer box. This is a constraint because the inner and outer boxes must be independent.
- The outer box supports only itself and part of the Multi-Foil insulation.

Each face of the outside box is a plate supported on four sides. The plate configurations considered were corrugated sheets and honeycomb sandwich panels. Corrugated sheets carry out-of-plane loads in one-way action only, and require edge members to carry in-plane shear forces. In addition, the joints involve long, multiple, S-type welds. Sandwich panels are structurally efficient since the skins are optimally placed at the full depth of the panel and the panels carry loads in two-way action.

A-2999

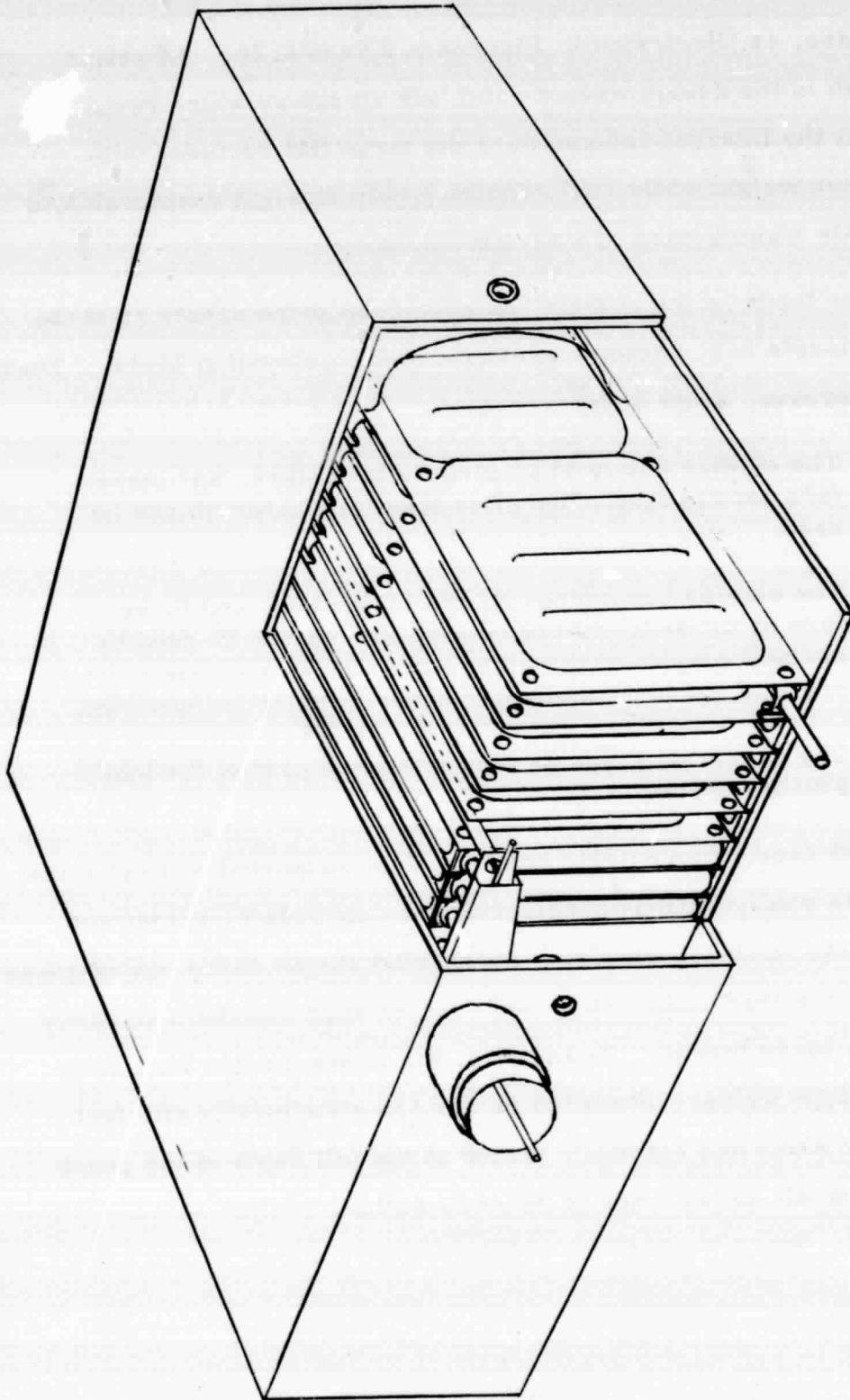


Figure 6.25 Multi-Foil Insulation Around Inner Box

19-1078

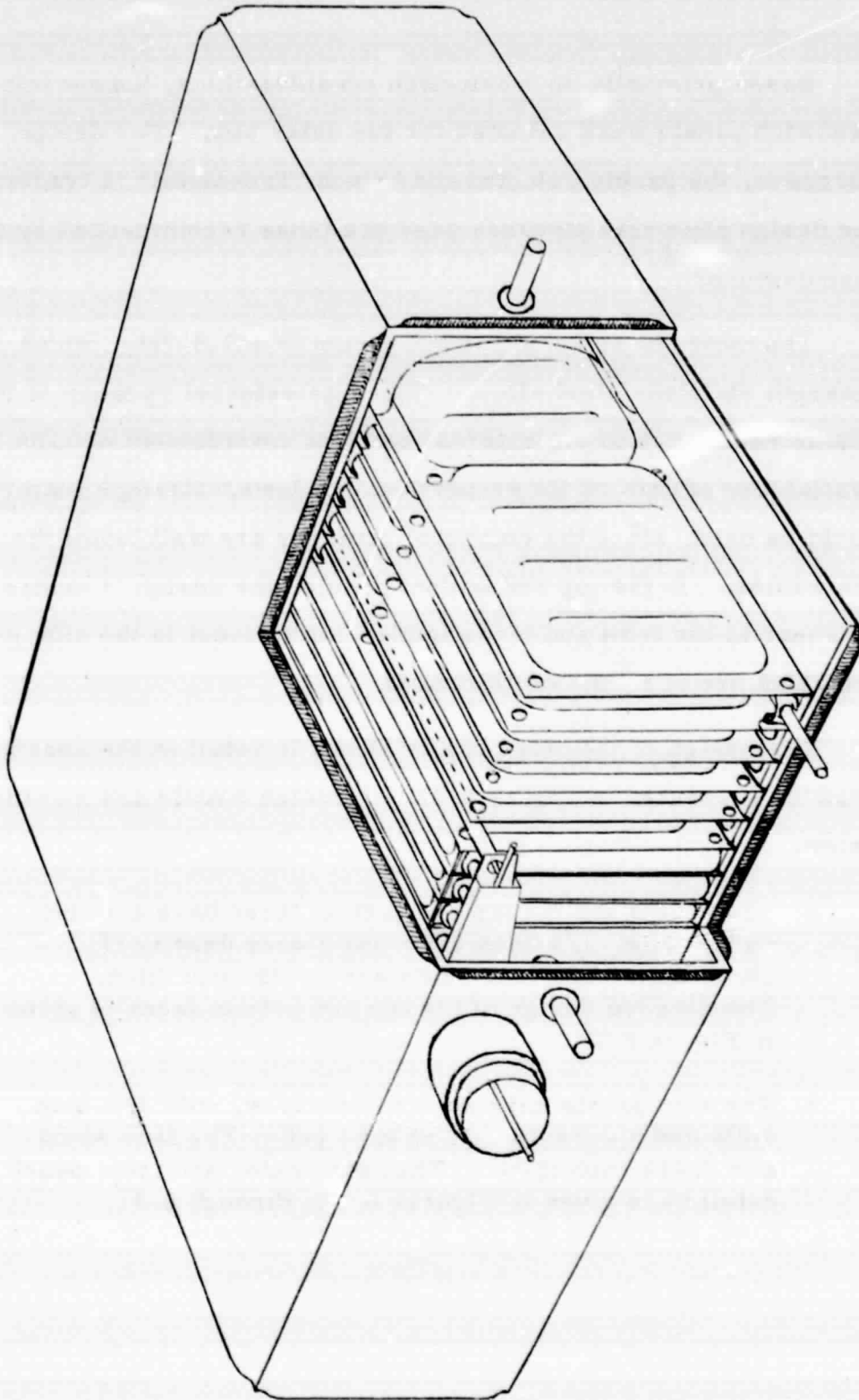


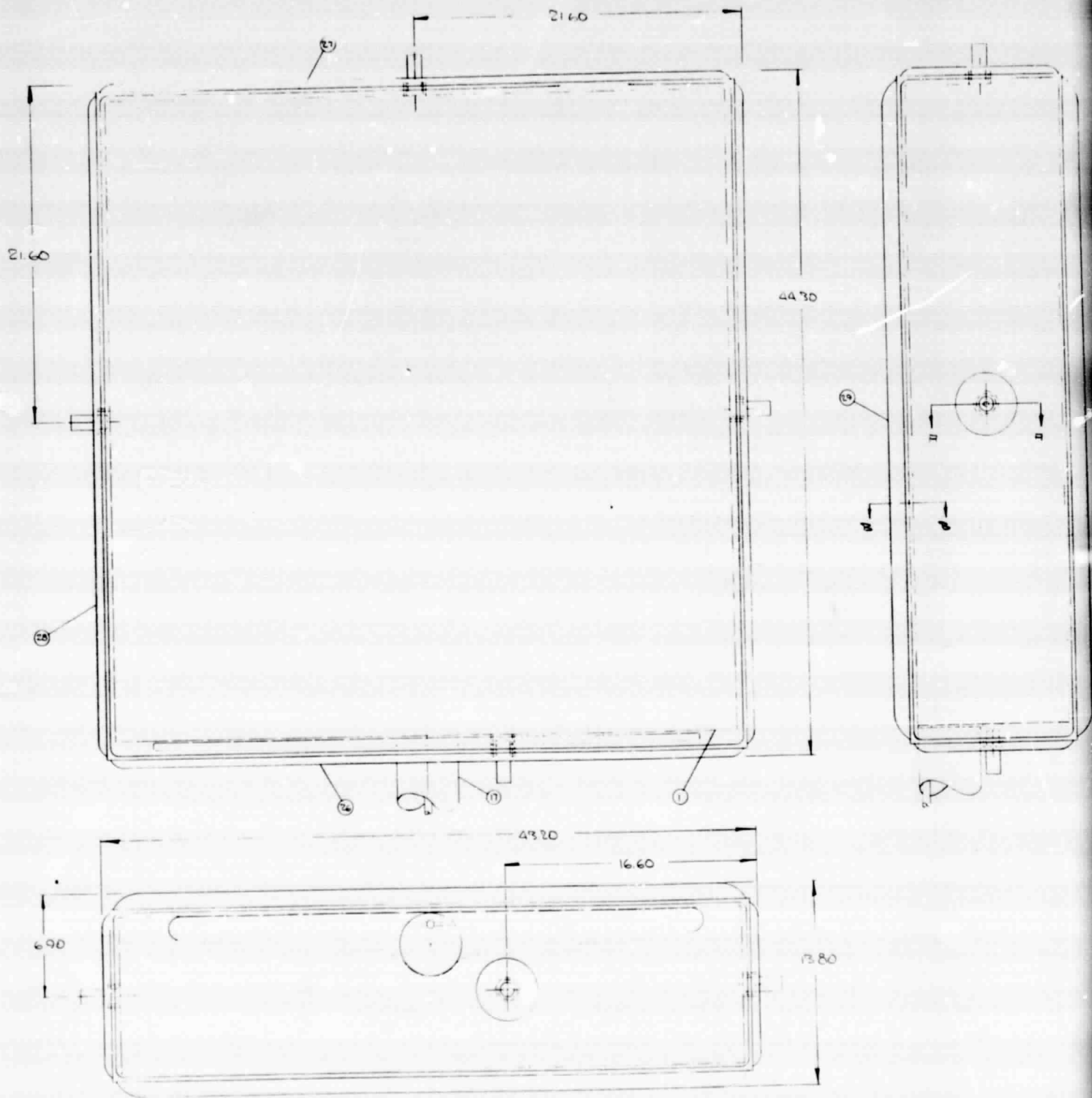
Figure 6.26 Honeycomb Outer Box to Provide Vacuum in Multi-Foil Insulation

Based primarily on fabrication considerations, honeycomb sandwich panels were selected for the outer box. For design purposes, the panels selected are Astech "Tre-Metal" (a trademark); the design allowable stresses used are those recommended by the manufacturer.⁴

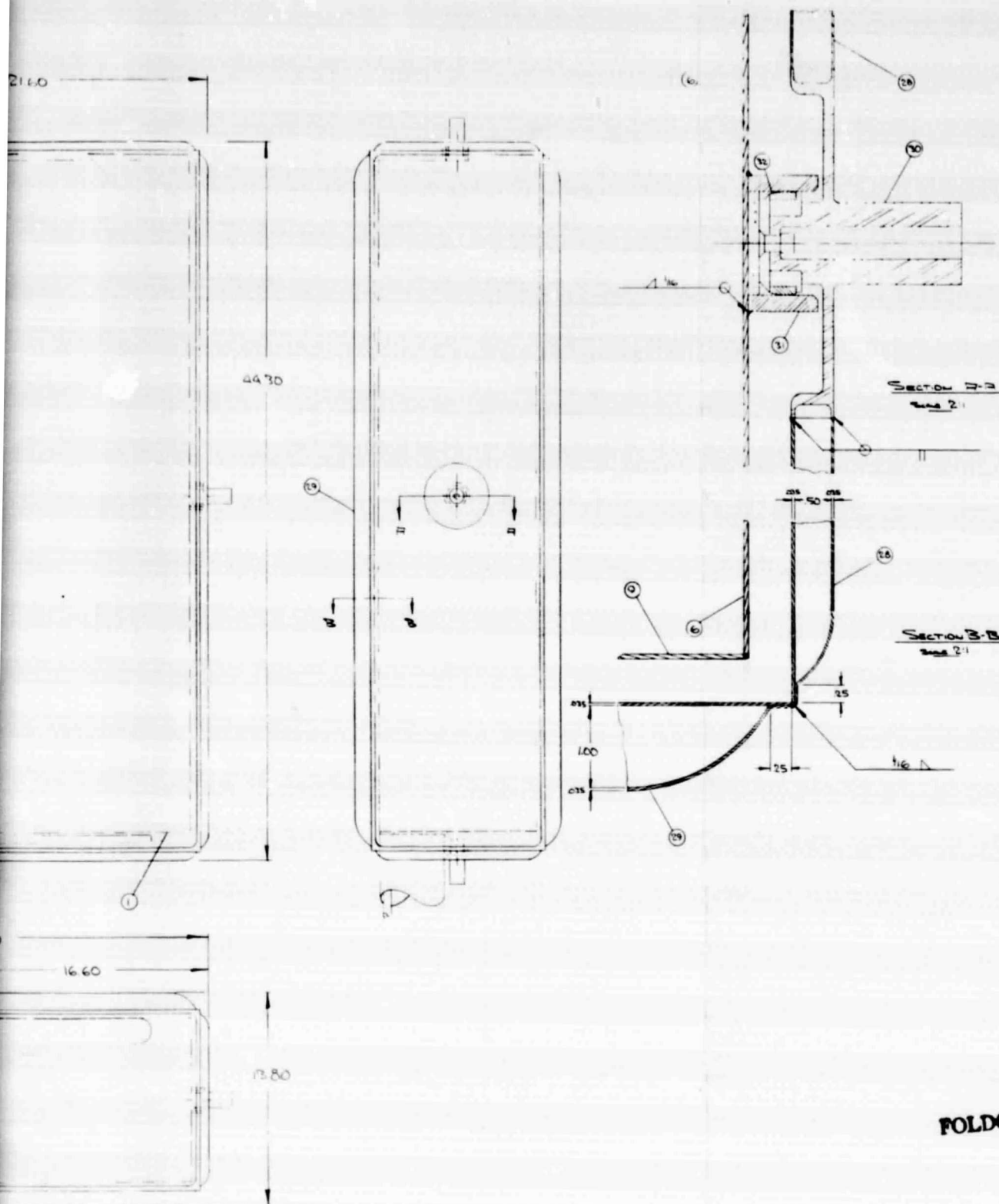
The material selected for the panels is PH15-7Mo, which is a high-strength stainless steel alloy. This was selected because of its corrosion resistance to the external ambient environment and the ready availability of data on its properties. A lower-strength material could be used, since the computed stresses are well below the allowables. In the top and bottom panels, the design is controlled by shear in the core and by deflection limitations; in the side panels, the skins are of minimum thickness.

The design of the outer box is shown in detail in the assembly drawing presented in Figure 6.27. Design details are summarized below:

- The panels for the top and bottom faces have a 1-inch core, with 1/4-inch cells and a core density of 10.33 pcf. The face skins are 0.035-inch thick. The detailed design of the top and bottom faces is given in Figure 6.28.
- The side panels have an 0.5-inch core, with 1/4-inch cells and a core density of 9.61 pcf. The face skins are 0.012-inch thick. The rear, side, and front panel details are given in Figures 6.29 through 6.31.



FOLDOUT FRAME



FOLDOUT FRAME 2

Figure 6.27 Assembly Drawing of Outer Box with Details of Pin Support

A-3001

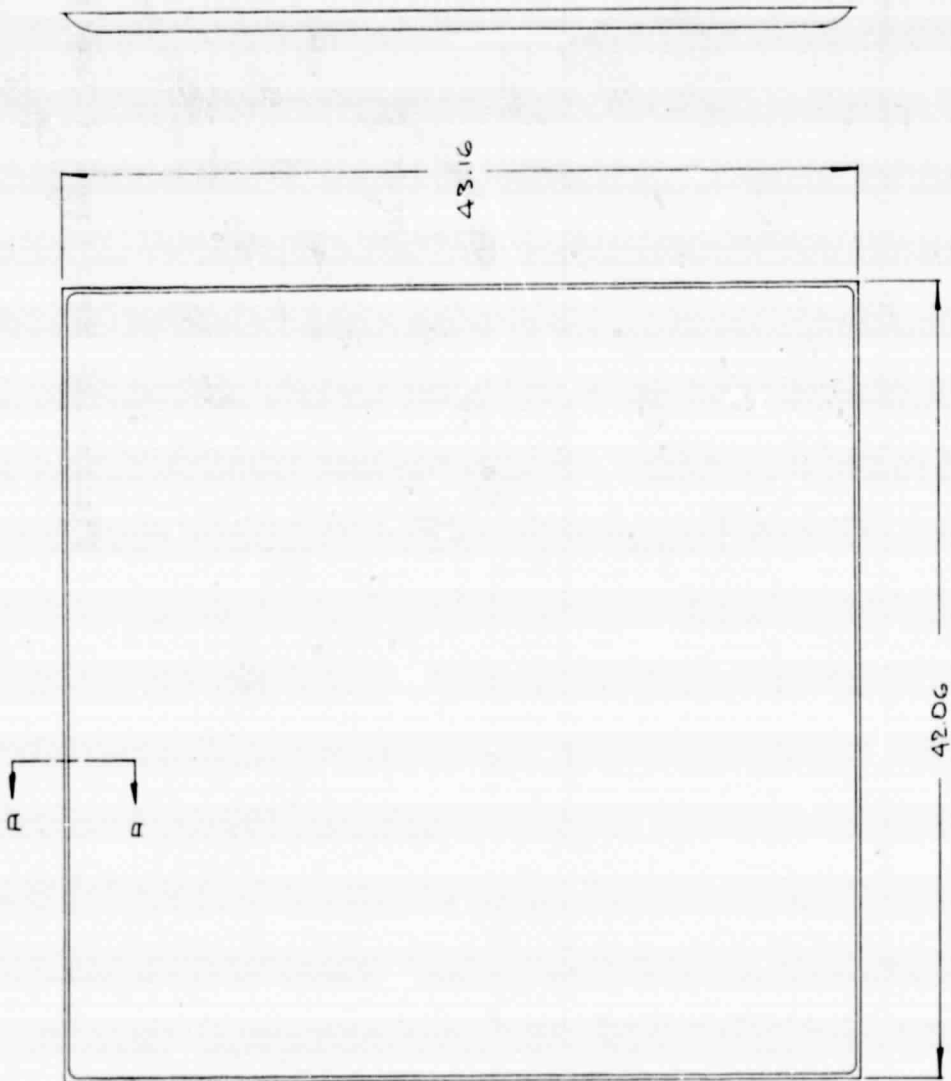
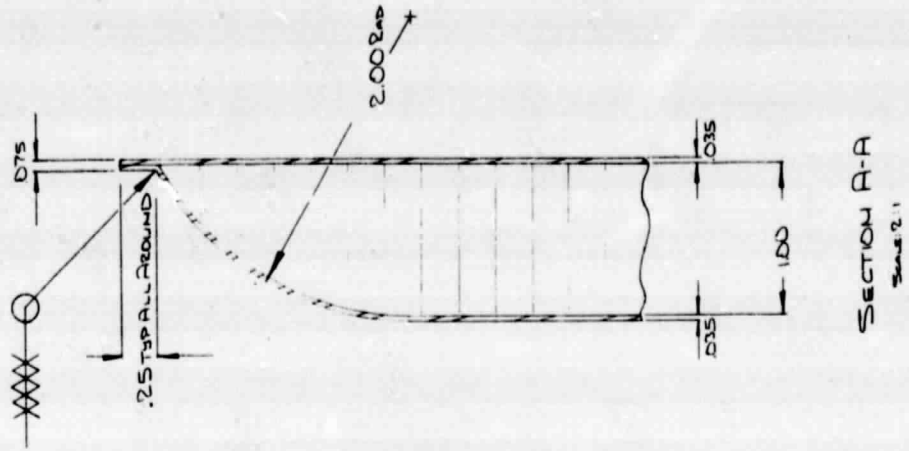


Figure 6.28 Top and Bottom Panels of Outer Box

A-3002

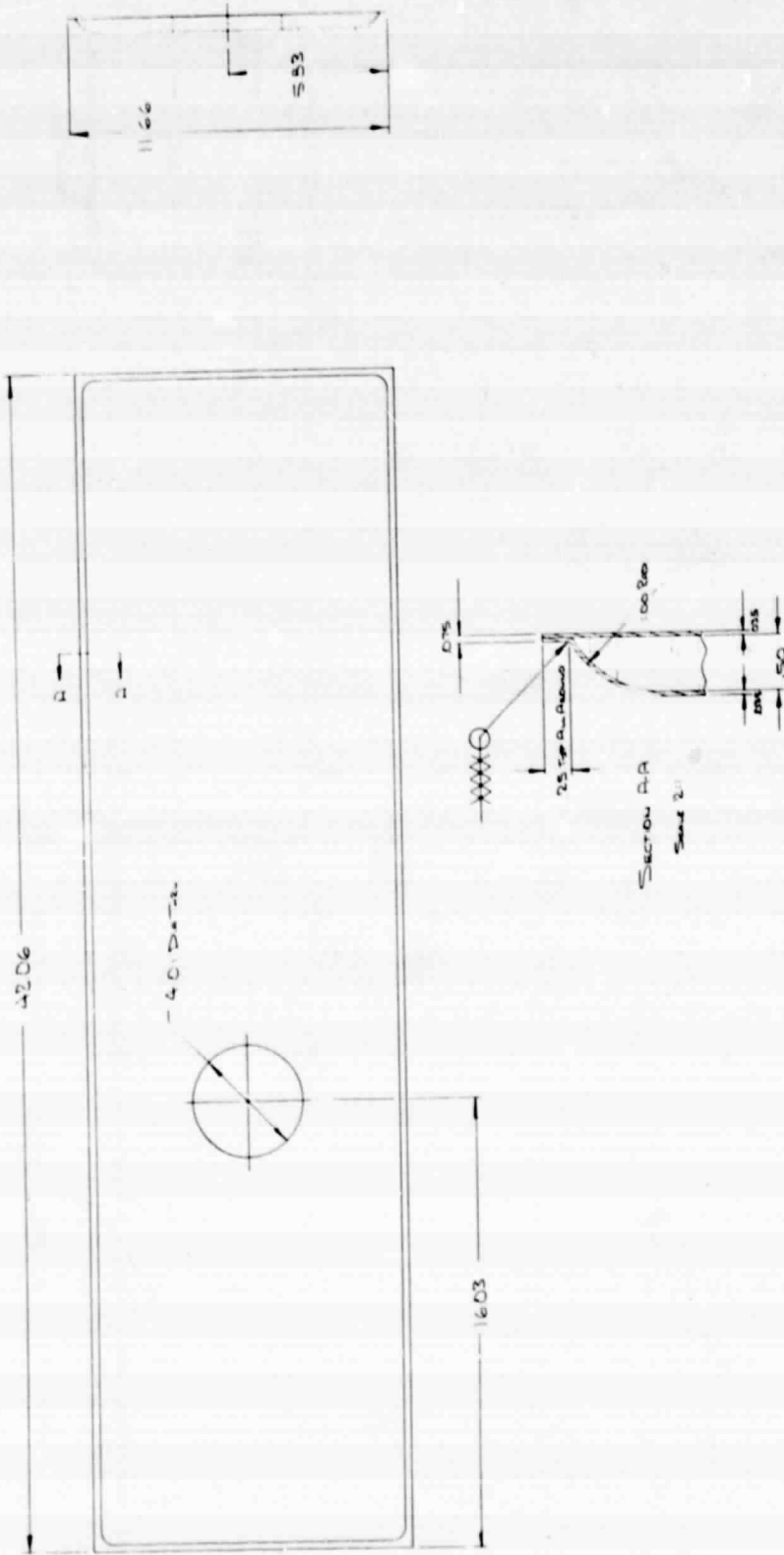


Figure 6.29 Rear Panel of Outer Box

A-3003

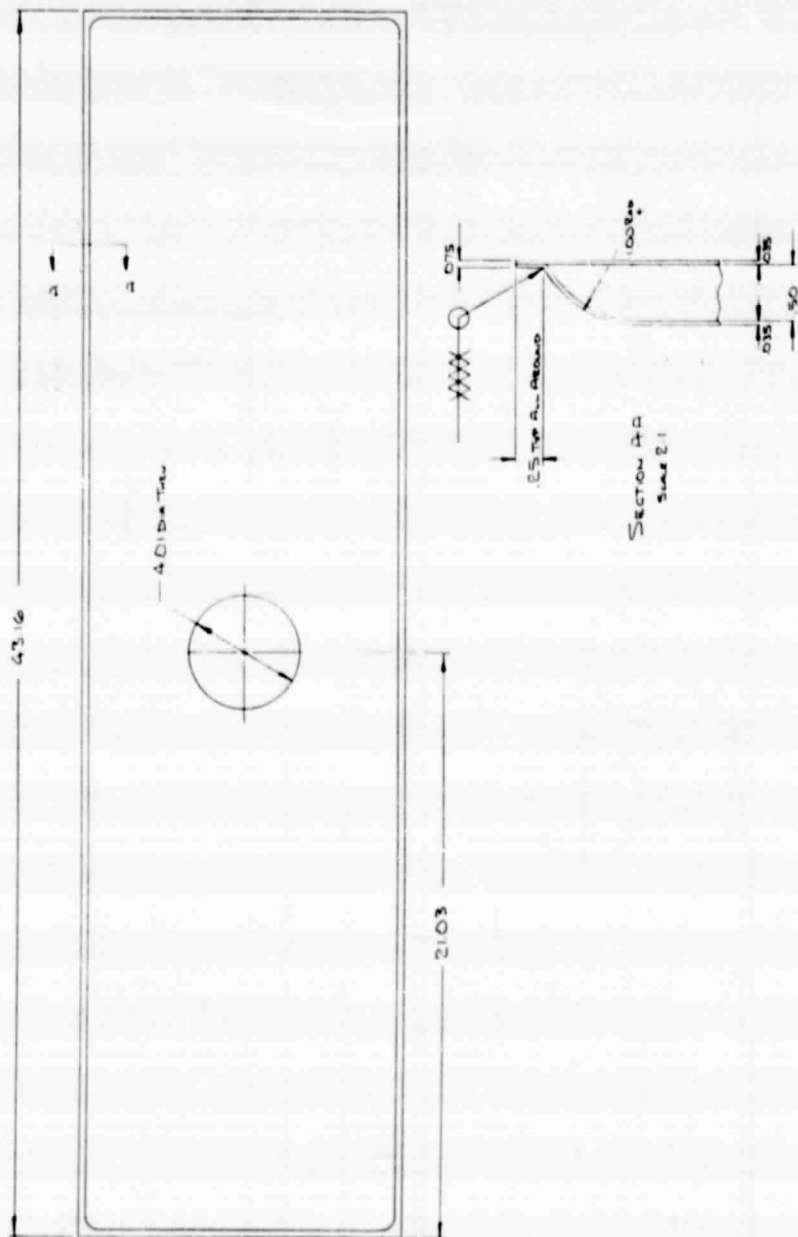


Figure 6.30 Side Panel of Outer Box (2 Req'd)

A-3004

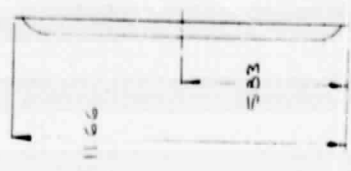
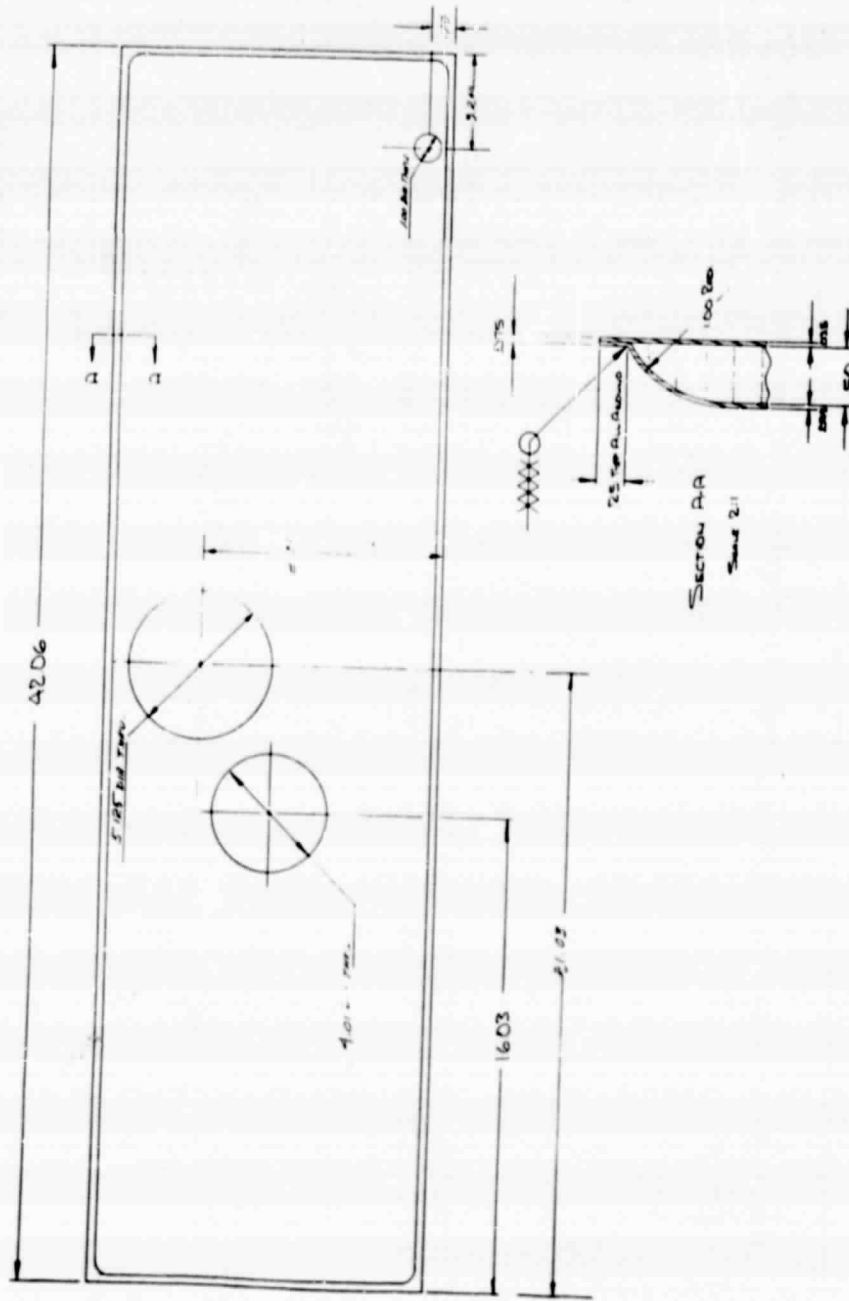


Figure 6.31 Front Panel of Outer Box

- The box is supported by the four pins which also support the inner box. The pins are welded to the outer box. In Figure 6.27, a cross section of the pin support arrangement for both the inner and outer boxes is presented, with part details given in Figures 6.32 and 6.33.
- A 5-inch diameter pipe surrounds the 4-inch diameter pipe from the manifold as it passes out of the outer box forming the space for the vacuum Multi-Foil insulation. At the appropriate distance from the outer box and near the Stirling engine the annulus between the pipes is sealed off by a bellows as illustrated in Figure 6.37 for the cylindrical unit assembly.
- The inside dimensions of the box are 43.25 in. x 42.125 in. x 11.625 in; the outside dimensions are 44.3 in. x 43.2 in. x 13.8 in; and the weight of the box is approximately 118 lbs.

The plan view of the outer box is not square, because space for the discharge heat pipe manifold is needed along one side of the inner box, which has a square plan.

The edge detail is based on one proposed by Astech for a similar panel. The vacuum tightness of the box depends on a single straight seam weld along each edge, and is in marked contrast to the intricate welding required at the intersection of corrugated sheets.

For pressure loads, the panels act as simply supported plates with lateral and in-plane forces. Acceleration loads must be carried to the four pin supports. For the outside box, acceleration loads arise out of their own mass and part of the Multi-Foil insulation. In general, local acceleration loads are carried by in-plane

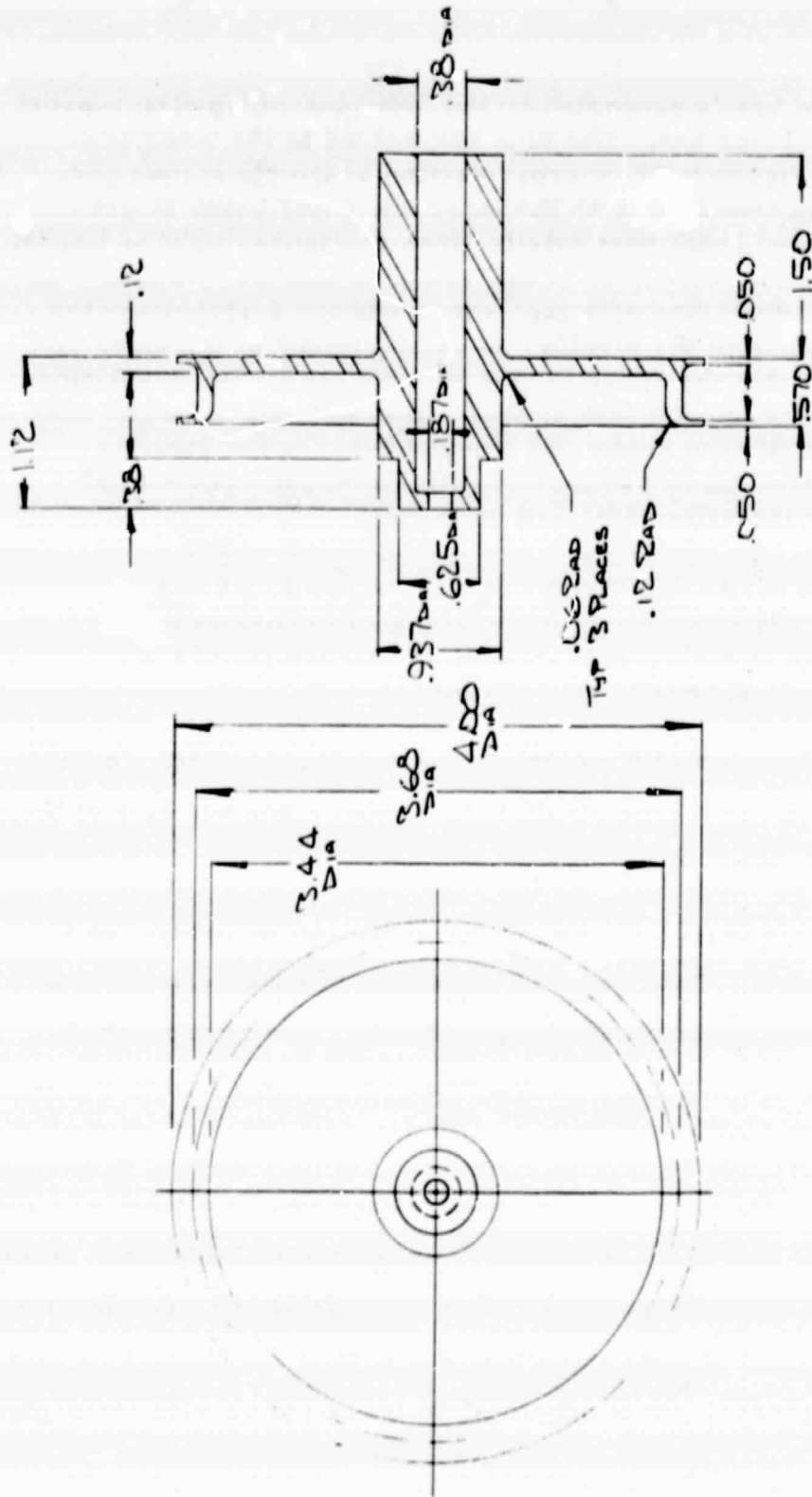


Figure 6.32 Pin Support Welded into Outer Box Opening

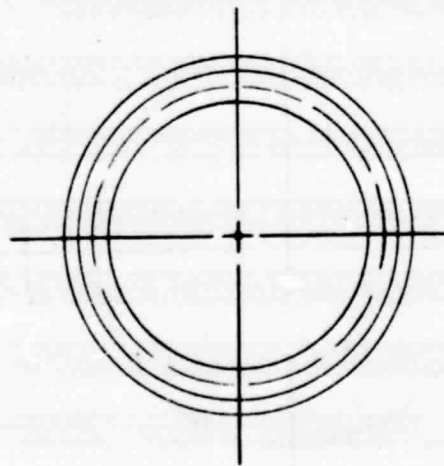
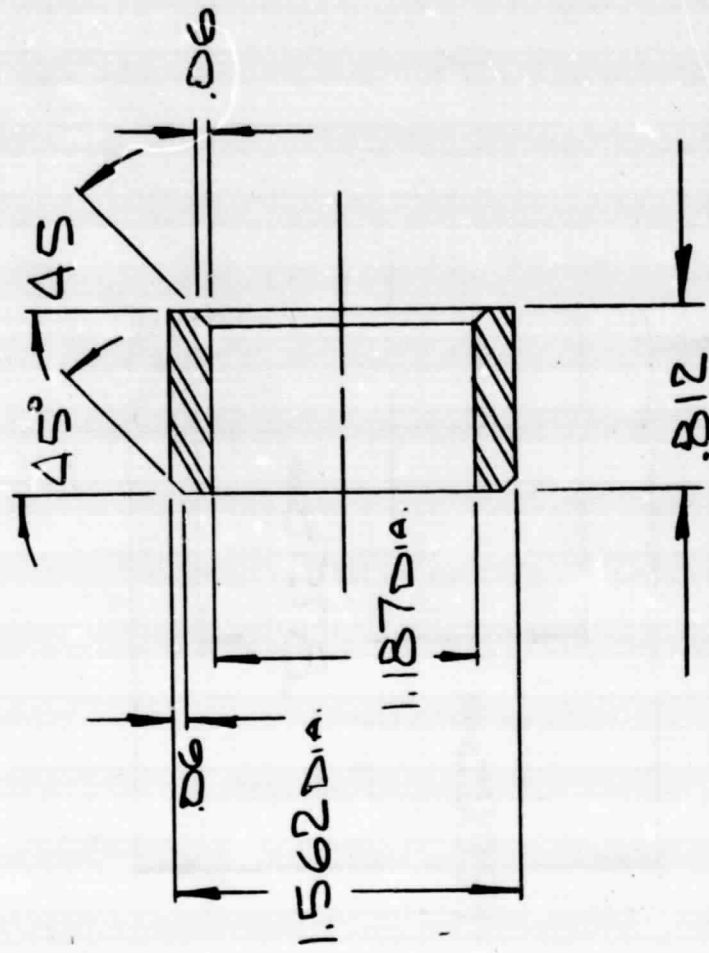


Figure 6.33a Support Bushing Welded to Trusses of Inner Box

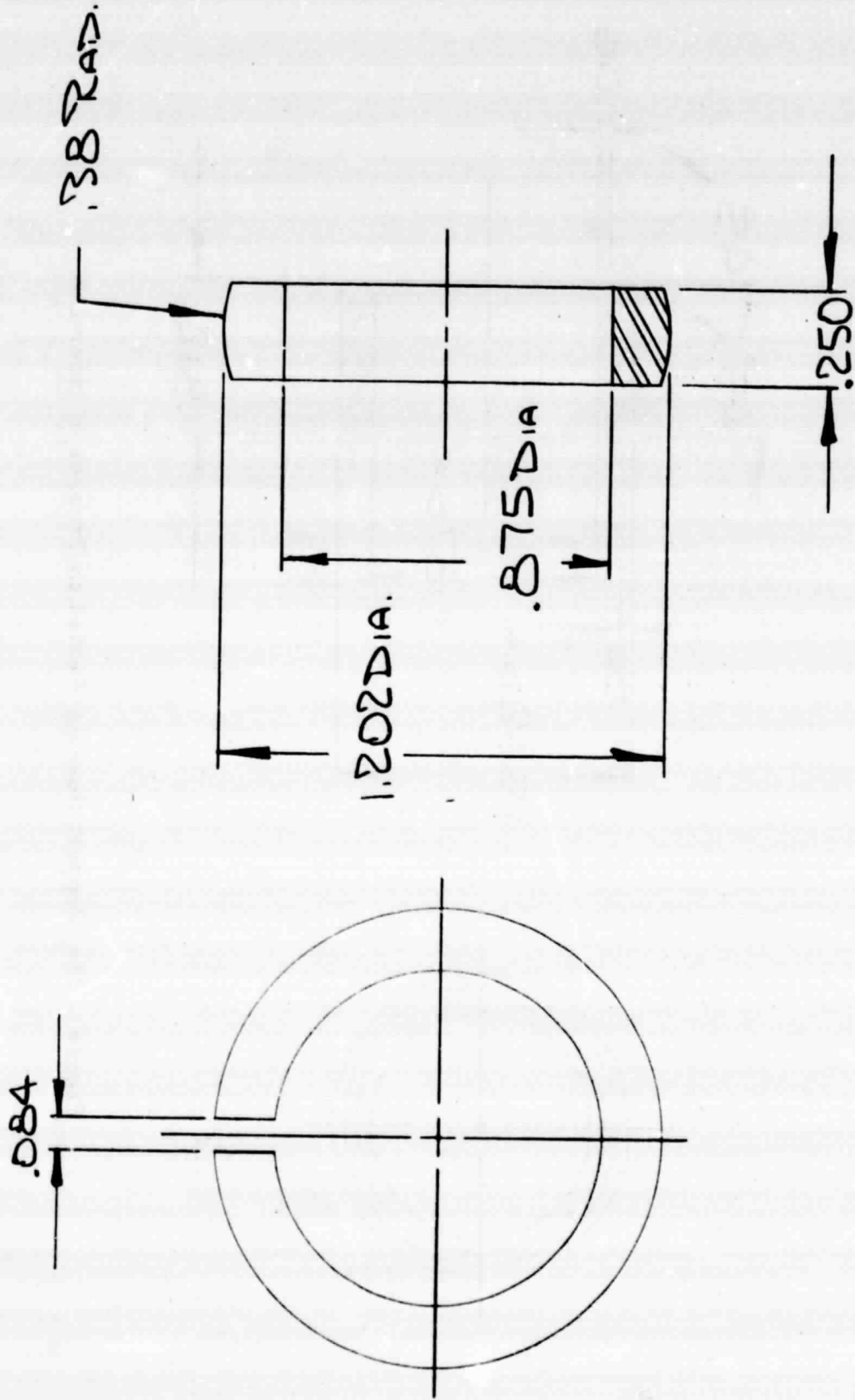


Figure 6.33b Support Ring for Inner Box

action to the pins or by out-of-plane bending of the panels to their edges; the loads delivered to the edges are then carried to the pins by panels acting as deep beams.

The inside dimensions of the outer box are selected to provide the required minimum 0.5-inch clearance for the Multi-Foil insulation between the boxes. These dimensions take into consideration the deflections of the outer box due to the external pressure load.

6.3.2 Miscellaneous Details

In the manufacturing procedure of Chapter 8, it is planned to use precast salt blocks for charging the salt capsules prior to welding of the salt capsules. In Figure 6.34, the dimensions of the tall and short salt blocks required are presented. The salt capsules will be cast with a small percentage of aluminum powder to act as a corrosion inhibitor, as discussed in Chapter 2. These dimensions allow room for the salt to expand on heating and melting. After welding, the capsules must be evacuated. Each salt capsule will have a pinch-off tube for evacuation and sealing, as illustrated in Figure 6.35. A small quantity of potassium will also be sealed in each salt capsule to equalize the internal capsule pressure with the external pressure.

In Figure 6.36, the tabs for tying each primary diaphragm to the top and bottom diaphragms and to the side trusses are illustrated.

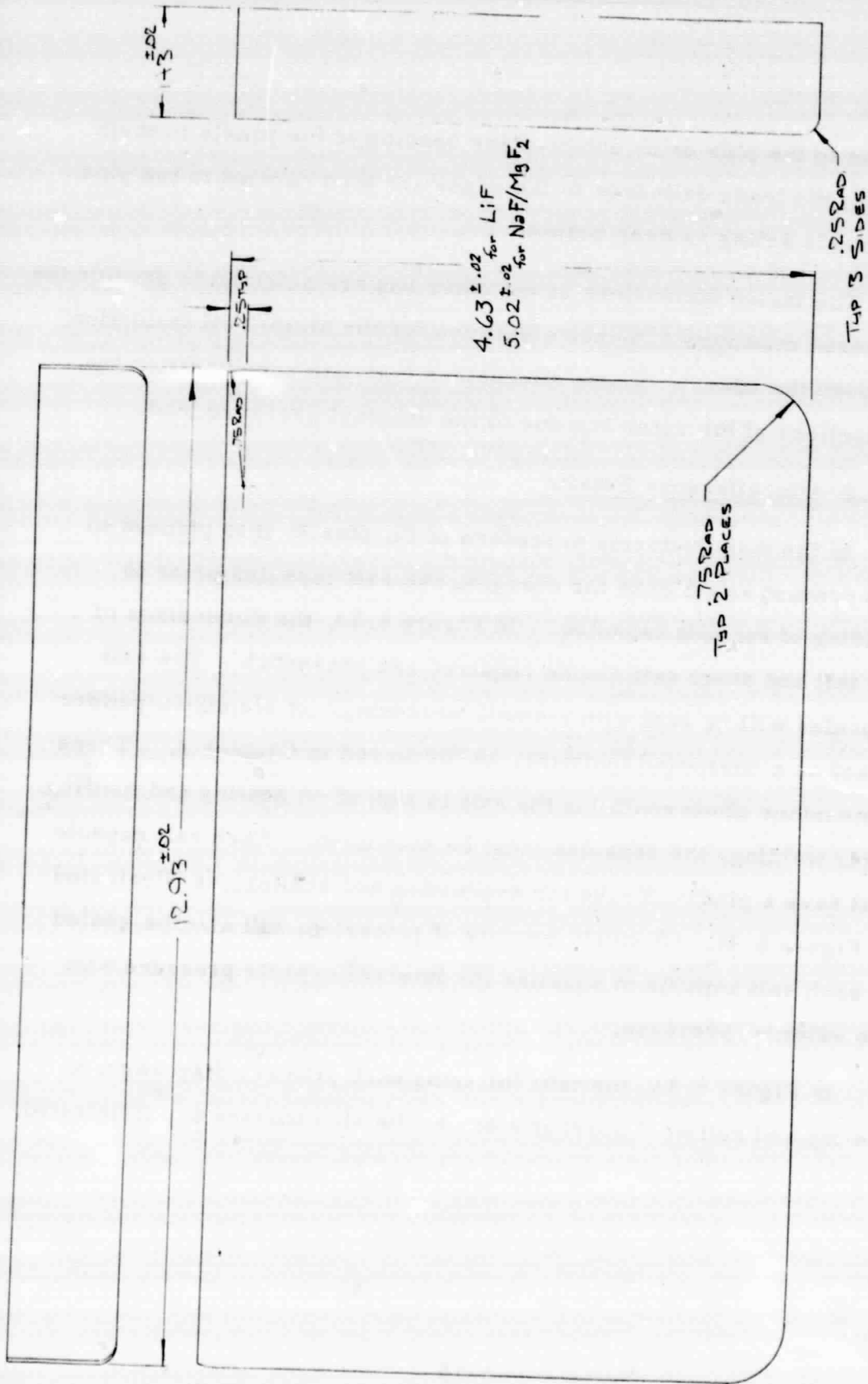


Figure 6.34a Molded Salt Capsules for Charging; Short (for End Capsules)

A-3009

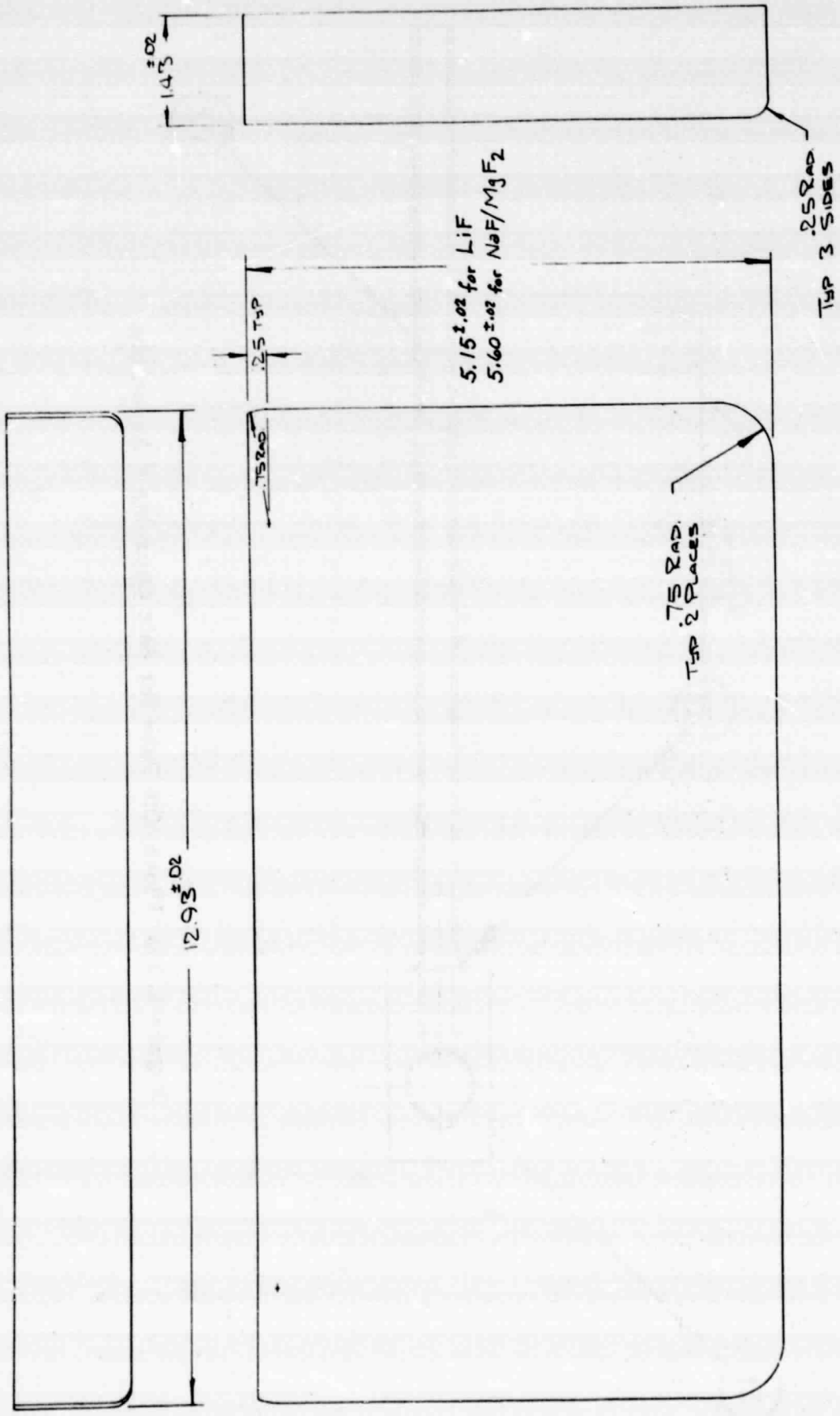


Figure 6.34b Molded Salt Capsules for Charging: Long (For all Except End Capsules)

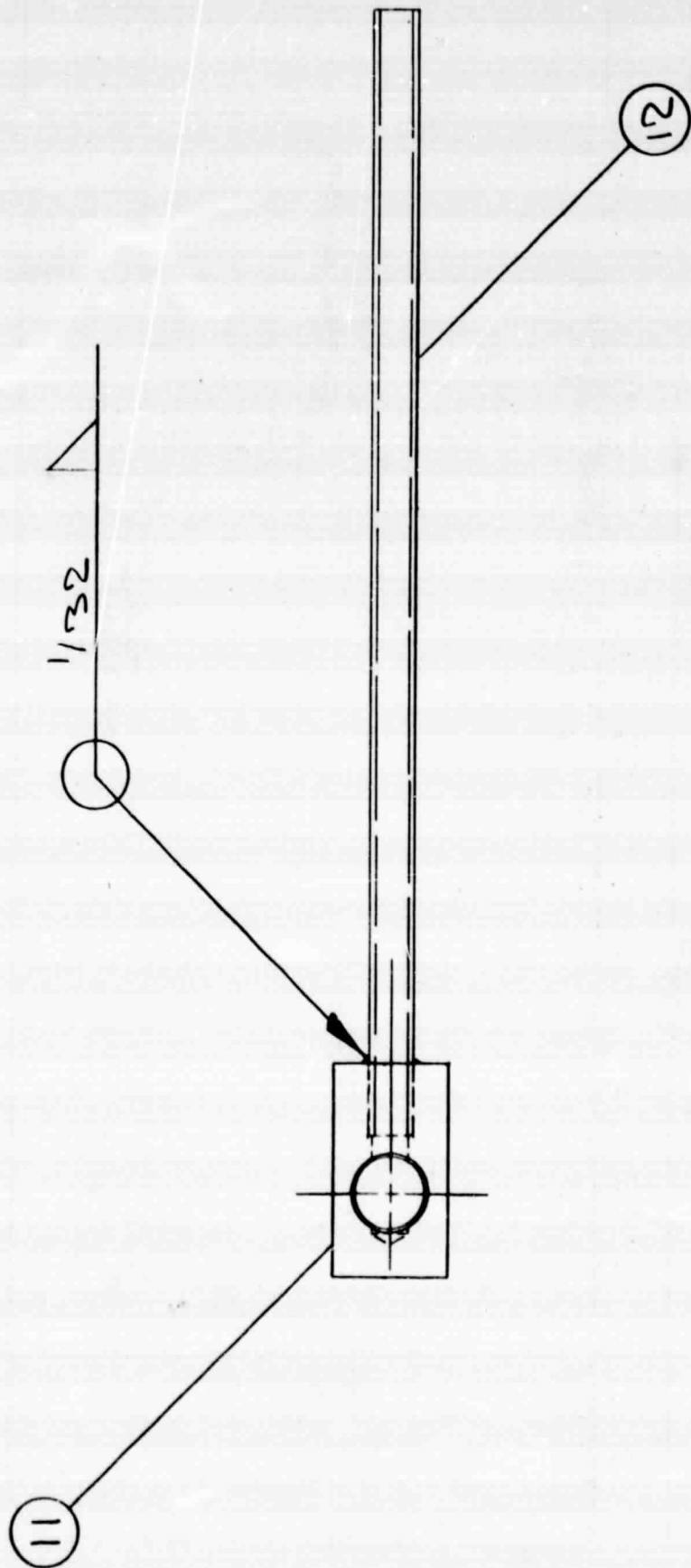


Figure 6.35a Pinch-Off Tube for Salt Capsules - Assembly

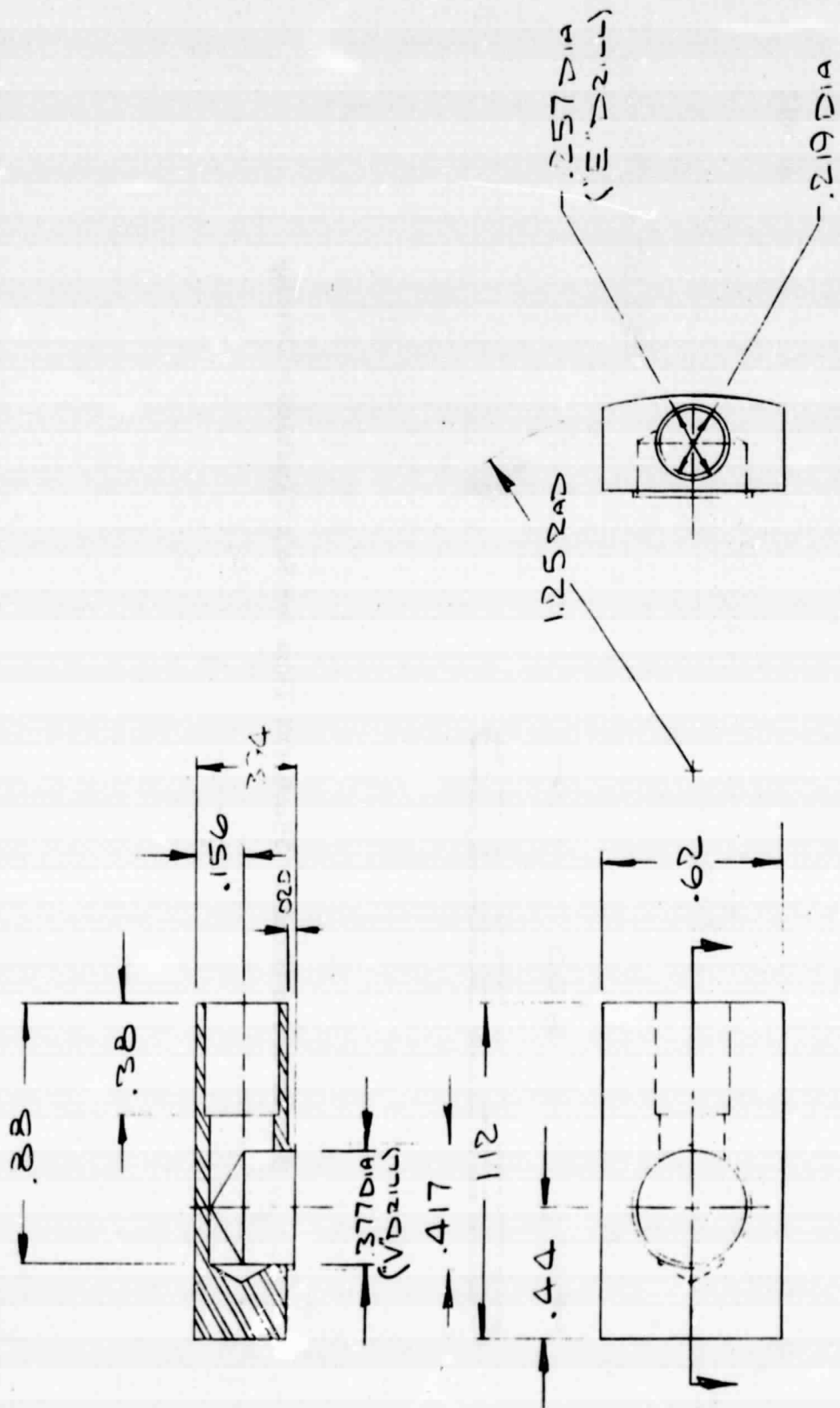
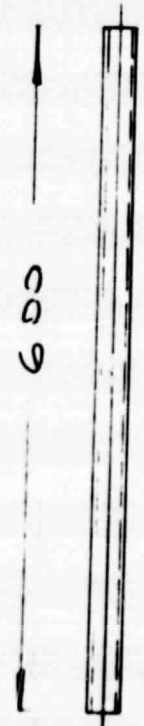


Figure 6.35b Pinch-Off Tube for Salt Capsules - Details

A-3012

1500D-532 Wall

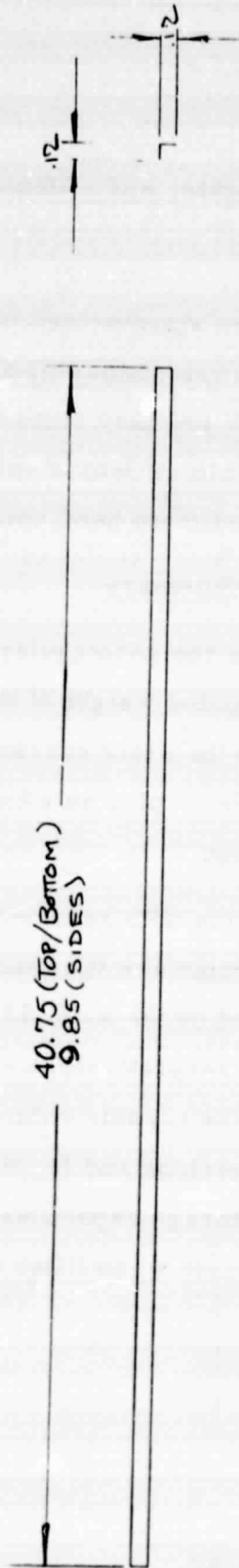


6-80

Figure 6.35b (Cont'd) Pinch-Off Tube for Salt Capsules = Details

ORIGINAL PAGE IS
OF POOR QUALITY

A-3013



THICKNESS = .010

Figure 6.36 Tabs for Tying Primary Diaphragms to Reinforcing Skin

6.3.3 Summary of Stresses, Weights, and Volumes

6.3.3.1 Stress Summary

Stresses for the inside box are summarized in Table 6.3, while stresses for the outside box are summarized in Table 6.4. As can be seen in these tables, all primary stress elements have been checked to have stresses within allowable values. The computed stresses are based on approximate hand computations.

6.3.3.2 Weight and Volume Summary

A breakdown of the weight for the rectangular box structure is given in Table 6.5. The estimated weight of the inner box is based on a unit weight of 0.32 lbs/in^3 ; this corresponds to the unit weight of Inconel 617 (0.302 lbs/in^3), plus an allowance of 5 percent for connections and local stiffening.

In Table 6.6, a summary of the TES reservoir characteristics is presented. Of particular interest are the fractions of the total TES reservoir weight represented by the salt, 59.5 percent and 64.0 percent for LiF and NaF/MgF₂, respectively; and the fraction of the total volume represented by the capsule volume, 44.7 percent and 75.3 percent for the outer envelope and for the inside of the inner box, respectively. The storage capacities are 169 kwhrth when filled with LiF, and 125 kwhrth when filled with NaF/MgF₂.

TABLE 6.3
INNER RECTANGULAR BOX OF INCONEL 617
STRESS SUMMARY

Result No.	Element	Loading or Result No.	Type of Stress	Stress (ksi)	Allowable Stress (ksi)
1	Primary diaphragm (t=0.015)	Internal pressure	Stretching, direction Y	3.0	3.0
2	Primary diaphragm (t=0.015)	Internal pressure	Stretching, direction Z	3.0	3.0
3	Primary diaphragm (t=0.19)	Internal pressure	Stretching, direction Y	0.4	3.0
4	Primary diaphragm (t=0.19)	Internal pressure	Compression, direction Z	0.4	-
5	Primary diaphragm (t=0.19)	Internal pressure	Bending, direction Z	2.5	-
6	Primary diaphragm (t=0.19)	4 + 5	-	2.9	3.0
7	Top/Bottom diaphragm (t=0.05)	Internal pressure	Stretching, direction X	3.0	3.0
8	Top/Bottom diaphragm (t=0.05)	Gravity	Stretching/compression, direction Y	0.5	3.0
9	Top/Bottom diaphragm (t=0.05)	Acceleration Y	Stretching due to bending, direction X	0.2	-
10	Top/Bottom diaphragm (t=0.05)	7 + 9	Stretching	3.2	16.0

A-3023b

TABLE 6.3 (cont.)
 INNER RECTANGULAR BOX OF INCONEL 617
 STRESS SUMMARY

Result No.	Element	Loading or Result No.	Type of Stress	Stress (ksi)	Allowable Stress (ksi)
11	Top/Bottom diaphragm (t=0.05)	Acceleration Z	Stretching/compression, direction Y	1.6	-
12	Top/Bottom diaphragm (t=0.05)	8 + 11	Stretching	2.1	16.0
13	Cylindrical shells	Internal pressure	Hoop tension	3.0	3.0
14	End caps	Internal pressure	Hoop tension	3.0	3.0

A-3024

TABLE 6.4
OUTER RECTANGULAR BOX OF TRE-METAL
STRESS SUMMARY

Result No.	Element	Loading or Result No.	Type of Stress	Stress	Allowable Stress
1	Top/Bottom Panels	External pressure	Bending of panel, stretching of skin	38.7 ksi	150.0 ksi
2	Top/Bottom Panels	External pressure	Shear in core	265.0 lb/in.	265.0 lb/in.
3	Edge strip of top/bottom panels	External pressure	Bending	26.9 ksi	150.0 ksi
4	Edge strip of top/bottom panels	External pressure	Shear	5.7 ksi	90.0 ksi
5	Side panels	External pressure	Bending of panel, stretching of skin	43.7 ksi	117.0 ksi
6	Side panels	External pressure	Shear in core	82.5 lb/in.	145.0 lb/in.
7	Edge strip of side panels	External pressure	Bending	100.0 ksi	150.0 ksi
8	Edge strip of side panels	External pressure	Shear	5.2 ksi	60.0 ksi

TABLE 6.5
SUMMARY OF STRUCTURAL WEIGHT
RECTANGULAR BOX

		<u>lbs</u>
● Inner Box		
23 diaphragms,	$t = 0.015''$	45.3
2 diaphragms,	$t = 0.19''$	24.9
2 diaphragms,	$t = 0.05''$	53.8
24 edge pieces,	$t = 0.01''$	21.2
2 end pieces,	$t = 0.07''$	38.6
26 capsules,	$t = 0.01''$	57.7
4 trusses,	$t = 0.05''$	<u>27.7</u>
Subtotal		269
● Outer Box		
2 square panels,	$t_f = 0.035''$	93.7
4 rectangular panels,	$t_f = 0.012''$	22.1
edges		<u>2.3</u>
Subtotal		118
● Total Structural Weight		387
● Multi-Foil Insulation Weight		95
● Heat Pipe Weight		25
● Total TES Reservoir Weight Less Salt		507 (230 kg)

TABLE 6.6

SUMMARY OF WEIGHTS, VOLUMES,
HEAT TRANSFER AREAS, AND TES CAPACITY
FOR RECTANGULAR CONFIGURATION

Internal Capsule Volume	12,000 in ³	
Volume of Inner Box (Inside)	15,670 in ³	
Volume of Outer Box (Outside)	26,410 in ³ (0.433 m ³)	
Surface Area of Salt Capsule	19,000 in ² (132 ft ²)	
Surface Area of Discharge Heat Pipe Tubes (OD)	2,672 in ² (18.6 ft ²)	
Surface Area of Recharge Heat Pipe Tube (OD)	111.3 in ² (0.773 ft ²)	
Total TES Reservoir Weight Less Salt	507 lb (230 kg)	
Capsule Volume/Total Volume	0.447	
Capsule Volume/Inner Box Volume (Inside)	0.753	
	LiF	NaF/MgF ₂
Weight of Salt (Capsules 94% Full of Liquid at Melting Point)	744 lb (337 kg)	901 lb (409 kg)
Storage Capacity (Salt Only, 800°K- 1150°K)	172 kwhrth	127 kwhrth
Total TES Reservoir Weight	1251 lb (567 kg)	1408 lb (639 kg)
Salt Weight/Total TES Reservoir Weight	0.595	0.640

6.4 CYLINDRICAL DESIGN

The most common pressure vessel design is the circular cylindrical unit with spherical or ellipsoidal heads. For the TES reservoir a cylindrical design is also feasible; however, to accommodate the required 300 kg of salt within the packaging constraints, two cylindrical reservoirs are required. The outside dimensions chosen for each of the two units, except for local stiffeners, are a 50-inch long, 15-inch diameter cylinder with two ellipsoidal heads of 5.5-inch rise. The primary drawback of the cylindrical design is the lower packaging efficiency; nevertheless, two cylinders may prove to integrate into a car design as well as one rectangular unit. The cylindrical units are easier to fabricate than the rectangular unit, and would require less development for automated, high volume production.

6.4.1 Design Approach

There are many similarities in the design approach for the cylindrical and rectangular configurations. For the cylindrical design concept, the design requirements led to the selection of two congruent pressure vessels, each a cylindrical body with two ellipsoidal heads, that are positioned one-half of an inch apart to provide the volume for the Multi-Foil insulation. To allow for thermal expansion of the inner container to occur freely, a four-pin support system as previously described for the rectangular unit is used. The support plane was chosen as the symmetry plane that contains a circumference of the cylinder.

Once a pressure vessel configuration has been adopted, the primary design consideration is the method of containing the salt. A concept of individual salt capsules, shaped approximately as slices of a cylinder, was chosen. In this approach, the salt containers are stacked loose inside the inner pressure vessel; to physically restrain the salt capsules and prevent their crushing under acceleration loads, a series of restraining rings is used. These rings perform a dual role in that they also strengthen the thin shell of the pressure vessel. Strengthening is required at discontinuities such as the support plane and the head-to-cylinder intersection.

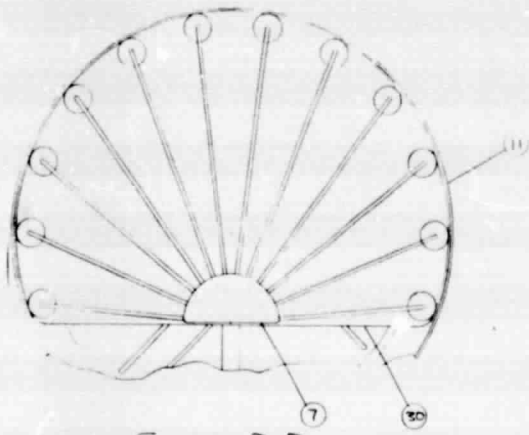
The pressure loading is such that the inside vessel is in tension (internal pressure from the potassium vapor) and the outside vessel is in compression (outside pressure from the atmosphere) as for the rectangular configuration. Under internal pressure the meridional and hoop stresses in the inner cylinder and in its ellipsoidal heads are tensile. Buckling is therefore not a consideration; nevertheless, the rings that are required for other purposes can also work to prevent buckling under external pressure should the vacuum in the insulation space be accidentally lost. The atmospheric pressure causes compressive meridional and hoop stresses in the outer pressure vessel. To prevent buckling of the thin shell, stiffening rings are necessary. Two of these rings also serve to channel the dead weight of the shell to the supports.

In summary, the cylindrical design consists of two congruent pressure vessels, with Multi-Foil insulation in between. Each pressure vessel is thin-walled, and therefore stiffened by rings. The salt is stored in short cylindrical capsules stacked in the inner pressure vessel. Discharge and charge heat pipes are incorporated in a fashion similar to that for the rectangular unit with tubes forming the wall separating the discharge/TES reservoir heat pipes. An assembly drawing of the entire unit is given in Figure 6.37, and perspective illustrations of the construction of the system are presented in Figures 6.38 - 6.41.

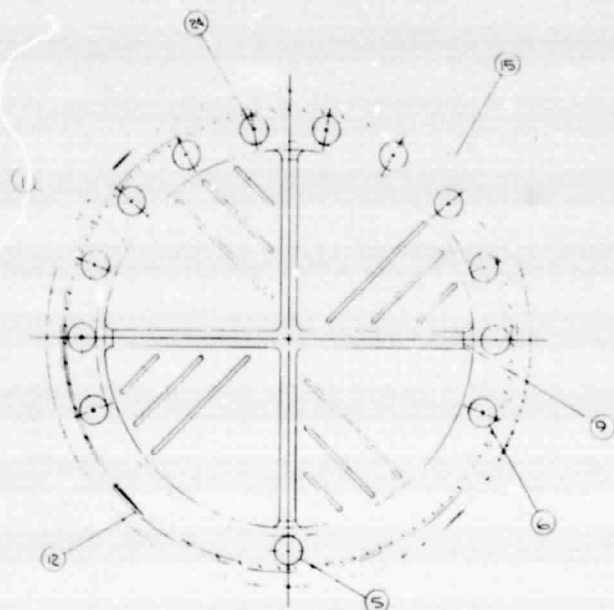
6.4.1.1 Inner Cylinder

The inner cylinder will be made of Inconel 617, for the reasons given earlier. The design and allowable stresses for this material are shown in Table 6.7.

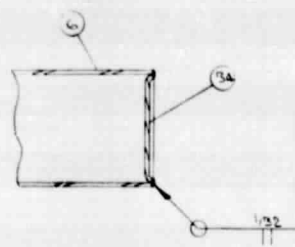
The several design concepts studied can be classified into two groups: (1) designs in which the salt containers are units independent of the pressure vessel, and (2) designs in which the salt containers are an integral part of the inner cylinder. The advantage of the first group is that the resulting cylinder is easy to fabricate, since, in essence, it is a conventional pressure vessel; the disadvantage is that the salt units are independent, and some motion or rattling must be expected. The decision was made that a design concept should not be disqualified merely because of rattling, that is, if the design concept is structurally sound. The advantage of a design with integral salt containers lies in its one-piece aspect; this advantage, however, is gained at a significant increase in fabrication complexity. Because



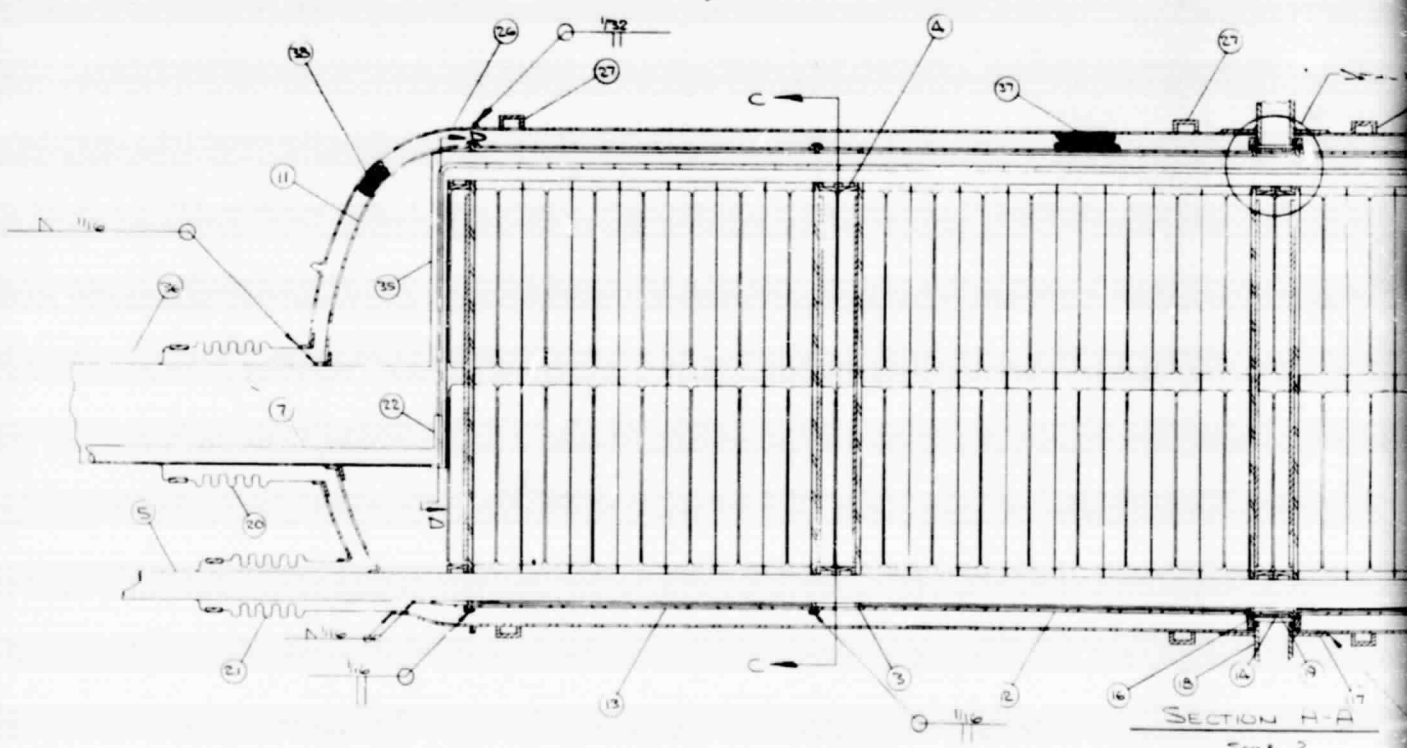
SECTION D-D
Scale 1/2



SECTION C-C
Scale 1/2



METAL II
Scale 2:1



SECTION H-A
Scale 2

FOLDOUT FRAME

A-3014

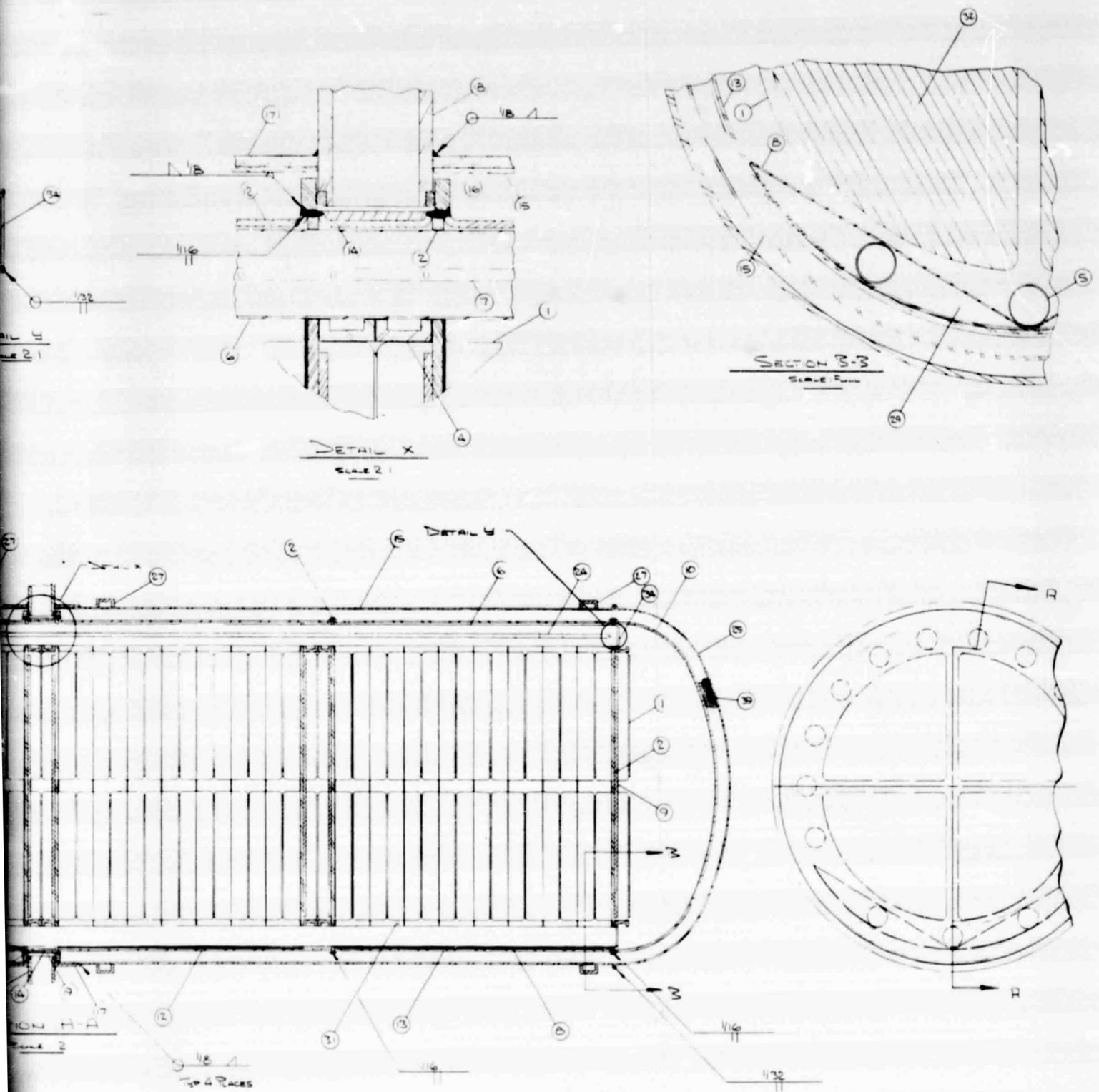


Figure 6.37 Assembly Drawing of Cylindrical TES Reservoir (Dwg. No. 035-01-000) 6-91

FOLDOUT FRAME 2

A-3015

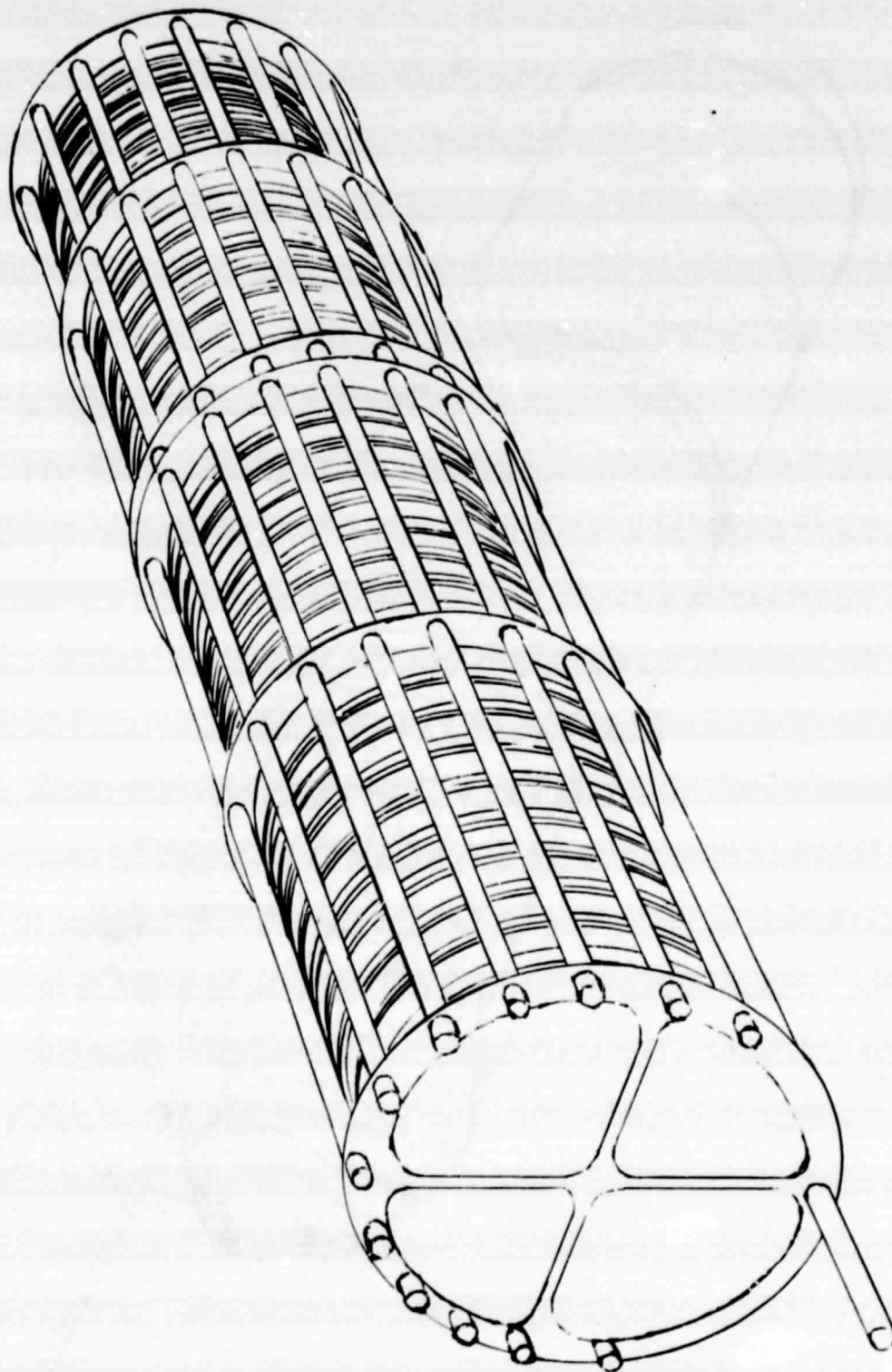


Figure 6. 38 Stock of Salt Inventory Capsules with Reinforcing Rings and Discharge/Charge Heat Pipe Tubes Incorporated

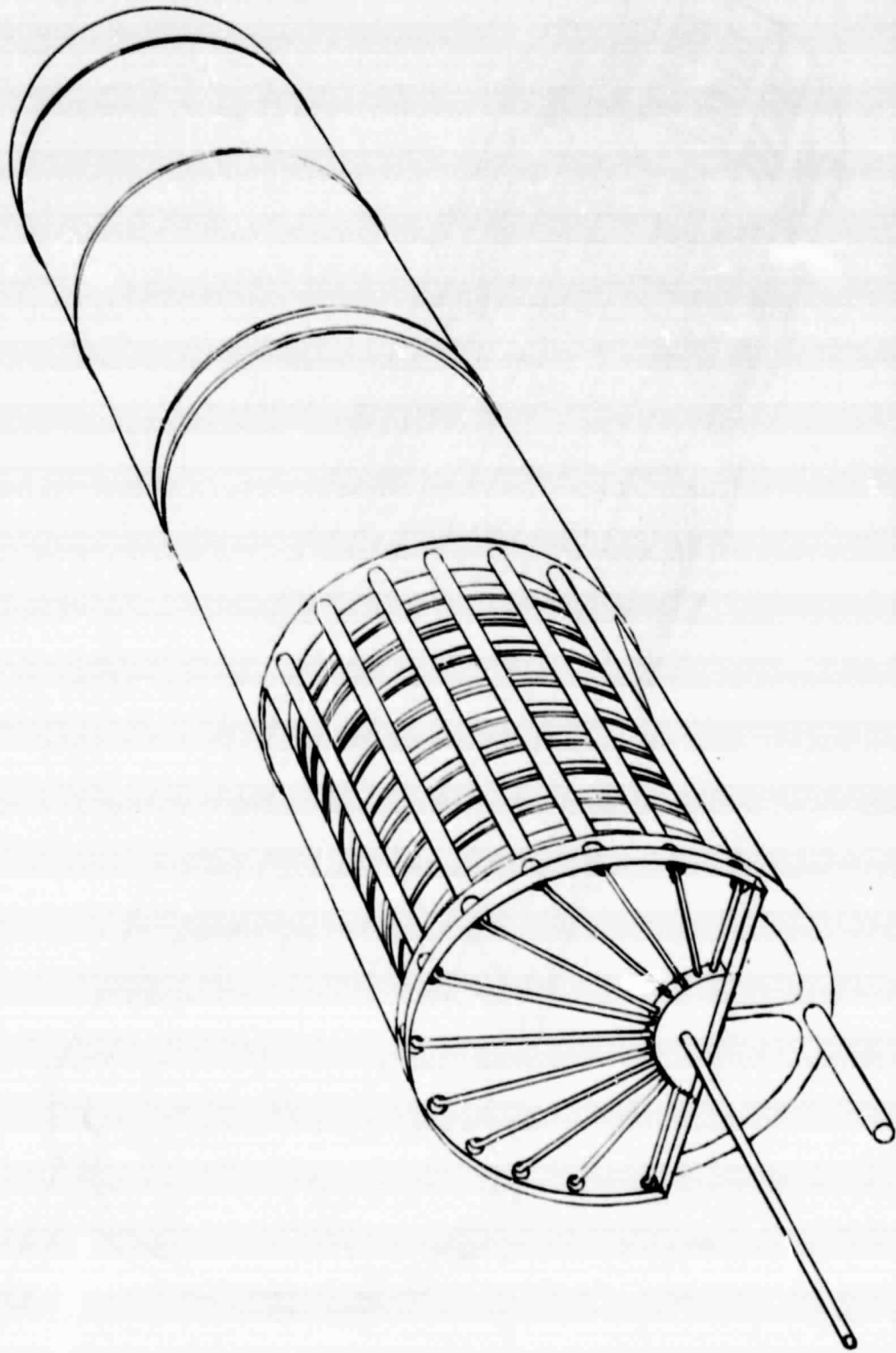


Figure 6.39 As In Figure 6.38 with Part of Inner Pressure Shell and Part of Discharge Heat Pipe Header Incorporated

A-3016

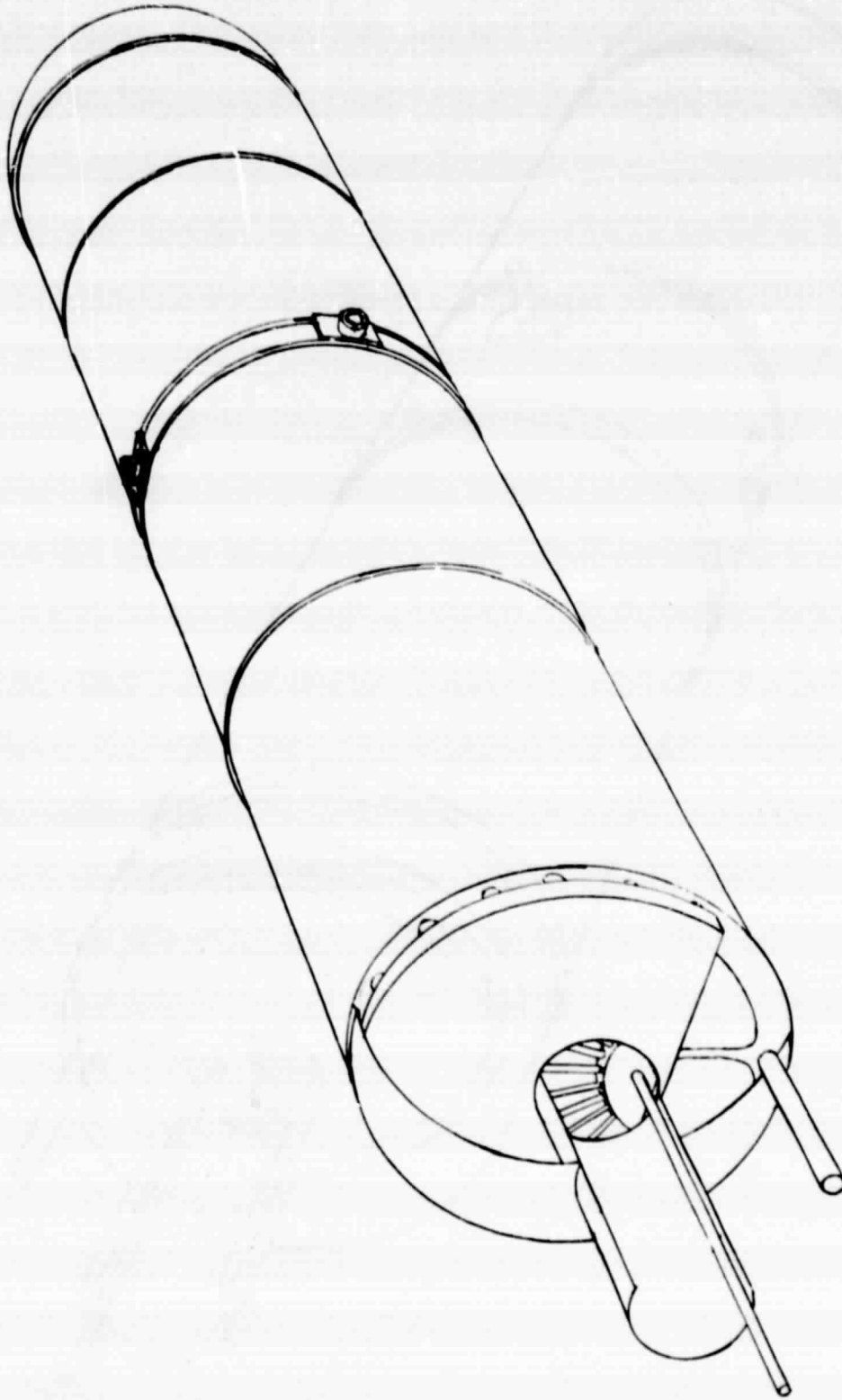


Figure 6.40 Complete Inner Pressure Vessel

21-1078

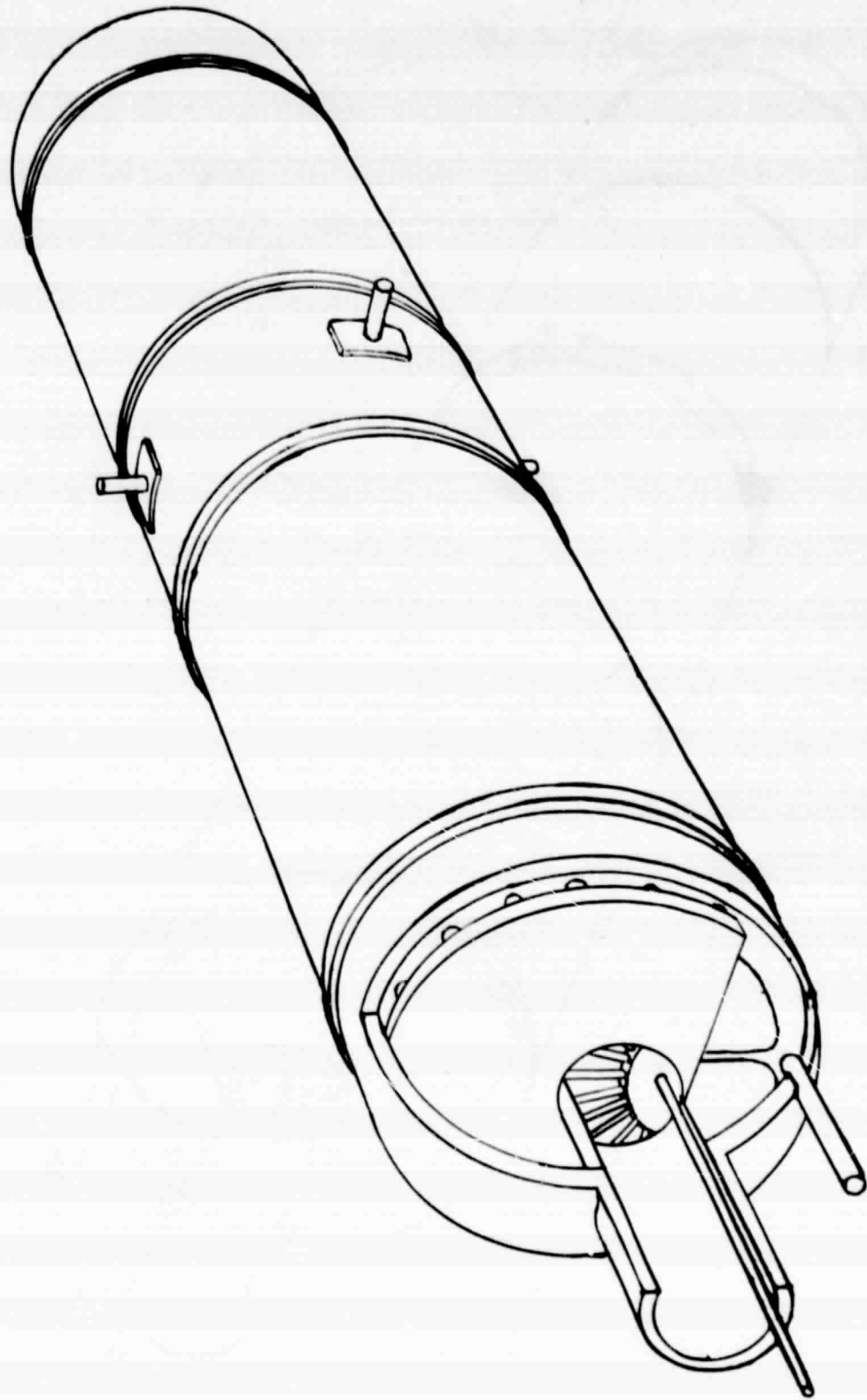


Figure 6.41 Installation of Multi-Foil Insulation, Outer Pressure Vessel With Stiffening Rings, and Support Pins

TABLE 6.7
INNER CYLINDRICAL CONTAINER OF INCONEL 617
STRESS SUMMARY

Result No.	Element	Loading or Result No.	Type of Stress	Stress (ksi)	Allowable Stress (ksi)
1	Cylinder	Internal pressure	Hoop primary membrane	3.0	3.0
2	Cylinder	Internal pressure	Meridional primary membrane	1.5	-
3	Cylinder	Gravity	Meridional primary membrane	0.6	-
4	Cylinder	Internal pressure	Hoop secondary bending	0.8	-
5	Cylinder	Internal pressure	Meridional secondary bending	2.8	-
6	Cylinder	2 + 3	-	2.1	3.0
7	Cylinder	1 + 4	-	3.8	6.7
8	Cylinder	2 + 3 + 5	-	4.9	6.7
9	Cylinder	3.5 g vertical	-	2.1	16.0
10	Ring at Center	Internal pressure	Hoop tension	1.0	-
11	Ring at Center	Gravity	Bending	1.0	-
12	Ring at Center	10 + 11	Combined	2.0	3.0
13	Ellipsoidal head	Internal pressure	Primary membrane at crown	2.1	3.0
14	Ellipsoidal head	Internal pressure	Primary membrane at cylinder junction	1.5	3.0
15	Ellipsoidal head	Internal pressure	Secondary bending at cylinder junction	1.5	-
16	Ellipsoidal head	14 + 15	-	3.0	6.7

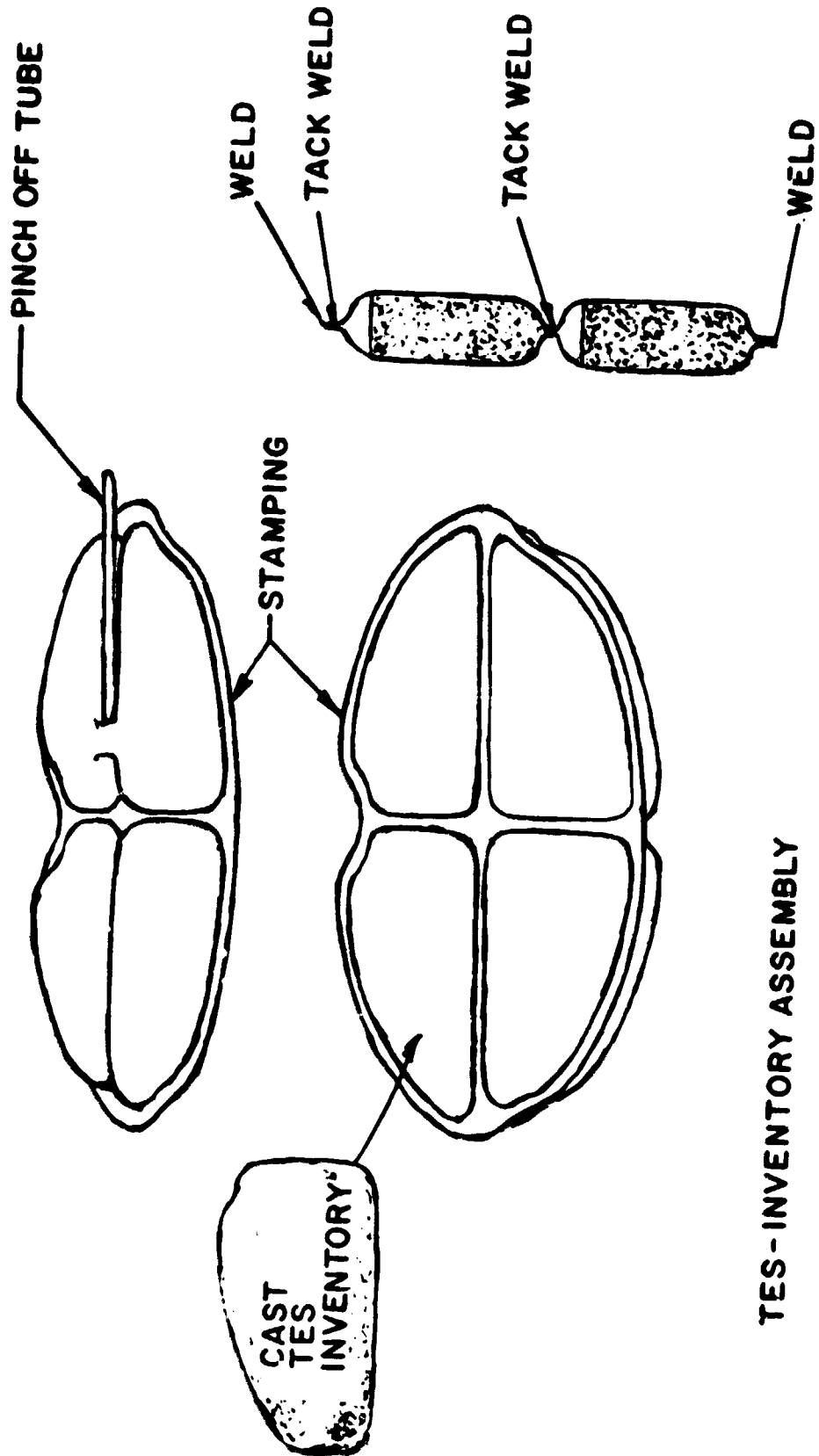
of these fabrication complexities, many of the advantages of a cylindrical pressure vessel are lost when the capsules are integral with the containment walls. A design of this type shares many of the conceptual aspects of the rectangular design, such as closely spaced diaphragms.

A design of either of the two previously discussed groups must be considered, a priori, as feasible. Since a design of the one-piece approach would be similar to the rectangular box, it was decided to pursue the design with independent salt containers. The decision implies that the rectangular and cylindrical designs are conceptually quite different; at a later stage in the program, a one-piece cylinder could be pursued and a cost comparison performed. Once a pressure vessel design with independent salt containers is selected, a number of design questions arise:

- What are the required pressure vessel thicknesses for the cylindrical portion and for the heads, based on primary membrane effects? Are the thicknesses selected to carry primary bending sufficient to carry discontinuity stresses (e. g., at the head to cylinder junction)?
- What shall the support system be? Are the thicknesses of the vessel sufficient to carry the additional stresses that arise near the supports?
- What shall be the configuration of the salt containers? How shall the salt containers be supported?

The design arrived at after investigating the preceding questions, in addition to the all-encompassing issue of fabricability of the container, is shown in Figures 6.37 through 6.42. A summary description of the inner pressure vessel is given below.

- Material selected, Inconel 617
- Cylindrical portion of the pressure vessel is 50 inches long, 14 inches outside diameter, with a wall thickness of 0.07 inch (70 mil).
- The ellipsoidal head is an oblate spheroid, with a minor axis of 5 inches, a major axis of 7 inches (both of these are outside dimensions), and a wall thickness of 70 mil.
- The inner cylinder is supported at its midlength by four pins which cantilever inwards from the exterior. These pins slide into four bearings equally spaced around the cylinder. Local stiffening is used to distribute the loads from the bearings to the cylinder walls; 1.25-inch diameter bushings provide the sliding interface with the pins.
- Eight stiffening rings are used, one at each end of the cylinder, two at the center, and two at each quarter point. The stiffening rings perform several functions; support for the pressure vessel, for the salt containers, and for the twelve 7/8-in diameter discharge heat pipe tubes. The two rings at the center of the cylinder distribute gravity and acceleration loads from the cylindrical shell to the four supports; the two rings at the ends of the cylinder stiffen the head-to-cylinder junction; and all eight rings provide support to the salt containers and the discharge heat pipe tubes.
- Each stiffening ring consists of a four-spoke wheel stamped out of a 120-mil thick sheet. The rim and the spokes, which are stiffened by a 120-mil thick



TES- INVENTORY ASSEMBLY

Figure 6.42 Salt Capsule Assembly Illustration

cross-like plate, serve as supports to the salt containers for acceleration loads in the longitudinal direction. Each rim has 12 circular holes through which pass the discharge heat pipe tubes.

- The salt containers are made of two identical pieces, press drawn to a thickness of 10 mil, and welded along the circumference. Each salt container is 1.56-inches wide, including 10-mil deep stiffeners stamped onto the sides. One- to 2-mil thick spray-on wicking may be used. A circumferential edge strip protects the weld from damage from impact against the heat pipe tubes.
- The 4-inch diameter pipe of the discharge heat pipe, which transports K vapor from the TES to the Stirling engine, passes through the center of one of the heads.

The inner cylindrical container was checked for pressure loads, gravity, and acceleration loads. A straightforward pressure vessel analysis was performed for the shell; both primary membrane and secondary bending stresses were checked. Gravity and acceleration loads are transmitted from the salt containers to the shell, to the rings located at the center of the cylinder, and finally to the bearings.

For accelerations normal to the axis of the cylinder, each half of the inner container acts as a cantilever member with circular cross section; the overall bending moment is carried by meridional membrane action; and the overall shear is carried in the shell by in-plane shear to the support rings, which act as a diaphragm in transferring the load to the bearings. For accelerations parallel to the axis, the cylindrical shell acts primarily as a tension/compression element with meridional stresses.

The salt containers are loose inside the vessel. Every eight contiguous capsules are restrained in the axial direction by two rings, one at each end of the group of eight. These rings provide support along the axial direction. When the TES experiences longitudinal accelerations, each capsule of the group will bear on the adjacent capsule; since the first capsule is restrained by a ring, so are the remaining capsules. The criterion used for selecting the size of allowable stacking of capsules is that every capsule maintain its structural integrity, without excessive deformations or wall buckling. Conceptually, the problem is similar to determining the stacking height for cardboard boxes. When the TES experiences accelerations in the transverse direction, each capsule bears against the heat pipes. The circumferential edge strip around the capsules protects the heat pipes against punching damage from the capsules, and also protects the circumferential weld of the capsule from abrasion. Even though the salt containers will be stacked tight, some movement of the capsules is expected; some testing will be required to determine the effects of the movements.

6.4.1.2 Outer Cylinder

The outer cylinder is at ambient temperature. Since buckling, rather than stress, is the primary design concern of pressure vessels under external pressure, any carbon steel with a yield $\geq 40,000$ psi can be used, for example, AISI 1040.

Consistent with the geometry of the inner cylinder, a 50-inch long, 15-inch diameter cylinder was selected with a wall thickness of 55 mil; two ellipsoidal heads with a minor axis of 5.5 inches and

a 55-mil wall thickness were selected. The design of the tank was performed in accordance with the ASME Boiler and Pressure Vessel Code, Section VIII, Division 1. Four circumferential stiffener rings are used, located at ± 2 inches and ± 18 inches from the tank centerline. The two rings closer to the heads are sized to prevent shell buckling; the two rings close to the center serve the dual purpose of preventing buckling and distributing the gravity and acceleration loads to the pin supports. The cylindrical portion between the central rings, which is 4 inches wide, is made of 0.15-inch thick material. This extra thickness, supplemented by local stiffeners next to the support pin, is sufficient to deliver the gravity and acceleration loads to the pin supports.

A 5-inch diameter pipe extends from the head towards the engine; this pipe surrounds the 4-inch pipe, of the discharge heat pipe, that goes from the inner cylinder to the engine, with the space between filled with Multi-Foil insulation. At a location near the Stirling engine, the annulus between the pipes is sealed off by a bellows. A transition piece may be required to weld the Inconel 617 heat pipe to the carbon steel outside pipe.

6.4.2 Summary of Results

6.4.2.1 Stress Summary

Stresses for the inside cylinder are summarized in Table 6.7. The computed stress values are based on well-established methods of shell theory, and on formulas, figures, and tables given in the ASME Boiler and Pressure Vessel Code. The outer shell is designed in accordance with the ASME Code Section VIII, Division 1; and since this does not require the calculation of stresses, none are tabulated.

6.4.2.2 Weight and Volume Summary

A breakdown of the weight for the inner and outer containers is given in Table 6.8. For the inner cylinder, a unit weight of 0.32 lbs/in³ is used; this corresponds to the unit weight of Inconel 617 plus an allowance of 5 percent for connections and local stiffening.

In Table 6.9, a summary of the TES reservoir characteristics is presented. The capsule volume/total volume ratio of 0.45 is almost identical to that of the rectangular configuration. The ratio of salt weight to total reservoir weight of 0.53 for LiF and 0.58 for NaF/MgF₂ is about 10 percent less than that for the rectangular configuration. It should be noted, however, that the cylindrical configuration is definitely able to withstand one atmosphere pressure in the Multi-Foil chamber without buckling (with vacuum in the inner box), whereas the rectangular configuration may not. Thus, air-leakage into the Multi-Foil could be catastrophic to the rectangular unit; whereas the cylindrical unit could probably be repaired and put back in service. Two modifications to the design could also improve the salt/total weight ratio for the cylindrical configuration. From the detailed layout of Figure 6.37, it appears that one more salt capsule can be added to the inner cylindrical envelope, resulting in a 2.9 percent increase in the salt/total weight ratio to 0.549 and 0.596 for LiF and NaF/MgF₂, respectively. It also may be possible to eliminate the cross-web indentations in the capsule, by the addition of internal supports in the capsules — thereby adding about 10 percent to each capsule internal volume. This additional modification would bring the salt/total weight ratio to 0.604 for LiF and 0.656 for NaF/MgF₂, which is comparable to the weight ratio for the rectangular configuration.

TABLE 6.8
SUMMARY OF STRUCTURAL WEIGHT
CYLINDRICAL CONTAINERS

			<u>lbs</u>
● Inner Container			
2	Cylindrical walls,	t = 0.07"	98.0
4	Ellipsoidal heads,	t = 0.07"	22.6
5	Stiffening rings		51.6
4	Support details		3.0
64	Capsules,	t = 0.01"	<u>61.0</u>
	Subtotal		236
● Outer Container			
2	Cylindrical walls,	t = 0.055"	76.6
4	Ellipsoidal heads,	t = 0.055"	21.0
3	Stiffening rings		27.6
4	Support details		<u>19.2</u>
	Subtotal		144
● Total Structural Weight, 2 cylinders			380
● Multi-Foil Insulation Weight (2 cylinders)			100
● Heat Pipe Weight (2 cylinders)			16
● Total TES Reservoir Weight Less Salt			496 (225 kg)

TABLE 6.9

SUMMARY OF WEIGHTS, VOLUMES, HEAT TRANSFER AREAS,
AND TES CAPACITY FOR CYLINDRICAL CONFIGURATION
(TWO CYLINDERS)

Internal Capsule Volume	9,320 in ³
Volume of Inner Cylinder (Inside)	17,070 in ³
Volume of Outer Cylinder (Outside)	20,640 in ³ (0.338 m ³)
Surface Area of Salt Capsule	22,000 in ² (153 ft ²)
Surface Area of Discharge Heat Pipe Tubes (OD)	1,650 in ² (11.5 ft ²)
Surface Area of Recharge Heat Pipe Tube (OD)	137 in ² (0.954 ft ²)
Total TES Structure Weight Less Salt	496 lbs (225 kg)
Capsule Volume/Total Volume	0.452
Capsule Volume/Inner Box Volume	0.546

	LiF	NaF/MgF ₂
Weight of Salt (Capsules 95% Full of Liquid at Melting Point)	579 lb (262 kg)	700 lb (318 kg)
Storage Capacity (Salt Only, 800°K-1150°K)	134 kwhrth	98.6 kwhrth
Total TES Reservoir Weight	1075 lb (487 kg)	1196 lb (542 kg)
Salt Weight/Total TES Reservoir Weight	0.533	0.579

6.5 DISCUSSION

6.5.1 Alternate Designs

Several alternate designs were considered for the inner rectangular box. The primary concepts were:

- A honeycomb sandwich panel box similar to the design of the proposed outside box. This was discarded because it is too heavy and because of the uncertainty about the behavior of honeycomb sandwich panels at temperatures of $\sim 1600^{\circ}\text{F}$.
- A box with sides made of corrugated sheet. Such a design requires diaphragms adjacent to the corrugated sheets to carry in-plane compression normal to the direction of the corrugations; the design also requires at least four, and possibly eight, edge members or longerons to carry dead weight and acceleration loads. This design was discarded primarily because it is too heavy, but also because of the difficulty and expense of welding multiple S-shaped seams.
- A honeycomb sandwich panel box with closely spaced interior diaphragms. The design approach is similar to that adopted, with parallel diaphragms used to cut down the bending span of the panels that are the sides of the box. In this design approach the honeycomb sandwich panels replace functionally the multiple adjacent cylindrical shells, the top and bottom diaphragms, and the perimeter trusses of the proposed rectangular box. The spacing of diaphragms in this design must be chosen to minimize the material weight of diaphragms and panels and the fabrication cost. If a spacing of either 1.5 inches or 3.0 inches is selected, the salt containers may be attached to the diaphragms as in the proposed rectangular design; if a spacing larger than 3.0 inches is selected, individual salt capsules would be required. A honeycomb sandwich panel box with

interior diaphragms is an interesting alternative that should be studied further. It was not selected in this study, because of the lack of data for sandwich panels operating at the high temperatures required for this application.

An altogether different possibility is to use two rectangular boxes instead of one. Any of the design approaches described before could be used. Two boxes could be considered for packaging efficiency, and to cut down on the span of the faces of the inner and outer boxes.

The use of corrugated sheets for the outer box was considered and discarded. The problems are the multiple S-welds, the need for longerons and extra diaphragms, and the increase in weight. Fabrication costs are much larger than for the proposed honeycomb sandwich panel box.

The only alternative considered for the cylindrical design is one in which the salt containers are an integral part of the inner unit. This alternative has been discussed in Section 6.4.1.

6.5.2 Potential Problems

Several technical uncertainties exist in these designs which can only be resolved by experimental testing and/or more extensive design evaluation. Foremost is the need to establish the behavior of Inconel 617 in contact with solid and liquid salt, and with potassium liquid and vapor, in the temperature range of 800°K – 1150°K. Corrosion rates and the effect of temperature cycling on corrosion and on the creep characteristics should be established. To minimize the

structural weight, thin plates (0.010-inch thick) are used where stress conditions permit. Although the manufacturer indicates that Inconel 617 is readily weldable, welding techniques for the thin plates to provide an absolutely vacuum-tight weld will require some development. Where the Multi-Foil insulation is ended, (see Figure 6.37), a vacuum-tight welded connection is required between the Inconel 617 heat transport tube and the outer carbon steel and/or stainless steel envelope. A graded connector will probably be required, permitting welding to Inconel 617 on one end and to carbon steel and/or stainless steel on the other.

The cylindrical design incorporates independent salt containers which are not completely restrained. Some movement of these capsules under dynamic loading may occur, with potential problems from material fretting and abrasion and from noise.

A loss of vacuum in the Multi-Foil drastically reduces the effectiveness of the insulation, so that the outer box or cylinder will be heated if the TES reservoir is charged with hot salt. The insulation approaches the effectiveness of a stagnant air gap (the small spacing between foils minimizes convection), and thus is not completely lost. Consequently, the surface temperature will be somewhat less than the salt temperature, with the exact temperature depending on the ambient around the TES reservoir. A rough calculation for a surface in free air indicates a surface temperature (C) of $\sim 600^{\circ}\text{F}$ with 1600°F salt temperature. If this temperature is high enough, the strength of the outer container (of carbon steel or stainless steel) will be affected, with the possibility of some deformation of the outer container. In

addition, the high surface temperature would represent a fire hazard for the vehicle.

A more serious consequence of loss of vacuum may be buckling of the inner container. If the loss of vacuum is from a leak to the atmosphere, the outer container will no longer be under external pressure, while the differential pressure on the inner container will initially be lower than the design pressure. As the inner container cools down, the internal pressure may drop to below 1 atmosphere, and the unit would then be under external pressure. No calculations have been performed for the inner containers under external pressure. However, in the cylindrical design, the inner cylinder is thicker, has a smaller radius, and has stiffening rings more closely spaced than the outside cylinder; it therefore should not buckle. In the rectangular box, the only elements that could buckle are the primary diaphragms; however, these are restrained by the salt. In any event, should further study indicate a stability problem, one-way pressure release valves may be incorporated into the design to prevent failure of the inner containers due to external pressure.

If the loss of vacuum is from a leak of potassium vapor, the inner unit would no longer be under pressure and the external container would be under reduced external pressure, but would be in contact with the hot potassium, with possible corrosion problems.

The normal operation of the TES reservoir is such that the temperature is expected to be uniform, and nonuniform temperature distributions are unlikely to occur under any conditions. The effect

of nonuniform distributions was therefore not considered. If nonuniform temperature distributions become possible, stresses could develop with nonuniform thermal expansion of the structure — resulting in distortion and possible joint fracture. Differential pressures could also develop across the salt capsule walls due to a difference in potassium vapor pressures inside and outside of the capsules.

The consequences of a leak of salt from one or two salt containers is not believed to be serious, since the reservoir heat pipe is sealed — preventing migration of the salt to the Stirling engine. The salt in the reservoir heat pipe would probably end up around the charge heat pipe and, if excessive, would prevent recharging. Gross leakage would obviously prevent functioning of the TES system. No structural effects would be expected.

The designs presented in this report are based on criteria and specifications set in the contract. These criteria could be extended and modified for a more realistic and detailed evaluation relative to structural response in a vehicle. Thus, criteria for transverse accelerations where the vehicle is struck from the side, or for puncture resistance of the outer skin, could be included. Dynamic response to random vibrations in the 10-20 cycle/sec range should also be evaluated, particularly with respect to the dynamic amplification for accelerations that vary harmonically in the 10-20 cycle/sec range. With regards to restricting the natural frequencies, it must be noted that the rectangular unit may have relatively high overall natural frequencies (not computed in this study) with low local frequencies for out-of-plane vibrations of the

diaphragms. The cylindrical unit is also expected to have high overall natural frequencies; however, the salt containers are loose — a known natural frequency of zero.

6.5.3 Comparison and Evaluation

The design specification indicated a 500 kg total system weight, with a volume of $\leq 0.4\text{m}^3$. Since the designs did not exactly match this specification, the system characteristics are extrapolated linearly to this specification — so that a direct comparison can be made. No allowance is made here for the rest of the system weight, comprising the heat transport pipe to the Stirling engine, the E-M pump, and the controls. Results are given in Table 6.10.

Both designs satisfy the volume specification of $\leq 0.4\text{m}^3$.

6.6 CONCLUSIONS

The two structural concepts developed for the TES meet the basic design requirements of the contract. In the rectangular unit, the salt capsules are welded to the structure, and the design requires a considerable amount of vacuum-tight seam welds. For the cylindrical design, two units are required, the salt capsules are stacked inside, without connection to the structure, and much less vacuum-tight welding is required.

A testing program will be needed to confirm material properties, to determine structural performance, to check for feasibility of fabrication in an industrial environment, and eventually to establish which configuration is preferable.

TABLE 6.10

A-2970

COMPARISON OF CYLINDRICAL AND RECTANGULAR CONFIGURATIONS
AFTER NORMALIZATION TO 500 kg TOTAL RESERVOIR WEIGHT

	LIF		NaF/MgF ₂	
	Rectangular	Cylindrical	Rectangular	Cylindrical
Structure/Heat Pipe/Insulation				
Salt	203 kg	231 kg	180 kg	208 kg
Total Envelope Volume	297 kg	269 kg	320 kg	293 kg
Storage Capacity	0.38 m ³	0.35 m ³	0.34 m ³	0.31 m ³
Storage Capacity/500 kg	152 kwhrth	138 kwhrth	99 kwhrth	91 kwhrth
Storage Capacity/(Structure/Heat Pipe/Insulation Mass)	0.364 $\frac{\text{kwhrth}}{\text{kg}}$	0.276 $\frac{\text{kwhrth}}{\text{kg}}$	0.198 $\frac{\text{kwhrth}}{\text{kg}}$	0.182 $\frac{\text{kwhrth}}{\text{kg}}$
Storage Capacity/Envelope Volume	0.749 $\frac{\text{kwhrth}}{\text{kg}}$	0.597 $\frac{\text{kwhrth}}{\text{kg}}$	0.550 $\frac{\text{kwhrth}}{\text{kg}}$	0.438 $\frac{\text{kwhrth}}{\text{kg}}$
Equivalent U.S. Gallons and Weight of Gasoline at 41 kwhrth/gal	400 $\frac{\text{kwhrth}}{\text{m}^3}$	398 $\frac{\text{kwhrth}}{\text{m}^3}$	291 $\frac{\text{kwhrth}}{\text{m}^3}$	292 $\frac{\text{kwhrth}}{\text{kg}}$
	3.7 gal	3.4	2.4	2.2
	10.9 kg	10.0 kg	7.1 kg	6.5 kg

REFERENCES FOR CHAPTER 6

1. "High Temperature Alloy, Hot Performance Guide," 8/77 Revision, and "Inconel Alloy 617," 20 M 9-72 T-46, Huntington Alloys, Inc., Huntington, W. Va.
2. "ASME Boiler and Pressure Vessel Code," Section VIII: Pressure Vessels, Division 1 and Division 2: Alternative Rules, 1977 Edition. (Also ANCI/ASME BPV-VIII-1 and BPV-VIII-2.)
3. Harris, C.M. and Crede, C.E. (Editors), "Shock and Vibration Handbook" in Three Volumes, McGraw-Hill Book Company, Inc., New York, N.Y., 1961.
4. "Astech Design Allowables Manual," Report ADAM-100, TRE Corporation, Santa Ana, CA., May, 1977.

7. THERMOELECTRIC-ELECTROMAGNETIC PUMP DESIGN

An electromagnetic pump is used to control the flow of potassium in order to regulate the thermal conductance of the discharge heat pipe. Since the pressure head of such a pump is much greater than that due to capillary forces, the diameter of the discharge heat pipe can be smaller than if a wick return were used. Electromagnetic pumps also have the advantage of no moving parts and have been used successfully in sodium-cooled nuclear reactors, as well as in other high-temperature, liquid-metal pumping applications.

The potassium vapor transport characteristics for the reference case duct (4 in DIA x 4 ft L) are shown in Figure 7.1. To meet system specifications, a maximum potassium flow rate of 2.2 gal/min at a pressure head of 1 psi is required. For these flow conditions, a d-c Faraday conduction electromagnetic pump requires a power input of only 4.2 watts (ideal pumping power of 0.96 watt). Although this power requirement is insignificant, it must be supplied at a high current (83 amp) and low potential (0.05 volt), an inconvenient impedance for most power sources. However, a thermoelectric module can match this impedance. This design concept of using the output of a short-circuited thermoelectric module to drive an electromagnetic pump has been successfully demonstrated on SNAP 10A, the only space reactor power supply launched by the United States. In this system, NaK was circulated by the electromagnetic pump through the reactor to the thermoelectric power conversion system and back. The electromagnetic pump was powered by a short-circuited PbTe thermocouple operating between the NaK outlet temperature (990° F) and a cold junction determined by a small pump radiator at 600° F.

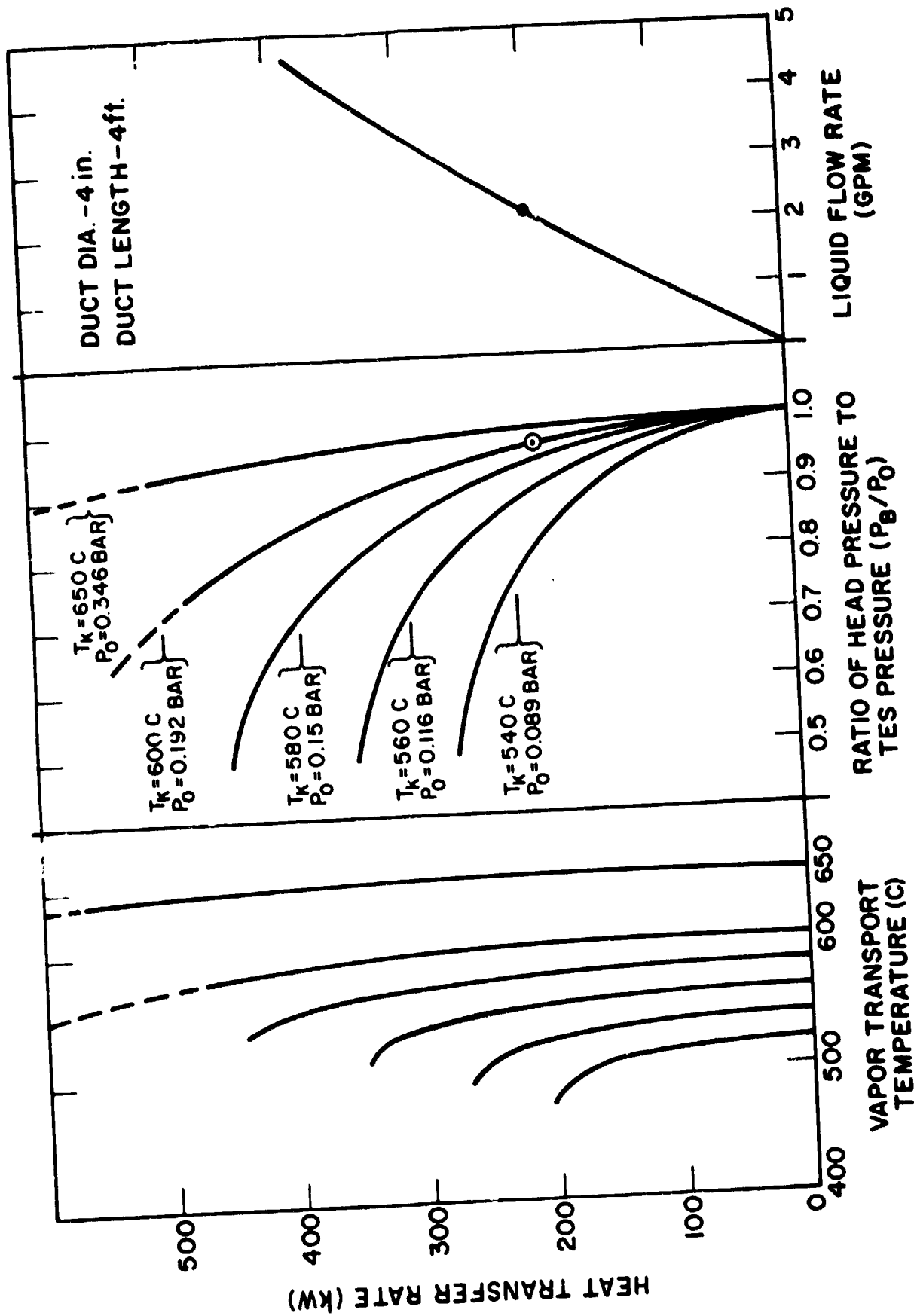


Figure 7.1 Potassium Vapor Transport Characteristics

The pump magnetic field was supplied by a permanent magnet. With a flow rate of 13 gal/min versus a ΔP of 1.1 psi, this pump required a thermal power of 625 watts with the above operating conditions.¹

The physical arrangement of the thermoelectric-electromagnetic (TE-EM) pump proposed for the TES system is illustrated in Figures 7.2 and 7.3. The close integration of the thermoelectric and pump components is evident in these figures. This design does not require long, high-current leads. The heat for the thermoelectric generator is provided by the potassium flowing through the pump. The pumping rate is controlled by rotating the permanent magnet to vary the field strength to the current flow through the pump. The total current output from the thermoelectric module flows through the EM pump at all times.

The design considerations for the thermoelectric module and the EM pump will be discussed in the next two subsections. The operation of the thermal control has been described in Section 3.

7.1 THERMOELECTRIC MODULE

The term "module" usually denotes an array of thermocouples. For the present application, a single semiconductor thermocouple is sufficient. However, if a different EM pump design point or a thermoelectric (TE) material with a low Seebeck voltage were used — two, or more, thermocouples would be required.

For the TE-EM pump design shown in Figures 7.2 and 7.3, the "N" and "P" legs are concentric, with the tube containing the flowing potassium. Each leg is electrically insulated from, but thermally connected to, the potassium tube.

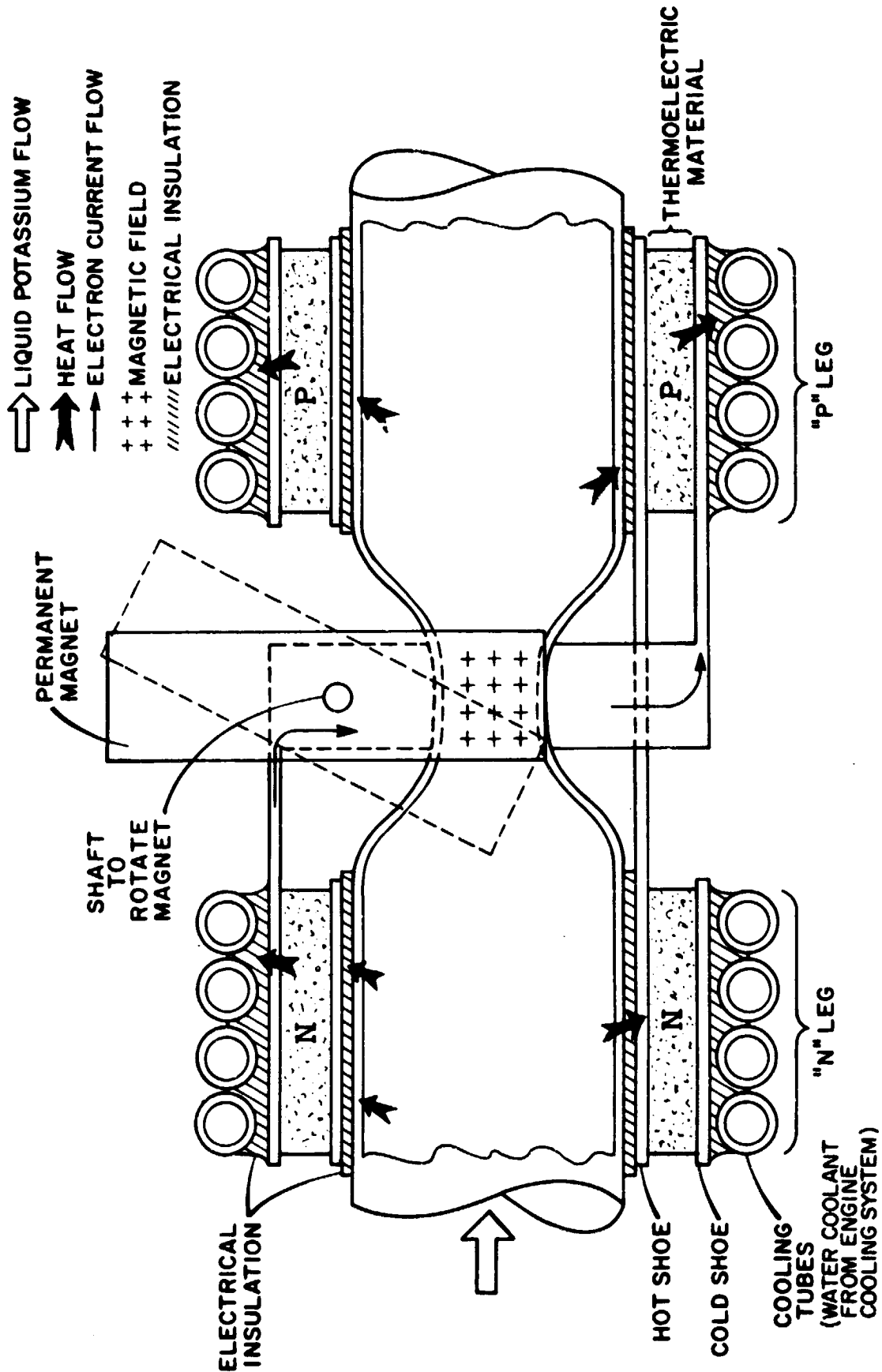


Figure 7.2 Thermoelectric-Electromagnetic (TE-EM) Pump Concept

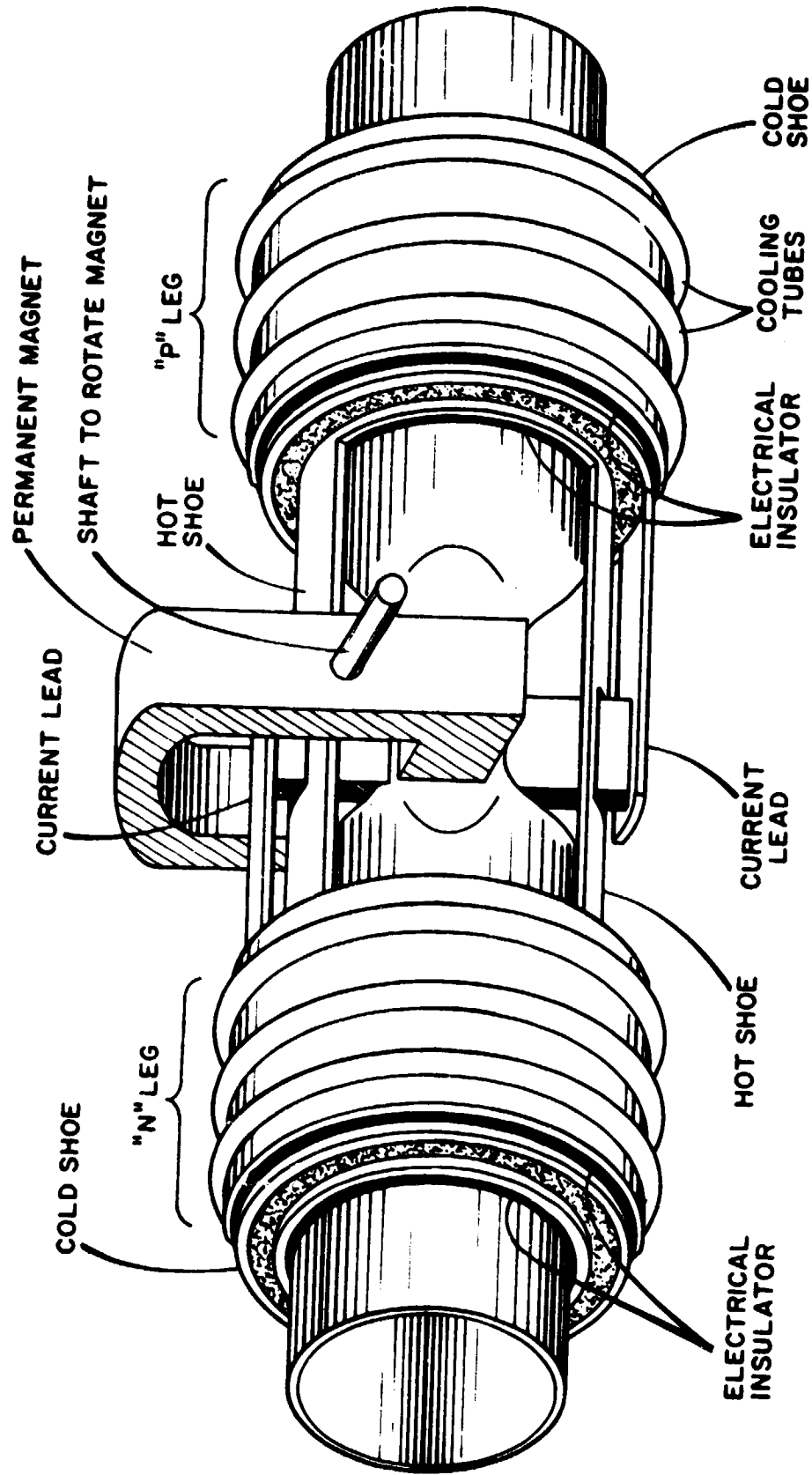


Figure 7.3 Thermoelectric-Electromagnetic (TE-EM) Pump Perspective Diagram

The TE output current is conducted through short, heavy leads into the EM pump section, where the current flow is perpendicular to the field of the permanent magnet. The resulting pumping force is proportional to the vector product of the current and magnetic field. The current loop through the "N" leg, EM pump and "P" leg is completed by the "hot shoe" (see Figure 7.3). The cooling tubes are connected to the Stirling engine radiator cooling system. An evaluation of available thermoelectric materials is given in Table 7.1. Any of the semiconductor materials in this tabulation would probably be adequate; however, the efficiency of bismuth telluride is marginal. The thermoelectric efficiency is given in Figure 7.4 as a function of hot junction temperature for the semiconductor materials under consideration. Silicon-Germanium is attractive, but its low thermal expansion (relative to other materials in the system), would present some matching problems. Gadolinium selenide has a high efficiency, but there is yet little experience with this material. Based on all considerations (i. e., efficiency, maximum hot junction temperature, bonding, cost and experience), lead telluride has been chosen for the reference design. Cylindrical lead telluride TE modules have been built by Westinghouse.

A summary of the TE-EM pump reference design is shown in Table 7.2. A samarium-cobalt magnet is assumed to minimize weight; however, the magnetic field conditions could be met with a heavier Alnico magnet.

TABLE 7.1
THERMOELECTRIC MATERIAL PROPERTIES

MATERIAL	MAXIMUM HOT JUNCTION TEMPERATURE (°C)	THERMOELECTRIC EFFICIENCY FROM 600°C TO 150°C (PERCENT)	COMMENTS
CUPRON/TOPHEL	600	<1	UNACCEPTABLY LOW EFFICIENCY. BEST METAL THERMOCOUPLE.
BISMUTH TELLURIDE	500	3	MARGINAL EFFICIENCY. HOT JUNCTIONS CAN BE BONDED.
SILICON-GERMANIUM	1000	5	MODERATE EFFICIENCY. DIFFICULT THERMAL EXPANSION MATCHING. BEST AT HIGH TEMPERATURES.
LEAD TELLURIDE	550	9	GOOD EFFICIENCY. DIFFICULT TO BOND HOT JUNCTION. CHOSEN FOR REFERENCE DESIGN.
GADOLINIUM SELENIDE	900	~14	HIGH EFFICIENCY. THERMOELECTRIC PROPERTIES AND VAPORIZATION ARE CURRENT DEPENDENT. LITTLE OPERATIONAL DATA.

9-778

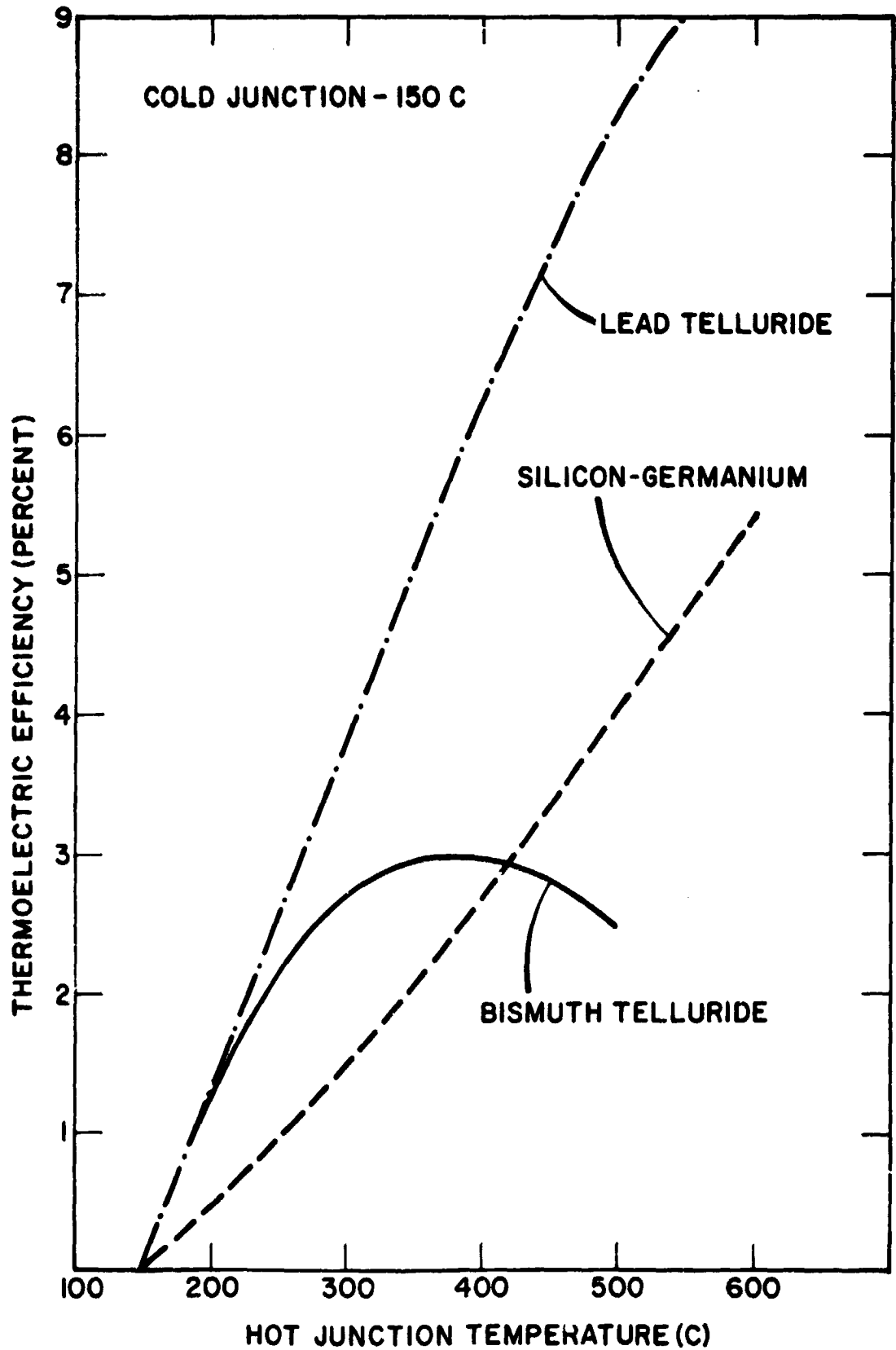


Figure 7.4 Thermoelectric Efficiency Versus Hot Junction Temperature

TABLE 7. 2

**THERMOELECTRIC-ELECTROMAGNETIC
REFERENCE PUMP SUMMARY**

Maximum Pump Rate - 2. 2 gal/min Potassium

Pressure Head - 1 psi

Potassium Temperature - 650°C

Duct Dimensions

Length - 0. 400 in.

Inside Height of Chamber = 0. 100 in.

Inside Width - 0. 706 in.

Wall Thickness - 0. 005 in.

Samarium-Cobalt Permanent Magnet

Magnetic Field - 4500 gauss

Area of Field - 0. 282 in.²

Electrical Input

Current - 83 amp

Potential - ~50 millivolts

Power - 4. 2 watt

Electromagnetic Pump Efficiency - 22. 8 percent

Thermoelectric Material - Lead Telluride

Maximum Hot Junction Temperature - 550°C

Cold Junction Temperature - 150°C

Thermoelectric Efficiency - 9 percent

Number of Couples - One

Thermoelectric Element Dimensions

Inside Diameter - 0. 5 in.

Outside Diameter - 1. 00 in.

Length - 1. 120 in.

7.2 ELECTROMAGNETIC PUMP

The electromagnetic pump operates on the Lorentz force principle: a body containing an electric current in the presence of an externally applied magnetic field experiences a force perpendicular to both the current and the field. Thus, an electrically conducting fluid, such as liquid potassium, can be made to flow through a duct, as shown in Figure 7.5, in the absence of any other moving parts.

Figure 7.6 presents a lumped parameter analytical model of Figure 7.5, incorporating the back emf (e) induced by the flowing fluid and the power loss (R_e) due to eddy currents at the field boundaries. The model assumes a constant velocity profile, which, as shown below, is the case for liquid potassium in the range of temperatures and flow rates specified by the design.

On the basis of the equations given in Figure 7.6, pump operating currents, voltages, power consumptions, and efficiencies were determined as functions of dimensions and magnetic field. It was assumed that the tubing material was 0.005-inch wall 304 stainless steel, and that the working fluid was liquid potassium flowing at 2.2 gal/min, with a 1.0 psi head (ΔP). Figure 7.7 shows typical operation curves for a series of EM pump designs, including the one selected as a practical optimum:

- B - 4500 Gauss
- I - 83 amps
- V - 0.05 volt
- L - 0.400 inch
- D - 0.716 inch
- S - 0.100 inch

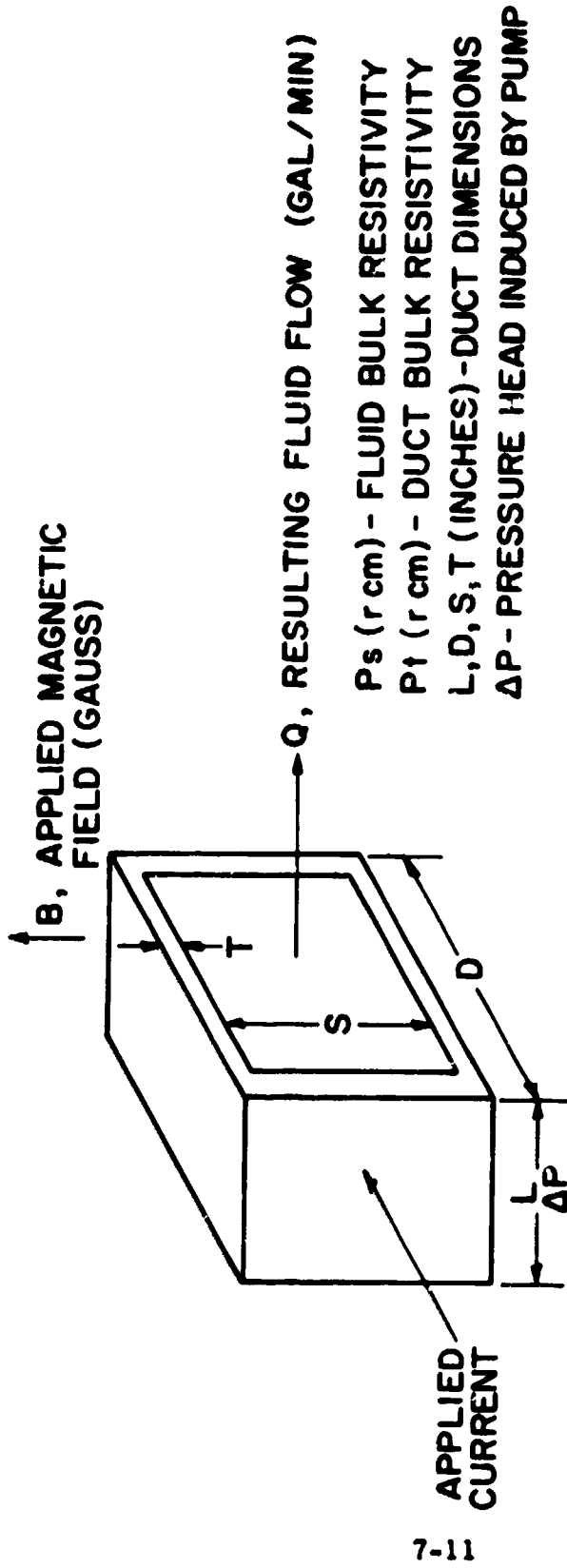
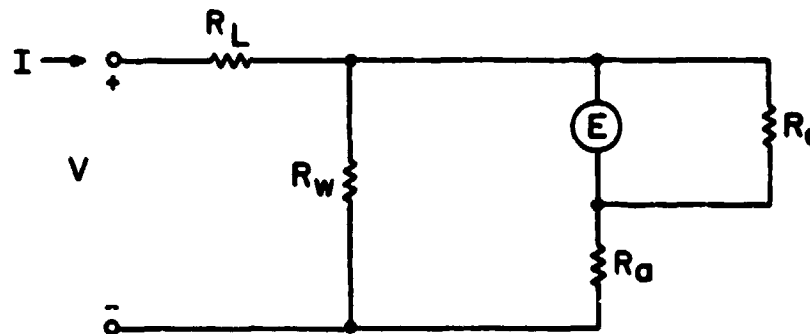


Figure 7.5 Electromagnetic Pump



$E = 2.48 \times 10^{-7} BQ/\rho_t$, back emf induced by Fluid Flow

$R_L =$ lead resistance

$R_w = \rho_t D/5.08TL$, duct wall shunting resistance

$R_a = [\rho_s D + 2T(\rho_t - \rho_s)]/2.54LS$, device resistance series

$R_e = 1.44\rho_s/S$, back voltage resistance shunted across

$$I = \frac{2.48 \times 10^{-7} BQ}{SR_e} \left\{ 1 + \frac{R_e}{R_w} + \frac{R_a}{R_w} \right\} + \frac{S\Delta P (1 + R_a/R_w)}{5.71 \times 10^{-7} B}$$

$$V = \frac{2.48 \times 10^{-7} BQ}{S} \left\{ 1 + \frac{R_a}{R_e} + \frac{R_L}{R_e} \left(1 + \frac{R_e}{R_w} + \frac{R_a}{R_w} \right) \right\} + \frac{S\Delta F}{5.71 \times 10^{-7} B} \left\{ R_a + R_L (1 + R_a/R_w) \right\}$$

Figure 7.6 Lumped Parameter Model of Electromagnetic Pump

789-31

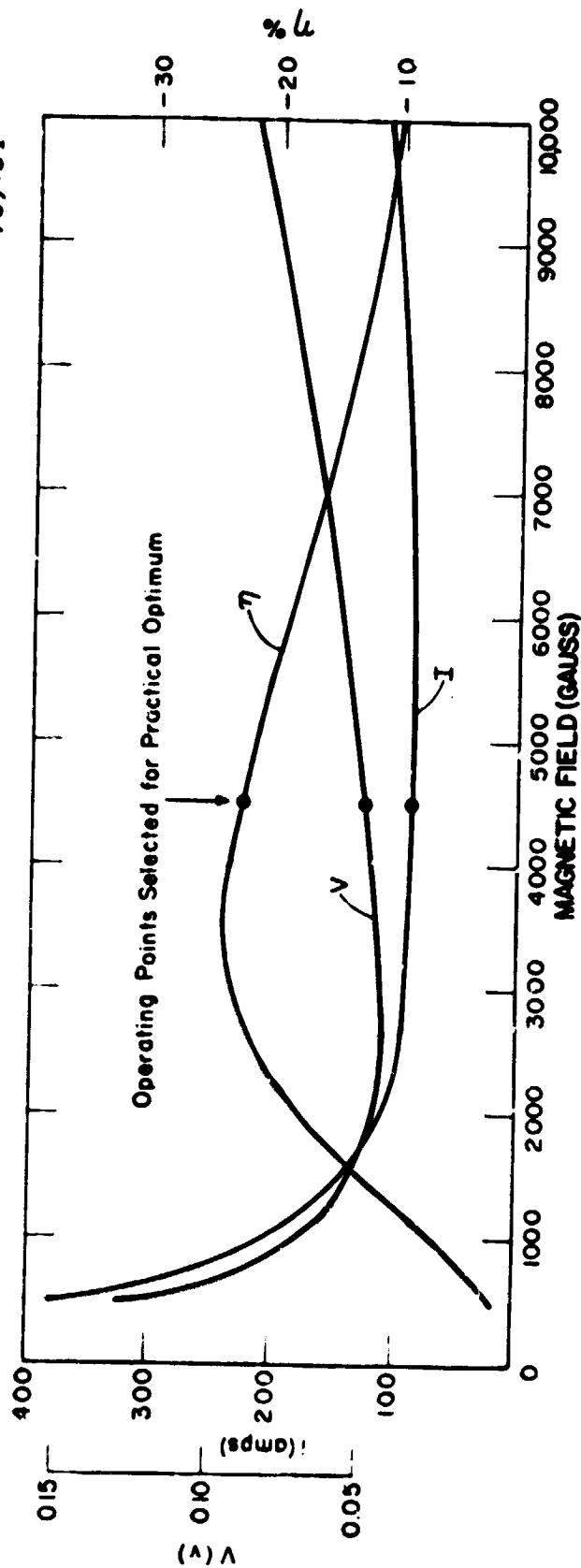


Figure 7.7 Operating Characteristics of an EM Pump

Channel Length L = 0.400 - inches

Channel Width D-2T = 0.706 - inches

Channel Height S = 0.100 - inches

It is apparent from Figure 7.7 that slight variations in magnetic fields have little effect upon voltage and current requirements. The reference design pump consumes 4.2 watts electrical power and has an efficiency of 23 percent; with a thermoelectric module efficiency of ~9%, the thermal power requirement from the circulating liquid potassium is 47 watts. The magnetic field is furnished by the Samarium-Cobalt magnetic alloy² (Sm Co₅) - which is known to have a residual induction of between 7500 and 9000 gauss and can function up to 900° C. The pump duct cross section can be generated by deforming a 0.50 inch-diameter tube which is identical to the size used for the liquid return line.

Calculations were made to determine the pressure losses in the pump and its associated plumbing. The results are enumerated in Table 7.3. Liquid potassium is less dense and less viscous than water.³ Flow in the EM pump would be associated with Reynolds number [$Re = 2SD\sqrt{p}/\mu(S + D)$] on the order of 10^5 , and thus would be turbulent and have a flat cross-sectional velocity profile. Pressure losses in the discharge heat pipe vapor duct were determined parametrically from Figure 7.1. Hydrostatic head requirements were computed on the basis of a one-half meter liquid height. Frictional losses in the short rectangular EM pump duct are only about 2 percent of its pressure generating capability. Entrance - exit losses⁴ were taken as 10 percent of the loss calculated assuming abrupt entrance-exit, since efficient inlet - outlet diffusers are used to reduce the entrance-exit losses. Calculations for pressure losses in the return plumbing are based upon four feet of turbulent flow in a 3/4-inch diameter return pipe. As seen from the right hand column of Table 7.3, total pressure drops anywhere in the conceivable

TABLE 7. 3

PRESSURES (psi) REQUIRED TO COMPENSATE FOR FRICTIONAL LOSSES
IN THE EM PUMP AND ITS ASSOCIATED PLUMBING

T(°C)	Pressure Losses, psi					ΔP Total
	Frictional Loss In Pump Duct	Entrance- Exit	Return Tube	Hydrostatic Head	Vapor Duct**	
540	0.022	0.048	0.114	0.508	0.268	0.960
560	0.022	0.048	0.112	0.504	0.192	0.884
580	0.021	0.047	0.112	0.501	0.148	0.828
600	0.021	0.047	0.110	0.497	0.123	0.798
650	0.021	0.046	0.108	0.489	0.066	0.730

* Liquid Return Line from Stirling engine to TES reservoir (4-ft length x 0.50-in. diameter)

** Vapor Duct Transporting Vapor from TES reservoir to Stirling engine (4-ft lengths x 4-in. ID)

operating temperature range are well under the 1 psi ΔP capability designed into the pump, particularly considering that the hydrostatic head is recoverable and thus not really a pressure loss unless the TES reservoir is located substantially higher in elevation than the engine. The EM pump as designed should be adequate for all TES system flow requirements.

REFERENCES FOR CHAPTER 7

1. Dieckamp, H. M. , Nuclear Space Power Systems, Atomics International, Canoga Park, California, September, 1964.
2. L. R. Moskowitz, Permanent Magnet Design and Application Handbook, Cahner Books International, Inc. , Boston, 1976.
3. R. N. Lyon, ed. , Liquid Metals Handbook, U.S. Government Printing Office, Washington, D. C. , 1953.
4. W. M. Kays and A. L. London, Compact Heat Exchangers, McGraw-Hill Book Co. , New York, 1964.

8. CUSTOMER ACCEPTANCE AND APPLICATION CONSIDERATIONS

In the preceding discussion, prime attention has been given to technical considerations in the development of a technically feasible system. Many other requirements related to socio-economic factors must be satisfied before a new system can be considered for large-scale application. These include items such as safety, recharging energy source, environmental impact, and system cost. Many of these questions do not have an absolute answer, and can be considered only in a relative sense to other alternative means of achieving the desired function. For others, only preliminary projections are possible.

8.1 MANUFACTURING COST

An obviously important issue is the initial cost to the customer. A manufacturing cost estimate for fabrication of both the rectangular and the cylindrical reservoir configurations has been prepared. This cost does not include the items required for a complete business, such as sales force, engineering force, administrative force, etc., but represents estimates of the raw material cost and burdened cost of hands-on labor, that is, the direct manufacturing cost. The cost to the consumer will thus be somewhat greater than the costs given here.

The cost estimate was prepared by an experienced industrial engineer on the basis of producing 200,000 units per year of the

designs presented in Chapter 6. It was assumed that automated machinery would be utilized as much as possible, in particular for all seam welding operations. A complete manufacturing flow diagram was developed, for each configuration, as illustrated in Figures 8.1 and 8.2. For each operation in the manufacturing process, man-minute time estimates were made by simulation of the proposed operation. Vendor contact was used to determine the raw material costs for the items comprising the structure. In short, we believe the manufacturing cost estimate to be reasonably accurate for a mass-produced system and a good basis on which to evaluate the potential system cost.

The results of the cost estimate are presented in Table 8.1 for the rectangular configuration and Table 8.2 for the cylindrical configuration. The manufacturing cost of the basic structure is estimated at \$5830 for the rectangular design and \$5170 for the cylindrical design (two cylinders). Most of this cost results from the use of Inconel 617 for all high-temperature parts of the system; the Inconel 617 sheet cost amounts to 51 percent of the structure manufacturing cost for the rectangular design, and to 73% for the cylindrical design. An important development goal is obviously replacement of Inconel 617 with a less expensive material.

The charged reservoir cost is presented for both LiF and NaF/MgF₂ eutectic, using costs of \$2.75/kg for LiF and \$0.20/kg for NaF/MgF₂, approximate lower limits as given by Eichelberger¹ for large-volume production. In terms of cost per unit thermal storage capacity, the rectangular design has a cost of \$39/kwhrth when charged with LiF and \$47/kwhrth when charged with NaF/MgF₂; the corresponding

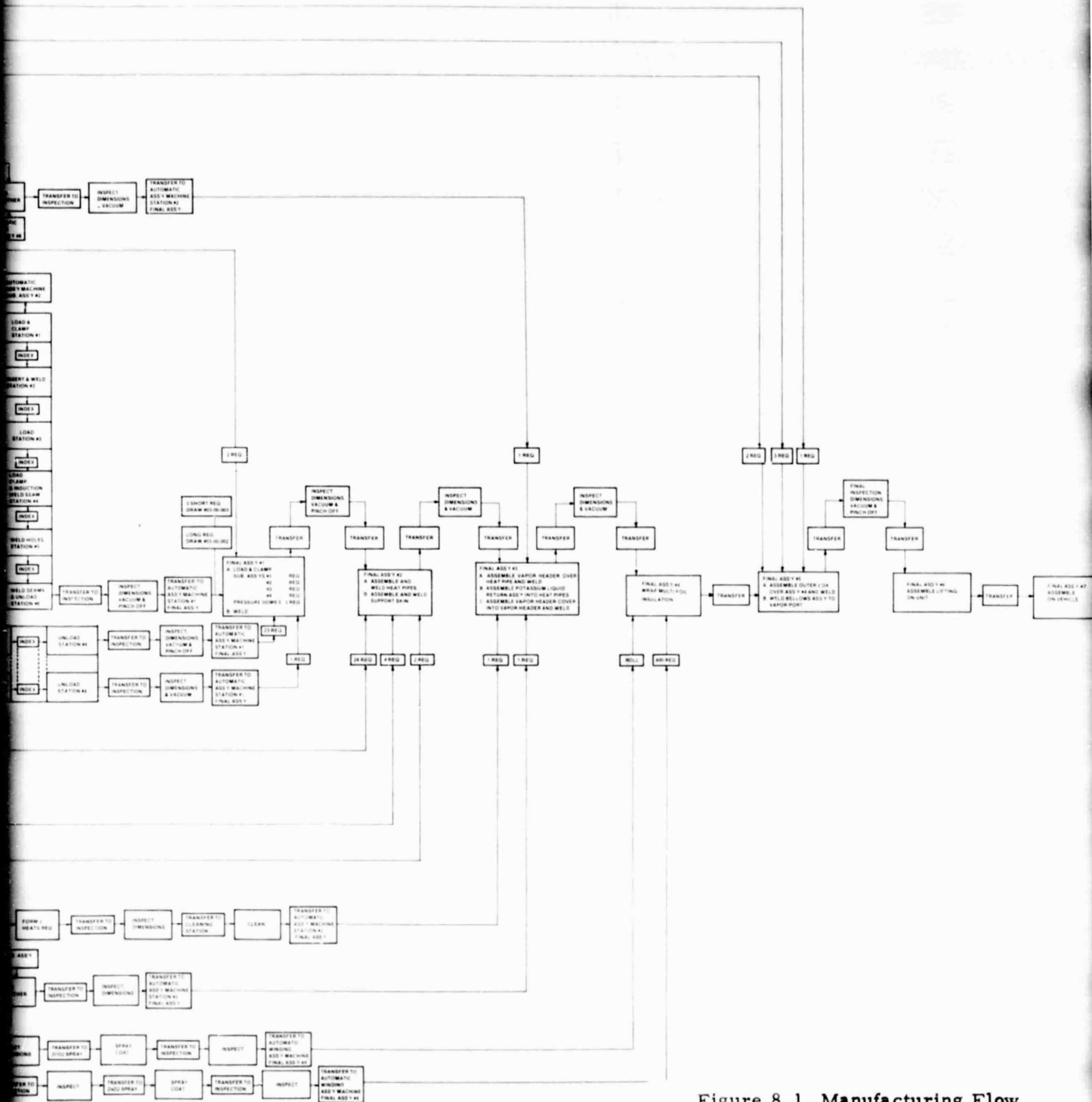
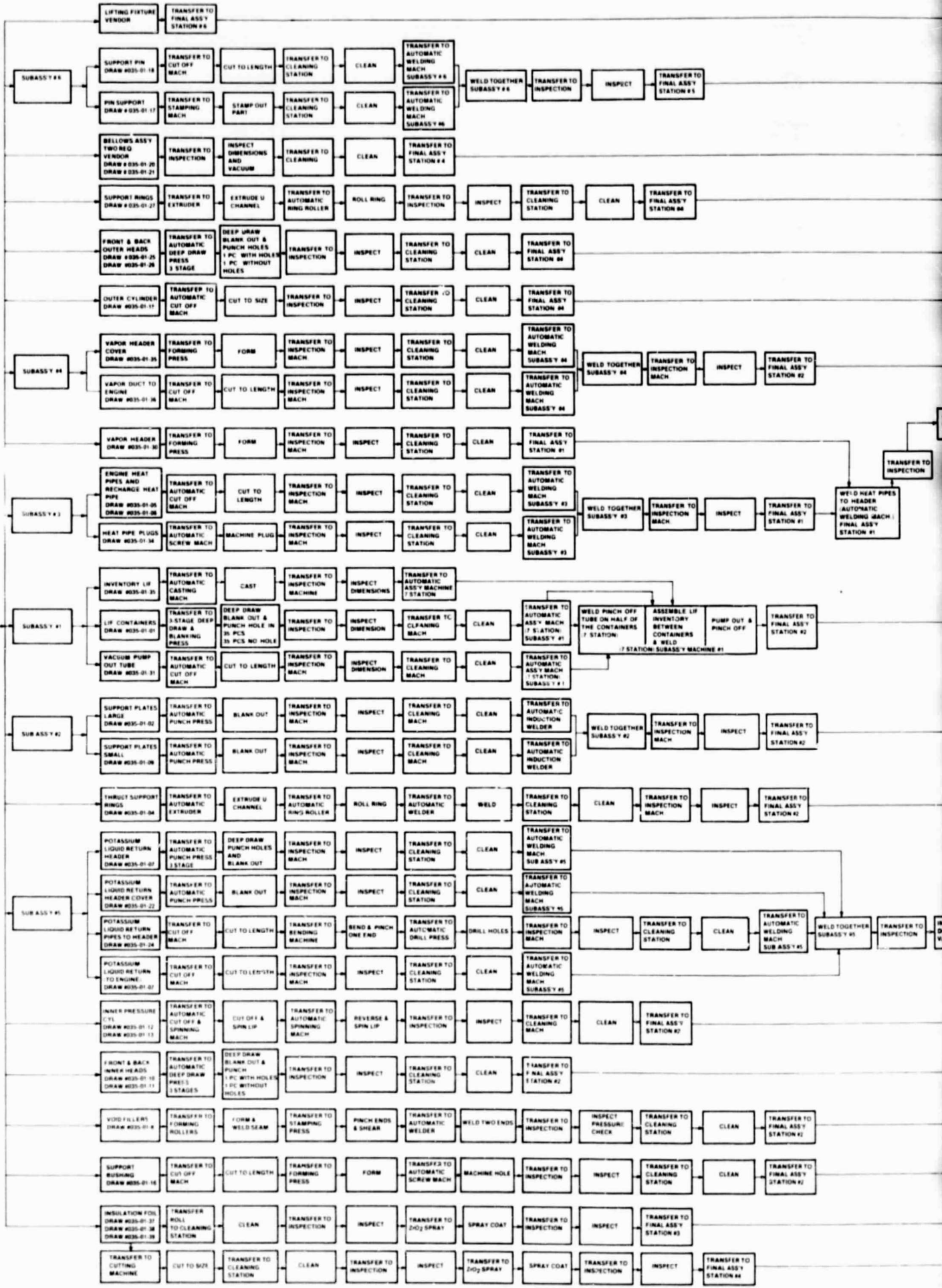


Figure 8.1 Manufacturing Flow Diagram for Rectangular Configuration

RECEIVING
A. VERIFICATION
OF MATERIAL
B. INSPECT
DIMENSIONS &
C. DOCUMENTATION



FOLDOUT FRAME

PRECEDING PAGE BLANK NOT FILMED

TABLE 8.1

MANUFACTURING COST ESTIMATE FOR
RECTANGULAR TES RESERVOIR CONFIGURATION

Units/Year	200,000
Finished Structural Weight	230 kg (507 lb)
Structural Raw Materials	
Inconel Sheet and Tubing	
Weight	217 kg
Cost	\$ 2976
Multi-Foil Insulation	
SS Weight	39.6 kg
Cost	\$ 258
Al Weight	5.3 kg
Cost	\$ 34
Honeycomb For Outer Box (Carbon Steel)	
Weight	53.5 kg
Cost	\$ 42
Total of Above Weights	315 kg
Total of Above Costs	\$ 3310
Miscellaneous Parts Costs	
Bellows	\$ 185
Welding Rod	\$ 250
Total Raw Materials Cost	\$ 3745
Direct Labor	
Manhours	48 1/2 Manhours
Burdened Cost (at \$ 25/Manhour)	\$ 1212
Assumed % of Units Scrapped Because of Manufacturing Defects	15%
Total Structure Manufacturing Cost (Raw Material Plus Labor)	\$ 5832

TABLE 8. 1 (cont.)

MANUFACTURING COST ESTIMATE FOR
RECTANGULAR TES RESERVOIR CONFIGURATION

Manufacturing Cost Charged With LiF (at \$ 2. 75/kg LiF)

LiF Mass	337 kg
Total Reservoir Mass	567 kg
LiF Cost	\$ 927
Total Reservoir Manufactured Cost	\$ 6759
Storage Capacity	172 kwhrth
Cost Per Unit Storage Capacity	39. 3 \$ /kwhrth

Manufacturing Cost Charged With NaF/MgF₂ Eutectic
(at \$ 0. 20/kg)

NaF/MgF ₂ Mass	409 kg
Total Reservoir Mass	639 kg
NaF/MgF ₂ Cost	\$ 82
Total Reservoir Manufactured Cost	\$ 5914
Storage Capacity	127 kwhrth
Cost Per Unit Storage Capacity	46. 6 \$ /kwhrth

TABLE 8.2

MANUFACTURING COST ESTIMATE FOR
CYLINDRICAL TES RESERVOIR CONFIGURATION

Units/Year	200,000
Finished Structural Weight	225 kg
Structural Raw Materials	
Inconel Sheet and Tubing	
Weight	275 kg
Cost	\$3786
Multi-Foil Insulation	
SS Weight	41.7 kg
Cost	\$272
Al Weight	5.6 kg
Cost	\$37
Outer Cylinder (Alloy Steel)	
Weight	68.5 kg
Cost	\$182
Total of Above Weights	391 kg
Total of Above Costs	\$4277
Miscellaneous Parts Costs	
Bellows	\$185
Welding Rod	\$125
Total Raw Materials Cost	\$4587
Direct Labor	
Manhours	13 Manhours
Burdened Cost (at \$25/Manhour)	\$324
Assumed % of Units Scrapped Because of Manufacturing Defects	5%
Total Structure Manufacturing Cost (Raw Materials Plus Labor)	\$5169

TABLE 8. 2 (cont.)

MANUFACTURING COST ESTIMATE FOR
CYLINDRICAL TES RESERVOIR CONFIGURATION

Manufacturing Cost Charged With LiF (at \$ 2. 75/kg LiF)

LiF Mass	262 kg
Total Reservoir Mass	487
LiF Cost	\$ 720. 5
Total Reservoir Manufactured Cost	\$ 5890
Storage Capacity	134 kwhrth
Cost Per Unit Storage Capacity	44. 0 \$ /kwhrth

Manufacturing Cost Charged With NaF/MgF₂
Eutectic (at \$ 0. 20/kg)

NaF/MgF ₂ Mass	318 kg
Total Reservoir Mass	543 kg
NaF/MgF ₂ Cost	\$ 64
Total Reservoir Manufactured Cost	\$ 5233
Storage Capacity	98. 6 kwhrth
Cost Per Unit Storage Capacity	53. 1 \$ /kwhrth

values for the cylindrical design are \$44/kwhrth and \$53/kwhrth. Thus, from an economical point of view, it is preferable to use LiF as the storage salt, even though its cost per charge is about 11 times that of NaF/MgF₂ (\$720 versus \$64 for the cylindrical design). This attractiveness of LiF results from the high cost of the basic structure and the extra storage capacity when charged with LiF instead of NaF/MgF₂. Basically, the structural cost overrides the cost of the charging salt. It should be noted that the raw materials cost does not include a credit for recycle of manufacturing scrap. This credit can be a significant factor in reducing the cost, since each unit has considerable scrap that can easily be recycled.

8.2 ENERGY SOURCES AND RECHARGING

In Chapter 3, the recharging concept was described via a recharging heat pipe incorporated as part of the TES system and a separate combustor heat source, incorporated as part of the vehicle garage, which can be automatically engaged to the vehicle for overnight recharging. The question arises as to what nonpetroleum fuel will be available for recharging that may not be suited for direct use on the vehicle.

In Figure 8.3, a schematic diagram is presented of potential nonpetroleum energy sources and how they might be utilized for automotive propulsion. All three options can be used to produce electric power, which can easily be used for recharging the TES system. If advanced batteries are developed that have a competitive gravimetric and volumetric energy storage density to TES and that

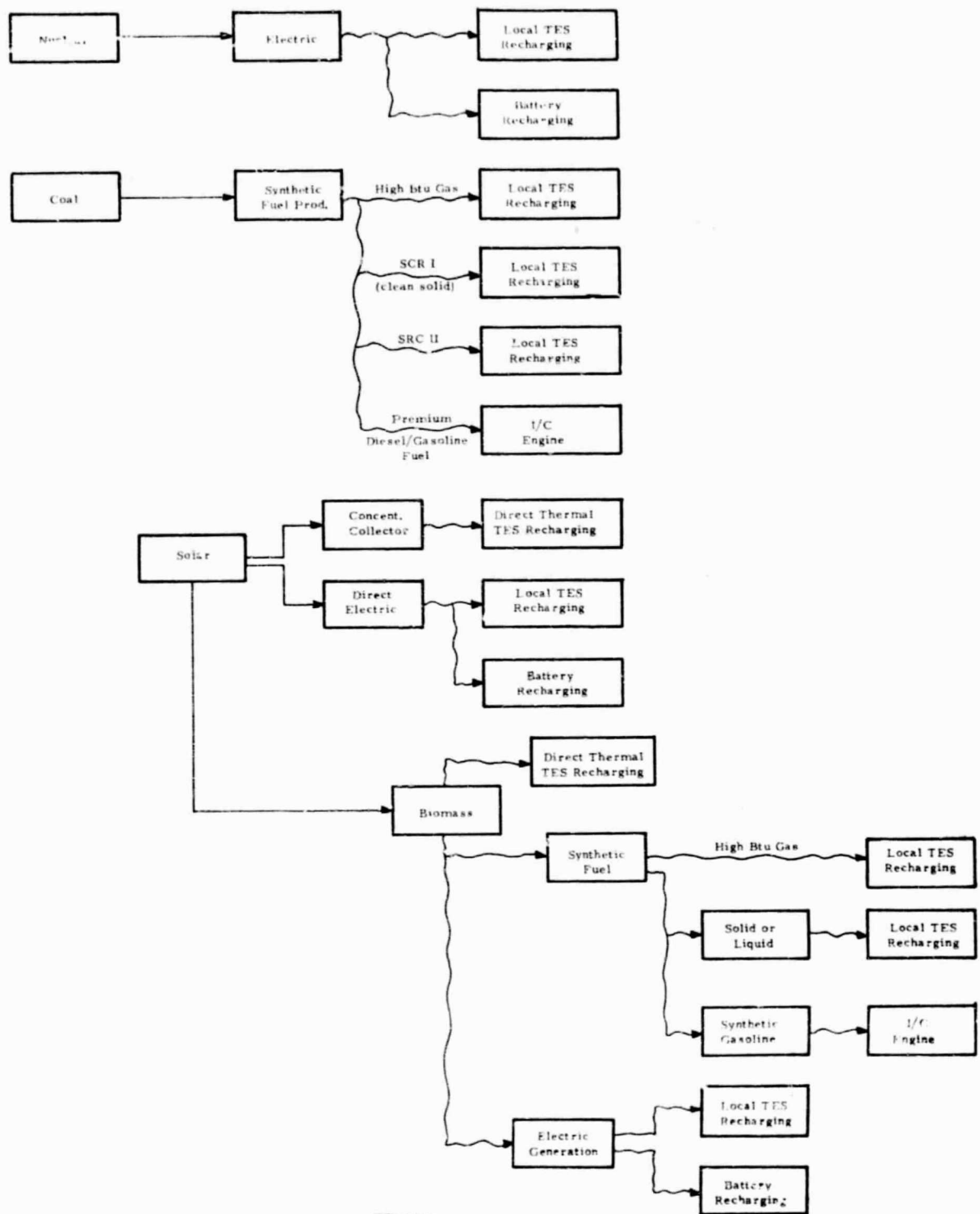


Figure 8.3 Nonpetroleum Energy Sources and Options for Automotive Propulsion

have an acceptable recharge cycle life, cost, etc., — the use of batteries would represent the best means of utilizing electric power for automotive propulsion. However, it is not clear whether such a battery will be developed.

The TES/Stirling system is competitive to electric battery storage systems in terms of gravimetric and volumetric storage density and thus represents a viable alternative for use of electric power for automotive propulsion. Although arguments can be made against the use of electric power as a thermal energy source on the basis of efficient utilization of energy, it is a convenient thermal energy source, universally available, and capable of production from any of the nonpetroleum energy sources. For these reasons, electric power is used extensively for applications such as residential water heating and, in certain areas, residential space heating. Whether or not electric power is used as the primary energy source, we believe any TES system should include the capability of electric recharging for emergency use when the system might be discharged with no means of recharging from a combustion source. The universal availability of electric energy would permit partial or complete electric recharging so that the vehicle could return to its home base for recharging from a combustion heat source.

The most attractive option for recharging relative to energy efficiency is the direct use of combustion from nonpetroleum-derived fuels. Synthetic gas from coal, for example, represents an excellent combustion energy source that may be widely available in the future and that is not suitable for direct utilization for

automotive propulsion. In most sections of the country, natural gas is used extensively for residential space and water heating as well as for commercial and industrial heating. To support this system, an immense and expensive pipeline network has been developed.

The existing system provides an extremely powerful incentive to develop synthetic gas production from coal to supplement, and eventually replace, natural gas in these pipelines as our gas reserves are depleted.

Thus, a reasonable conclusion could be made that natural and/or synthetic gas will be delivered to homes and to commercial/industrial establishments for many years in the future. Particularly with overnight recharging when the normal gas demand is low, this synthetic gas can be used for recharging TES/Stirling automobiles. Furthermore, gas is an extremely clean-burning fuel with very low emissions and requires a simple and compact burner/furnace because of its ease of combustion. The use of synthetic gas delivered to the home, just as natural gas is now delivered, can represent an important future energy source for the TES/Stirling automobile.

The use of synthetic liquid fuels depends on the grade of fuel. If synthetic gasoline or synthetic diesel fuel is produced, the most appropriate mode of use is direct storage on the vehicle and use with an I/C engine (or Stirling engine coupled with liquid fuel/TES as a dual-mode system). Thermal energy storage would thus be suited best for liquid fuels with characteristics that were not suited for direct on-board vehicle utilization, such as a high freezing point or poor combustion characteristics. These fuels might still have

properties suitable for home heating and could be cheaper to produce and more energy-efficient in production than the premium liquid fuels. This type of fuel could be used as a replacement for the petroleum-based heating oil now used extensively in certain areas of the country, particularly the Northeast, and an extensive infrastructure again exists for this function. If used for home heating, this liquid fuel could be used in a special burner for recharging the TES/Stirling automobile with the same convenience as home heating is now performed. The convenience would be the same as with gas, although a somewhat larger combustor would be required.

Synthetic solid fuels, such as SRC-I, represent another potential energy source. However, the use of this type of fuel would be more difficult than that of the liquid or gaseous fuels for which the distribution system and utilization equipment for local use already exist. Still, as recently as 30 to 40 years ago, coal was extensively used for home heating, either with manual fueling or with automatic stoker-fed furnaces. If the potential advantages of SRC-I or similar synthetic fuel (high energy production efficiency, minimum production cost) resulted in its development and extensive use for home heating, the fuel could be used for recharging the TES/Stirling car with as much convenience as its use for home heating.

In summary, relative to synthetic fuels from either coal or biomass, we believe that synthetic gas and/or synthetic liquid fuels will be developed and used for residential heating for many years in the future. The use of these fuels can be readily extended to local combustion recharging of the TES/Stirling car.

Finally, direct use of solar thermal energy for recharging appears to be difficult. The recharging temperature is high (up to 1600° F), requiring a high-temperature concentrating collector; the energy is available only during the day when automobiles are normally used so that separate TES would be required for the charging system to permit nighttime recharging of the vehicle; and coupling the recharging system to the vehicle for recharging would be difficult. Still, if some of the high-temperature solar developments supported by DOE for electric power generation become feasible from an economic point of view, this technology could undoubtedly be adapted and used for TES/Stirling car recharging. Such a utilization of solar energy will be many, many years in the future. The most immediate sources of nonpetroleum energy for use with this system are the synthetic fuels that are developed for home utilization, but that are not suitable for direct use on the vehicle. Electric energy provides a useful backup energy source.

8.3 VEHICLE RANGE

The vehicle range represents an extremely important characteristic relative to customer acceptance. The parameters determining the range are:

$$R = \frac{(\Delta H)(\bar{W})(f)}{(QPL)}$$

where R = vehicle range, km

ΔH = TES media gravimetric storage capacity,
kwhrth/kg

W = total TES system weight, k

f = fraction of TES system weight that is
TES media

QPL = thermal energy required per unit length
of travel by vehicle, kwhrth/km

Contract specifications indicated a QPL for a compact car of 0.627 kwhrth/km for steady speed cruise at 88.5 km/hr and 0.824 kwhrth/km for the SAE Metropolitan Driving Cycle (SAEJ-227), based on calculations performed by MTI² using the ERDA 4-98 Stirling engine performance map. The calculations were based on a vehicle gross weight of 3700 lb (1678 kg), automatic transmission, and the performance map given in Figure 8.4. The SAE J-227 driving cycle is illustrated in Figure 8.5. With the calculated energy requirements and using the TES storage capacity for the rectangular design after normalization to a total TES reservoir weight of 500kg (See Table 6.10), the vehicle range is as summarized in Table 8.3.

As a check on these values, and to provide additional information on the effect of Stirling engine efficiency on the vehicle range for a given TES system, the vehicle simulation program at Thermo Electron Corporation was used with two Stirling engine performance maps, one reported by the Ford Motor Co.³ for the 4-98 Stirling engine with rollsock seals as given in Figure 8.6, and one for the United Stirling P-75 Stirling engine as given in Figure 8.7.⁴ The peak engine power for the FOMOCO 4-98 engine is very near 100 hp, and the P-75 map was normalized to this peak power. Calculations were

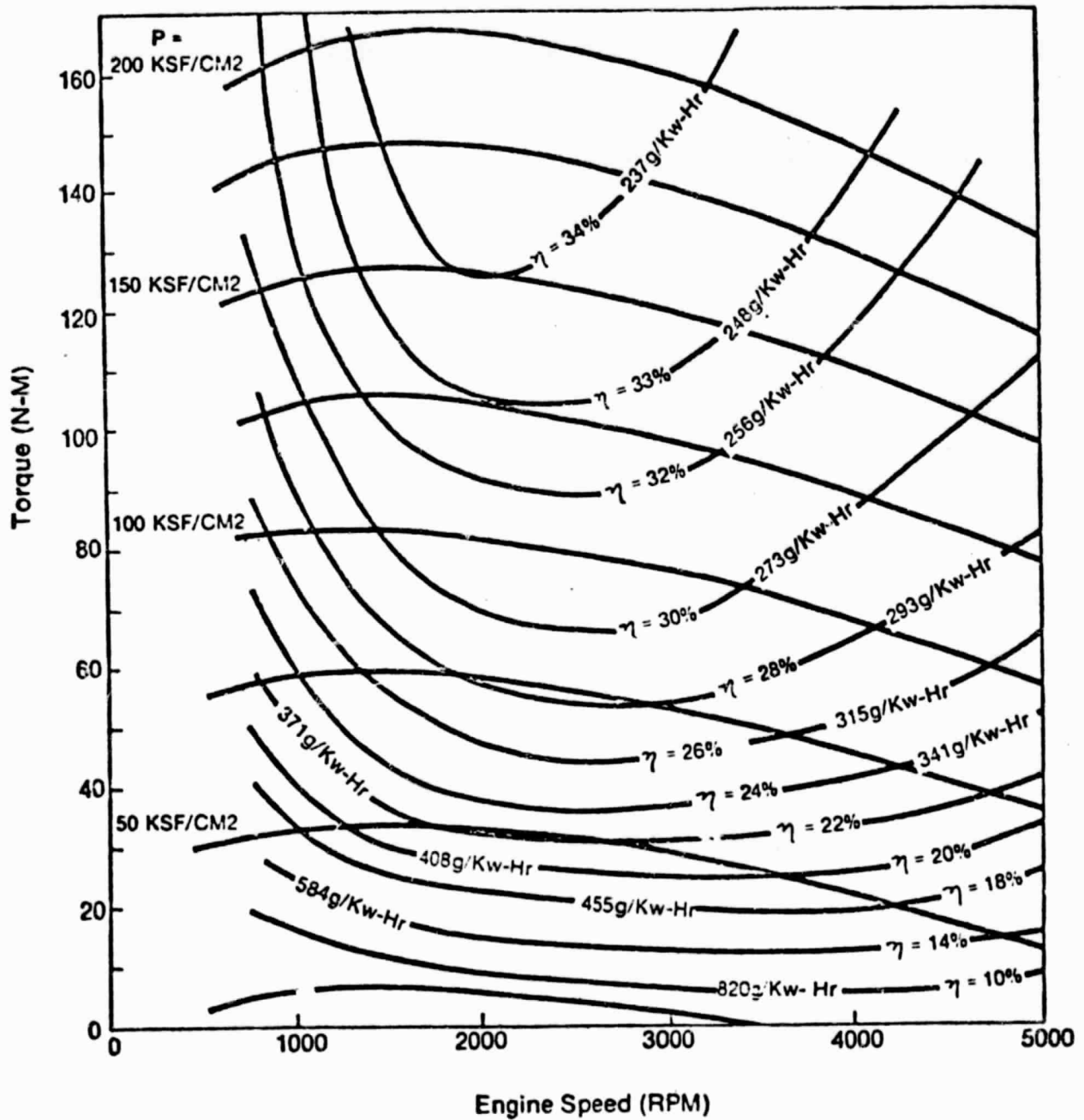


Figure 8.4 Performance Map for ERDA-4 98DA Stirling Engine²

A-3017

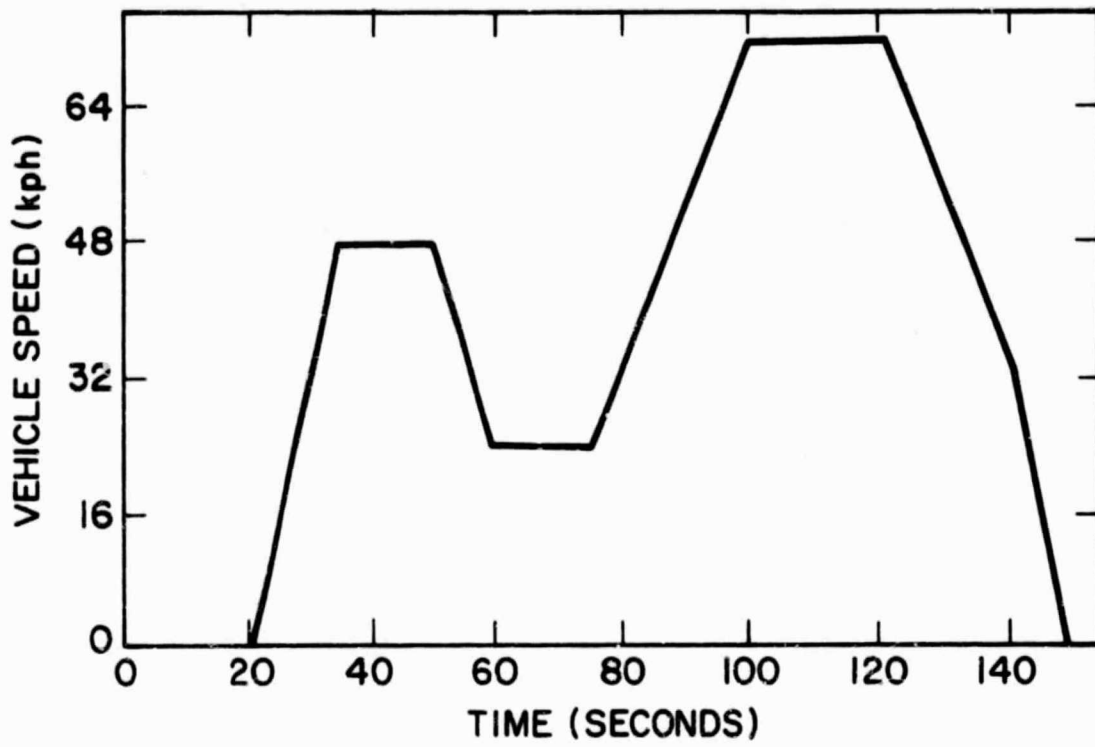


Figure 8.5 SAE Metropolitan Area
Driving Cycle, SAE J-2272

TABLE 8.3
VEHICLE RANGE FOR 500 kg TES RESERVOIR WEIGHT

Salt	LiF	NaF/MgF ₂
Storage Capacity	152 kwhrth	99 kwhrth
Range		
Cruise at 88.5 km/hr*	242 km	158 km
SAE Metropolitan Cycle**	184 km	120 km

* 0.627 kwhrth/km

** 0.824 kwhrth/km

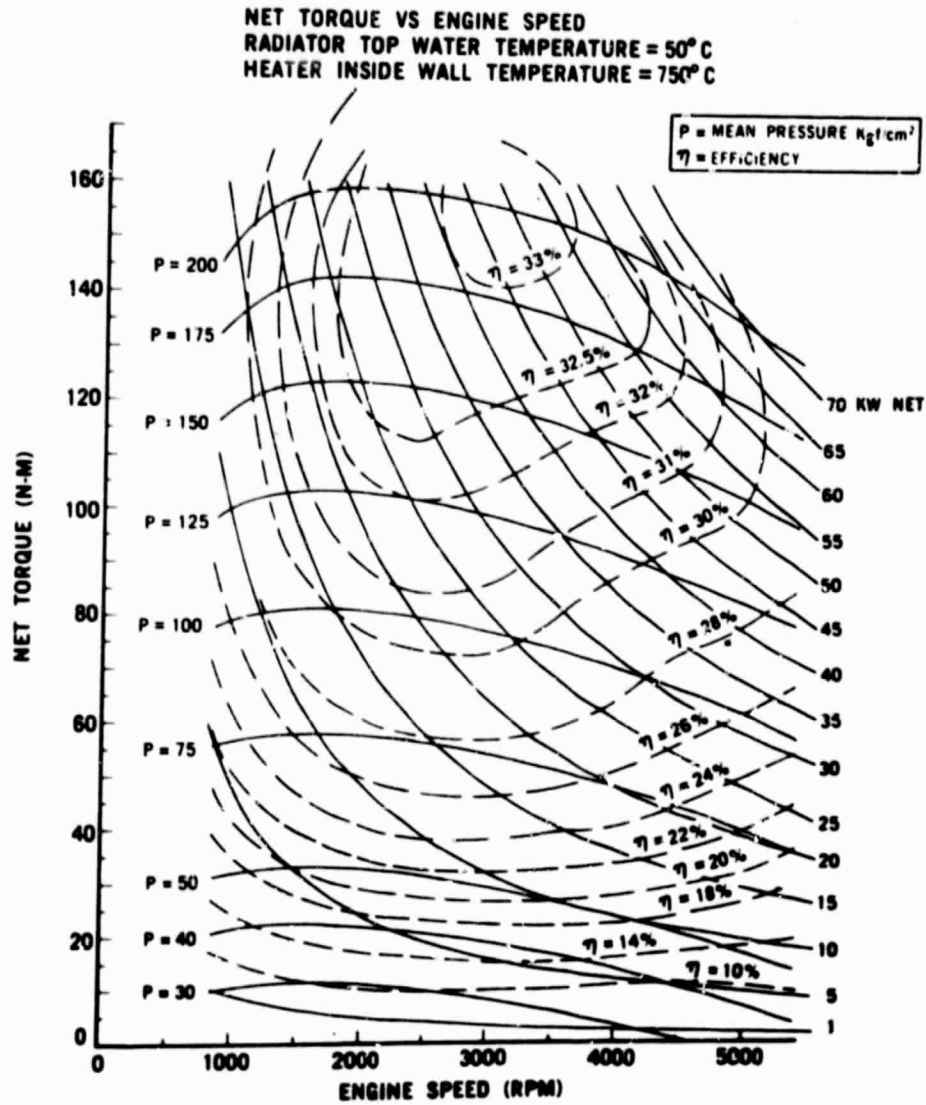


Figure 8.6 Performance Map: 4-98 Stirling Engine with Rollsock Seals

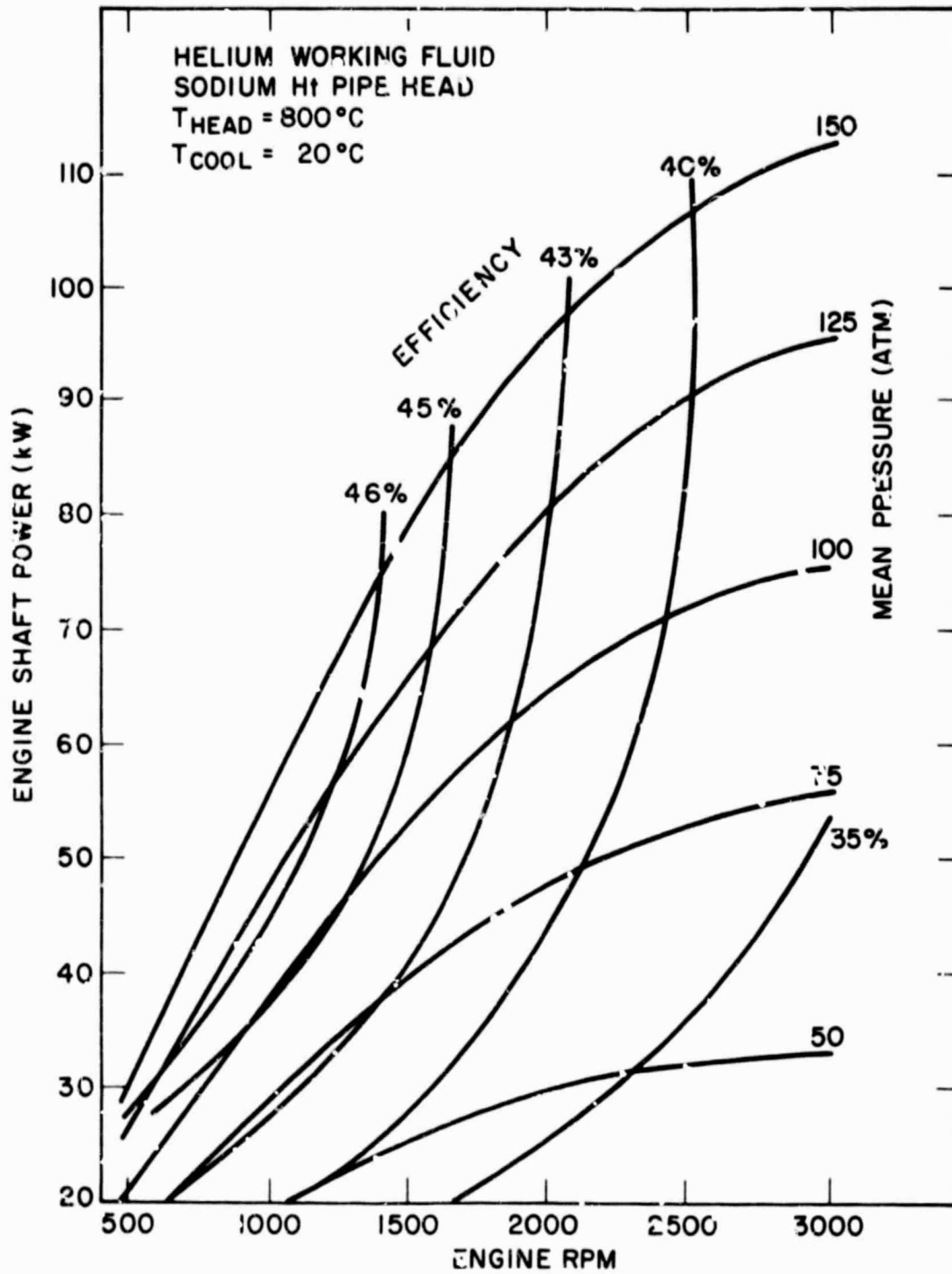


Figure 8.7 P-75 Stirling Engine Performance Map

performed for a vehicle gross weight of 3700 lb. The required wheel power for the vehicle was estimated by the following relation:

$$\begin{aligned} \text{HP} = & \frac{V}{550} \frac{W}{65} \left[1 + (1.4 \times 10^{-3})(V) + 1.2 \times 10^{-5} V^2 \right] \\ & + 1/2 \rho C_d A_f V^2 \\ & + \frac{W}{32.2} \frac{dV}{dt} Z \end{aligned}$$

where HP = wheel horsepower

V = vehicle velocity, ft/sec

W = gross vehicle weight, lb

C_d = drag coefficient (~0.35)

A_f = frontal area, ft²

Z = Constant factor for manual transmission to account for rotary inertia of engine, auxiliaries, and drivetrain (~1.01 for calculations).

ρ = air density, slugs/ft³

L = time, sec.

The calculations are based on the use of a four-speed manual transmission. The efficiencies of the transmission are taken as 96 percent for 1st gear, 97 percent for 2nd gear, and 98 percent for 3rd and 4th gear. The drive shaft gear efficiency is 96.5 percent. The shift points are: shift from 1st gear to 2nd gear at 25 mph, shift from 2nd gear to 3rd gear at 40 mph, and shift from 3rd gear to 4th gear at 62 mph. For the windage loss, the product $C_d A_f$ was taken as 10 ft².

Results of the calculated thermal energy requirement for steady-speed operation and for the Federal suburban and city driving cycles are given in Table 8.4. Performance calculations for acceleration and gradability are also presented in Table 8.4. The thermal energy requirement/distance is considerably higher than that predicted by MTI for the 4-98 engine map. The P-75 engine predictions are approximately equal to those of MTI, even though the engine map has a substantially higher efficiency. The reason for the discrepancy between the two estimates is not known at present. In any case, the estimated vehicle range from a 500 kg TES reservoir is respectable. From Part B of Table 8.4, the acceleration performance and gradability from the 100 peak hp engine is more than adequate. In fact, a somewhat smaller engine could be justified.

8.4 SAFETY CONSIDERATIONS

Any system containing a molten salt at 1150°K and using potassium (or sodium) as a heat transfer media obviously represents a safety hazard, particularly when located in close proximity to personnel in a mobile vehicle operating at high speed and subject to collision. However, the same hazard exists in the operation of a vehicle that contains 15 to 20 gallons of highly volatile and highly flammable fuel (gasoline). The hazard resulting from the TES should, therefore, be considered relative to current automobiles to provide a proper perspective on the hazard. It should be noted that a detailed safety hazard analysis would require extensive analysis as well as experimental work outside the scope of this program. The approach followed has been to make a conscious effort in the design to make

TABLE 8-4

ENERGY REQUIREMENT AND PERFORMANCE PREDICTIONS
(THERMO ELECTRON CORPORATION CALCULATIONS)

Vehicle Weight 3700 lb
 $C_{Df} A_f$ 10 ft.²
 Four-Speed Manual Transmission

A. ENERGY REQUIREMENT PER UNIT DISTANCE AND RANGE FOR
152 kwhrth STORAGE

Driving Cycle	FOMOCO 4-98 Max		United Sterling P-75 Max	
	Energy Req'd (kwhrth/km)	Range (km)	Energy Req'd (kwhrth/km)	Range
30 mph	0.944	161	0.642	237
40 mph	0.776	196	0.547	278
50 mph	0.844	180	0.631	241
60 mph	0.986	154	0.743	205
70 mph	0.960	158	0.718	212
80 mph	1.12	136	0.850	179
Suburban	1.04	146	0.794	191
City	1.45	104	0.907	168

$$1 \frac{\text{kwhrth}}{\text{km}} = 21 \frac{\text{Miles}}{\text{U. S. Gallon}}$$

TABLE 8.4 (cont'd)

A-2976b

ENERGY REQUIREMENT AND PERFORMANCE PREDICTIONS
(THERMO ELECTRON CORPORATION CALCULATIONS)B. VEHICLE ACCELERATION AND GRADABILITY
PERFORMANCE (PEAK ENGINE POWER = 100 hp)

	4-98 MAP	P-75 MAP
0-60 MPH	14.9 Sec	12.9 Sec
25-70 MPH	17.6 Sec	15.9 Sec
50-80 MPH	19.0 Sec	17.4 Sec
0-65 MPH, 5%	29.4 Sec	24.5 Sec
0 MPH	53%	52.6%
20 MPH	32%	33.7%
40 MPH	15.2%	15.8%
60 MPH	10%	9%

the system as safe as possible without compromising its functional performance. It should be noted that Boser of the North American Philips Corporation has reported on safety considerations for high-temperature energy storage in fluoride salts.⁵

The TES reservoir designs presented in Chapter 6 have a low profile (height) specifically so that they may be packaged underneath the floorboard of the vehicle and between the wheels. This location provides maximum protection of the TES reservoir from front, rear, or side collisions of the vehicle, minimizing the possibility of major physical damage to the reservoir in the event of a collision. Collision stresses have also been considered in a preliminary manner in the design of the cylindrical and rectangular configurations and their supporting pins. It should be noted that, if the TES reservoir is breached and molten salt leaks to the outside, freezing of the salt around the edges of the leaking materials naturally restricts movement of the molten salt and reduces the possibility of contact with and ignition of flammable material (or personnel contact). The fluoride salts are very stable compounds and will not react chemically with ambient surroundings at high temperature.

An additional design feature to minimize leakage of molten salt is the use of many individual capsules for containing the salt. Thus, even if major damage to the TES reservoir occurs, it can be anticipated that only a relatively small fraction of the salt capsules will be breached, thereby limiting the potential salt leakage. In addition, where leakage does occur, freezing of salt around the leakage site will tend to seal the leak, preventing further leakage.

Another potential hazard results from the use of potassium (or sodium) as a heat transport medium. As discussed in Chapter 4, the only feasible method of transporting the heat from the TES material to the Stirling engine heater head appears to be the use of either sodium or potassium vapor transport. Because of a smaller transport pipe diameter, potassium has been selected as the reference material. Potassium is a very reactive material with either oxygen or water and its use raises safety questions relative to the use of such a reactive material. This issue is addressed in the following discussion.

Our basic approach to this issue has been to reduce to a bare minimum the potassium inventory required for operation of the system. If this inventory is sufficiently small, the hazard from the use of potassium as a heat transport medium will be insignificant relative to the hazard resulting from other sources of stored energy or from operation of the vehicle. A major criterion in our design work has thus been to minimize the sodium inventory. In Table 8.5 the estimated potassium inventory in the system is presented. The tabulation is based on the liquid inventory, since the vapor inventory is negligible relative to the liquid inventory. It should be noted that the exact inventory is difficult to estimate due to uncertainty in the amount of liquid clinging to the walls in the system or in a wick structure. Based on these estimates as well as prior experience in sodium and potassium heat pipes, we believe that the total potassium inventory will be no more than ~ 1 kg for the rectangular configuration and no more than ~ 1.5 kg for the cylindrical configuration. As an example of the inventory in a specific heat pipe,

TABLE 8.5

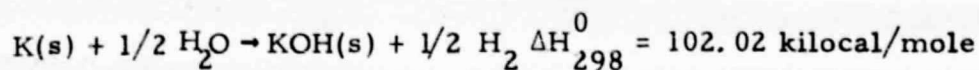
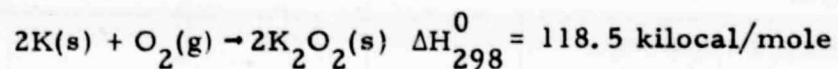
ESTIMATED POTASSIUM CHARGE FOR SYSTEM

Item	Potassium Mass, grams			
	Rectangular Configuration		Cylindrical Configuration*	
	Per Item	Total	Per Item	Total
A. Recharge Heat Pipes	6	6	12	12
B. TES Reservoir Heat Pipe		280		440
Potassium Sump	110		255	
Clingage to TES Containers	135		155	
Clingage to Reservoir Walls	35		30	
C. Discharge Heat Pipe		255		260
Potassium Reservoir	40		40	
Liquid Return Line and E/M Pump	135		135	
Wick Structure	75		80	
Clingage to Engine Tubes	5		5	
D. Total Estimated	-	541	-	712
Allowance for Overcharge and Uncertainty (20% → 100%)	-	108 → 541	-	142 → 712
E. Estimated Potassium Inventory Range	-	650 → 1080	-	850 → 1420

*For two cylinders.

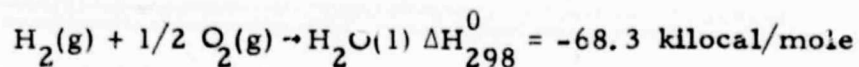
a heat pipe with 4.5-in diameter by 6-ft length, operating at 1900°F (1040°C), has been constructed and tested at Thermo Electron. This heat pipe had wick on the entire interior surface and was charged with 450 gm of sodium. The liquid inventory for the TES system is minimized by the use of a small-diameter liquid return line (rather than wick), as well as by minimizing liquid holdup at all parts of the system.

If the potassium inventory can be held to the range of 1 kg to 1.5 kg, the hazard due to potassium should be acceptable. The major sources of hazard are reactions with O₂ and water as indicated below:



Both reactions are quite energetic with exothermic heat releases corresponding to 2730 Btu/lb of potassium for the first reaction and 4700 Btu/lb of potassium for the second reaction. In fact, the reaction of potassium with water usually generates sufficient heat to ignite the H₂ generated by the reaction (if mixed with the proper amount of air), thereby increasing the potential hazard.

For comparison with the above reaction energies, the heat of combustion of a hydrocarbon fuel is about 18,500 Btu/lb of fuel. The heat of combustion of hydrogen is 61,500 Btu/lb of hydrogen:



The tabulation below summarizes the energy releases, corresponding to the above reactions, for 1.5 kg of potassium, the estimated upper limit on the potassium inventory.

Potassium Combustion with O ₂	9,030 Btu
Potassium Reaction with Water	15,540 Btu
H ₂ Generated by Water Reaction	77.3 gm
Hydrogen Combustion with O ₂	10,430 Btu

We believe that these potential energy releases are small enough so that any potential hazard from this source is acceptable, relative to the other hazards involved in operating either conventional or TES/Stirling engine automobiles.

Finally, in the construction of the large 4.5-in by 6-ft sodium heat pipes described earlier, it was sometimes necessary to reprocess the units containing a full charge (450 gm) of sodium. The sodium charge was solidified at one end of the heat pipe. The end of the heat pipe was then cut off with a hack saw. This procedure was carried out in normal room atmosphere and at room temperature. The exposed sodium was slowly covered by a film of sodium oxide and/or sodium hydroxide without vigorous reaction. The reaction rate was slow initially and stopped within a few minutes.

Removal of the sodium from the heat pipe was performed by the use of a large quantity of cold water, either by the use of a hose or by dunking in a barrel of water. The reaction was vigorous, with rapid hydrogen evolution as expected. The washing was performed outside with no explosion occurring.

During testing of one of the large heat pipes while it was being heated by a gas-fired burner, a crack developed in the heated part, permitting sodium to leak out (the operating sodium pressure was greater than atmospheric). The presence of the leak was noticed because of the formation of the yellow-colored flame by the sodium instead of the customary blue flame of the gas burner. The heat pipe continued to function as the burners were turned off. Upon shutdown, as the heat pipes cooled, the internal sodium pressure became less than atmospheric with leakage of air into the heat pipe. No observable effects occurred. Subsequent inspection revealed the location of the crack by small amounts of sodium oxide and sodium hydroxide around the crack.

An additional design consideration is to minimize the chances of breaching the system in the event of a collision. As discussed earlier, the optimum location for the TES unit to provide maximum protection in the event of a collision is between the wheels and side frame members, and underneath the floor board. This location also minimizes the reduction of useful vehicle space by the TES system. From Table 8.5, the total potassium inventory is divided into three separate heat pipes, with the largest amount in the TES reservoir. Thus, the system containing about 55 percent of the total potassium inventory has the best protection in the event of a collision, and it has the greatest potential for being hardened to a 35-mph collision. It would appear difficult to prevent rupture of the heat pipe connecting the TES module to the Stirling engine in the event of a major collision. However, this heat pipe is estimated to contain only about 40 to 50 percent of the total potassium inventory.

One consideration is the possibility of fires produced by the hot, outer surface of the TES reservoir if vacuum is lost in the Multi-Foil insulation. During normal operation, the insulation is so effective that the outside surface temperature in ambient air is estimated to be only about 10°F above the air temperature. Even if vacuum is lost, however, the Multi-Foil insulation serves to minimize convective heat transfer as well as radiation through the air so that the surface temperature is relatively low, even in this case. Estimates based on the thermal conductivity of air with a 0.5-in. gap thickness indicate that, with an internal temperature of 1150°K, the surface temperature will be 150 → 500°F above the ambient air temperature with external surface convective/radiation heat transfer coefficients of 1 to 10 Btu/hr-ft²-°F. These surface temperatures are low enough to prevent ignition of practically all flammable materials.

8.5 ENVIRONMENTAL CONSIDERATIONS

Potential environmental effects of the large-scale use of TES for automotive propulsion can be divided into four categories:

- Mining and Production of Basic Materials
- Manufacturing
- Use
- End-of-Life Disposal

Potential problems from the mining and production of the basic materials are no worse than those from other minerals and materials required for our society, providing reasonable ore deposits can be

located so that extraction from low assay ores is not required. Environmental problems in manufacturing can be readily handled since none of the materials required for the system are highly toxic. In normal use, some loss of the fluoride salt can be expected by leakage during collision or by component failure. This amount of leakage and its possible environmental effects should be small and totally negligible compared to other practices now routinely followed, such as the use of CaCl_2 for highway ice removal.

The most important factor in reducing environmental effects is end-of-life disposal. The entire system should be recycled, thus minimizing potential environmental effects from the mining and production of basic materials. Indeed, the cost of high-temperature metal parts and of LiF will provide a strong economic incentive for recycling of these materials. With some additional effort, all materials, both high and low cost (such as NaF/MgF_2), can be recycled, eliminating any potential environmental effects from end-of-life disposal. Such recycling should be easily implemented and carried out.

8.6 MATERIAL AVAILABILITY CONSIDERATIONS

The major material availability question is the cobalt, nickel, chromium and molybdenum content of the high-temperature alloys required for the hot parts of the system. For a TES system with a structural weight of ~ 250 kg, approximately 70 percent or 175 kg (386 lb), of the total structure weight is high-temperature alloy, specifically Inconel 617. Inconel 617 has a composition of

54 percent nickel, 22 percent chromium, 12.5 percent cobalt, 9 percent molybdenum, and 1 percent aluminum. Thus, for each vehicle, the following approximate quantities of these metals are required:

Nickel	95 kg (208 lb)
Chromium	38 kg (85 lb)
Cobalt	22 kg (48 lb)
Molybdenum	16 kg (35 lb)

In Table 8.6, the total quantity required for 100,000,000 vehicles is compared to the current (1973) world production and to identified resources for these metals⁷. It is apparent that sufficient worldwide resources exist for TES systems for 100,000,000 vehicles, though the cost will be high. The U.S. resources of these metals are low, introducing balance-of-trade problems for large-scale utilization.

With continued development, and possibly with some reduction in the peak operating temperature of the TES system (and of the Stirling engine), use of iron-based alloys may prove feasible, thus reducing the cost and availability difficulties. Such an effort at locating substitute materials of construction to replace Inconel 617 represents an important goal for future development.

8.7 DUAL-MODE TES/LIQUID FUEL SYSTEM

An automobile based on the use of stored thermal energy as a propulsion energy source has a number of limitations and disadvantages that raise questions of public acceptance:

TABLE 8.6
COMPARISON OF QUANTITY OF STRATEGIC METALS
FOR 100,000,000 VEHICLES TO CURRENT WORLD
PRODUCTION AND ESTIMATED RESERVES

A-2977

Metal	Metric Tonnes Required	World Production 1973 (Metric Tonnes)	Identified [*] Resources (Metric Tonnes)	Average Abundance In Earth's Crust (ppm)
Nickel	9,500,000	560,000	112,000,000	75
Chromium	3,800,000	2,165,000	1,800,000,000	100
Cobalt	2,200,000	26,000	4,300,000	25
Molybdenum	1,600,000	82,000	28,600,000	1.5

* Does not include nickel and cobalt associated with seabed manganese nodules.

- The TES is expensive, relative to the rest of the vehicle.
- The vehicle daily range is limited to ~ 160 km (100 miles) for a 500-kg (1100-lb) TES system, since recharge is necessarily slow. Overnight recharging appears most practical.
- The large mass of very high-temperature liquid salt coupled with potassium or sodium raises psychological barriers to public acceptance of such a system because of safety fears.
- The large volume and mass introduce vehicle design problems, relative to packaging, and reduce the energy efficiency of the vehicle.

In short and stated bluntly, who wishes to pay a premium price for a car that can travel only 100 miles before requiring an overnight recharge and that requires the passengers to sit directly over ~ 600 lbs of molten salt at 1600°F?

The system developed in this study is ideally suited for use in a dual-mode approach in which the vehicle can be operated either from fuel carried on-board, as in current automobiles, or from the TES system recharged overnight from an external combustion energy source. This concept was described conceptually in Chapter 3. With this approach, the TES system is greatly reduced in size and used only for short-range trips such as daily commuting or local

shopping trips. Whenever the TES system is discharged, operation is diverted to the use of the liquid fuel in a combustor/heater that provides heat to the Stirling engine via the TES system (see Figure 3.5). In this mode of operation, the TES system operates as a thermal flywheel permitting the combustor to operate at a relatively steady rate with transient peak thermal requirements for high power from the Stirling engine (wide-open-throttle acceleration) supplied from the TES system. Steady combustion should result in very low emission levels from the combustor, relative to the highly transient combustion required for direct-firing of the Stirling engine.

The primary goal in using TES for automotive propulsion is to eliminate the use of premium liquid hydrocarbon fuels. Although the dual-mode approach does not completely eliminate the use of liquid fuels, it does provide an opportunity for a very significant savings of premium liquid fuels. In Figure 8.8, an estimate of the distribution of trip mileage and fuel consumption is given.⁶ Trips of 5 miles or less consume more than 30 percent of all automotive fuel consumption, and trips of 10 miles or less, almost 50 percent of all automotive fuel consumption. It is apparent that even a TES system with only a 10-mile range could result in an extremely important fuel savings for automotive propulsion. Such a system would have a size and weight approximately one-tenth of that described in Chapter 6, namely about 50 kg (110 lb) total weight with a corresponding reduction in volume. Coupling this TES into a dual-mode system with liquid hydrocarbon fuel would provide the convenience and flexibility of current automobiles; i. e., it would permit long

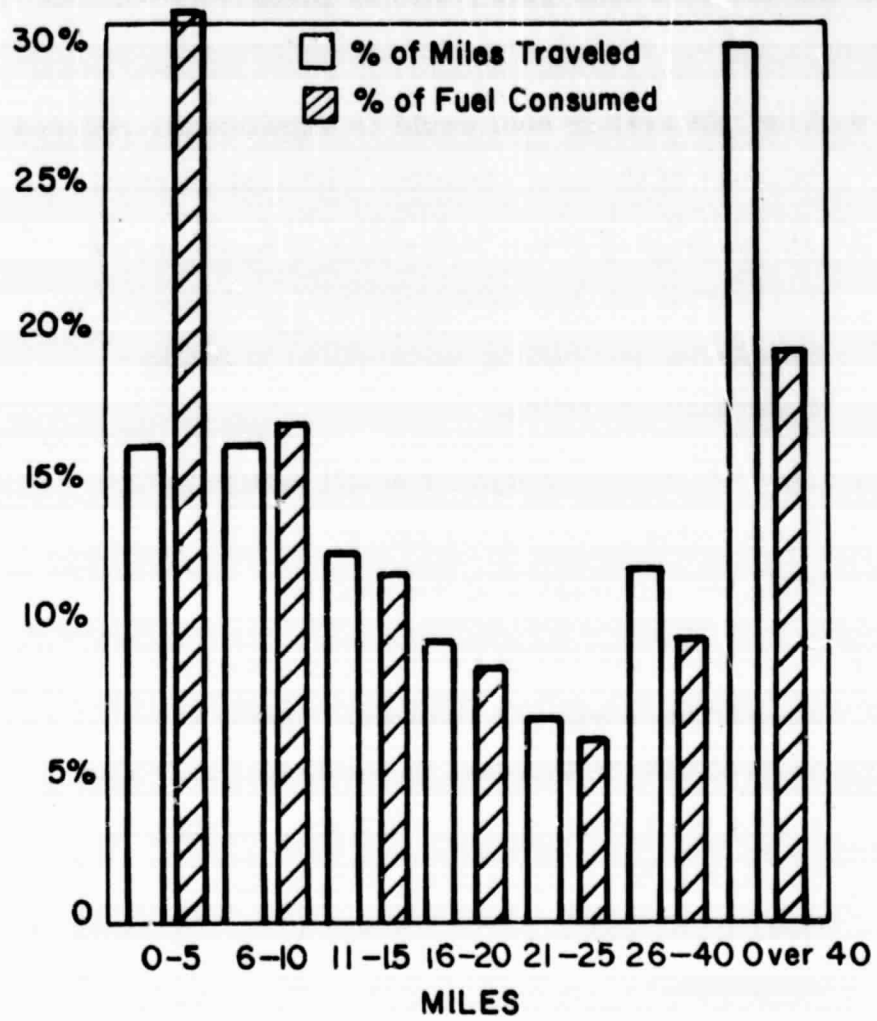


Figure 8.8 Distribution of Trip Mileage and Fuel Consumption

trips with one-minute recharging (refill of gasoline tank). In addition:

- The TES system cost would be significantly reduced because of the much smaller TES system required.
- The packaging of the TES would be much easier because of the approximately one-tenth reduction in volume, permitting automobiles to retain their current styling.
- The TES system weight is small enough to have a negligible effect on the energy efficiency, handling, and suspension of the vehicle.
- Because of the use of the heat pipe heating of the Stirling engine, helium working gas can be used with an increase in power (for the same engine displacement) and efficiency relative to the direct-fired H_2 engine. Elimination of H_2 without performance degradation is an important advantage.
- Decoupling of the burner/heater from the Stirling engine permits the use of a larger burner/heater with lower pressure drop. The parasitic power can thus be reduced, resulting in an additional overall system efficiency improvement. In addition, the burner/heater

can be located away from the engine (as in the trunk with the engine in front) with coupling by a small diameter (~ 1-in. D) potassium vapor line.

- The TES system can be sized and used for different purposes, ranging from a very small TES used only as a thermal flywheel, to a unit one-tenth the size of that described in this report and used for dual-mode operation. This permits gradual evolution of TES systems for automotive use.

REFERENCES FOR CHAPTER 8

1. Eichelberger, J. L., "Investigation of Metal Fluoride Thermal Energy Storage Materials: Availability, Cost, and Chemistry," Report to U. S. Energy Research and Development Administration, Report No. C00-2990-6, Pennwalt Corporation, King of Prussia, Pennsylvania, December 1976.
2. Folsom, L. R. and Artiles, A. A., "Thermal Energy Storage/Heat Engine for Highway Vehicle Propulsion," paper presented at ERDA Highway Vehicle Systems Contractor's Coordination Meeting, Dearborn, Michigan, October 4-6, 1977.
3. "Stirling Engine Feasibility Study of an 80-100 HP Engine and of Improvement Potential for Emissions and Fuel Economy," Report No. C00-2631-22, Ford Motor Co., Dearborn, Michigan, November 1977.
4. Percival, W., Consultant Personal Communication, Washington, D. C., July 1978.
5. Boser, O., "Safety Considerations for High Temperature Thermal Energy Storage in Fluoride Salts," 12th IECEC, Paper No. 779092, pp. 575-582 of Proceedings, August 1977.
6. Shanks, D. B., Loebel, A. S., and Patterson, P. D., Transportation Energy Conservation Data Book, Edition 2, ORNL-5320, Oak Ridge National Laboratory, Oak Ridge, Tenn., October 1977 (p. 283).
7. Mineral Facts and Problems, 1975 Edition, Bureau of Mines Bulletin 667, U. S. Department of the Interior, 1976.

9. CONCLUSIONS

Conclusions based on this study are summarized below:

- The TES/Stirling engine vehicle is technically feasible and meets all operational requirements for a practical vehicle.
- The TES system cost is high, primarily because of the necessity for high-alloy metals for all high-temperature parts of the system.
- Overnight recharging is most practical.
- The dual-mode fuel/TES system offers many advantages relative to a TES-only system.
 - Size and weight of the TES system are reduced by a factor of ~10. The cost would also be significantly reduced and should be acceptable even with use of Inconel 617.
 - Substantial savings (up to 50 percent) of premium liquid fuels for automotive propulsion are obtained.
 - Current vehicle flexibility is retained.
 - Introduction of TES by this approach is a smaller perturbation to current automobiles facilitating implementation.
 - Implementation can be initiated by a very small TES used only as a thermal flywheel to permit steady combustion, with a gradual evolution to larger sizes and dual-mode or TES-only operation.

- Use of potassium or sodium heat pipes is the only feasible method for transport of heat from the TES reservoir to the Stirling engine and for recharge of the TES system. With the use of the metal-vapor heat pipe,
 - He working gas can be used in the Stirling engine instead of H_2 , with better power and efficiency from the same displacement engine; the engine size is also reduced.
 - Precise control of the engine heater temperature, with isothermal heater temperature (no hotpots), is easily accomplished with little danger of overheating the engine.
 - The combustor/heater is decoupled from the engine, permitting the use of a larger combustor/heater with lower pressure drop. The lower parasitic power loss improves the overall system efficiency. The combustor/heater can be located remotely from the engine.
 - H_2 working gas for the Stirling engine can introduce problems in operation of the discharge heat-pipe due to H_2 diffusion through the Stirling heater tubes. Experimental work is required to determine if the H_2 diffusion can be satisfactorily handled, thereby permitting the use of H_2 working gas in the engine.

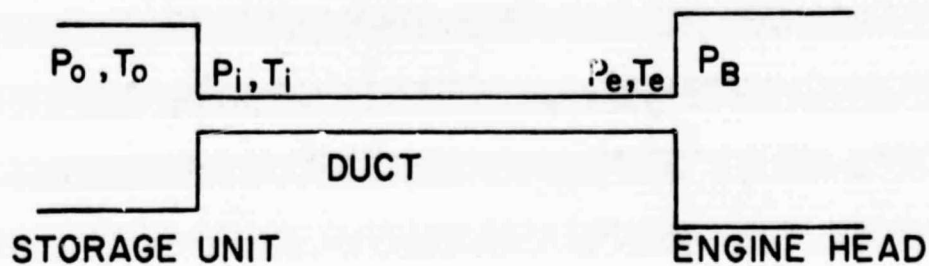
- Use of three-coupled heat pipes is a unique and key feature in meeting all operational requirements.
- The mass of potassium (or sodium) can be maintained low enough in all three heat pipes so that the hazard from the potassium reactivity is negligible.
- A unique E-M pump design was developed for return of the liquid in the discharge heat pipe. Incorporation of this pump provides precise control of the heat delivery rate from the TES to the engine without moving parts and reduces the vapor transport pipe to its minimum size to transport 200 kwth.
- The optimum TES media for the Stirling engine is LiF, provided that cost and availability are acceptable. Sufficient information is not available to eliminate LiF on these grounds. The best material without LiF is a NaF/MgF₂ eutectic, but its gravimetric and volumetric storage densities are inferior to those of LiF.
- Vacuum Multi-Foil thermal insulation provides an effective thermal conductivity that is a factor of ~20 lower than any type of fiber insulation even under vacuum. This low thermal conductivity leads to a significantly lower volume (thickness), weight, and cost when compared to other types of thermal insulation, all factors highly important for the automotive application. The structural design problems introduced by the vacuum enclosure are difficult, but have been

successfully resolved for both the cylindrical and rectangular configurations.

- For the TES-only system, the optimum location for the TES reservoir is beneath the floorboard and between the wheels and sideframes. This provides maximum collision protection to the TES reservoir, maintains a low vehicle center of gravity, and gives an equal weight distribution on the wheels.
- With this location of the TES reservoir and design for minimum potassium inventory, the hazard of this system should be no greater than that due to TES by up to 20 gallons of gasoline.

APPENDIX A
MODEL USED FOR HEAT TRANSPORT CALCULATIONS FOR
DISCHARGE HEAT PIPE DUCT

The flow schematic is shown in the following figure.



The properties of the vapor of liquid metal at low pressure obey the ideal gas law. If we assume that the flow of vapor from the storage unit to the entrance of the duct behaves like the flow in a converge nozzle, the relationships of pressure and temperature between these two locations is:

$$\frac{P_o}{P_i} = \left(1 + \frac{K-1}{2} M_i^2\right)^{\frac{K}{K-1}} \quad (1)$$

$$\frac{T_o}{T_i} = 1 + \frac{K-1}{2} M_i^2 \quad (2)$$

where K = the ratio of specific heats

M_i = the Mach number of flow velocity at the entrance of the duct

Shapiro¹ gives the relationship of adiabatic flow of a perfect gas in a constant area duct with friction:

$$4\bar{f} \frac{L}{D} = \frac{k+1}{2k} \operatorname{hr} \left[\frac{\left(1 + \frac{k-1}{2} M_i^2\right) M_i^2}{\left(1 + \frac{k-1}{2} M_i^2\right) M_i^2} \right] - \frac{1}{k} \frac{M_i^2 - M_e^2}{M_i^2 M_e^2} \quad (3)$$

$$\frac{P_e}{P_i} = \frac{M_i}{M_e} \left[\frac{1 + \frac{k-1}{2} M_i^2}{1 + \frac{k-1}{2} M_e^2} \right]^{\frac{1}{2}} \quad (4)$$

$$\frac{T_e}{T_i} = \frac{1 + \frac{k-1}{2} M_i^2}{1 + \frac{k-1}{2} M_e^2} \quad (5)$$

Where \bar{f} = the average friction factor. For the values of the Reynold's number between 5000 to 300,00,

$$f = 0.0791 N_{re}^{-1/4} \quad (6)$$

L = length of the duct

D = diameter of the duct

M_i = the Mach number of the flow velocity at the exit of the duct

For the given conditions of P_o and T_o in the storage unit, the back pressure P_B at the engine head governs the flow in the duct. A reduction in back pressure P_B acts to increase the flow rate and pressure drop in the duct. No qualitative changes are to be observed until the back pressure is reduced to the value corresponding to the condition that the exit Mach number M_e is unity. Further reductions

in back pressure cannot produce further increases in flow rate, since M_e cannot become greater than unity. The back pressure, P_B , at the engine head is determined by the condensation temperature of the vapor.

REFERENCE FOR APPENDIX A

1. Shapiro A.H., The Dynamics and Thermodynamics of Compressible Fluid Flow, The Ronald Press Company, 1953.